NASA Contractor Report 170413

NASA-CR-170413
19840009552

Development of a Thermal and Structural Model for a NASTRAN Finite-Element Analysis of a Hypersonic Wing Test Structure

Jaap Laméris

Grant NSG 4008
February 1984

National Aeronautics and
Space Administration

NASA Contractor Report 170413

Development of a Thermal and Structural Model for a NASTRAN Finite-Element Analysis of a Hypersonic Wing Test Structure

Jaap Laméris
The University of Kansas Center for Research, Inc., Lawrence, Kansas 66045

Prepared for
Ames Research Center
Dryden Flight Research Facility
Edwards, California
under Grant NSG 4008

1984

National Aeronautics and
Space Administration
Ames Research Center
Dryden Flight Research Facility
Edwards, California 93523

This Page Intentionally Left Blank

ABSTRACT

As part of NASA's continuing research program into hypersonics, Dryden Flight Research Facility has conducted extensive heating and mechanical tests on a Hypersonic Wing Test Structure (HWTS). This structure was based on a structural concept developed for a hypersonic research airplane that would cruise at Mach 8. For future designs of structural concepts and space transportation systems operating at high temperatures, accurate prediction methods of thermal deflections and strains are required. An accurate prediction of the temperature distribution is a major prerequisite for obtaining this goal. In this context, the goal of NASA Dryden's HWTS project is to perform a coordinated analysis and test of a medium-sized existing specimen to obtain a detailed evaluation of state-of-the-art predictive techniques for thermal structures.

This report describes the development of a thermal and structural model for this HWTS structure using the NASTRAN finite-element method as its primary analytical tool. A detailed analysis was defined to obtain the temperature and thermal stress distribution in the whole wing as well as at the five upper and lower root panels.

During the development of the models, it was found that the thermal application of NASTRAN and the VIEW program, used for the generation of the radiation exchange coefficients, were deficient. Although for most of these deficiencies solutions could be found, the existence of one particular deficiency in the current thermal model has prevented the final computation of the temperature distributions at this date.

Despite this, valuable knowledge about the thermal application of NASTRAN and about VIEW has been gained, in addition to the information obtained during the use of an advanced finite-element generating program.

A SPAR analysis of a single bay of the wing, using data converted from the original NASTRAN model, indicated that local temperature-time distributions can be obtained with good agreement with the test data. The conversion of the NASTRAN thermal model into a SPAR model is recommended to meet the immediate goal of obtaining an accurate thermal stress distribution.

TABLE OF CONTENTS

Page

ABSTRACT i

TABLE OF CONTENTS. iii

LIST OF SYMBOLS. vi

LIST OF ACRONYMS vii

LIST OF FIGURES. viii

LIST OF TABLES xii

CHAPTER 1: INTRODUCTION 1

CHAPTER 2: THE HYPERSONIC WING TEST STRUCTURE PROGRAM 6

2.1 THE HYPERSONIC RESEARCH AIRPLANE CONCEPT 6

2.2 THE HYPERSONIC WING TEST STRUCTURE 8

2.3 LOADING TESTS DONE AT DFRF 14

2.4 INSTRUMENTATION. 24

CHAPTER 3: GENERAL DESCRIPTION OF THE ANALYSIS. 29

3.1 INTRODUCTION 29

3.2 DESCRIPTION OF EXISTING ANALYSIS 31

3.3 GENERAL DESCRIPTION OF THE CURRENT ANALYSIS. 37

3.3.1 INTRODUCTION. 37

3.3.2 THE HEAT TRANSFER ANALYSIS. 41

3.3.3 THE STRUCTURAL ANALYSIS 42

3.4 AVAILABLE COMPUTER RESOURCES AND PROGRAMS. 44

3.4.1 COMPUTER RESOURCES. 44

3.4.2 THE NASTRAN PROGRAM 44

TABLE OF CONTENTS (continued)

Page

3.4.3 THE PATRAN-G PROGRAM. 45

3.4.4 THE VIEW PROGRAM. 47

CHAPTER 4: THE THERMAL MODELS 48

4.1 INTRODUCTION 48

4.2 THE UPPER AND LOWER SURFACES OF THE WINGBOX. 51

4.3 THE SPARS AND RIBS OF THE WINGBOX. 52

4.4 THE HEAT SHIELDS AND THE THERMAL LOADING SYSTEM. . . . 55

4.5 THE INSULATION BLANKET 71

4.6 THE RADIATION ELEMENTS 71

4.7 THE RADIATION EXCHANGE COEFFICIENT MATRIX, RADMTX. . . 74

4.8 MATERIAL PROPERTIES AND DIMENSIONS 78

4.9 SUMMARY OF THE GENERATION OF THE THWTS MODEL 80

4.10 THE THERMAL QUARTER BEADED PANEL MODEL, TBPQTR 82

CHAPTER 5: THE STRUCTURAL MODELS. 85

5.1 INTRODUCTION 85

5.2 THE SHWTS MODEL. 85

5.3 THE SBPQTR MODEL 91

5.4 SUPPORTING PROGRAMS. 94

CHAPTER 6: COMMENTS ON THE NASTRAN AND SUPPORT PROGRAMS 95

6.1 INTRODUCTION 95

6.2 FATAL ERROR MESSAGES IN NASTRAN (COSMIC VERSION) . . . 95

6.2.1 SYSTEM FATAL MESSAGE 3102, LOGIC ERROR EMA-1264. 95

TABLE OF CONTENTS (continued)

Page

6.2.2 SYSTEM FATAL MESSAGE 1159: ROW POSITIONS OF ELEMENTS FURNISHED TO ZBLPKI OR BLDPKI ARE NOT IN A MONOTONIC INCREASING SEQUENCE. . . 96

6.2.3 USER FATAL MESSAGE 3031: UNABLE TO FIND SELECTED SET (11) IN TABLE (PLT) IN SUBROUTINE (TRL6) 96

6.3 DEFICIENCIES IN (COSMIC) NASTRAN 96

6.4 THE VIEW PROGRAM 99

CHAPTER 7: RESULTS OF THE THERMAL ANALYSIS. 106

7.1 INTRODUCTION 106

7.2 THE BAY H ANALYSIS 106

7.3 THE BAY H* ANALYSIS. 116

7.4 DISCUSSION 134

CHAPTER 8: DISCUSSION, CONCLUSIONS, AND RECOMMENDATIONS 143

8.1 INTRODUCTION 143

8.2 DISCUSSION 144

8.3 CONCLUSIONS. 148

8.4 RECOMMENDATIONS. 149

REFERENCES 152

APPENDIX A: DRAWINGS. 153

APPENDIX B: PROCEDURE OF THERMAL AND STRUCTURAL ANALYSIS OF THE HYPERSONIC WING TEST STRUCTURE. 203

APPENDIX C: COMPUTER PROGRAMS 214

LIST OF SYMBOLS

Symbol	Definition	Dimension
A	Area	m^2
F	View factor	--
h	Convective film coefficient	$W/m^2 - K$
k	Conductivity	W/m - K
T	Temperature	K
t	Time	sec
Greek Symbol		
ε	Emissivity	--
Subscript		
i,j	Element i to element j	

LIST OF ACRONYMS

Acronymn	Definition
CHBDY	Heat boundary element (NASTRAN)
COSMIC	Computer Software Management and Information Center
CQUAD4	Quadrilateral isometric plate element
CRINC	University of Kansas Center for Research, Inc.
CTRIA3	Triangular isometric plate element
HWTS	Hypersonic wing test structure
KU	University of Kansas
LOBEPA	Lower beaded surface panel submodel
LOHESH	Lower heat shield submodel
LOSURF	Lower surface of wingbox submodel
MSC	MacNeil-Schwindler Corporation
NASA	National Aeronautics and Space Administration
NASTRAN	NASA general purpose Structural Analysis program
SBPQTR	Structural model of quarter beaded panel
SHWTS	Structural model of HWTS
SPARRIBS	Spars and ribs submodel
TBPQTR	Thermal model of quarter beaded panel
THWTS	Thermal model of HWTS
UPBEPA	Upper beaded surface panel submodel
UPHESH	Upper heat shield submodel
UPSURF	Upper surface of wingbox submodel
VIEW	Computer program for generation of view factors

LIST OF FIGURES

Number	Title	Page
1	The Hypersonic Research Airplane and the HWTS.	2
2.1	Hypersonic Research Airplane Configuration. (Fuselage stations [F.S.] and dimensions in meters.)	7
2.2	Hypersonic Research Airplane Research-Mission Profile.	9
2.3	Time History for a Loads Maneuver of the Hypersonic Research Airplane.	10
2.4	Hypersonic Wing Test Structure Dimensions. (The most critically loaded panels are shaded and numbered 1 to 5 going aft. Fuselage stations, wing stations, and dimensions in meters.).	11
2.5	Beaded Panel for HWTS. (Dimensions in centimeters.).	13
2.6	Hypersonic Wing Test Structure..	15
2.7	Interior of HWTS Bay Showing Corrugated Webs of Spars and Ribs.	16
2.8	Applied Load Distributions on HWTS..	18
2.9	HWTS Loading Test Set-Up for the Room Temperature Tests.	19
2.10	Pressure Pan of the HWTS..	21
2.11	Temperature-Time for a Heating Zone, Simulating the Thermal Load during a Mach 8 Loads Maneuver. . . .	22
2.12	HWTS Loading Set-Up for Elevated Temperature Tests.	23
2.13	Strain Gage Locations. (Wing stations are in meters.)	25
2.14	Temperature Measurement Locations.	27
2.15	HWTS Deflection Measurement Locations.	28
3.1	Analysis Flow Chart of Original Analysis..	32

LIST OF FIGURES (continued)

Number	Title	Page
3.2	NWML, NASTRAN Model of the HWTS.	33
3.3	NASTR, NASTRAN Finite-Element Computer Model..	36
3.4	TWOBD, NASTRAN Finite-Element Computer Model..	36
3.5	Flow Chart of Proposed Analysis.	39
4.1	First Thermal Computer Model of HWTS..	49
4.2	Phase-One Construction of (Lower) Surface Wingbox.	53
4.3	Phase-Two Construction of (Lower) Surface Wingbox.	53
4.4	Phase-One Construction of Spar and Rib Webs.	56
4.5	Line Elements Representing Caps of Spars, Ribs, and Vertical Angles.	58
4.6	Heating Zones at Upper Heat Shield..	64
4.7	Heating Zones at Lower Heat Shield..	65
4.8	Compatability Requirement.	67
4.9	Phase-Two Construction of Upper Heat Shield.	68
4.10	Phase-Two Construction of Lower Heat Shield.	68
4.11	Construction of Insulation Blanket..	72
4.12	Subdivision of CHBDY Elements.	76
4.13	Lower Triangle of RADMATRIX, Position of Non-Zero View Factors.	76
4.14	RESURF, NASTRAN Computer Model of a Half Size Beaded Panel and Heat Shield..	79
4.15	SISURF, NASTRAN Computer Model of a Half Size Beaded Panel and Heat Shield as Simulated in Thermal Model.	79
4.16	Flow Chart of the Generation of the THWTS Model. . . .	81

LIST OF FIGURES (continued)

Number	Title	Page
4.17	NASTRAN Thermal Quarter Beaded Panel Computer Model, TBPQTR.	83
5.1	SHWTS, NASTRAN Structural Model of the HWTS.	88
5.2	Top View of the SHWTS Model.	89
5.3	Spar and Rib Elements in SHWTS Model..	90
5.4	NASTRAN Structural Quarter Beaded Panel Computer Model, SBPQTR..	92
6.1	Arrangement of Test Case VIEW.	102
7.1	PATRAN-G Hidden Line Plot of Wingbox and Insulation Blanket of THWTS Model.	107
7.2	PATRAN-G Hidden Line Plot of THWTS Model Including Heat Shields and Curtain Elements.	108
7.3	Isometric View of Thermal Model of Isolated Bay H, BAY H..	110
7.4	Results of NASTRAN COSMIC Analysis of BAY H Model, at F.S. 24.384 and W.S. 2.479..	111
7.5	Results of NASTRAN/MSC Analysis of BAY H Model, at F.S. 24.384 and W.S. 2.479.	112
7.6	Results of NASTRAN COSMIC Analysis of BAY H Model, with Rod Instead of Bar Elements, at F.S. 24.384 and W.S. 2.479..	114
7.7	Comparison of MSC and COSMIC Versions of NASTRAN for the Web Temperatures in the BAY H Model at F.S. 24.384 and W.S. 2.479 with the Heat Shield Temperatures..	115
7.8	Comparison of MSC and COSMIC Versions of NASTRAN for the Center Temperatures of the Surface Panels in the BAY H Model (F.S. 24.384 and W.S. 1.926). . . .	117
7.9	Results of the NASTRAN COSMIC Analysis of the BAY H* Model at F.S. 24.384 and W.S. 2.479..	119
7.10	Results of the SPAR Analysis of the BAY H* Model with Constant Material Properties at F.S. 24.384 and W.S. 2.479..	120

LIST OF FIGURES (continued)

Number	Title	Page
7.11	Results of the SPAR Analysis of the BAY H* Model with Variable Material Properties at F.S. 24.384 and W.S. 2.479..	121
7.12	BAY H* Results of Lower Surface along F.S. 24.384. (Test data given in solid symbols.)	132
7.13	BAY H* Results of Lower Surface along W.S. 1.926. (Test data given in solid symbols.).	133
7.14	BAY H* Results at W.S. 2.479 and F.S. 24.384 (Rib Cross Section). (Test data given in solid symbols.).	135
7.15	BAY H* Results at W.S. 1.372 and F.S. 24.384 (Rib Cross Section). (Test data given in solid symbols.).	136
7.16	BAY H* Results at W.S. 1.926 and F.S. 24.638 (Spar Cross Section). (Test data given in solid symbols.).	137
7.17	Unfolded Planform of BAY H(*) Models..	138
7.18	Possible Candidate Models for Investigation of Size Effect..	142

LIST OF TABLES

Number	Title	Page
4.1	PATRAN-G Directives for the Construction of the Lower and Upper Surfaces of Wingbox.	54
4.2	PATRAN-G Directives for the Generation of the Spar and Rib Webs.	59
4.3	Design of the Thermal Loading System..	62
4.4	Identification of Heating Zones Used in Tests and Models..	63
4.5	PATRAN-G Directives for the Construction of the Lower Heat Shield.	69
4.6	PATRAN-G Directives for the Construction of the Upper Heat Shield.	70
6.1	DMAP Alter Packet to Include Subcases in Transient Heat Analysis (Rigid Format 9)..	97
7.1	BAY H* Results for the Three Analysis Methods at the Lower Surface..	122
7.2	BAY H* Results for the Three Analysis Methods at the Right Rib Surface..	124
7.3	BAY H* Results for the Three Analysis Methods at the Left Rib Surface.	126
7.4	BAY H* Results for the Three Analysis Methods at the Front Spar Surface.	128
7.5	BAY H* Results for the Three Analysis Methods at the Cross Section along W.S. 1.926.	130

CHAPTER 1

INTRODUCTION

The utility of a hypersonic cruise vehicle depends on a low structural mass fraction in a high temperature environment. Various structural concepts have been investigated for application to hypersonic wings (References 1-5). They can be classified, in general, as heat sink, hot radiating, insulated, or actively cooled. In cold structures the primary load-carrying structural members are functioning at relatively low temperatures because of active cooling or an ablative or insulated covering. On the other hand, in hot structures the primary load-carrying members are required to function at an elevated temperature that approaches the practical limits of the materials used.

In the study of Reference 1, various combinations of promising hot structural concepts were evaluated with respect to weight, cost, performance, and reliability for the wing structure of a hypersonic vehicle. It was specified that this vehicle was to cruise at Mach 8 at a maximum dynamic pressure of 105.3 kN/m^2 for a 10,000 hour lifespan. The most ideal configuration appeared to be a semimonocoque wing structure with single sheet, chordwise-stiffened, beaded panels made of René 41; heat shields on the external surfaces made of corrugated René 41; and segmented leading edges of TDNiCr.

Using the structural concept of the previous investigation, a 7.9 square meter planform of a wing was designed and fabricated by a contractor (Reference 4). Figure 1 shows an artistic impression of the proposed form of the hypersonic research airplane (HRA) and the location of the Hypersonic Wing Test Structure (HWTS).

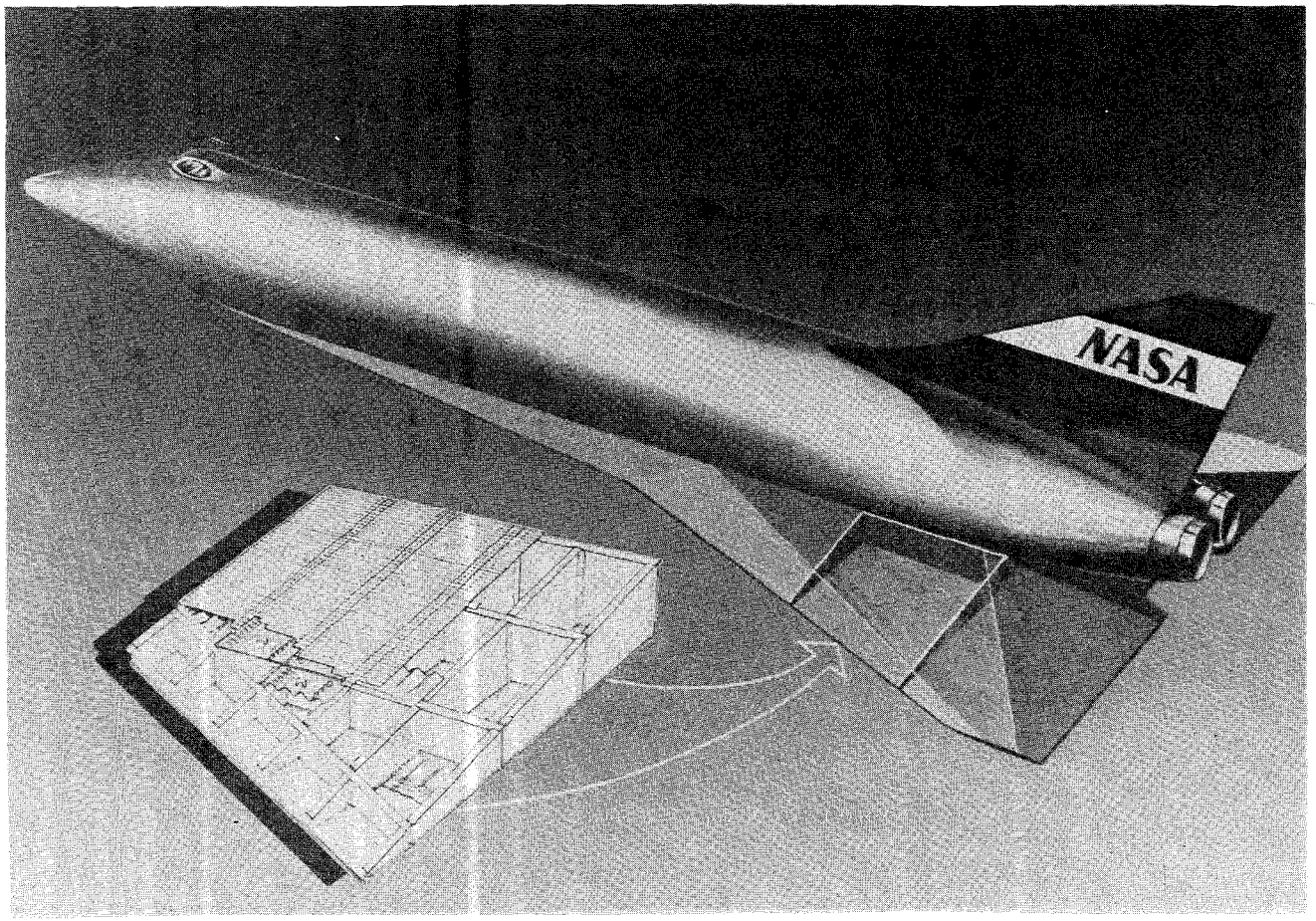

Figure 1: The Hypersonic Research Airplane and the HWTS.

At the Flight Loads Research Facility of Dryden FRF, the HWTS was subjected to a series of loading tests under different thermal environments, which were designed to establish the ability of the wing structure to withstand the design loads and to evaluate the flight loads instrumentation, high temperature calibration methods, and temperature simulation techniques (Reference 5). A separate investigation was done to determine the buckling behavior of a beaded panel with a finite-element method as well as with experimental tests (Reference 6).

The successful design of new structural concepts and efficient space transportation systems will require accurate prediction of thermal deflections and strains. Although predictions of thermal deflection and strains for simple structures have been found to be satisfactory (where the detailed temperature distribution is well defined), attempts to correlate test and analysis strain results on realistic structures have not produced useful results. The weak link in the analysis process is the determination of the temperature distribution throughout the structure with sufficient precision to produce accurate thermal stress predictions. The goal of the HWTS project is to perform a coordinated analysis and test of a medium sized, existing specimen to obtain a detailed evaluation of state-of-the-art predictive techniques for thermal structures.

During the processing of the test data and the comparison with the analytical data, derived from a simple finite-element model, the need for a better and more detailed predicting technique for the distribution of temperature and strains was presented. This came at the same time that new heat-transfer capabilities for existing finite-element programs,

such as NASTRAN and SPAR (References 7 and 8), were developed. However, there is not much experience in predicting temperature and thermal stress distributions in large, complex structures with these programs. This report covers the development of a thermal model as well as of a structural model of the HWTS for the prediction of the distribution of temperature and displacements/strains, using NASTRAN, a finite-element method developed by NASA. This study investigated the feasibility of such analysis for a large structure as an entire model as opposed to a piece-wise approach. This last approach was used in the analysis of the wing structure of the space shuttle, where a large number of isolated locations were modeled and an interpolation technique was used for obtaining the remaining temperature distribution. The inaccuracies involved in this approach and the complexity of the transfer of the data to the structural model can be avoided when the whole structure is modeled as one model. A second related objective is to get experience in conducting a thermal/structural analysis on such large scale and explore the capacities of NASTRAN and other supporting programs.

In Chapter 2, a description of the HWTS is presented. Chapter 3 presents a general treatment of the detailed modeling of the thermal and structural models compared to the earlier, simpler models, while Chapter 4 deals with the detailed development of the new thermal model. Chapter 5 describes the structural modeling in more detail. Chapter 6 describes in detail the experiences and particulars of NASTRAN and its support programs used in the analysis. In Chapter 7 the results of the thermal analysis are discussed. A summary of conclusions and recommendations concerning the modeling of the structure in particular is presented in Chapter 8.

Appendix A presents the drawings of the models, while in Appendices B and C the test procedure of the combined thermal and structural analysis and the corresponding support programs are described in more detailed form. Appendix D describes the management side of the project. Physical quantities in this report are given in SI units. The measurements were taken and the calculations were made in the US customary units.

CHAPTER 2

THE HYPERSONIC WING TEST STRUCTURE PROGRAM

2.1 THE HYPERSONIC RESEARCH AIRPLANE CONCEPT

The HWTS was designed as a part of the wing structure for a hypersonic research airplane concept as shown by the shaded area in Figure 2.1. The proposed hypersonic research airplane configuration is a single-place design with conventional takeoff and landing capability and an estimated gross weight of 322.8 kN. The plane has a length of 30.75 meters, has a wing span of 11.58 meters, and consists of a discrete wing-body with a single vertical tail. The fuselage cross section is circular, with two lower corner areas added to permit wing attachment and to provide a flat lower surface; additional fuselage volume; and a longitudinal carry-through area. The fuselage primary structure is of insulated, semimonocoque design. The main landing gear is attached and stowed below the wing plane and outboard of the inlet/ramjet components.

The wing and vertical tail are hot radiating structures. The wing is a low mounted, clipped double-delta design with leading-edge sweep angles of 85° and 70°. No twist, angle of incidence, or dihedral is included in the wing design. The basic delta wing has a symmetrical 30/70 Hex (modified) airfoil section which is 4% thick and has a leading-edge radius of 1.91 centimeters. The total wing planform area is 145.6 square meters. Wing loading at takeoff is estimated to be 2217 N/m^2.

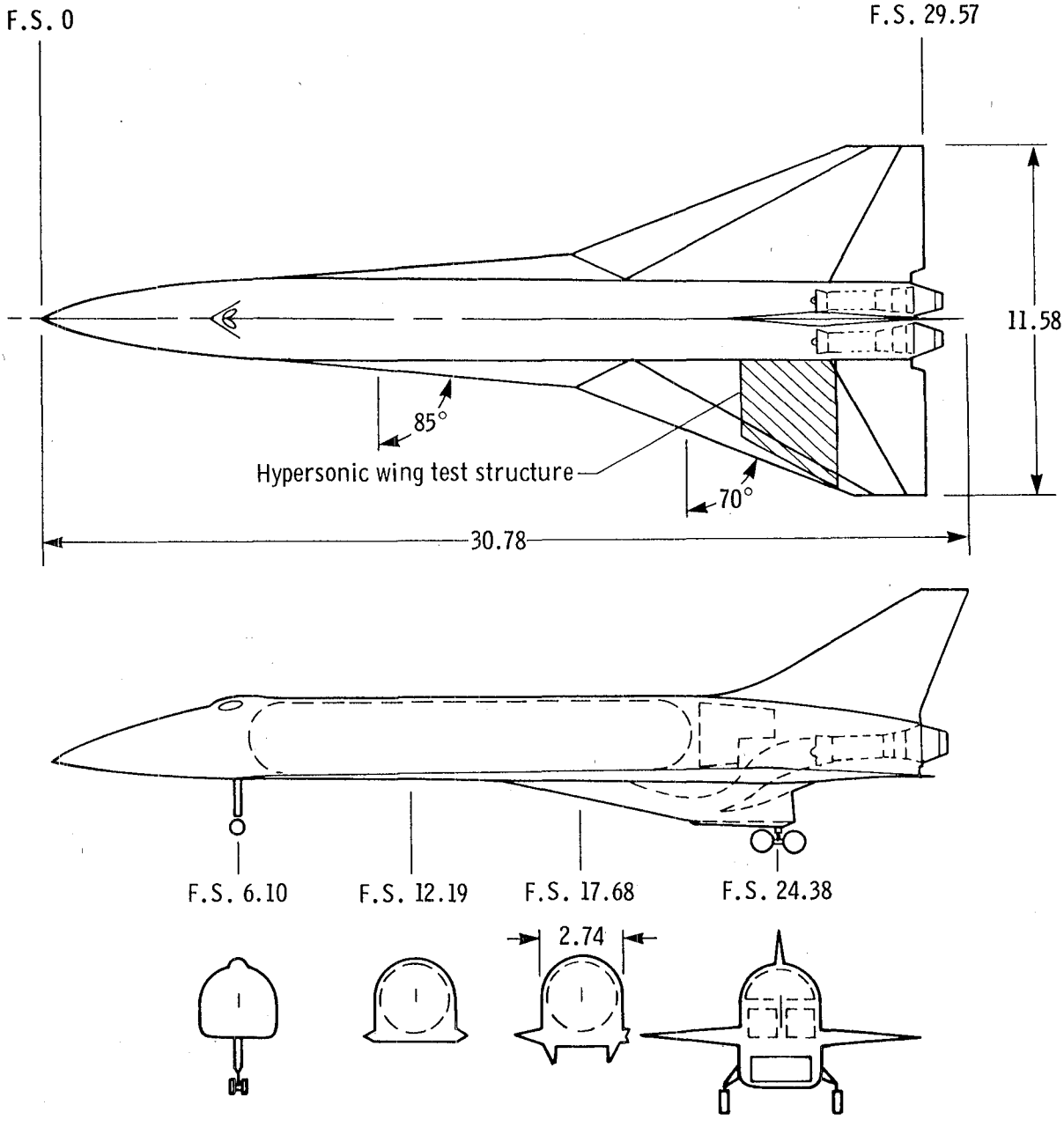

Figure 2.1: Hypersonic Research Airplane Configuration.
(Fuselage stations [F.S.] and dimensions in meters.)

The propulsion system consists of separate turbofan jets and ramjets with a common two-dimensional inlet design. The two turbofan jets, located in the aft fuselage bay, operate on hydrocarbon fuel at Mach numbers up to 2.8. The two hydrogen-burning ramjets, located beneath the aft fuselage, operate at Mach numbers from 0.8 to 8.0. The inlet is a mixed-compression, fixed-capture-area design with variable ramp geometry.

Figure 3.3 shows a nominal research mission profile for the HRA, consisting of a horizontal takeoff at 103 m/s, subsonic climb to a 7.32 km altitude, and acceleration at a dynamic pressure of 47.88 kN/m^2 to Mach 8 at an altitude of 30.8 km. A 5-minute cruise flight is performed at Mach 8 at altitudes between 30.8 and 35.8 km. Descent follows a constant 23.94 kN/m^2 dynamic pressure profile. Figure 2.3 presents a more specific time history for the loads maneuver indicated in Figure 2.2 by the dashed line profile. This maneuver is to be initiated at Mach 8 at an altitude of 27.4 km and consists of a -0.5 g push-over, a 2.5 g pull-up, and a return to the nominal research mission descent profile. The entire loads maneuver encompasses 42 seconds, and the maximum dynamic pressure obtained during the maneuver is 83.78 kN/m^2.

2.2 THE HYPERSONIC WING TEST STRUCTURE

Figure 2.4 shows the general dimensions and shape of the HWTS and of the transition section. The wing is cantilevered from wing station (W.S.) 1.067. The transition section is not part of the wing design

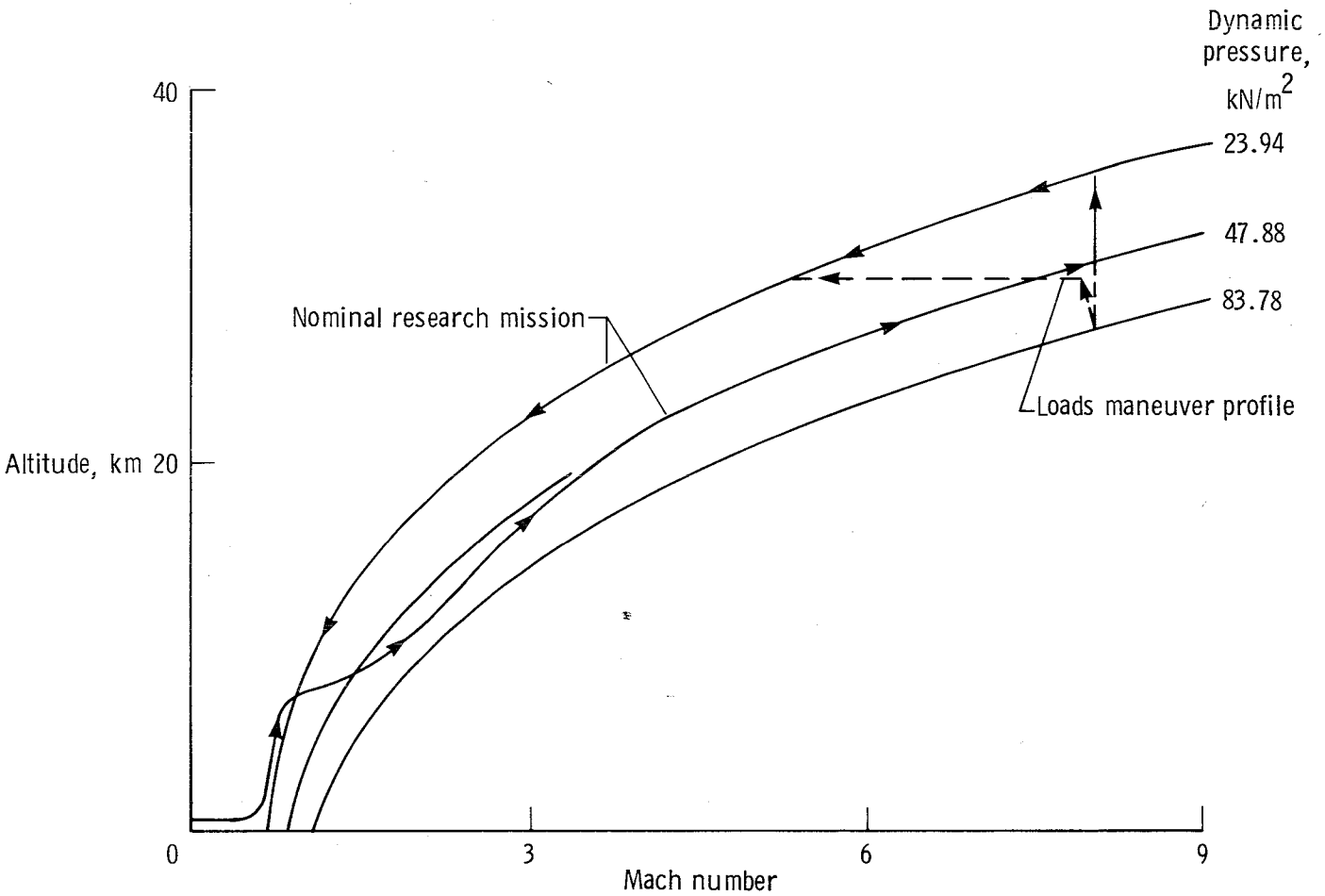

Figure 2.2: Hypersonic Research Airplane Research-Mission Profile.

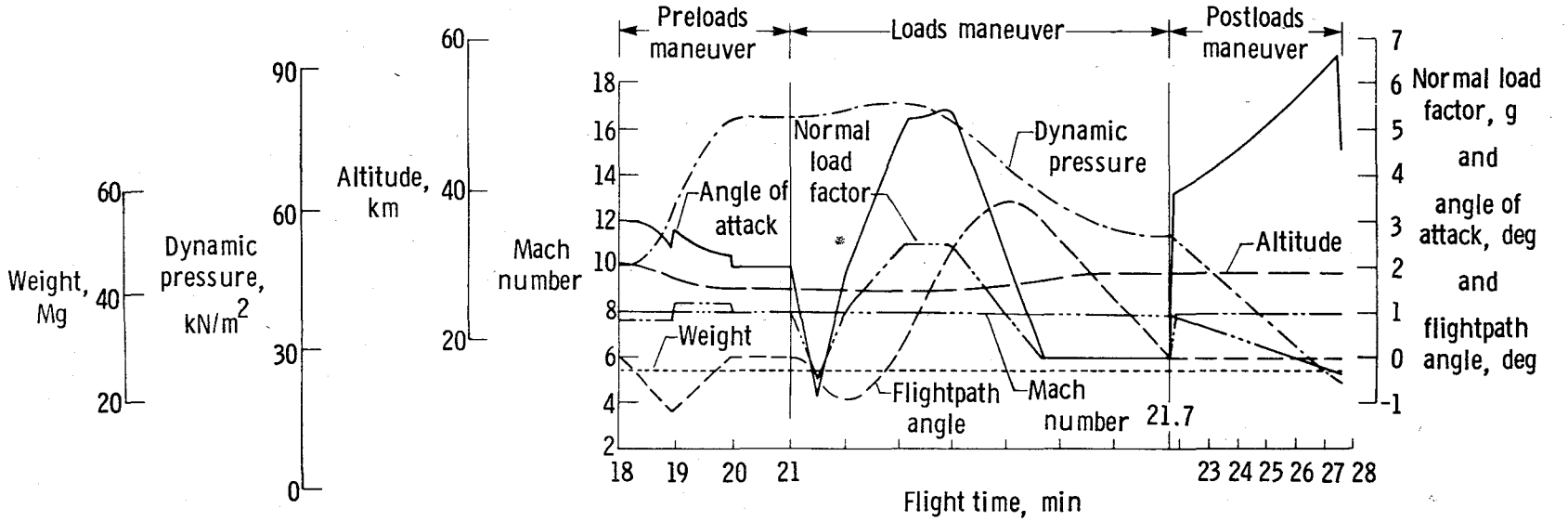

Figure 2.3: Type History for a Loads Maneuver of the Hypersonic Research Airplane.

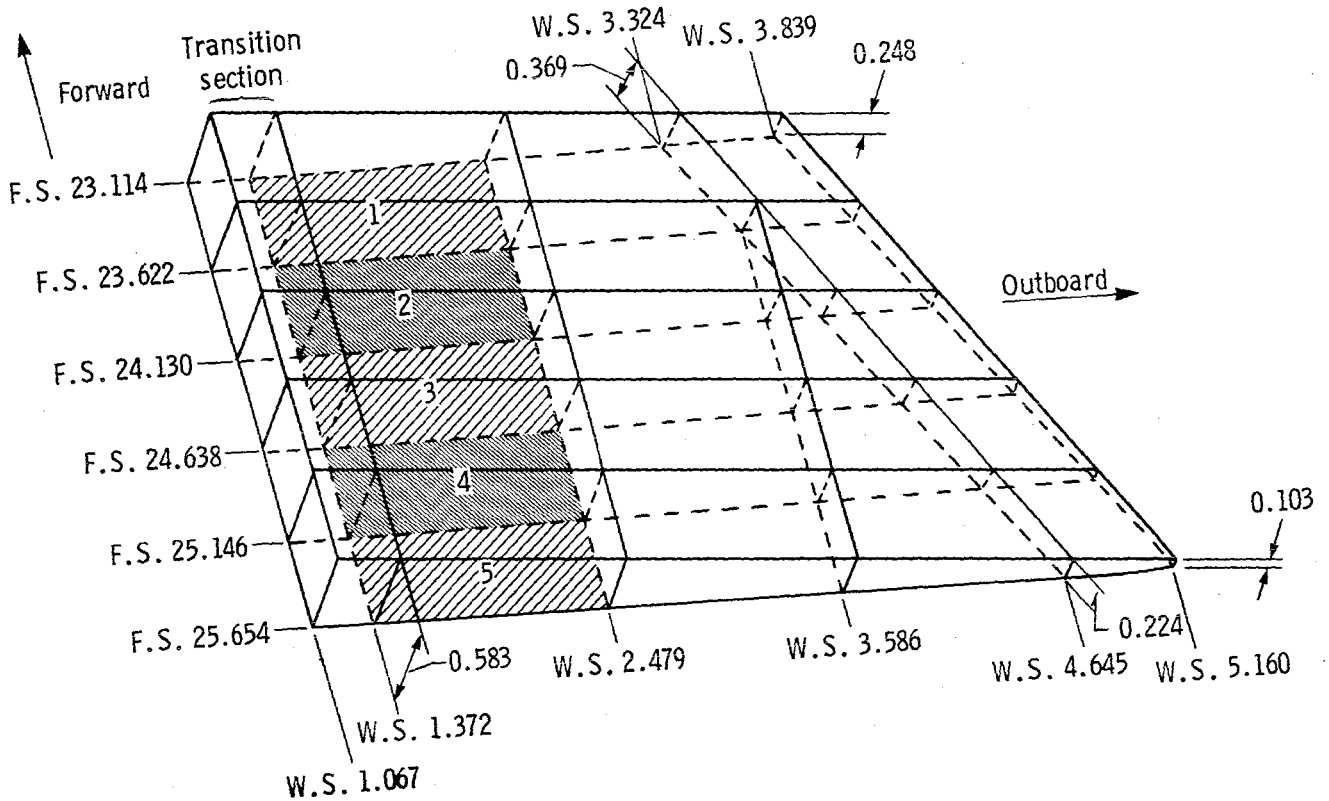

Figure 2.4: Hypersonic Wing Test Structure Dimensions.
(The most critically loaded panels are shaded and numbered 1 to 5, going aft.
Fuselage stations, wing stations, and dimensions in meters.)

but was included in the test specimen to provide a buffer between the support structure and the test portion of the wing. For economic reasons, the wing test structure geometry was modified between the leading edge and the 30% chord line by setting the leading edge parallel to the 30% chord. The wing was tested inverted for reasons of convenience of testing the compressively loaded upper surface of the actual vehicle. (In the remainder of this report, "upper surface" refers to the actual upper side in flight, and "lower surface" to the side nearest to the earth--not to the position in the laboratory). The five most critically compression-loaded panels are the upper root panels, which are shaded in Figure 2.4 and numbered 1 to 5 from fore to aft.

The primary load-carrying members of the HWTS are the René 41 beaded panels. In contrast to more conventional aircraft wing structures, the bending loads are carried in the HWTS mainly by the beaded panels instead of the spars. The panels are also subjected to shear loads resulting from wing torsion and to pressure loads normal to the surface resulting from internal pressure lag. A typical panel is shown in Figure 2.5. The panel was formed from a single sheet of René 41 with seven alternating up-and-down circular arc beads parallel to the span of the wing. Doublers are spot-welded to reduce excessive deformation by shear and to prevent local end failure. Z-shaped clips connect the beaded panels with the slightly-streamwise-corrugated heat shield.

The main purpose of these heat shields is to provide a thermal buffer between the hot boundary layer and the load-carrying structure

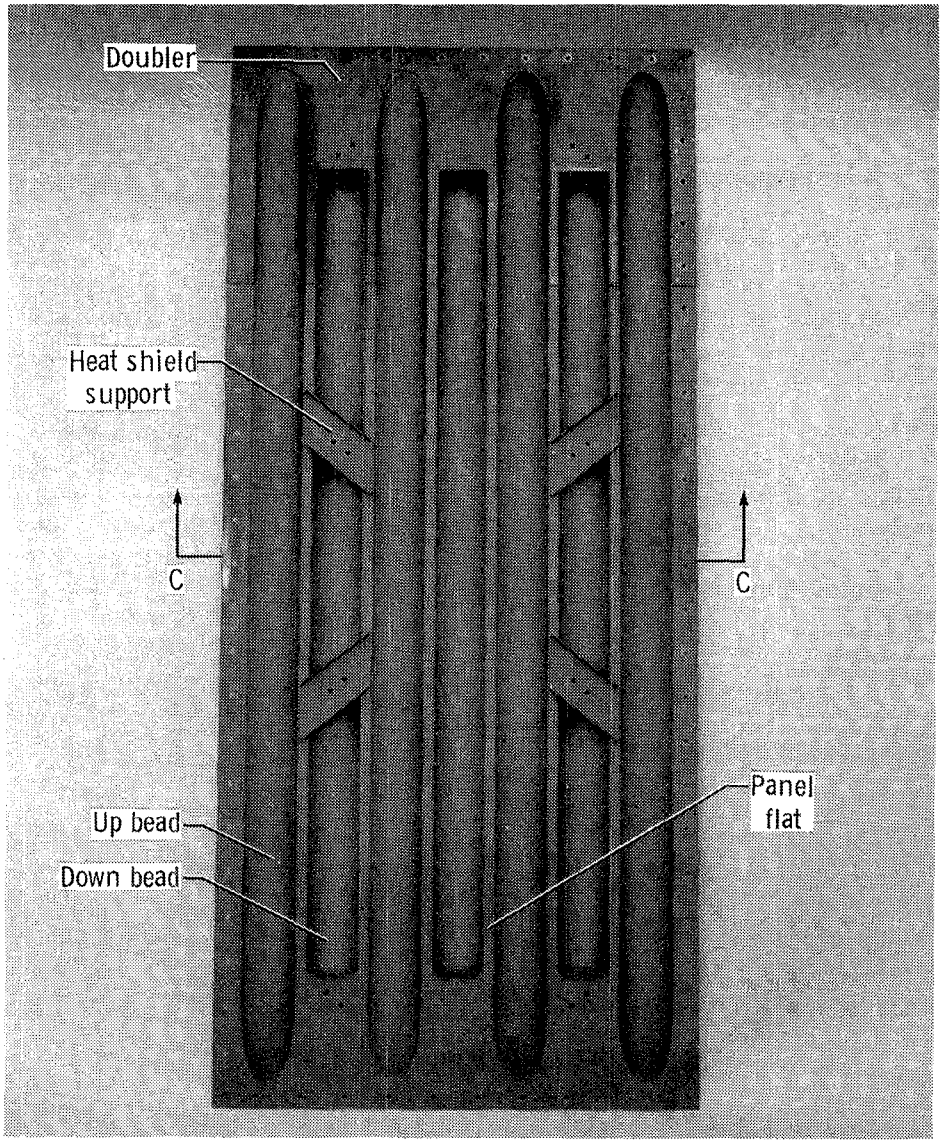

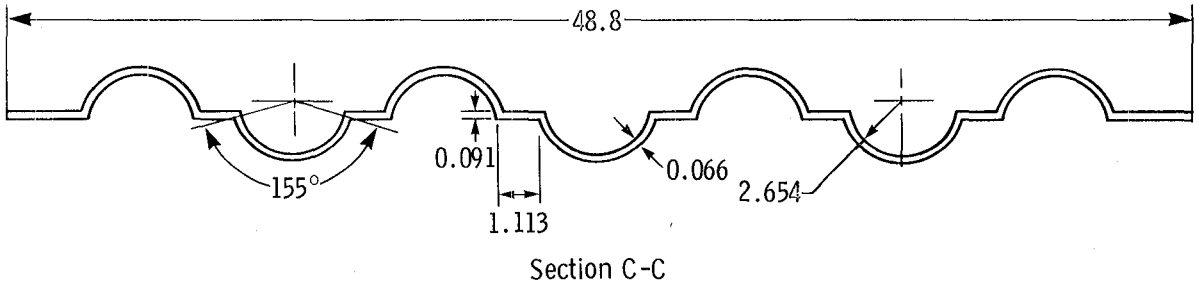

Figure 2.5: Beaded Panel for HWTS. (Dimensions in centimeters.)

as well as for aerodynamic smoothness. The panels of the lower heat shield between the 30% chord line and the leading edge are made from a more temperature-resistant, thorium-nickel-chromium alloy, TDNiCr, capable of operating under a maximum temperature of 1500 K. The outboard sections of the beaded panels are covered with an insulation blanket to keep the structural temperature below the operational limit. In general, two heat shields cover each full-size beaded panel. Heat shield extensions were also provided around the boundaries of the test structure to improve the simulation of the heating of the HWTS. The beaded panels are attached to the caps of orthogonal spars and ribs by screws.

The wing structure has six spars perpendicular to the fuselage centerline with adjacent ribs which produce 19 internal bays (and 5 in the transition section; see Figure 2.4). Both the spar and rib webs have sine wave corrugations to allow thermal expansion.

Figure 2.6(a) shows the HWTS mounted in a support fixture with the heat shields removed, while Figure 2.6(b) shows the HWTS with the heat shields installed. Figure 2.7 shows the interior of a HWTS bay showing the corrugated webs of spars and ribs. For this picture one of the upper beaded panels was removed.

2.3 LOADING TESTS DONE AT DFRF

A series of loading tests under three different heating conditions was conducted by the Flight Loads Laboratory of DFRF on the HWTS (Reference 5). These conditions can be classified as (1) room temperature;

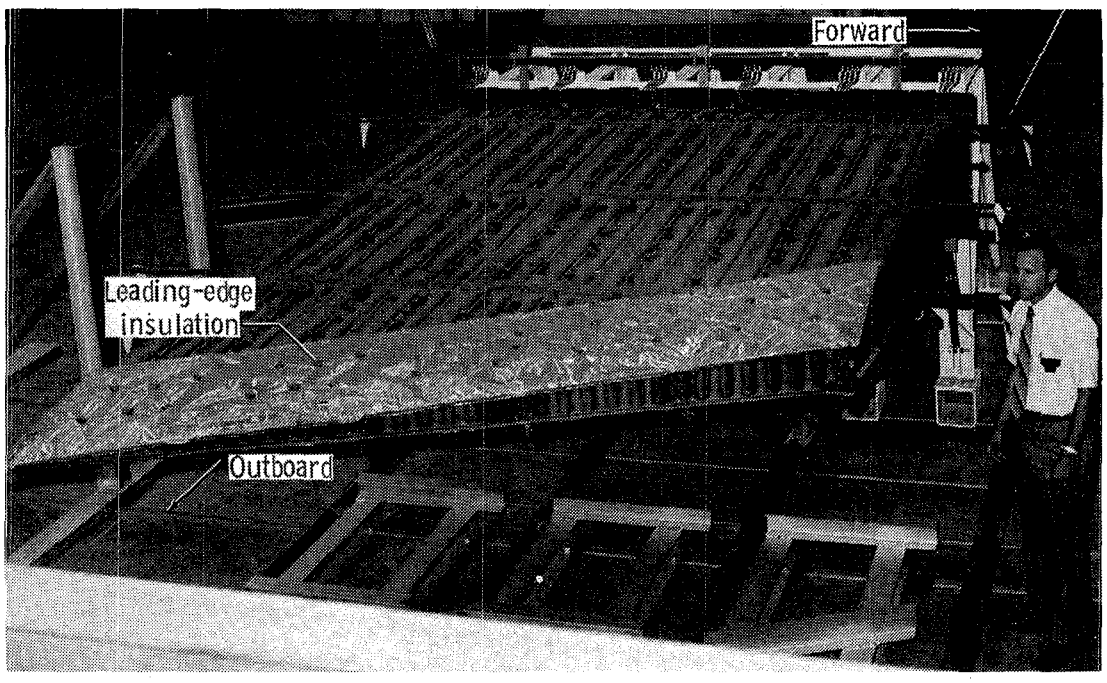

E 27650

(a) Heat shields removed.

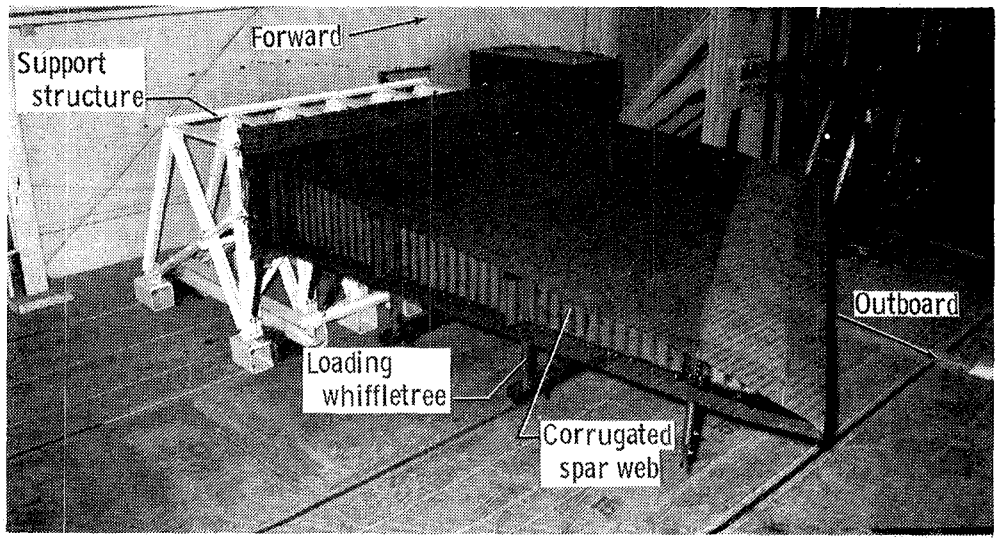

E 26145

(b) Heat shields installed.

Figure 2.6: Hypersonic Wing Test Structure.

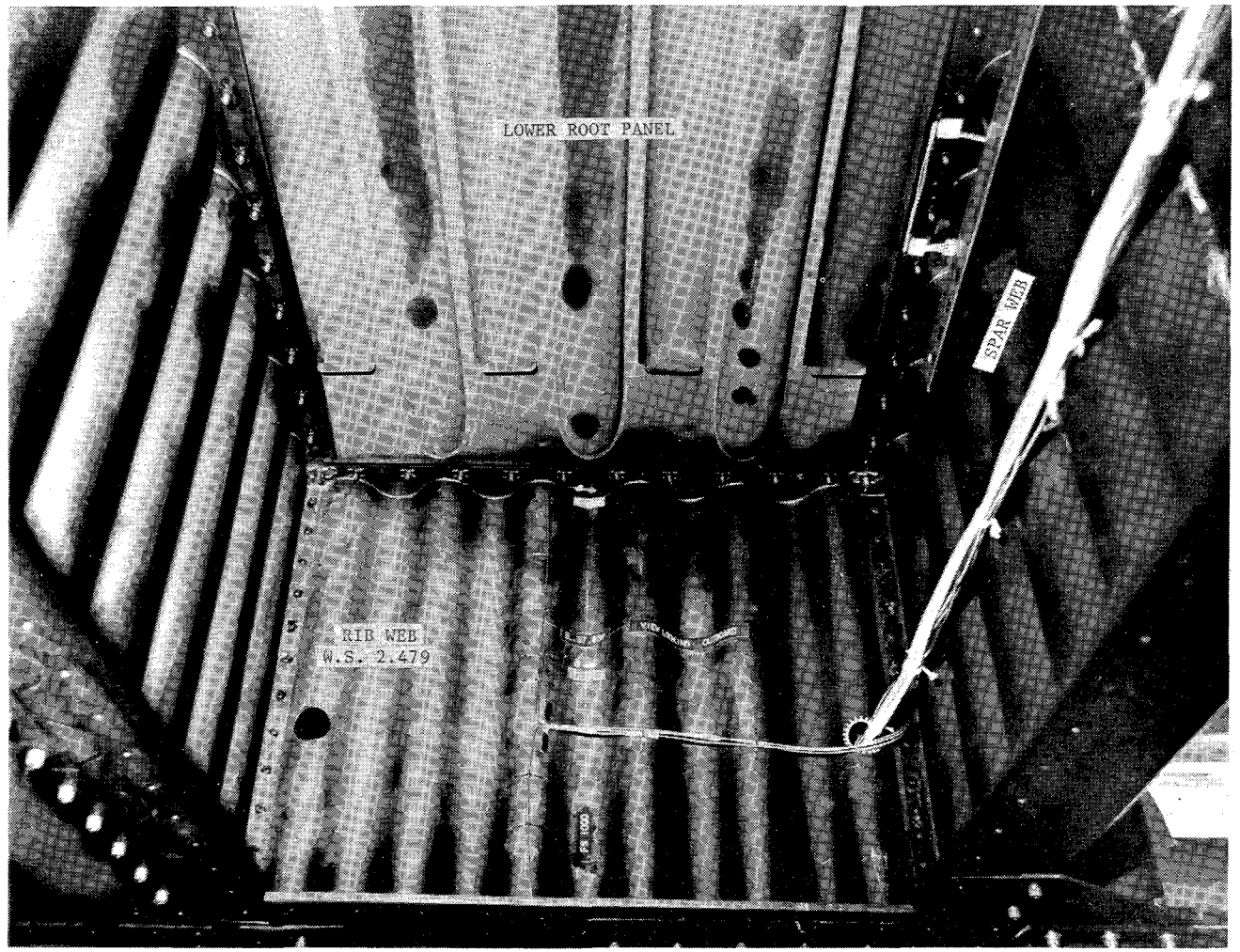

Figure 2.7: Interior of HWTS Bay Showing Corrugated Webs of Spars and Ribs.

(2) all heat shields heated uniformly to 561 K (550°F), not varying with time; and (3) all heat shield heated according to a predefined temperature-time history, simulating the 2.5 g load maneuver at Mach 8 shown in Figure 2.3. Each series of loading tests consisted of six or less cases with a different loading configuration. Figure 2.8 illustrates the applied load distribution during the six tests. The vectors in the figure indicate the direction and magnitude of the applied loads. The loads applied during tests 1 to 3 are the structural loads that would be experienced by this wing section during a 2.5 g load maneuver at Mach 8. In test 1, only vertical loads were applied to the structure. In test 2, the structure was loaded vertically and horizontally. The horizontal loads simulated loads predicted to be introduced into the HWTS area by the wing portions forward and aft of the HWTS area. In test 3, three types of loads were applied to the structure: horizontal loads, vertical loads, and internal pressure loads on the upper five inboard panels (Figure 2.4). The loads applied in this test are the predicted design ultimate loads for the wing portion represented by the HWTS. Tests 4 to 6 were designed to establish the failure envelope of the panels. This envelope defines the combinations of the in-plane shear and compression which produce panel failure.

Figure 2.9 shows a close-up of the room temperature loading set-up of the HWTS. Two-point whiffle trees can be seen in the lower portion of the picture with load cells and actuators attached to them. Horizontal loading jacks are visible on the right. Independent structures are used to support these horizontal jacks and the position

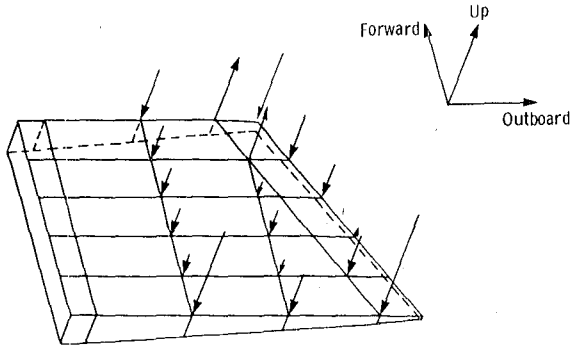

(a) Test 1.

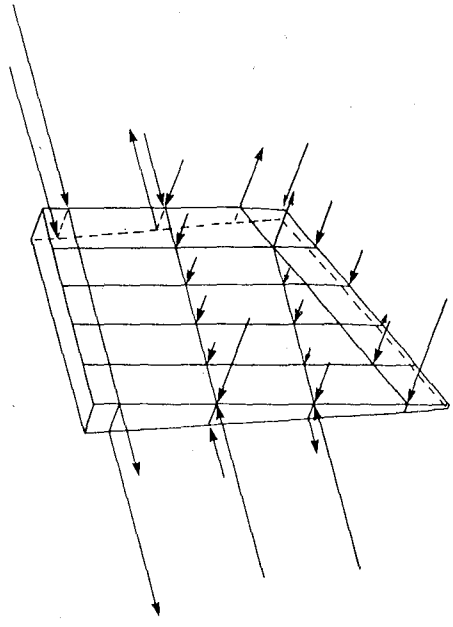

(b) Tests 2 and 3.

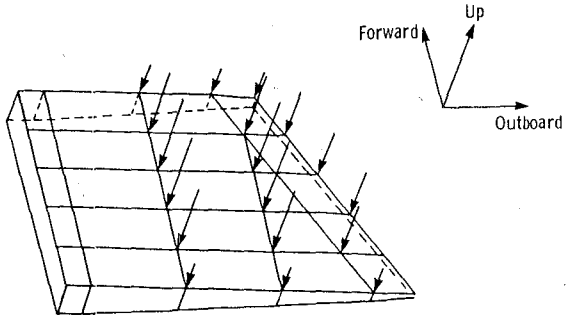

(c) Test 4.

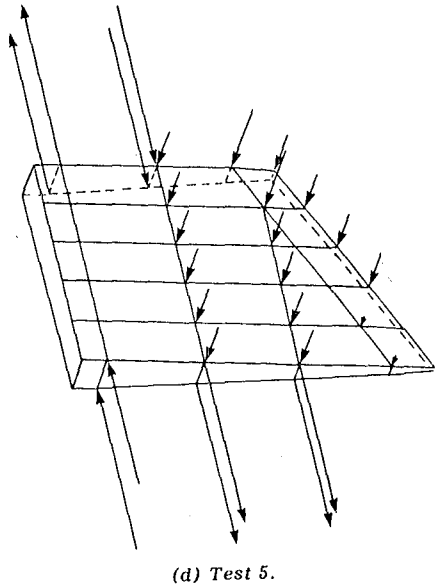

(d) Test 5.

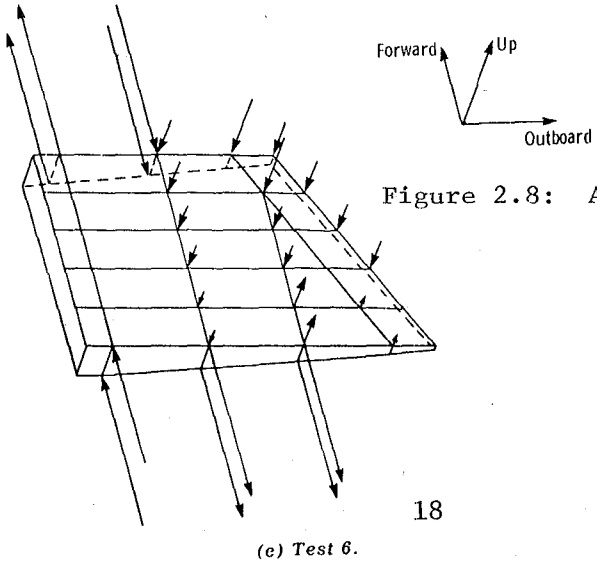

(e) Test 6.

Figure 2.8: Applied Load Distributions on HWTS.

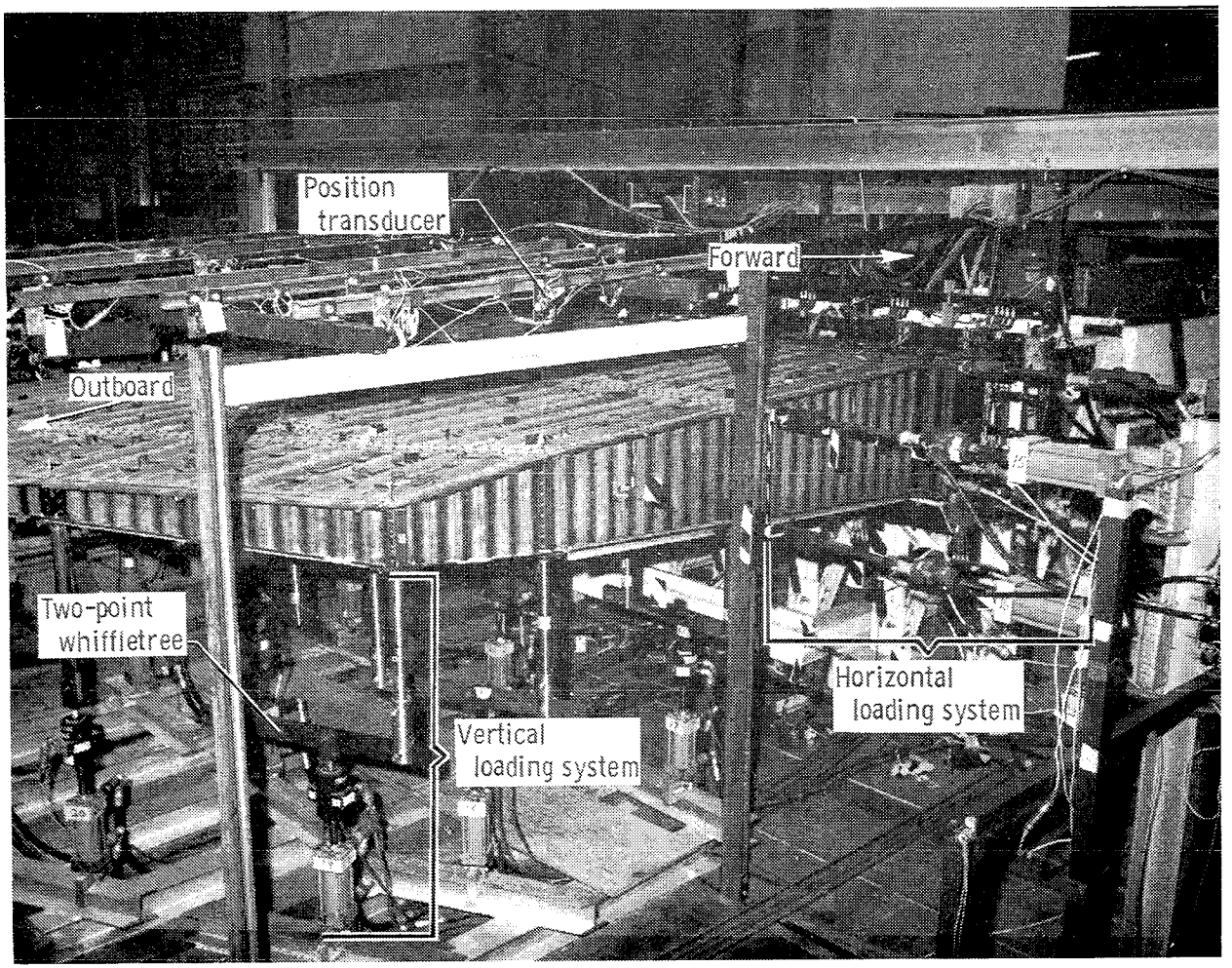

E 30865

Figure 2.9: HWTS Loading Test Set-Up for the Room Temperature Tests.

transducers. In order to apply pressure loads normal to the beaded panel surface, pressure pans were manufactured and connected to each of the five upper root panels at the inside. Figure 2.10 shows the top view of a pressure pan that was exposed by removing one of the lower beaded panels. Two lines are connected to the pan. The larger one is a pressure feed line, and the other is a pressure monitor line. An internal pressure of 5.2 kN/m^2 was applied to the panels during testing. For the test at elevated temperatures, the head shields were attached to the main wingbox; and two independent structures for the thermal loading were placed below and over the upper and lower heat shield, respectively. The thermal loading was accomplished by heating the heat shields with quartz lamps attached to the independent structure. Eighty-nine separate heating zones were independently controlled according to 41 different time-dependent temperature profiles, which simulate the thermal load during a typical load maneuver at Mach 8. Figure 2.11 shows a typical temperature-time history for such heating zone. The peak of the thermal loading takes place between 1200 and 1400 seconds and decreases till 2100 seconds. Thermocouples attached on each heating zone controlled the output of each set of quartz lamps according to precalculated temperature-time profiles. This means that the thermal loading is defined in these tests as enforced temperatures on different locations of the heat shields. Those temperatures have been calculated in a separate heat transfer program from thermal heat fluxes derived from the master program in Reference 9.

Figure 2.12 shows the HWTS loading set-up for testing at elevated temperatures. Rows of quartz lamps are attached to independent structures. Thermal blankets at the boundaries are used to prevent radiation

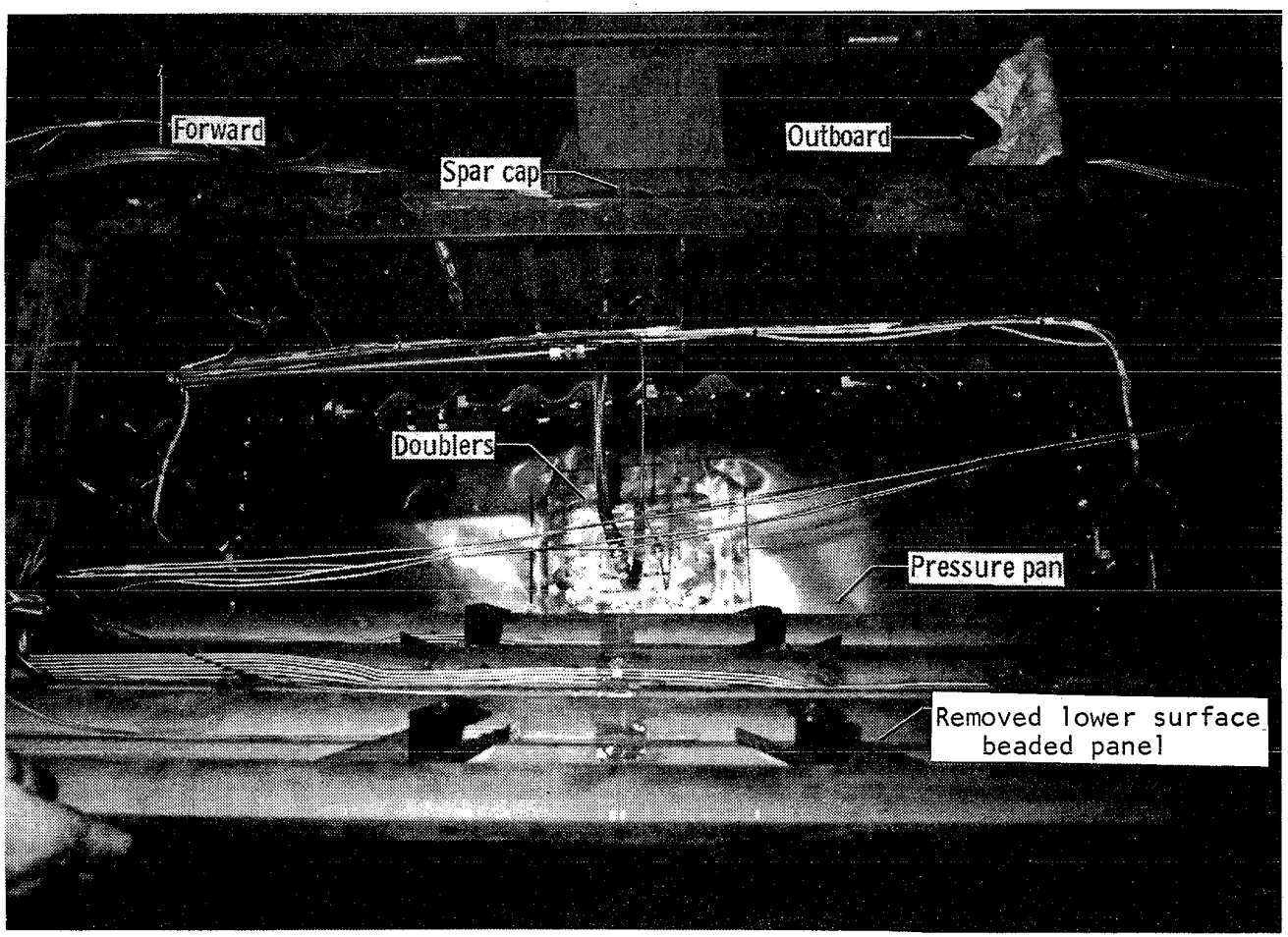

E 28432

Figure 2.10: Pressure Pan of the HWTS.

HWTS Mach 8 Temperature Profile of Heating Zone 1, Upper Heat Shield

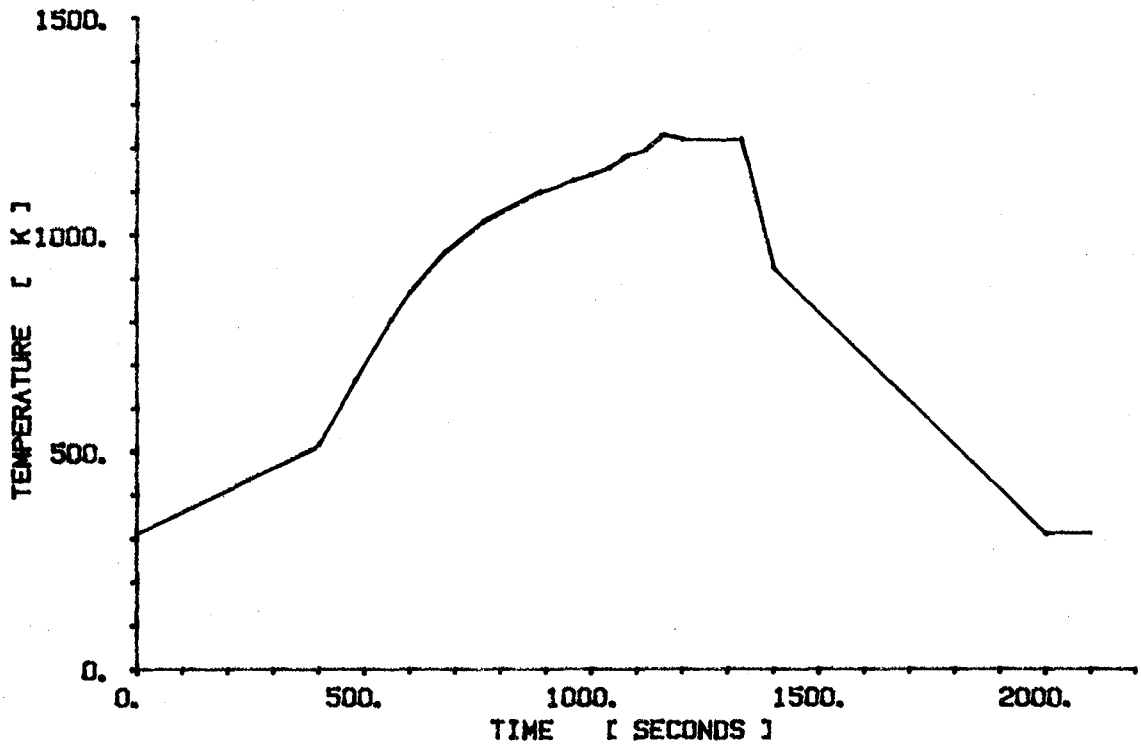

Figure 2.11: Temperature-Time for a Heating Zone, Simulating the Thermal Load during a Mach 8 Loads Maneuver.

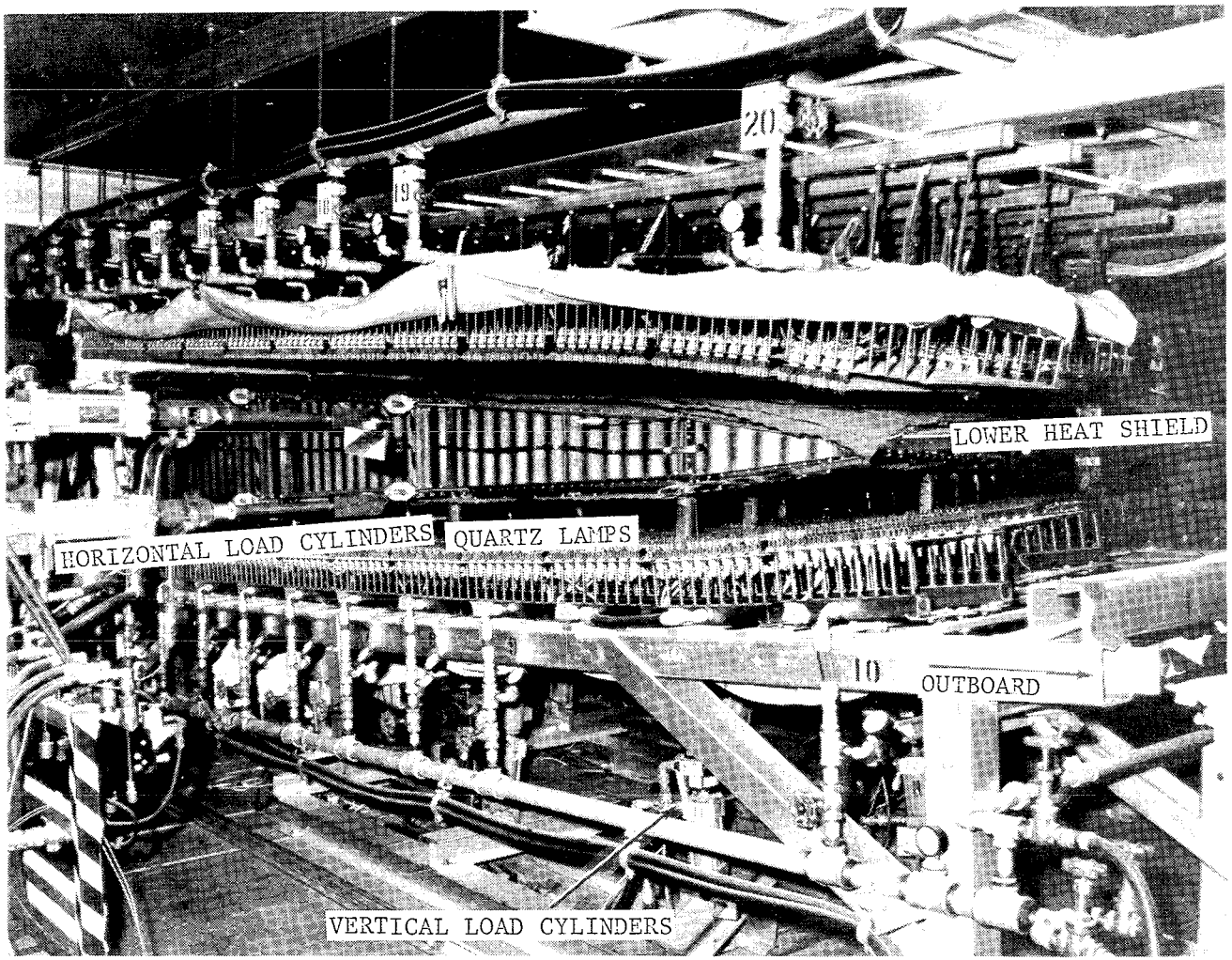

Figure 2.12: HWTS Loading Set-Up for Elevated Temperature Tests.

of heat outside the structure. Heat shield extensions were also provided around the boundaries of the test structure to improve the simulation of the heating of the HWTS outer spar and rib webs.

2.4 INSTRUMENTATION

Strain gages were located as shown in Figures 2.13(a) and 2.13(b). The two strain gages on the spar caps are single-gage axial gages in a T-configuration and are of a foil type. The strain gages on the spar web centerlines and on the panel flats are of the delta-rosette foil type. The strain gages on the panel up and down beads are single-gage axial strain gages of two types: foil and capacitance. Only the capacitance gages are capable of operating at temperatures above 600 K (Reference 5). Two of these strain gages, one of each type, were mounted end to end at each location shown by the circular symbols in Figure 2.13(b).

Figure 2.14 shows the locations of the thermocouples on the HWTS, while Figure 2.15 illustrates the deflection measurement locations. The accuracy of the data acquisition system for strain gage measurements at room temperature was +4.88 microstrain, which represents 0.3% of the strain gage calibration output.

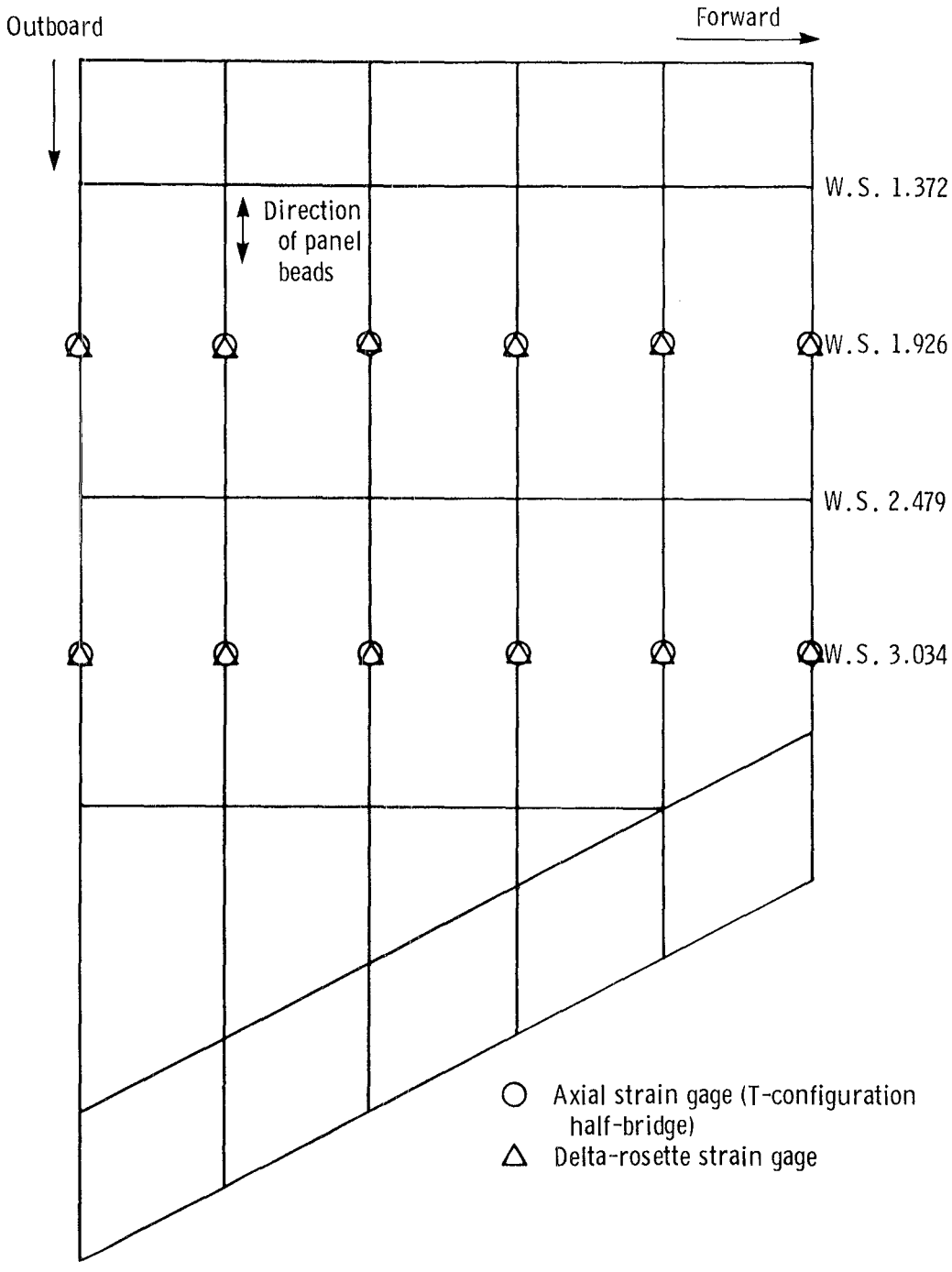

(a) Strain gage locations on spar caps and web (view looking down). Axial strain gages were installed on upper and lower spar caps, and delta-rosette strain gages were used on spar web centerlines.

Figure 2.13: Strain Gage Locations. (Wing stations are in meters.)

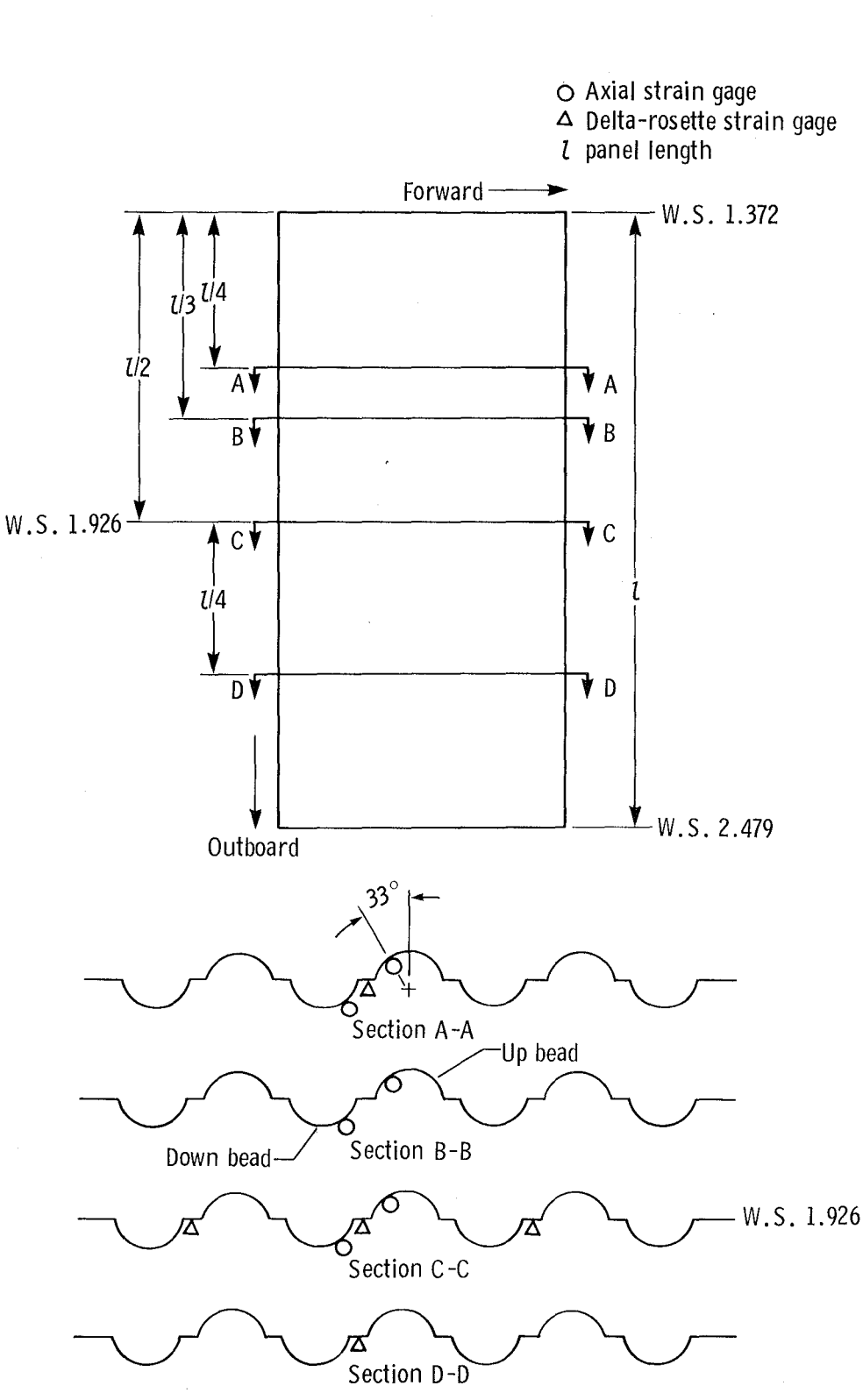

(b) Strain gage locations on upper root panels between W.S. 1.372 and 2.479. Instrumentation was identical for each root panel.

Figure 2.13: Concluded.

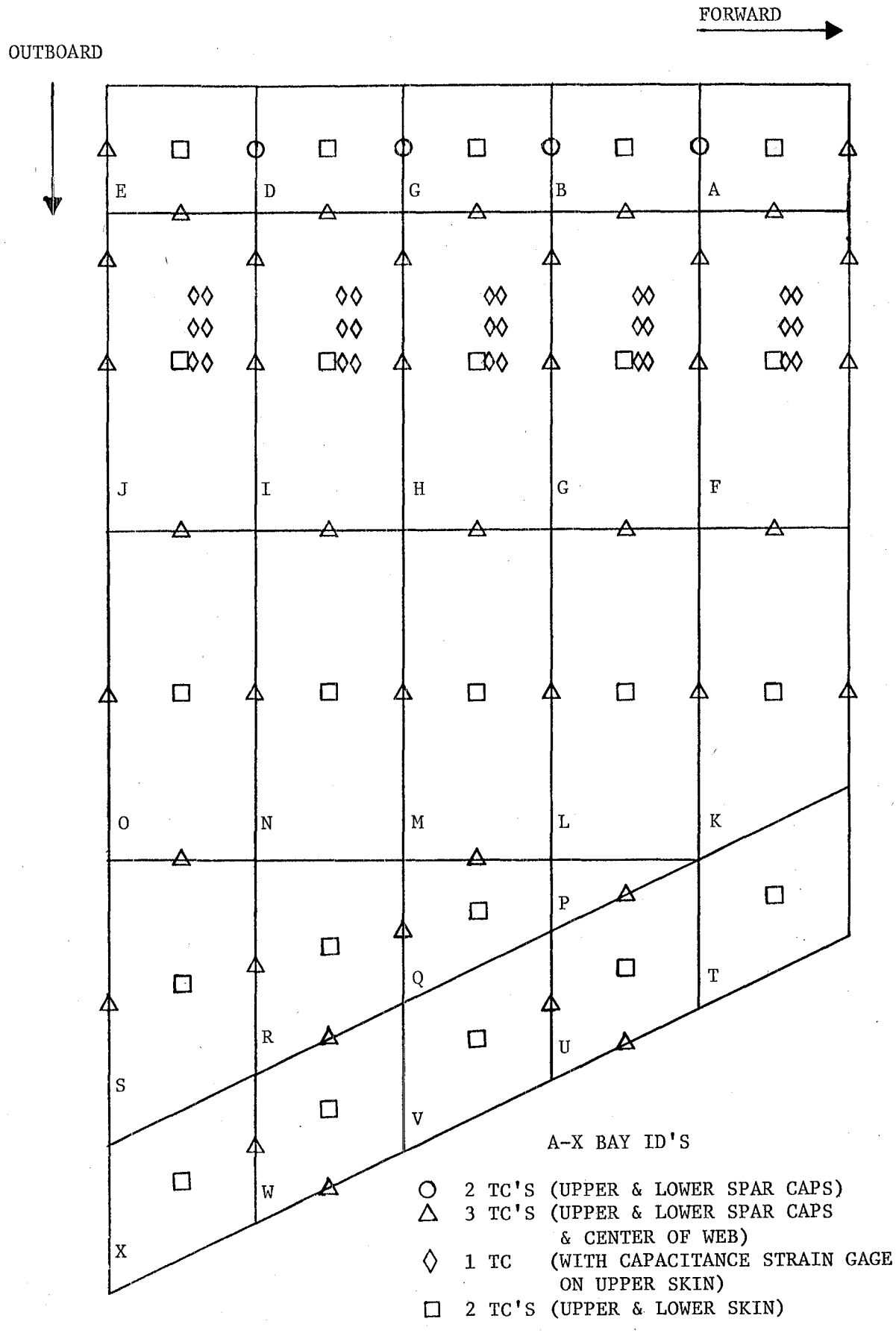

Figure 2.14: Temperature Measurement Locations.

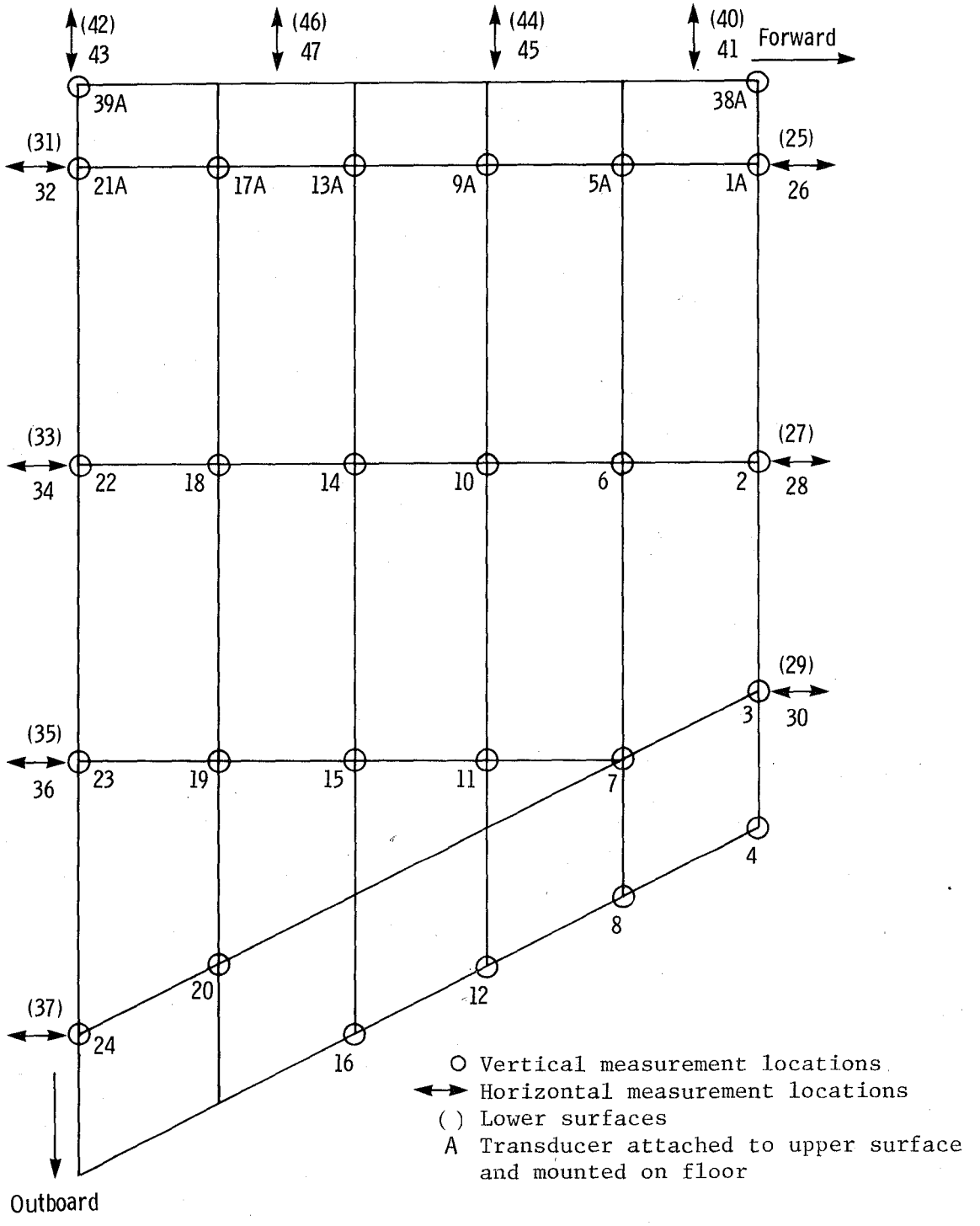

Figure 2.15: HWTS Deflection Measurement Locations.

CHAPTER 3

GENERAL DESCRIPTION OF THE ANALYSIS

3.1 INTRODUCTION

In the past the use of analytical methods for heat transfer and structural analysis of the HWTS for comparison with the test data was limited. For the room temperature tests a relatively simple NASTRAN model was used to calculate the stress distribution. NASTRAN is a general-purpose structural analysis computer program. Based on the finite-element principle, it was developed by NASA. A small number of NASTRAN and Fortran programs were further needed to produce sufficient accurate data for direct comparison with the measured strain distributions. Except for generating the external temperature distribution at the heat shields during the earlier design stages of the HRA program (Reference 7), no heat transfer analysis program was used. Interpolation of measured temperature data would be, therefore, the only tool for implementing the investigation of the influence of thermal stresses.

Comparisons of the measured strain distributions with the calculated distribution using a NASTRAN finite-element program were not completely satisfactory. Discrepancies were assumed to be caused by experimental errors, nonuniform loads introduced by the support structure, and the simplicity of the structural model. Another contribution to the discrepancies would be an insufficient knowledge of the temperature distributions for accurate thermal stress calculations. This lack of known temperature-time histories through the structure, and consequently the assumption of interpolated temperature-time histories,

proved to be a major reason for discrepancies in measured and predicted data in thermal stress calculations for other large, complex structures. Although it would be extremely difficult to determine quantitatively the exact share of each factor, it was felt that improvement of the structural model and a better input of the temperature distribution would result in closer agreement with the test data.

It is obvious that equipping a large and complex structure with high temperature strain gages and thermocouples for testing is expensive, so accurate analytical methods for predicting thermal stress data will be needed. During the last ten years, large general-purpose finite-element programs such as NASTRAN and SPAR have been supplemented with heat-transfer capabilitiies. Finite-difference-based programs such as the Lockheed Thermo-analyzer, SINDA, and MIDAS have more capabilities for heat transfer analysis but cannot be used for structural analysis. However, there is not much experience in predicting temperature and thermal stress distributions in large complex structures. Most of these programs have been used for relatively small and simple structures such as satellites and missiles.

All of these factors--discrepancies between the test data and the previous test model due to the simplicity of the NASTRAN model used, the need for more accurate analytical tools, and the lack of experience with large thermal computer programs--have contributed to the need for developing a better analytical predicting method for the HWTS structure.

As a basic tool, NASTRAN was chosen for both the heat transfer and the structural analysis. The main reasons were the relatively simple user-oriented nature of NASTRAN, the existing experience with

the program, and the supporting assistance obtained from COSMIC* and others. It is planned to model the HWTS later using SPAR for comparison with NASTRAN and to evaluate the use of complex analytical predicting methods.

Section 3.2 describes the analysis of the (room temperature) loading tests conducted by DFRF. Section 3.3 will describe the general consensus of the heat transfer and structural analysis as it is envisioned in the current investigation. Section 3.4 explains the computational resources and the main computer programs used during this investigation.

3.2 DESCRIPTION OF EXISTING ANALYSIS

A number of computer programs were used for generating and processing analytical data for comparison with the results of the tests. The flow chart in Figure 3.1 displays the sequence of the programs required. Depending on the nature of the applied load, as many as six programs were necessary. Briefly they are

1. NWML: a NASTRAN finite-element computer program of the hypersonic wing test structure. This model was used in the design of the wing portion and is shown in Figure 3.2. It is a relatively simple, coarse model consisting of 481 elements and 106 grid points (256 degrees of freedom). The spar and rib caps were modeled as rods, the spar and rib webs as flat shear panels, and the beaded panels as

*COSMIC: Computer Software Management and Information Center maintains and supports the NASTRAN program for NASA.

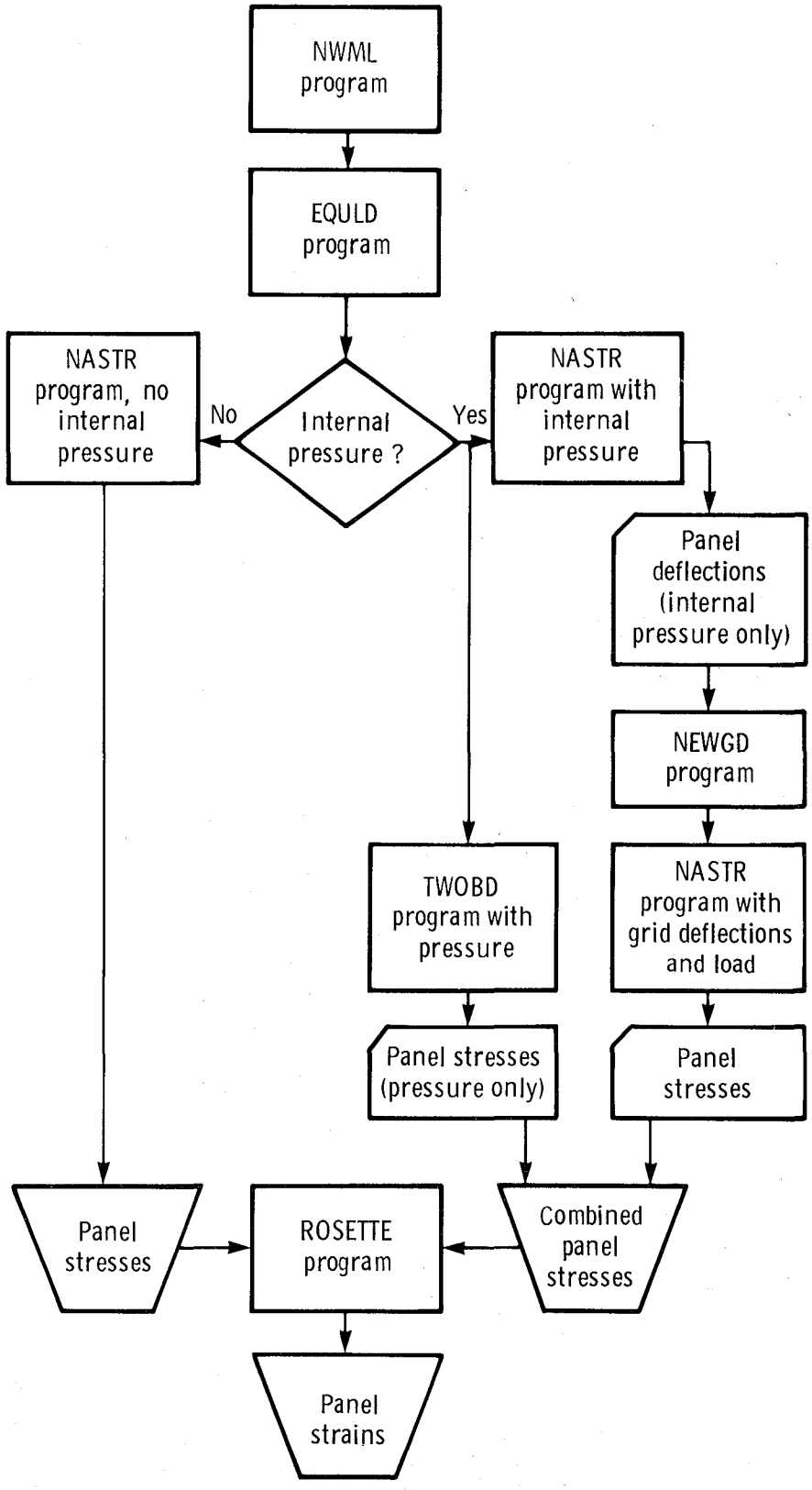

Figure 3.1: Analysis Flow Chart of Original Analysis.

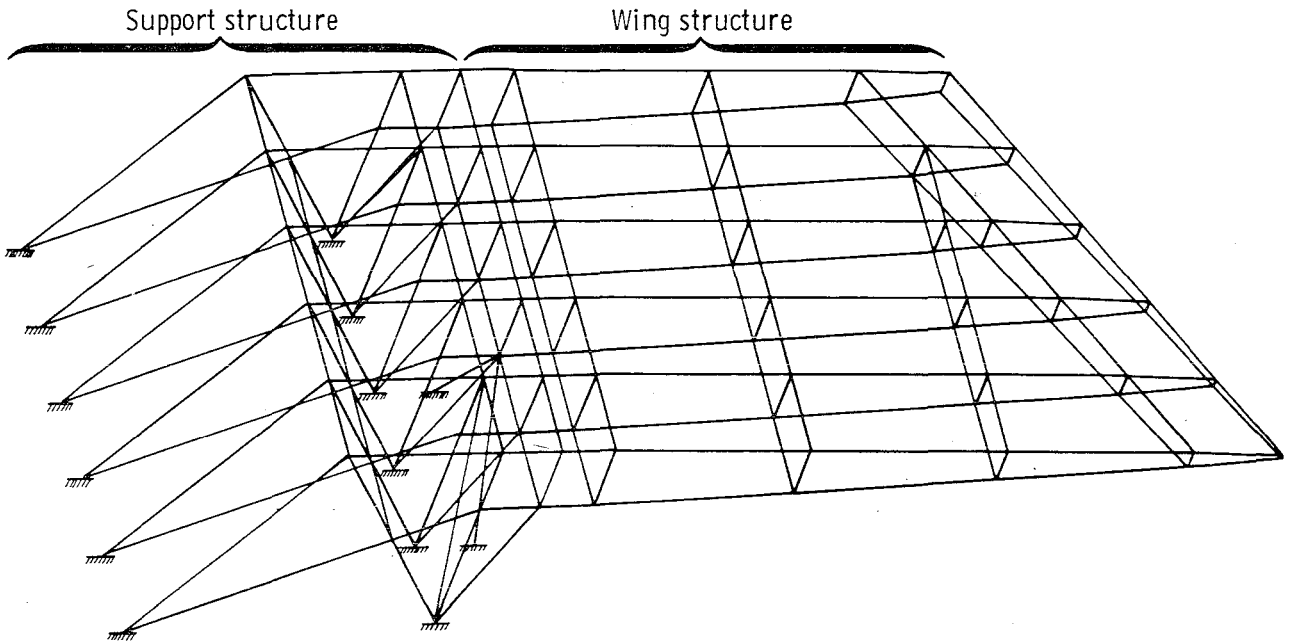

Figure 3.2: NWML NASTRAN Model of the HWTS.

four overlapping triangular membrane elements. No provisions were made to take account of the beaded and corrugated form of the panels and webs and/or of the influence of doublers, fittings, and pressure pans. The support structure was modeled by using bar elements.

Mechanical loads were applied at the grid points in the model that corresponded to the load points on the HWTS. For the elevated temperature tests, manually interpolated temperatures derived from the measured temperatures of a limited number of locations were used as input. Direct comparison between the test data for the beaded panels and the data for the NWML model could not be made because of the large size of the elements representing the beaded panels. Thus, comparisons between the results of a strain gage mounted on a specific location on a beaded panel and the calculated average stresses/strains of the model would not necessarily be accurate. It was necessary to develop the EQULD and NASTR programs. Internal pressure loads applied to some root panels could also not be adequately modeled by this NWML model.

2. EQULD: a Fortran program written to generate load data cards for input to the NASTR beaded panel model. This program divided up the loads per unit length of the panels, derived from the NWML program, and distributed them to the grid points of the NASTR model corresponding to the edges of the beaded panel. The same procedure was used to determine and distribute the shear forces.

3. NASTR: a NASTRAN finite-element computer model of one-fourth of a beaded panel. It consisted of 392 elements and 418 grid points (306 degrees of freedom). The model closely approximated the actual geometry of one-fourth of a beaded panel (see Figure 3.3). The elements were small enough in size that accurate comparisons could be made between the element stresses and the beaded panel stresses.

4. NEWGD: a Fortran program which generated a new grid point network for NASTR. In cases where internal pressure load was applied, the first of two runs of NASTR was done with internal pressure load data only. Deflections due to internal pressure loads were outputted on computer cards for subsequent use in NEWGD. This program added the deflections (equal to translations in the x, y, and z directions) to the original undeflected grid network. The second run of NASTR used this deflected grid combined with in-plane compression and shear load data from the EQULD program.

5. TWOBD: a NASTRAN finite-element computer model of two full-length panel beads as shown in Figure 3.4. This program was used because of unsatisfactory stresses from internal pressure load cases. It was assumed that (1) the beaded panels had zero stiffness in the plane of the panel in the direction perpendicular to the beads and that (2) the beads carried the internal pressure load as a beam in bending. The model was loaded with the same internal pressures as the test structure, and the resulting panel stresses were combined with the ele-

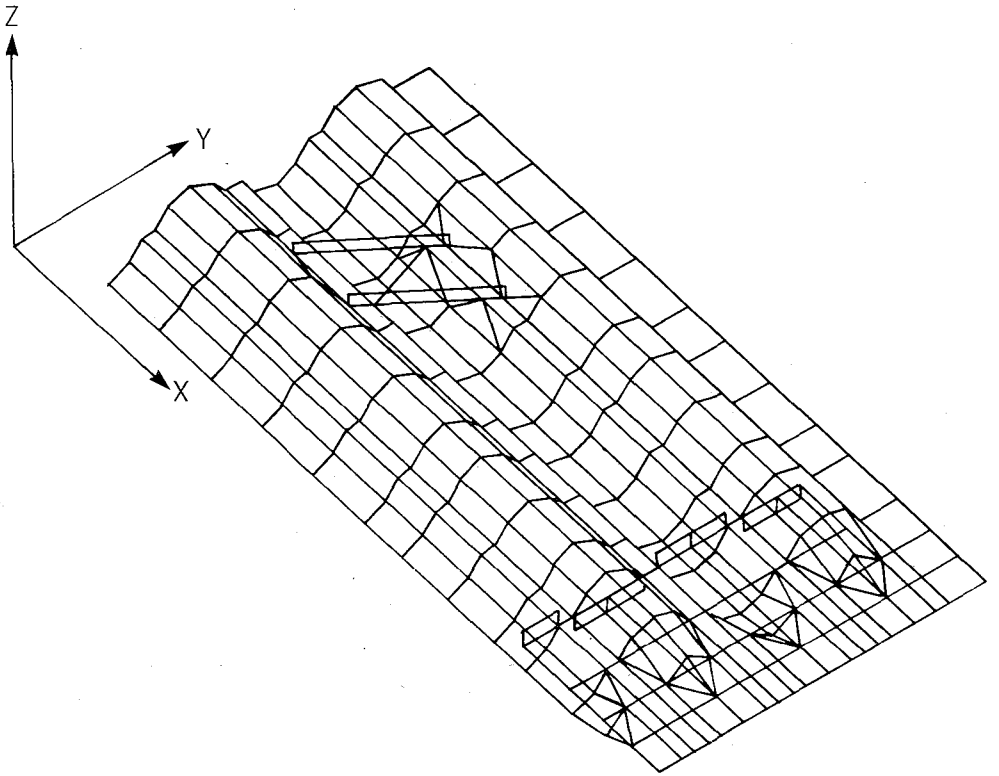

Figure 3.3: NASTR NASTRAN Finite-Element Computer Model.

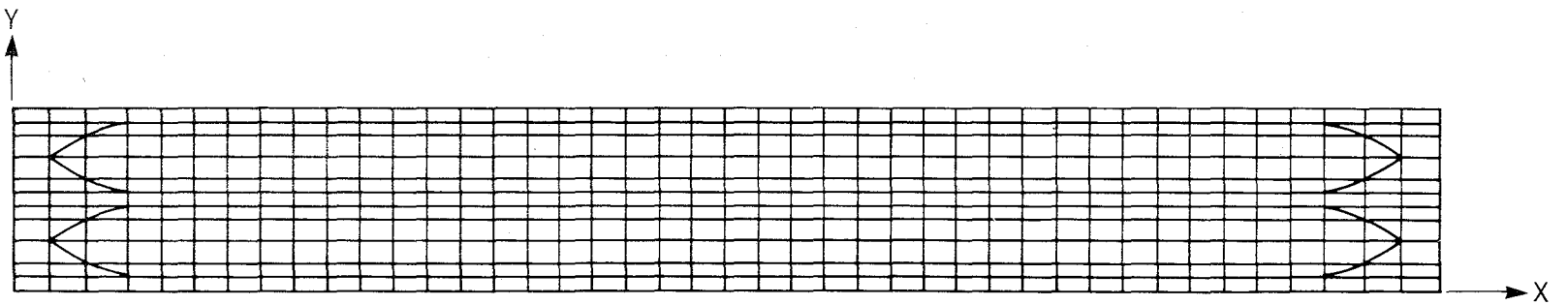

Figure 3.4: TWOBD NASTRAN Finite-Element Computer Model.

ment stresses output from the second execution of the NASTR program. The model consisted of 478 elements and 516 grid points.

6. ROSETTE: a Fortran program which converted stresses generated by the finite-element computer model to strains so that direct comparisons with experimental results could be made.

A more detailed description of the analysis and of the results can be found in Reference 5. In this analysis only one quarter of each panel of interest was analyzed, and stresses/strains in the remaining three quarters of the panel were obtained by assuming symmetrical load conditions.

3.3 GENERAL DESCRIPTION OF THE CURRENT ANALYSIS

3.3.1 INTRODUCTION

The current analysis is based on two sets of models. The first set consists of a detailed heat transfer model of the whole wing structure, except for the support structure, and of a thermal model of one quarter of a beaded panel. These models are used for the generation of temperature-time profiles throughout the structure and the beaded panel, respectively. The second set consists of two structural models and some support programs. Due to time constraints, no attempt was made to include internal pressure loads in the structural program. As many as ten different programs are necessary to generate and to process the strain distributions, resulting from ther-

mal and mechanical loads. Figure 3.5[8] presents a flowchart describing the proposed thermal and structural analysis. Briefly these programs are

1. THWTS: a NASTRAN finite-element heat transfer model of the HWTS.
2. VIEW: a Fortran program for computing view factors from NASTRAN bulk data for internal radiation and generating the proper input for NASTRAN heat transfer analysis.
3. TCHANGE: a Fortran program which converts temperatures generated by THWTS to thermal load data for input in the TBPQTR programs.
4. TBPQTR: a NASTRAN thermal model of one-fourth of a beaded panel. This model is the thermal equivalent of the structural SBPQTR model.
5. TEQUIV: a Fortran program written to equalize the temperatures at the grid points on the common edges of the four TBPQTR models in one panel.
6. SHWTS: a NASTRAN structural model of the HWTS. It includes the support structure but not the heat shields or the heat shield clips.
7. REDIST: a Fortran program written to convert the displacements of the grid points at the outside edges of the panel into enforced displacement cards (SPC) as input in the SBPQTR models.
8. SBPQTR: a NASTRAN structural model of one-fourth of a beaded panel. It was derived from the NASTR model described

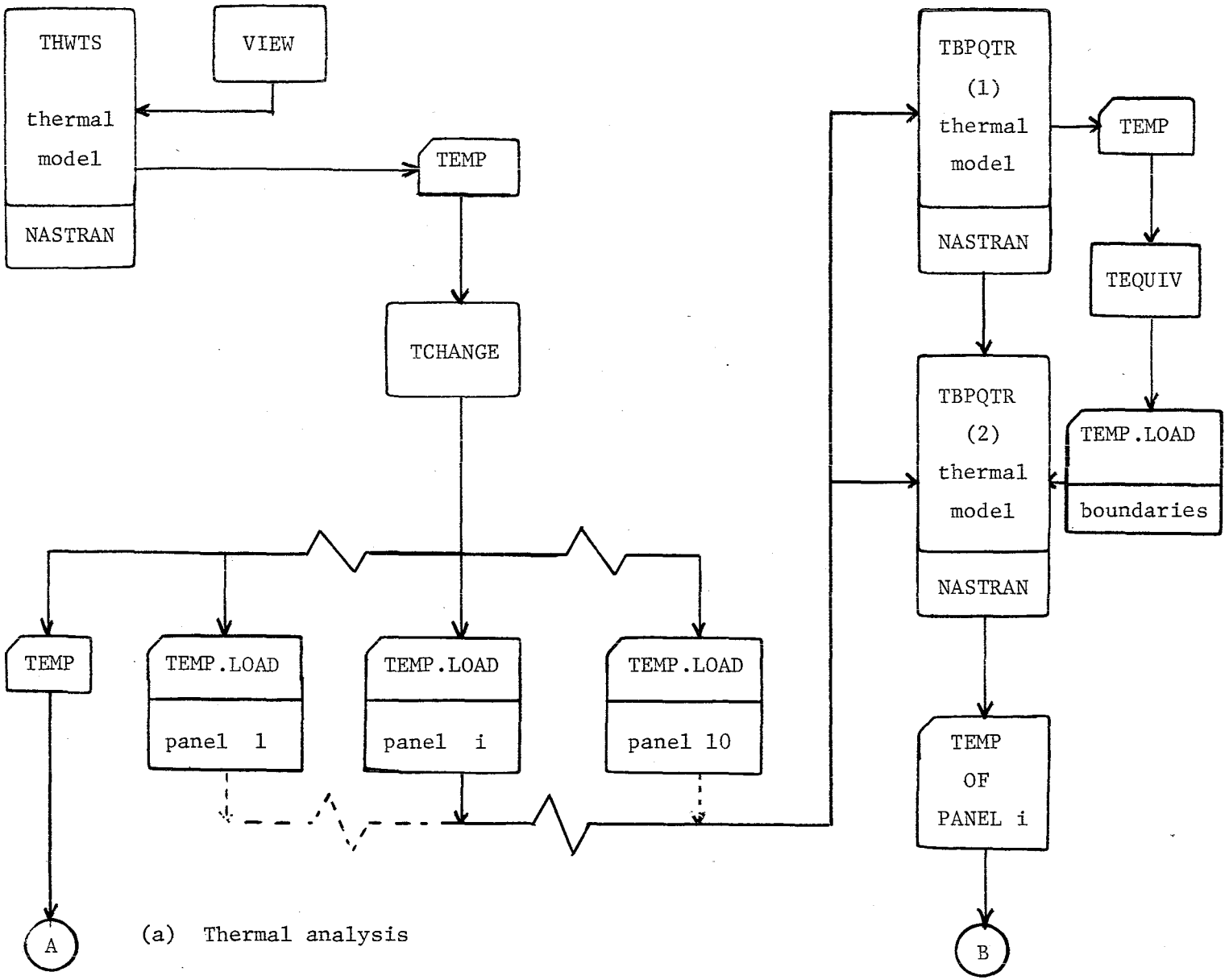

Figure 3.5: Flow Chart of Proposed Analysis.

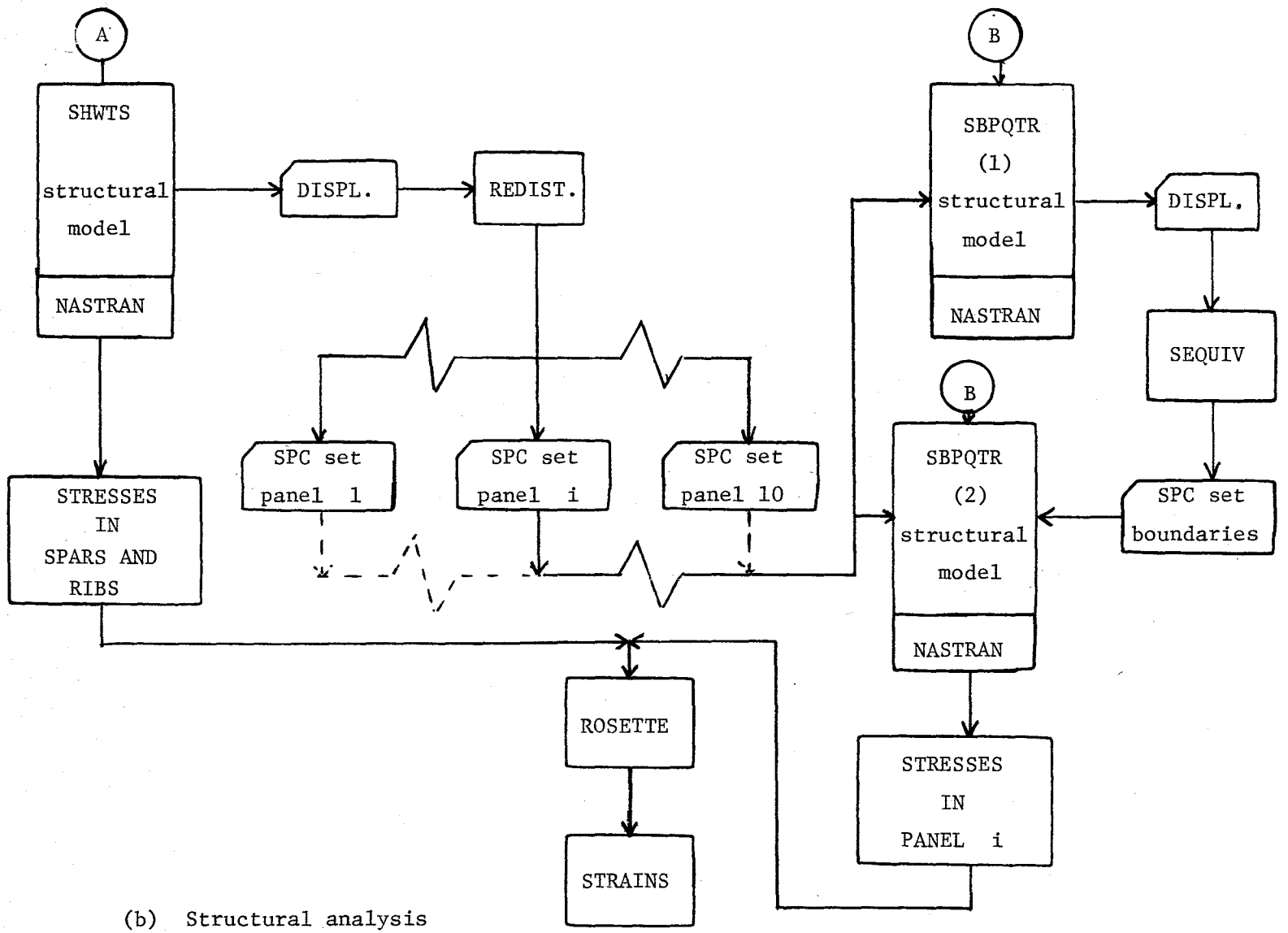

(b) Structural analysis

Figure 3.5: Continued.

in Section 3.2. Refinements were made to include grid points at the locations of the strain gages and thermocouples, as well as the influence of the doublers and the different thicknesses of the panel.

9. SEQUIV: a Fortran program which equalizes the displacements at the common edges of the four quarter models in a panel and converts them to load data cards.
10. ROSETTE: a Fortran program which converts stresses generated by SHWTS and the final runs of the SBPQTR models into strains so that direct comparisons can be made with the experimental data. This program was also used in the earlier analyses of Section 3.2.

A more complete description of the flowchart and of each program will be given in the following sections.

3.3.2 THE HEAT TRANSFER ANALYSIS

The finite-element computer model which represents the entire wing portion for heat transfer purposes is named THWTS. It consists of five submodels plus thermal load data and miscellaneous data. These submodels represent the upper and lower heat shields (UPHESH and LOHESH), the upper and lower beaded panel surfaces (UPBEPA and LOBEPA), and the spars and ribs (SPARRIBS). However, the subdivision in these five models was used only for reasons of convenience in generation and referencing of the elements. In the final version of THWTS, they are completely merged with the connecting elements and the thermal load data. Because of surface radiation effects between the heat shields

and the wingbox and in the wingbox itself, it was necessary to generate view factors. The computation of these view factors is done by a separate program, called VIEW (Reference 9).

The output of THWTS was stored on a permanent file. It consists of temperature cards for each time step for all the grid points that have corresponding locations in the structural model SHWTS. Sets of temperature cards also were generated for input in the thermal quarter beaded panel model, TBPQTR, after conversion by TCHANGE in thermal load data cards. TBPQTR generates the temperature distribution of a one-fourth beaded panel model, needed for the structural analysis. To obtain a unique temperature distribution along the edges of the four quarter models forming one beaded panel, a program named TEQUIV was written, which equalized the temperatures at the common grid points. A second run generated the final input data for the structural model, SBPQTR.

3.3.3 THE STRUCTURAL ANALYSIS

A structural model of the HWTS was developed for generating the stress distributions. This model, named SHWTS, is far more detailed than the NWML program of Section 3.2. However, flat elements do still represent parts of the beaded panels and the corrugated webs of the spars and ribs. The locations of strain gages and thermocouples and the effects of different thicknesses are incorporated in the model. Temperatures, derived from the thermal model program THWTS, are used as input for thermal loading. The computed stresses for the elements, representing the webs of spars and ribs, were converted into strains

by ROSETTE for the final comparison. Elements representing the beaded panels were, however, still too large for accurate representation of the stress distributions. As in the previous analysis, a one-fourth structural model of a beaded panel was used. This model, SBQTR, is derived from NASTR and extended with elements representing the doublers and the heat channels for the heat clips. A Fortran program, REDIST, is used to generate loading data cards for each panel from the output of the main SHWTS program. Enforced displacements at the edges of each quarter beaded panel model take care of the mechanical loading, as do the temperature cards, derived from the TBPQTR program for the thermal loading in the panel. In order to obtain equal boundary conditions, the displacements at the inside boundaries of the four models, representing one panel, will be averaged by SEQUIV. A second run of SBPQTR results in the final stress distribution of each panel. ROSETTE will again convert the computed stresses into strains.

To conduct a complete thermal/structural analysis of the HWTS and the five upper and lower root panels, numerous runs of NASTRAN and support programs have to be made. To help in the data management of the data files created during this analysis, a procedure was developed that explains the sequence and the type of files needed. This procedure is listed, and a detailed flowchart of these files presented, in Appendix B.

3.4 AVAILABLE COMPUTER RESOURCES AND PROGRAMS

3.4.1 COMPUTER RESOURCES

Most of the development of the first phase of the thermal modeling and all of the structural modeling was done in-house on the Cyber 73 computer of Dryden FRF. Entering of the input data was done by means of punched cards, while the data were stored as permanent or update files. In the second phase of the development of the thermal model, a VAX-11/750 computer system at Ames/Moffett Field was used. Entering data was accomplished from a terminal at Dryden or at Ames. In some instances the Ames Cyber 7600 and CRAY1 computers were used to obtain results of specific programs or for the NASTRAN analysis.

3.4.2 THE NASTRAN PROGRAM

As mentioned earlier, NASA's general purpose structural analysis program, NASTRAN, was used as the main analysis method. Two different versions of NASTRAN were used during the investigation. On the Dryden Cyber 73 computer the COSMIC version of NASTRAN was used for the first phase of the thermal model and for the structural model. At the Ames computers the MacNeil Schwindler Corporation version (MSC) of NASTRAN was installed. The main differences between both versions for the purpose are in the structure of the analysis program and in the availability of some plate element types, such as the isoparametric QUAD4 element in the MSC version that is not available in COSMIC. However, the differences in element types are minor.

3.4.3 THE PATRAN-G PROGRAM

In the second phase of the thermal modeling, the use of this program, developed by PDA Engineering, has enabled the generation of the thermal model in about two months, compared to the 12 months of the first phase thermal model. PATRAN-G is an interactive computer program that combines the best of two partners involved in the creation of a mathematical model: the engineer, with his or her experience, creativity, and decision-making expertise; and the computer, providing the speed, data management facilities, attention to details, and mathematical modeling tools (Reference 10). The framework for communication between man and machine is interactive graphics and alphanumeric question-and-answer by both parties.

PATRAN-G will output its data base for the mathematically defined model in a neutral format on a file called the neutral file. It is therefore possible that with the help of special translator programs, several finite-element models can be generated from the same geometric base. Translator programs do exist for finite-element programs like NASTRAN (COSMIC and MSC), SPAR, ANSYS, and others. Because this neutral file output operation is a bidirectional process, an existing model can be modified, expanded, or even converted into a different finite-element model with the use of PATRAN-G.

The generation of a model occurs in PATRAN-G in two phases, after which the data base is written on the neutral file.

In the phase I construction a continuous, mathematically defined geometry model is generated that closely approximates the physical

object. It defines the basic features, or regions, of the object, using a combination of three entities: one-dimensional "lines," two-dimensional "patches," and three-dimensional "hyperpatches." These entities are generated in PATRAN-G by the method of multilevel synthesis. Material property data also are defined during this phase.

Once a PATRAN-G geometry and properties model of the structure has been constructed, it can be subdivided during phase II to any required density for finite-element model generation. Seven basic operations form the base of the phase-II process:

1. GFEG or the subdivision of the geometric model into node points. The user must specify only the extent of the subdivision for a uniform mesh and the location of areas of nonuniform mesh refinement.
2. CFEG or connectivity generation, to define finite-elements. The user merely indicates the types of elements to be used to model each region.
3. Automatic "equivalencing," in which the ID numbers of congruent nodes are equated.
4. DFEG, or data generation, which applies external loads and constraints to the finite element model.
5. PFEG, or property generation, which assigns physical properties to the elements.
6. Node and finite element editing.
7. Node optimization, which redefines various aspects of the mathematical model with respect to certain criteria.

The last step of the PATRAN-G generation is the writing of the data base on the neutral file. A special program, PATNAS, translates the data base into a MSC NASTRAN finite-element model. The use of PATRAN-G will be discussed in more detail in the next chapter.

3.4.4 THE VIEW PROGRAM

This program was used for the generation of view factors for the thermal modeling of the HWTS structure. The VIEW program has been developed at NASA's Goddard Space Flight Center for computing the view factors for surface radiation effects in NASTRAN heat transfer analysis (Reference 9). The VIEW program is a modification of a (finite-element) view factor program called RAVFAC. The modifications included compatibility requirements for NASTRAN and RAVFAC input and capabilities to produce an output format directly usable for NASTRAN purposes. The MSC NASTRAN program contains a VIEW module that is based on the original program. However, it proved to be more efficient to run the separate VIEW program than to compute the view factors during a NASTRAN run. The VIEW program was installed on the Cyber computers of Dryden and Ames. The features and particulars of the VIEW program are discussed in more detail in the next chapter.

CHAPTER 4

THE THERMAL MODELS

4.1 INTRODUCTION

The development of the thermal model of the HWTS, THWTS, was actually done in two phases. During the first phase a model was developed that, based on the experiences of the then existing analysis, paid much attention to details of conduction paths and to radiation. Particular features in the HWTS are the beaded parts of the surface panels and the corrugated webs of the spars and ribs. In this model they were modeled as isolated, stretched flat elements, which took care of the real conduction paths; but they were still connected to the surrounding structure by means of special multipoint constraint definitions. Figure 4.1 presents some specific parts of this model. The heat shields were detailed because of the large number of heat clips connecting the shields to the surfaces of the wingbox.

However, the results of this first attempt to obtain a thermal model indicated some severe discrepancies. The calculated temperature distribution was much too low and did not match most of the measured temperatures. Also, the required computer time for one run was extremely long, despite the use of optimization techniques like BANDIT for reducing the bandwidth of the matrices. Based on the results of this model, it was concluded that a new model had to be created, which would incorporate the lessons learned during the (first phase) modeling. During this process several errors or discrepancies were detected in NASTRAN and in another support program. These and some solutions for them will be discussed in more detail later in Chapter 6.

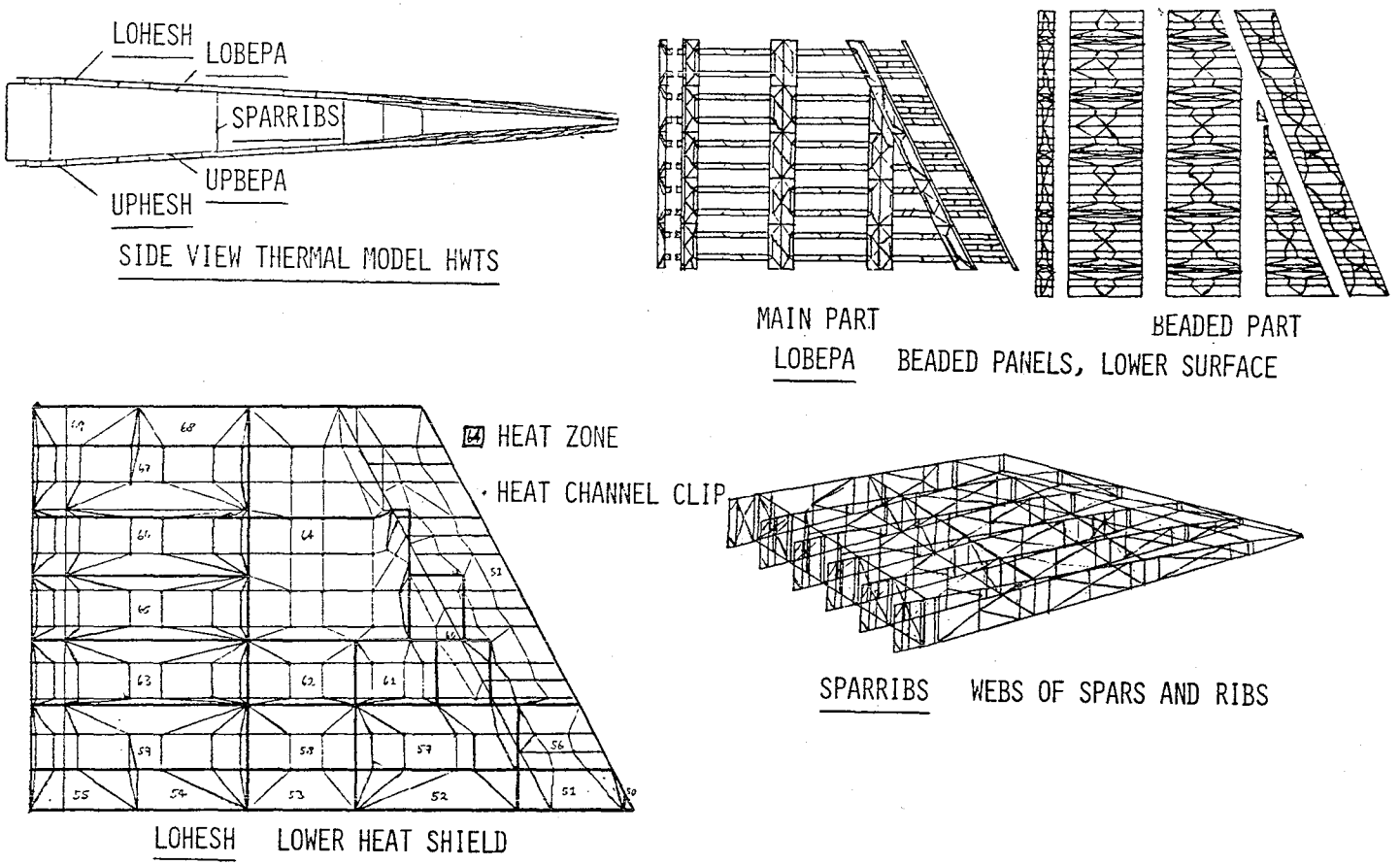

Figure 4.1: First Thermal Computer Model of HWTS.

The most important lessons learned from this first phase model were

1. The model should be as simple as possible but still represent the structure at a realistic level. The number of elements and grid points should result in run times and core memory requirements well within the confines of the available computer resources.
2. In a structure like the HWTS, the share of radiation in the heat transfer throughout the structure is much larger than the contribution of conduction. This is a result of the much higher temperatures experienced here than in similar existing structures like the space shuttle and the YF-12. The first phase model was deficient in the amount and size of radiation elements.
3. It is not possible to bring all the desired details together in one model as complex as this one within the available limits of sore size and CPU time.
4. Because the energy that an element receives from radiation is transferred to the surrounding elements through its corner grid points, the choice of the size of a radiating element should be made dependent on the size and importance of the structural elements at that location.
5. To obtain a sufficient temperature distribution along the webs of spars and ribs, the webs should be subdivided into at least three elements along the vertical axis.

6. The use of multipoint constraint (MPC) equations, which connect isolated parts of the structure with the main structure, is not efficient and should be avoided.

An important contribution to the decision to redo the development of the thermal model and not to try to make corrections to the old model was that the computer program PATRAN-G came at the disposal of Dryden FRC, together with the use of the VAX computer. With this interactive program it became possible to develop a new model very quickly and to make modifications or refinements to an existing model. Also, the long-term objective of the HWTS program--of comparing the value of several (thermal) finite-element programs--will be strongly helped by the use of PATRAN-G. Special translator programs for these finite-element programs exist which make use of the neutral data base generated by PATRAN-G.

In the remainder of this chapter, the development of this "second phase" thermal model is discussed. The use of PATRAN-G in the development of the different submodels of the THWTS model is, where possible, described with a listing of its directives. Appendix A displays in more detail the design of these submodels. The more important computer programs used in the development and analysis of the models are listed in Appendix C.

4.2 THE UPPER AND LOWER SURFACES OF THE WINGBOX

Each surface of the wingbox is composed of 19 beaded panels in the main section and five in the transition section. Figure 2.5 showed

the form of a beaded panel. A realistic modeling of the beads, in order to take into account the longer (conduction) length in the chord direction, would require too large a number of grid points (and therefore degrees of freedom). It was, therefore, decided to model the beaded parts in the panel as flat panels having the same mass but having a width equal to the projected length in the plane of the surface. Because most of the temperature and strain measurements were made in the center part of the wing, the internal bays in that area were modeled in more detail (bays G, H, I, and M in Figure 2.14).

Figure 4.2 displays the construction of the phase-one model of the lower wing surface. Only 19 grid points were directly defined with their coordinates, and 33 were generated by translation from other grid points. Patch elements define only the basic geometry of a group of regions that have identical geometrical and material properties. The upper surface of the wingbox in the phase-one model stage is created by a mirroring process around the horizontal plane. During the second phase of the PATRAN-G modeling, the patches are subdivided in subelements according to the desired mesh distribution. A listing of the PATRAN-G commands is given in Table 4.1. The final distribution of the surfaces is shown in Figure 4.3.

4.3 THE SPARS AND RIBS OF THE WINGBOX

Using the grid points generated during the phase-one construction of the surface models, patches were created representing the webs of the spars and ribs. Only one patch was sufficient for the phase-one

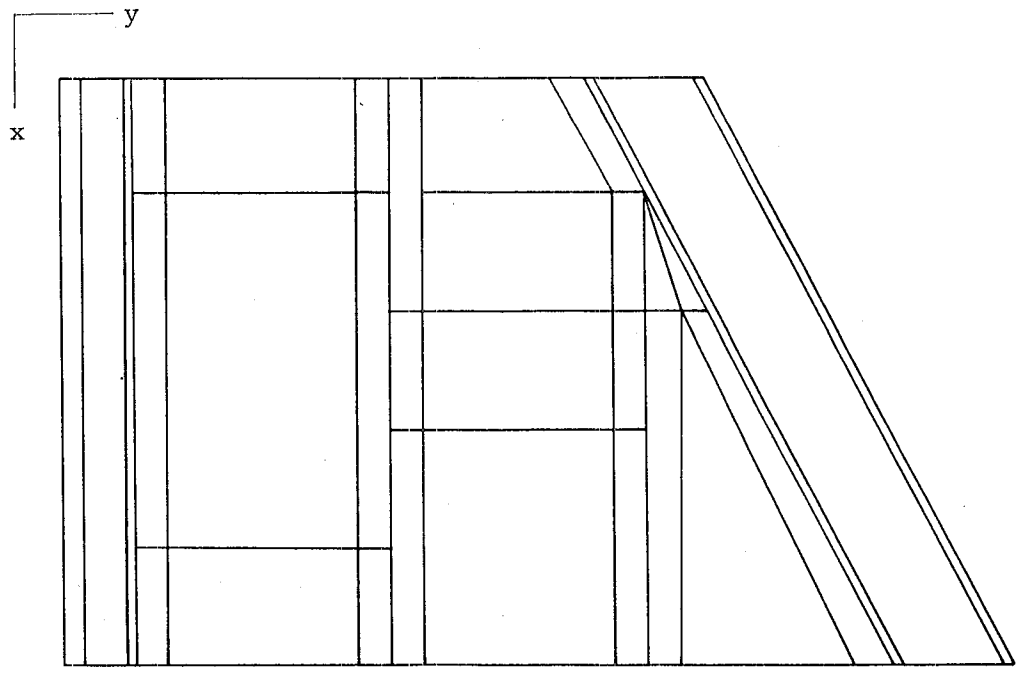

Figure 4.2: Phase-One Construction of (Lower) Surface Wingbox.

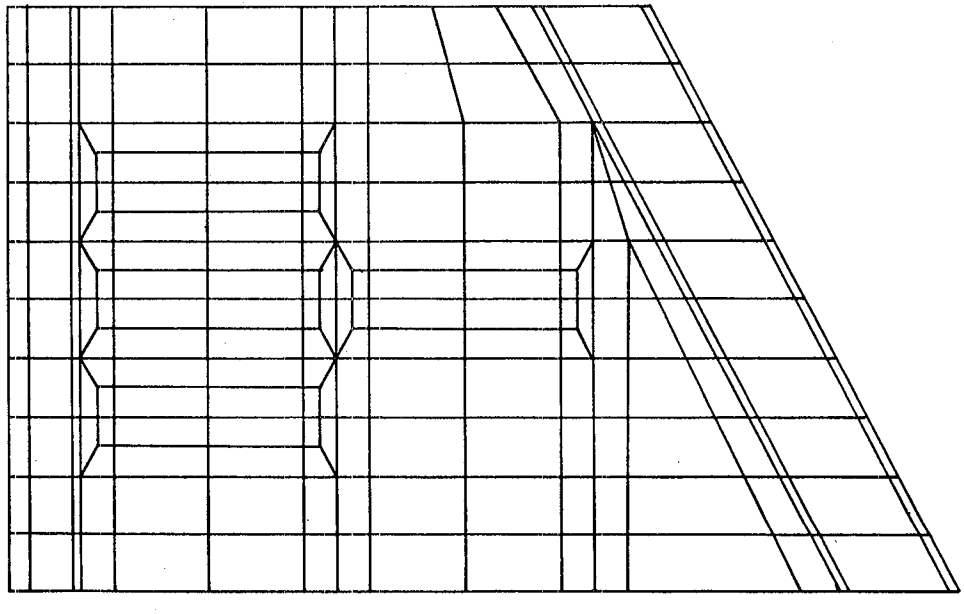

Figure 4.3: Phase-Two Construction of (Lower) Surface Wingbox.

Table 4.1: PATRAN-G Directives for the Construction of the Lower and Upper Surfaces of Wingbox.

```
GO
1
1
2
VI
1
0,0,0
VI
2
0,0,-90
GR,1,,910,42,10.019
GR,13,,910,151.160,3.425
GR,2,,910,45.34,10.019
GR,3,,910,52.65,10.019
WI
4
7
PL
GR,4,,910,54,10.019
GR,5,,910,59.632,9.71
GR,6,,910,92.003,7.931
GR,7,,910,97.635,7.621
GR,8,,910,103.267,7.312
GR,9,,910,125.1,6.112
GR,11,,910,132.519,5.603
GR,12,,910,149.513,3.617
GR,10,,910,130.872,5.795
GR,14T21,TR,100,1T8
GR,22T26,TR,20,4T8
GR,27T30,TR,80,4T7
GR,31,,930,135.639,5.553
GR,32,,930,141.2712,5.2236
GR,33T40,TR,20,25/26/31/32
GR,41/42,TR,40,38/40
GR,43T46,TR,100/51.996/-2.8570,10T13
GR,48,,950,147.232,4.896
GR,49,,950,151.6704,4.6522
GR,51,,1010,146.912,4.913
GR,52,,1010,176.472,3.2892
SET,NL,0
PAT,1,QU,,1/2/15/14
PA,2,Q,,2/3/16/15
PA,3,Q,,3/4/17/16
PA,4,Q,,4/5/23/22
PA,5,Q,,22/23/28/27
PA,6,Q,,27/28/18/17
PA,7,Q,,5/6/24/23
PA,8,Q,,23/24/29/28
PA,9,Q,,28/29/19/18
PA,10,Q,,6/7/25/24
PA,11,Q,,24/25/30/29
PA,12,Q,,29/30/20/19
PA,13,Q,,7/8/35/33
PA,15,Q,,33/35/36/34
PA,16,Q,,34/36/21/20
PA,17,Q,,8/9/31/26
PA,18,Q,,26/31/37/35
PA,19,Q,,35/37/38/36
PA,20,Q,,36/38/41/21
PA,21,Q,,9/10/32/31
PA,22,Q,,31/32/39/37
PA,23,Q,,37/39/40/38
PA,24,Q,,38/40/42/41
PA,25,Q,,32/32/48/39
PA,27,Q,,32/32/49/48
PA,28,Q,,39/48/51/42
PA,30,Q,,48/48/52/51
PA,32,Q,,48/49/43/52
PA,34,Q,,10/11/44/43
PA,35,Q,,11/12/45/44
PA,36,Q,,12/13/46/45
SET,NOFLIP,ON
DA,1,6(0),1,3(0),1,3(0),-1
PA,37,T67,MS,D1,1T13/15T25/27/28/30/32/34T36
SET,LAB1,OFF
END
2
1
2
SET,LABN,OFF
GF,P1T3,,11/2
GF,P4,,3/2
GF,P5,,7/2,,9/11/13
GF,P6,,3/2
GF,P7,,3/3
GF,P8,,13/3
GF,P9,,3/2
GF,P10,,3/2
GF,P11,,7/2,,2/4/6
GF,P12,,3/2
GF,P13,,5/2
GF,P15,,3/2,,5
GF,P16,,,5/2
GF,P17,,3/3
GF,P18,,3/3
GF,P19/20,,5/3
GF,P21/22,,3/2
GF,P23,,3/2,,2
GF,P24,,5/2
GF,P25/27,,3/2
GF,P28/30/32,,7/2
GF,P34T39,,11/2
GF,P40,,3/2
GF,P41,,7/2,,9/11/13
GF,P42,,3/2
GF,P43,,3/3
GF,P44,,13/3
GF,P45,,3/3
GF,P46,,3/2
GF,P47,,7/2,,2/4/6
GF,P48,,3/2
GF,P49,,5/2
GF,P50,,3/2,,5
GF,P51,,5/2
GF,P52/53,,3/3
GF,P54/55,,5/3
GF,P56/57,,3/2
GF,P58,,3/2,,2
GF,P59,,5/2
GF,P60/61,,3/2
GF,P62/64,,7/2
GF,P63,,7/2
GF,P65T67,,11/2
END
2
2
CF,P1,QU,1
CF,P2,QU,2
CF,P3,QU,1
CF,P4T6,QU,3
CF,P7T9,QU,4
CF,P10T13/15/16,QU,3
CF,P17T20,QU,4
CF,P21T24,QU,3
CF,P25/27,QU,5
CF,P28,QU,3
CF,P30,QU,4
CF,P32,QU,3
CF,P34,QU,6
CF,P35,QU,7
CF,P36,QU,6
VI
1
0,0,-90
VI
2
0,0,-90
SET,LABP,ON
CF,P37,QU,1
CF,P38,QU,2
CF,P39,QU,1
CF,P40T42,QU,3
CF,P43T45,QU,4
CF,P46T51,QU,3
CF,P52T55,QU,4
CF,P56T59,QU,3
CF,P60/61,QU,5
CF,P62,QU,3
CF,P63,QU,4
CF,P64,QU,3
CF,P65,QU,6
CF,P66,QU,7
CF,P67,QU,6
VI
1
-90,0,-90
VI
2
0,23,34
PL
END
8
5
```

model of a rib web (see also Figure 4.4). Similar to the beaded parts of the surface panels, the corrugated webs of spars and ribs were modeled as flat elements with thickness compensated for the real mass. During the phase-two construction these patches were subdivided along their x or y axes in such a way that they are compatible with the surface elements. Each web was divided along the z axis into three elements, giving four data points for the computation of the temperature distribution in the vertical plane.

The caps of the spars and ribs are represented in the model by bar elements. The mass of the connecting elements between surface panel and spar/rib caps--such as nutplates, fittings, and the two doublers at the edges--are added to the mass of the bar elements representing the caps of the adjacent spars and ribs. Figure 4.5 shows the line elements used in the phase-one construction of the lower and upper caps. The line elements representing the upper caps were derived from the lower elements by a mirroring process around the x-y plane.

Bar elements also represent the vertical angles connecting the webs of spars and ribs at their intersecting points. Table 4.2 presents the PATRAN-G directives for the generation of the spar/rib elements.

4.4 THE HEAT SHIELDS AND THE THERMAL LOADING SYSTEM

The basic components of the heat shield structure are (a) the slightly corrugated panels, made from René 41, or TDNiCr; (b) two support beams for each panel to minimize the pressure bending moments; and (c) flexible supports under the beams connected with the surface panels of the wingbox. The support clips were made flexible in bending

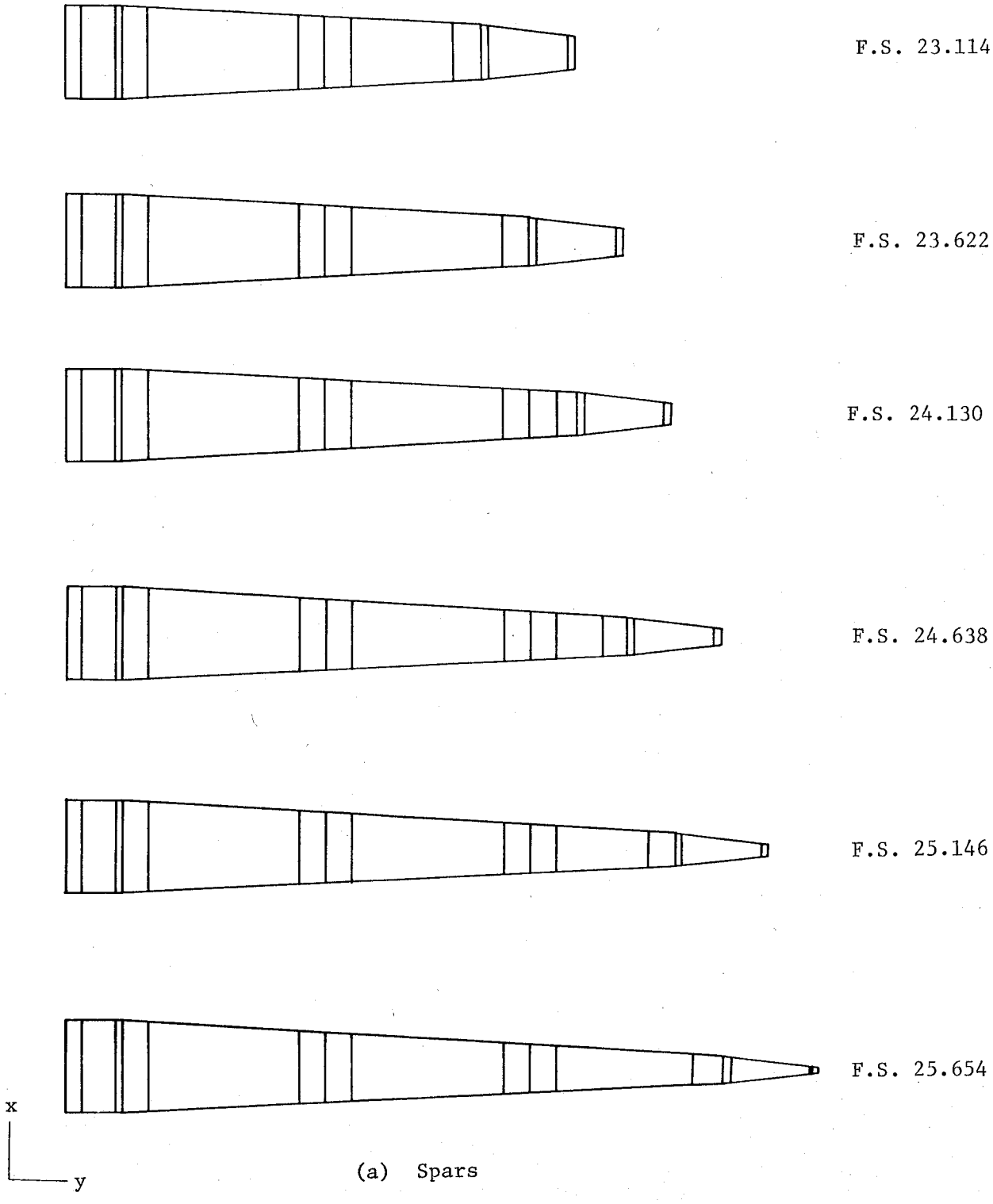

(a) Spars

Figure 4.4: Phase-One Construction of Spar and Rib Webs.

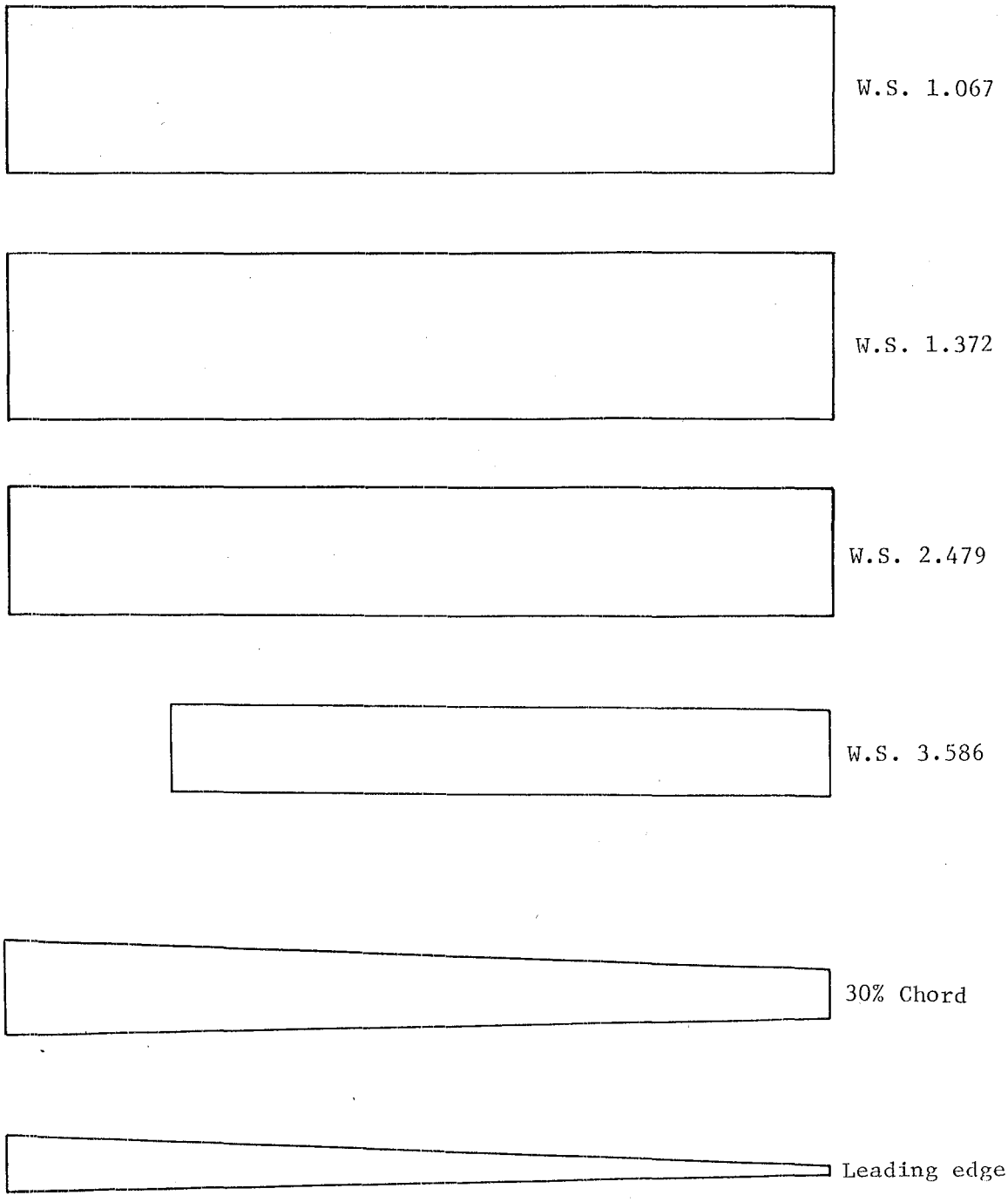

(b) Ribs

Figure 4.4: Concluded.

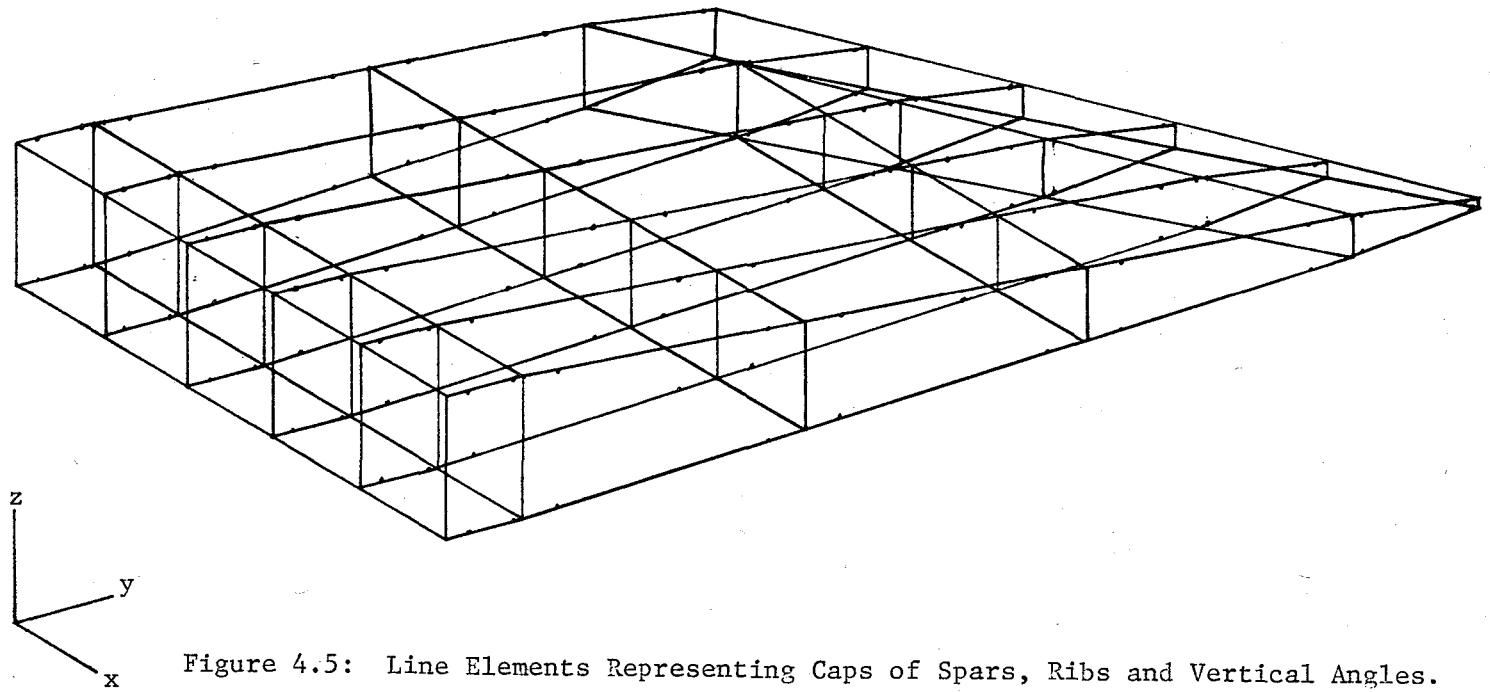

Figure 4.5: Line Elements Representing Caps of Spars, Ribs and Vertical Angles.

Table 4.2: PATRAN-G Directives for the Generation of the Spar and Rib Webs.

```
GO
3
2
2
VI
2
0,23,34
GR,200,,970,156.9787,4.3604
GR,201,,970,156.9787,-4.3604
GR,202,,990,166.7253,3.8248
GR,203,,990,166.7253,-3.8248
GR,204,,970,147.1253,4.9017
GR,205,,970,147.1253,-4.9017
GR,206,,990,147.0187,4.9073
GR,207,,990,147.0187,-4.9073
GR,208/209,TR,20,40/90
GR,210T211,TR,20/10.3992/-0.5714,49
GR,212,TR,20/10.3992/0.5714,93
GR,213,TR,20/10.3992/0.5714,212
GR,214T225,TR,20/10.3992/-0.5714,11T13
GR,226T237,TR,20/10.3992/0.5714,97T101B2
PA,70,Q,,1/14/56/53
PA,71,TR,0/12/0,70
PA,72,Q,,7/20/74/71
PA,73,Q,,32/42/91/88
PA,74,Q,,10/43/96/87
PA,75,Q,,13/46/102/101
PA,76,Q,,1/2/54/53
PA,77,Q,,2/3/57/54
PA,78,Q,,3/4/59/57
PA,79,Q,,4/5/61/59
PA,80,Q,,5/6/67/61
PA,81,Q,,6/7/71/67
PA,82,Q,,7/8/75/71
PA,83T117,TR,20,76T82
PA,118,Q,,8/9/81/75
PA,119,Q,,26/31/82/83
PA,120T123,TR,20,119
PA,124,Q,,9/10/87/81
PA,125,Q,,31/32/88/82
PA,126T129,TR,20,125
PA,130,Q,,39/48/92/89
PA,131,Q,,48/49/93/92
PA,132,Q,,40/204/205/90
PA,133,Q,,208/206/207/209
PA,134,Q,,42/51/94/91
PA,135,Q,,204/200/201/205
PA,136,Q,,206/202/203/207
PA,137,Q,,51/52/95/94
PA,138,Q,,200/210/212/201
PA,139,Q,,202/211/213/203
PA,140,Q,,52/43/96/95
PA,141,Q,,10/11/97/87
PA,142,Q,,11/12/99/97
PA,143,Q,,12/13/101/99
PA,144,Q,,32/214/226/88
PA,145,Q,,49/215/227/93
PA,146,Q,,210/216/228/212
PA,147,Q,,211/217/229/213
PA,148,Q,,43/44/98/96
PA,149,Q,,214/218/230/226
PA,150,Q,,215/219/231/227
PA,151,Q,,216/220/232/228
PA,152,Q,,217/221/233/229
PA,153,Q,,44/45/100/98
PA,154,Q,,218/222/234/230
PA,155,Q,,219/223/235/231
PA,156,Q,,220/224/236/232
PA,157,Q,,221/225/237/233
PA,158,Q,,45/46/102/100
PL
LI,1,ST,,1,2
LI,2,ST,,2,3
LI,3,ST,,3,4
LI,4,ST,,4,5
LI,5,ST,,5,6
LI,6,ST,,6,7
LI,7,ST,,7,8
LI,8,ST,,8,9
LI,9,ST,,9,10
LI,10,ST,,10,11
LI,11,ST,,11,12
LI,12,ST,,12,13
LI,13T47,TR,20,1T7
LI,48,ST,,26,31
LI,49,ST,,31,32
LI,50T57,TR,20,48/49
LI,58T72,TR,20/10.3992/-0.5714,10T12
LI,73,ST,,39,48
LI,74,ST,,48,49
LI,75,ST,,40,204
LI,76,ST,,204,200
LI,77,ST,,200,210
LI,78,ST,,208,206
LI,79,ST,,206,202
LI,80,ST,,202,212
LI,81,ST,,42,51
LI,82,ST,,51,52
LI,83,ST,,52,43
LI,84,ST,,1,14
LI,85,ST,,4,17
LI,86,ST,,7,20
LI,87,ST,,32,42
LI,88,ST,,10,43
LI,89,ST,,13,46
SET,NOFLIP,ON
LI,90T178,MI,Z,1T89
LI,200,ST,,1,53
LI,201T205,TR,20,200
LI,206T211,TR,0/12,200T205
LI,212,ST,,7,71
LI,213T217,TR,20,212
LI,218,ST,ST,,10,87
LI,219,ST,,32,88
LI,220T223,TR,20,219
LI,224,ST,,49,93
LI,225,ST,,210,209
LI,226,ST,,212,211
LI,227,ST,,43,96
LI,228,ST,,13,101
LI,229,ST,,222,234
LI,230,ST,,223,235
LI,231,ST,,224,236
LI,232,ST,,225,237
LI,233,SY,,46,102
END
2
1
2
GF,P70T72,,4/11
GF,P73,,4/9
GF,P74T75,,4/11
GF,P76T79/83T102,,4/2
GF,P80/103T107,,4/3
GF,P81/82/108T117,,4/2
GF,P118T123,,4/3
GF,P124T158,,4/2
GF,1LT4/6/7/9T32,,2
GF,5L/8/33T37/48/50T53,,3
GF,38LT47/49/54T83,,2
GF,84LT86,,11
GF,87L,,9
GF,88LT89,,11
GF,200LT233,,4
GF,90LT93/95T96/98T121,,2
GF,94L/97/122T126/137/139T142,,3
GF,127LT136/138/143T172,,2
GF,173LT175,,11
GF,176L,,9
GF,177L/178,,11
END
2
VI
1
-90,0,-90
VI
2
0,23,34
CF,P70,QU,10
CF,P71T158,QU,20
CF,1LT83,BAR,,100
1
G
14
4
CF,84LT89,BAR,,400
1
G
14
4
CF,200LT233,BAR,,300
1
G
14
4
CF,90LT172,BAR,,200
1
G
14
4
CF,173LT178,BAR,,500
1
G
14
4
END
8
5
```

to accommodate the heat shield differential thermal expansion. These clips as well as the support beams were modeled in the first thermal model as bar elements but are deleted in the latest version. For reasons of simplification, the corrugated heat shield panels are modeled as flat quadrilateral or triangular (radiation) elements. For the same reasons parts of the shield before wing station 1.118, positioned over the support structure, were deleted. The form and modeling of the heat shields are closely related to the design of the thermal loading of the HWTS. One of the main assumptions in the thermal modeling was that the heat flow into the heat shields from aerodynamic heating of the boundary layer (convection) and the resulting temperature distribution on both heat shields are already known. This means that, as in the loading tests, the thermal load is defined in terms of temperature distributions of the heat shields as function of time and location. In this way, the analytical prediction method will have the same thermal loading as that used in the experimental tests, independent of the real flight conditions; thus, results from the two methods can be compared directly with each other.

Forty-two and forty-seven heating panels with quartz lamps were used for heating the upper and lower heat shield surfaces--successfully, according to 41 different temperature-time profiles. Thermocouples attached to characteristic locations of the heat shield's 89 different heating zones control the heat input of each set of quartz lamps. These temperatures were derived from calculations of the heat flux input on the shields for the whole wing structure during the Mach 8 flight and load maneuver (Reference 11).

The approach used for simulating the thermal loading in the NASTRAN model was based directly on the known temperatures of the heat shield. It uses grounded spring elements to prescribe the desired temperatures at the grid points representing the heat shields. Table 4.3 describes the equations and the matching NASTRAN cards. By grounding the scalar end of the spring, the temperature of that scalar point is set to the absolute zero point. By multiplying the desired temperature with the spring factor, the correct temperature at the grid point will be obtained according to the equation

$$Q = K(T_B - T_A),$$

where $T_A = 0$ (grounded end).

According to this equation, the temperature of point B on the heat shield should be equal to the heat flux divided by the spring constant. Substituting the desired grid point temperature and an arbitrary large value of K, the required thermal load will be defined.

Although there were 89 different heating panels used in the heating tests, most of these zones used the same temperature-time profile. In the current model, 41 different heating profiles are used to control the temperatures of a total of 81 elements. That more elements were used than there are unique profiles can be explained by the presence of several different planes in the heat shields and by the differences in locations. Table 4.4 relates, in combination with Figures 4.6 and 4.7, the different identification numbers used in the heating tests and in the current model.

Table 4.3: Design of Thermal Loading System

As modeled:

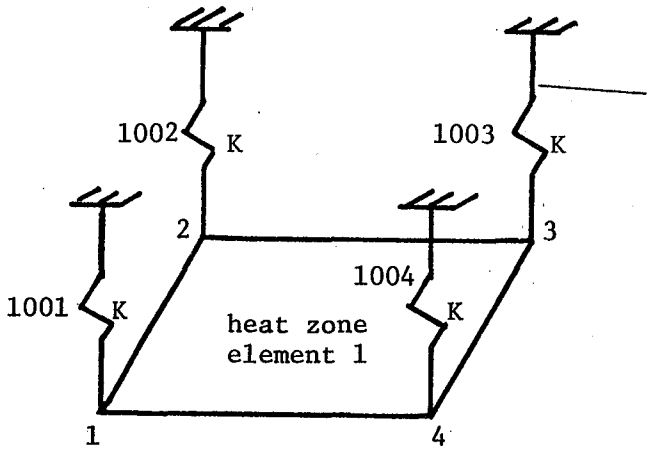

elastic spring with spring constant K and one grounded scalar endpoint

Each gridpoint in heat zone 1, 1 thru 4, has the same temperature-time profile, F(t).

Theory:

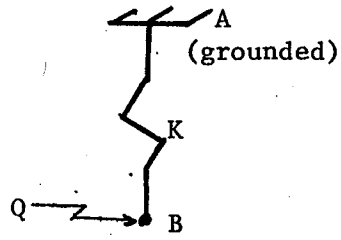

thermal load on point B: $Q = K(T_B - T_A)$

$= KT_B \quad (T_A = 0)$

OR: $T_B = Q/K$

Q is defined in NASTRAN as: Q = A f(t) on TLOAD2card

define A = K (large value $\simeq 10.0 \times 10^{10}$), defined on DAREA card.

f(t) = F(f) desired temperature-time profile, defined on TABLED1 cards.

K and elastic spring element defined on CELAS2 cards.

NASTRAN CARDS:

```
TLOAD1,1,1,,,1

                                TABLED1,1,,,,,,,,+TB11
                                +TB11,0.,100.,--,ENDT.

DAREA,1,1,10.0+10
DAREA,1,2,10.0+10
DAREA,1,3,10.0+10
DAREA,1,4,10.0+10

CELAS2,1001,10.0+10,1,1
CELAS2,1002,10.0+10,2,1
CELAS2,1003,10.0+10,3,1
CELAS2,1004,10.0+10,4,1
```

Table 4.4: Identification of Heating Zones Used in Tests and Models.

Heating Zone Tests	Temperature-Time Profile	Heating Zone Model
	UPPER HEAT SHIELD	
1, 7, 14, 21	1	3101 thru 3104
2, 8, 15, 22	2	3105 thru 3111
3, 9, 23	3	3112, 3113, 3126
4, 10, 11	4	3114, 3115
5, 12, 13	5	3116 thru 3118
6	6	3119, 3120
16	7	3121
17, 18	8	3122
19, 20	9	3123 thru 3125
24	10	3127
25	11	3128
26	12	3129, 3130
27, 33, 38	13	3131, 3132
28, 34, 39	14	3133 thru 3136
29	15	3137
30, 31, 32	16	3138 thru 3140
35	17	3141
36, 41	18	3143
37	19	3144, 3145
40	20	3142
42	21	3146, 3147
	LOWER HEAT SHIELD	
50	22	None
51, 52, 65, 66, 72, 73, 79, 80, 85, 86, 91, 92	23	3001 thru 3005
53, 54	24	3006
55	25	3007
56	26	3008
57	27	3009, 3010
58, 59	28	3011
60, 61	29	3012
62	30	3013
63, 64	31	3014, 3015
67, 74	32	3016 thru 3019
68	33	3020
69	34	3021
70, 71	35	3022, 3023
75, 76, 81, 82, 87, 88, 93, 94	36	3024, 3025
77, 78	37	3026, 3027
83, 84	38	3028, 3029
89, 90	39	3030, 3031
95	40	3032
96	41	3033, 3034

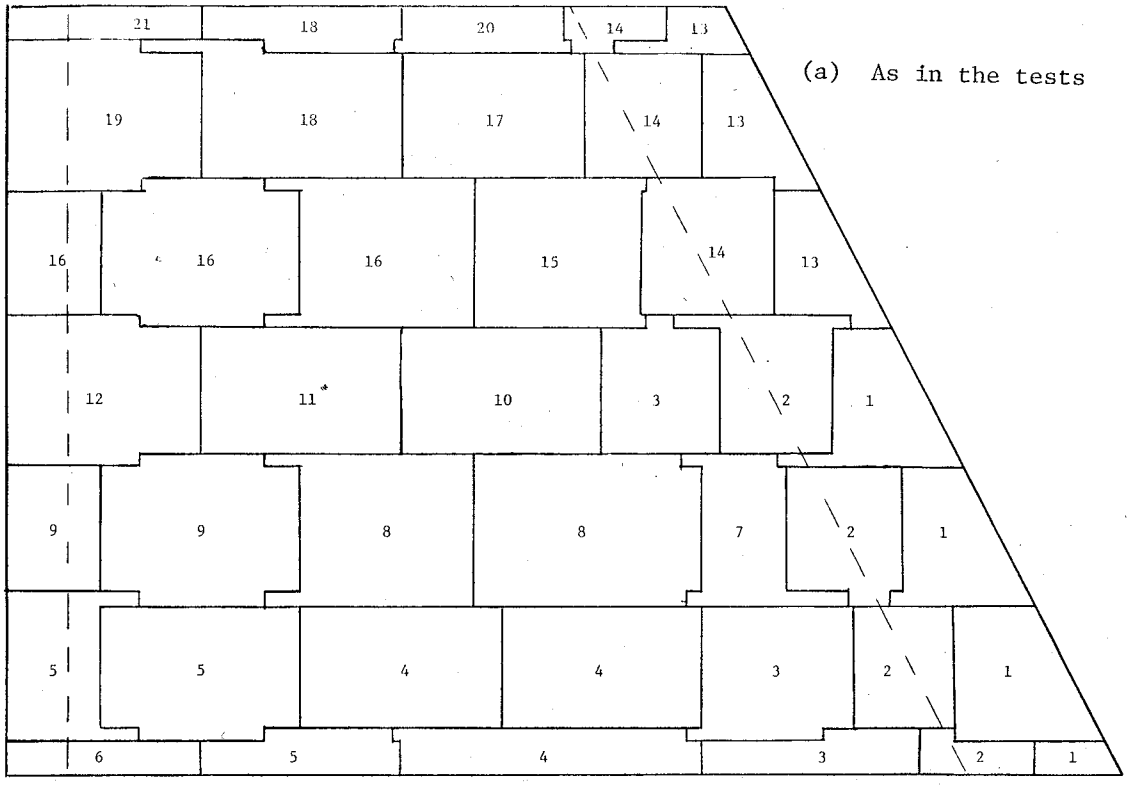

(a) As in the tests

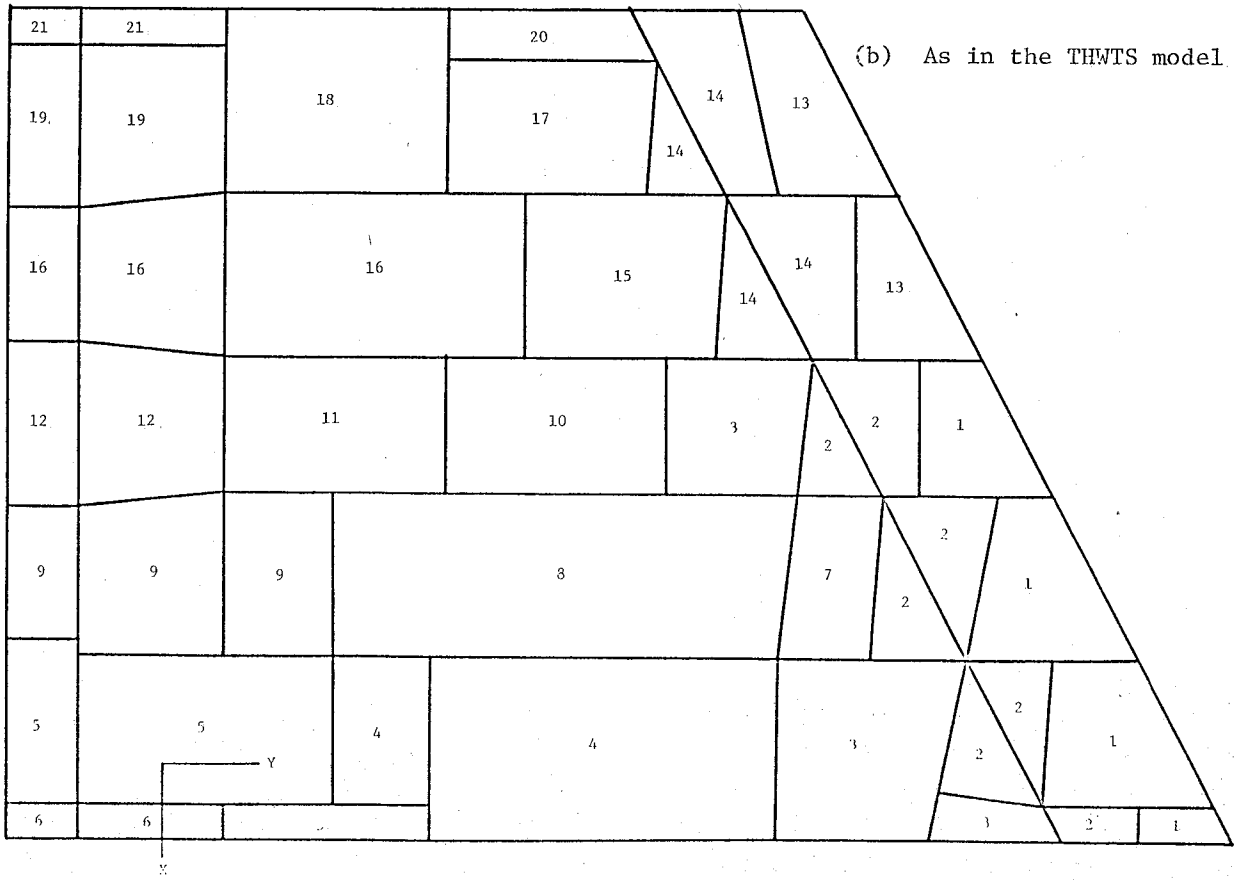

(b) As in the THWTS model

Figure 4.6: Heating Zones at Upper Heat Shield.

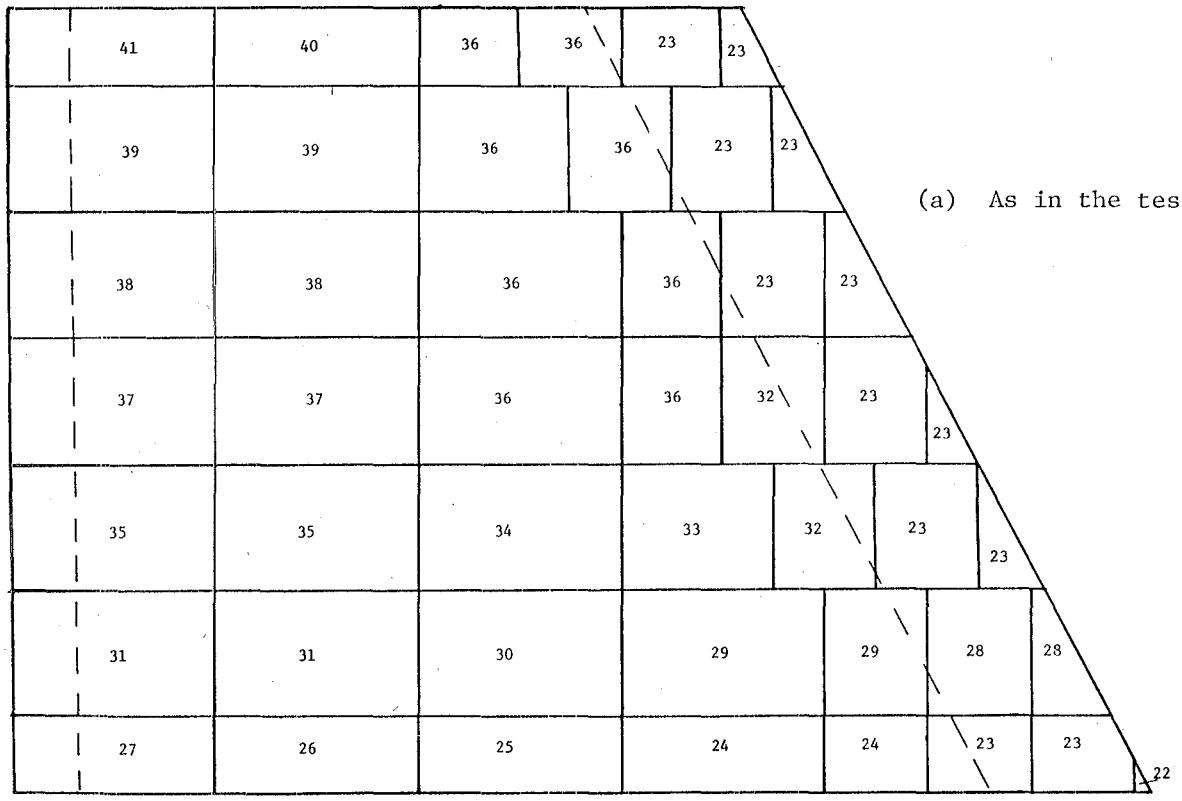

(a) As in the tests

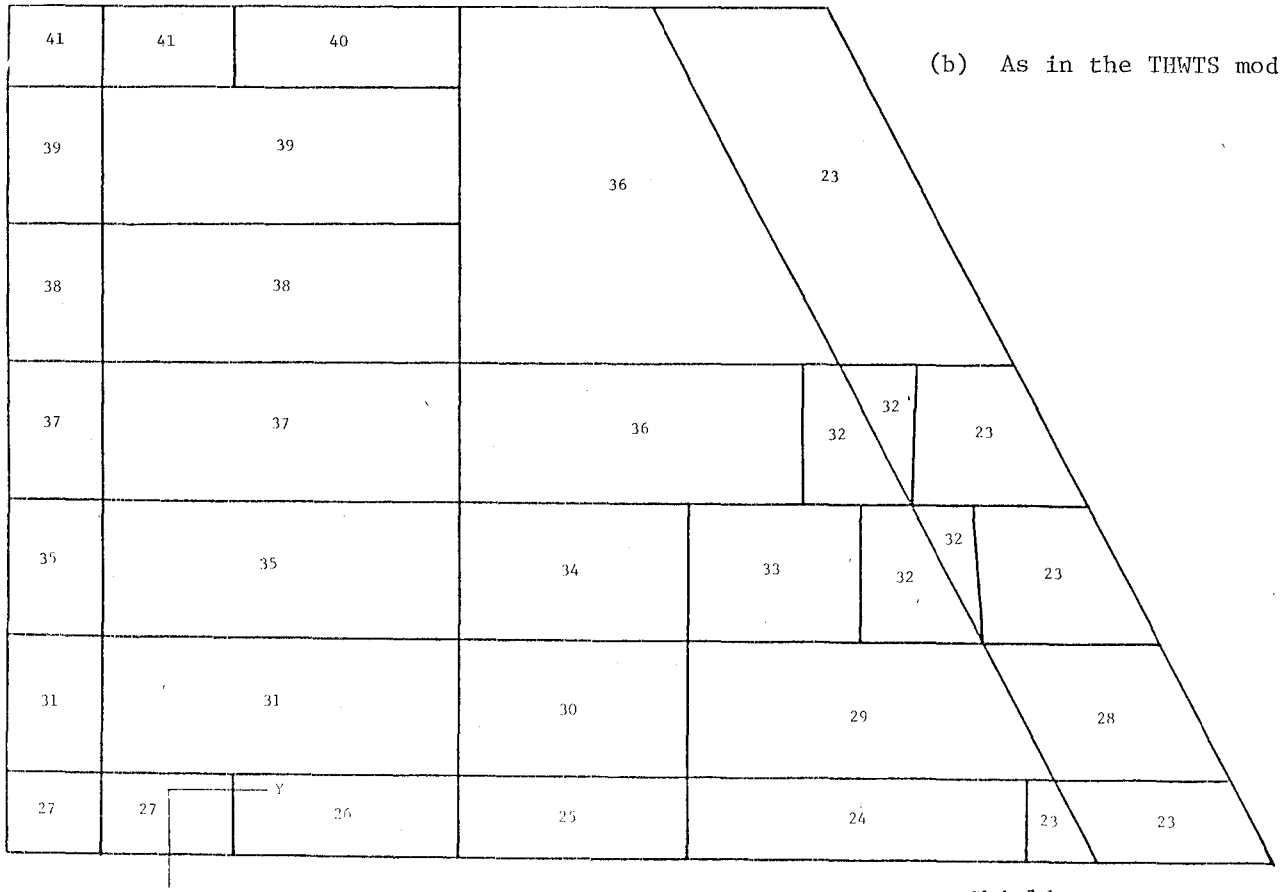

(b) As in the THWTS model

Figure 4.7: Heating Zones at Lower Heat Shield.

A characteristic feature of the PATRAN-G program was used for the application of the thermal load at the boundaries of two or more heating zones. During the generation of a quadrilateral element, four separate node points (or three for a triangular element) are created. In the equivalencing process, node points having the same coordinates are merged into one node point. By modeling the heat zones as separate entities, each with its own node points, and by deleting the equivalencing process, each heating zone will have its own set of grid points, to which a specific temperature-time loading profile can be attached. This method, where each heating zone has its own set of grid points, has the additional advantage that the number of elements can be reduced because of the absence of the requirement of compatability. This means that a grid point that is located on a boundary line between elements does not have to be a part of all the elements around that grid point (see Figure 4.8).

Because no conduction between heat shield and wingbox was assumed in this model, there was no necessity to use structural elements for the heat shields. Only radiation elements in the form of CHBDY elements are used. However, because PATRAN-G cannot generate these CHBDY elements, it was necessary to first generate structural elements, which later will be converted into CHBDY elements (see Section 4.6).

Figures 4.9 and 4.10 show the phase-two construction of the upper and lower heat shields, while in Tables 4.5 and 4.6 the corresponding PATRAN-G directives are listed.

IN STATICS:

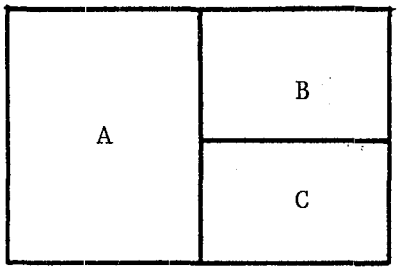

WRONG

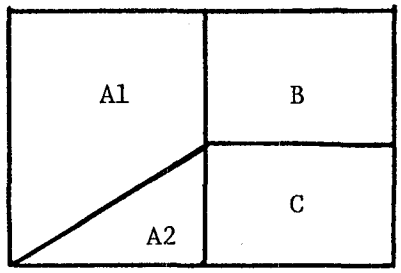

CORRECT

ACCORDING TO COMPATIBILITY REQUIREMENT.

IN THERMO ANALYSIS AS USED AT HEAT SHIELDS:

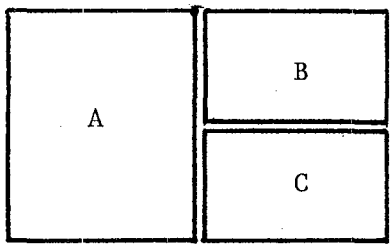

A, B, and C are heat zone elements
with own set of independent gridpoints
(no conduction from A to B and C)

COMPATIBILITY RULE NOT REQUIRED.

Figure 4.8: Compatibility Requirement

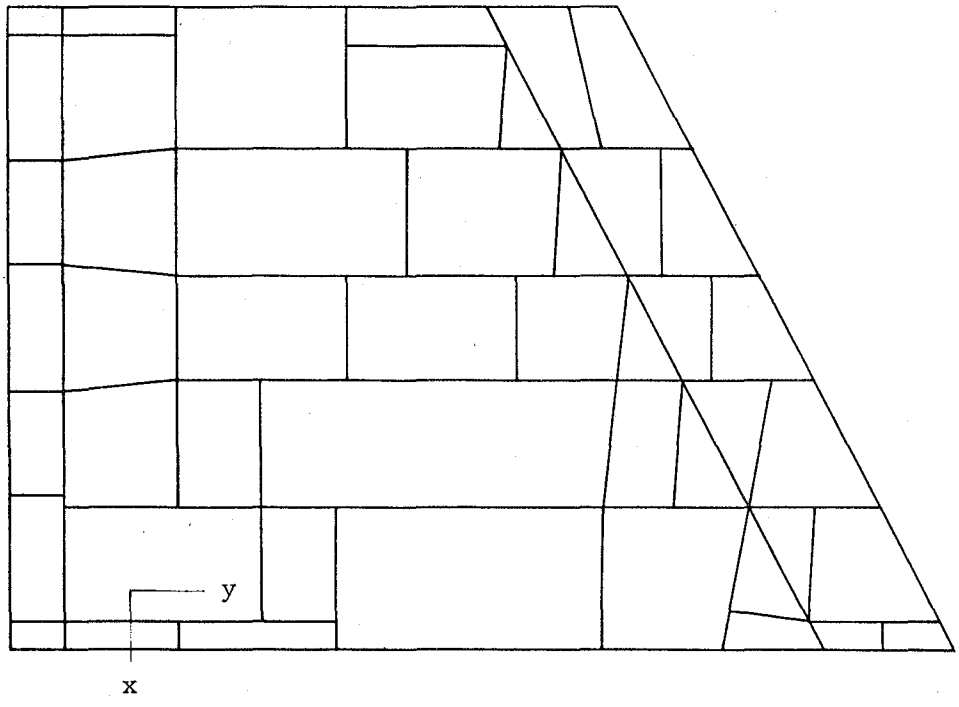

Figure 4.9: Phase-Two Construction of Upper Heat Shield.

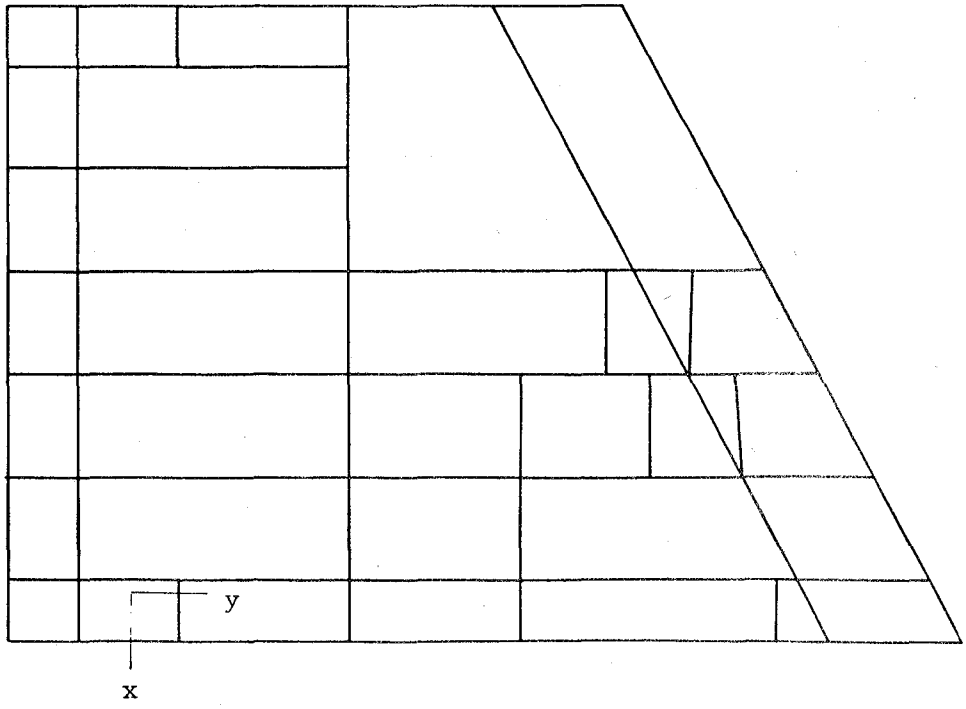

Figure 4.10: Phase-Two Construction of Lower Heat Shield.

Table 4.5: PATRAN-G Directives for the Construction of the Lower Heat Shield.

```
GO
1
1
2
VI
2
0,0,-90
GR,3001,,904,,44.5,11.573
GR,3162,,1016,208.779,1.657
WI
4
7
PL
GR,3002,,915.02,44.5,11.573
GR,3003,TR,0,3002
GR,3004,,933,44.5,11.573
GR,3005,TR,0,3004
GR,3006T3011,TR,18,3004/3005
GR,3012T3013,TR,17.98,3008/3011
GR,3014,TR,11.02,3012
GR,3015,TR,0/9.5,3001
GR,3017T3018,TR,11.02,3015/3015
GR,3021T3022,TR,17.98,3017T3018
GR,3025T3030,TR,18,3021T3022
GR,3037/3038,TR,17.98,3027/3030
GR,3041,TR,11.02,3037
GR,3043,,904,73.831,10.483
GR,3044,TR,0,3043
GR,3045T3047,TR,11.02,3043/3044/3044
GR,3048T3050,TR,89.96,3045T3047
GR,3051/3052,TR,11.02,3048/3049
GR,3053,,904,103.286,8.864
GR,3054,TR,0,3053
GR,3055T3057,TR,11.02,3053/3054/3053
GR,3058T3060,TR,17.98,3055T3057
GR,3061T3069,TR,18,3058T3060
GR,3070/3071,TR,18,3061
GR,3072T3075,TR,17.98,3063/3066/3069/3071
GR,3076/3077,TR,11.02,3072/3073
GR,3078,,904,127.752,7.520
GR,3079,,969,132.742,7.246
GR,3080T3081,TR,0,3079
GR,3082T3085,TR,18,3079T3081/3081
GR,3086T3089,TR,17.98,3082T3085
GR,3090T3091,TR,11.02,3086/3087
GR,3092,,904,132.742,6.937
GR,3093,TR,0,3092
GR,3094,,915.02,133.482,7.205
GR,3095,TR,0,3094
GR,3097,TR,0,,3061
GR,3117,,951,152.19,6.177
GR,3121,,951,162.197,5.008
GR,3133,,969,169.561,4.727
GR,3142,,998.57,176.925,4.818
GR,3150,,1004.98,180.258,4.635
GR,3153,,1016,,185.988,4.320
GR,3148,,1016,176.925,4.818
GR,3154,,987,193.7,2.486
GR,3156,,1004.98,203.049,1.972
GR,3158,,1011.39,206.381,1.789
GR,3160,,1016,206.381,1.937
GR,3118/3122/3134,TR,0,3117/3121/3133
GR,3143/3151,TR,0,3142/3150
GR,3155/3157/3149,TR,0,3154/3156/3148
GR,3159/3161,TR,0,3158/3160
GR,3119,,904,150.543,4.857
GR,3120,,924.98,161.452,4.258
GR,3123,,944.98,171.851,3.687
GR,3141,,964.98,182.25,3115
GR,3110,,951,147.470,6.436
GR,3111/3112,TR,0,3110
GR,3114,,969,147.47,6.436
GR,3115T3116,TR,0,3114
GR,3124,,969,154.834,6.032
GR,3125,TR,0,3124
GR,3127,,987,154.834,6.032
GR,3128T3129,TR,0,3127
GR,3130,,969,161.550,5.663
GR,3132,TR,0,3130
GR,3135,,987,170.909,5.148
GR,3136/3137,TR,0,3135
GR,3138,,987,176.925,4.446
GR,3139/3140,TR,0,3138
GR,3144,,1004.98,176.925,4.818
GR,3145T3147,TR,0,3144
GR,3105,TR,0,3117
GR,3104,TR,0,3078
GR,3100,,951,174.98132,3.51424
GR,3101,,969,184.3406786,2.99993
GR,3102,,987,170.90904,5.14861
GR,3103,,1004.98,180.25799,4.63487
SET,NL,0
PA,1,Q,,3151/3153/3162/3157
PA,2,Q,,3147/3149/3153/3151
PA,3,Q,,3134/3137/3154/3101
PA,4,Q,,3121/3132/3101/3100
PA,5,Q,,3104/3117/3100/3119
PA,6,Q,,3089/3091/3148/3145
PA,7,Q,,3075/3077/3090/3087
PA,8,Q,,3050/3052/3076/3073
PA,9,Q,,3038/3041/3051/3049
PA,10,Q,,3013/3014/3041/3038
PA,11,Q,,3102/3150/3156/3155
PA,12,Q,,3085/3088/3103/3136
PA,13,Q,,3071/3074/3086/3083
PA,14,Q,,3030/3037/3072/3066
PA,15,Q,,3011/3012/3037/3030
PA,16,Q,,3130/3130/3135/3133
PA,17,Q,,3118/3118/3130/3122
PA,18,Q,,3125/3129/3135/3130
PA,19,Q,,3112/3116/3130/3118
PA,20,Q,,3081/3084/3127/3124
PA,21,Q,,3070/3069/3082/3080
PA,22,Q,,3029/3027/3063/3065
PA,23,Q,,3010/3008/3027/3029
PA,24,Q,,3067/3068/3114/3110
PA,25,Q,,3054/3097/3105/3078
PA,26,Q,,3028/3026/3062/3064
PA,27,Q,,3009/3007/3026/3028
PA,28,Q,,3022/3025/3061/3059
PA,29,Q,,3005/3006/3025/3022
PA,30,Q,,3018/3021/3058/3056
PA,31,Q,,3003/3004/3021/3018
PA,32,Q,,3044/3047/3055/3053
PA,33,Q,,3015/3017/3045/3043
PA,34,Q,,3001/3002/3017/3015
END
2
1
2
GF,P1T34,,2/2,,,3001
END
2
2
CF,P1T15,QUAD,,13,3001
CF,P16T17,TRI,T1,13,3016
CF,P18T34,QUAD,,13,3018
END
8
4
1
LOWER HEAT SHIELD --LOHESH--
N
5
```

Table 4.6: PATRAN-G Directives for the Construction of the Upper Heat Shield.

```
GO
1
1
2
VI
2
0,0,-90
GR,1,,904,44.5,-11.573
GR,200,,1016,208.779,-1.657
WI
4
7
PL
GR,2,TR,5,1
GR,4,TR,27,1
GR,6,TR,45,1
GR,8,TR,67,1
GR,10,TR,85,1
GR,12,TR,107,1
GR,14,TR,112,1
GR,3T13B2,TR,0,2T12B2
GR,86T99,TR,0/9.5,1T14
GR,31,,904,73.797,-10.485
GR,32,TR,0,31
GR,33T35,TR,5,32/32/32
GR,36T38,TR,20,33T35
GR,39T41,TR,22,36T38
GR,42T44,TR,18,39T41
GR,17,,991,73.797,-10.485
GR,15,,991,54,-11.573
GR,16/18,TR,0,15/17
GR,45/46,TR,42,42/43
GR,47T48,TR,5,45/46
GR,219,,969,88.421,-9.681
GR,62,,904,103.327,-8.862
GR,64T66,TR,7,62/62/62
GR,67T69,TR,18,64T66
GR,70T72,TR,22,67T69
GR,73T75,TR,18,70T72
GR,207,,991,101.327,-8.862
GR,208,TR,0,207
GR,56,,991,88.421,-9.681
GR,57T59,TR,0,56
GR,76,,1011,101.327,-8.862
GR,78/79,TR,5,76/76
GR,80,,929,113.831,-8.285
GR,81/82,TR,0,80
GR,83T84,TR,22,80/81
GR,101,,904,127.752,-7.520
GR,19,,911,131.39175,-7.320169
GR,20/21,TR,0,19
GR,108,,929,130.069,-7.393
GR,111,,951,132.665,-7.250
GR,114/115,TR,18,111/112
GR,112,TR,0,111
GR,22,,929,140.7511,-6.805854
GR,121,,951,139.271,-6.884
GR,130,,969,150.015,-6.296
GR,131T133,TR,0,130
GR,136,,991,147.579,-6.430
GR,137T139,TR,0,136
GR,60,,1011,88.421,-9.681
GR,61,TR,0,60
GR,140/141,TR,25,136/137
GR,142,,904,142.128,-5.840
GR,149,,929,147.482,-6.019
GR,148,,904,150.543,-4.857
GR,151,,929,157.93,-4.799
GR,24,,951,152.1903,-6.1772
GR,27,,951,157.930,-5.5066
GR,26,,929,163.5421,-4.1428
GR,25/28,TR,0,24/27
GR,157,,951,166.556,-4.499
GR,160,,951,174.982,-3.514
GR,162,,969,161.55,-5.663
GR,163/170,TR,0,162
GR,164,,969,166.556,-5.078
GR,105,,991,159.992,-5.748
GR,134,,991,172.9889,-5.0343
GR,107/215,TR,0,134
GR,185,,991,184.431,-3.697
GR,187,,1009,169.546,-5.223
GR,104,,1016,168.2071,-5.2971
GR,196,,1011,196.181,-2.969
GR,198,,1016,196.181,-3.129
GR,29,,969,184.3407,-2.9999
GR,30,,991,195.7799,-2.3713
GR,103,,1011,206.1792,-1.7999
GR,194,,1011,183.3882,-4.4629
GR,193,,1016,185.988,-4.320
GR,171,,969,176.971,-3.8610
GR,172,TR,0,171
GR,216,TR,0,24
GR,220/63/77/102,TR,0,219/62/76/101
GR,109/23/122,TR,0,108/22/121
GR,143/150/158/161,TR,0,142/149/157/160
GR,165/106/135/186,TR,0,164/105/134/185
GR,188/195/197/199,TR,0,187/194/196/198
GR,225/152,TR,0,194/151
PA,1,Q,,196/103/200/199
PA,2,Q,,185/30/103/195
PA,3,Q,,171/29/30/215
PA,4,Q,,158/161/29/165
PA,5,Q,,225/197/198/193
PA,6,Q,,135/135/186/225
PA,7,Q,,135/135/194/188
PA,8,Q,,170/170/172/134
PA,9,Q,,170/170/134/106
PA,10,Q,,25/25/162/132
PA,11,Q,,25/157/164/162
PA,12,Q,,187/194/193/104
PA,13,Q,,139/107/104/141
PA,14,Q,,208/137/140/79
PA,15,Q,,59/208/76/61
PA,16,Q,,45/77/78/48
PA,17,Q,,16/57/60/97
PA,18,Q,,11/96/97/12
PA,19,Q,,98/46/47/99
PA,20,Q,,13/98/99/14
PA,21,Q,,133/163/105/138
PA,22,Q,,220/131/136/58
PA,23,Q,,43/219/56/18
PA,24,Q,,94/43/17/15
PA,25,Q,,9/94/95/10
PA,26,Q,,112/24/130/115
PA,27,Q,,72/111/114/75
PA,28,Q,,41/71/73/44
PA,29,Q,,92/40/42/93
PA,30,Q,,7/92/93/8
PA,31,Q,,151/126/160/28
PA,32,Q,,143/148/26/150
PA,33,Q,,22/152/27/216
PA,34,Q,,22/22/216/122
PA,35,Q,,21/21/22/109
PA,36,Q,,102/142/149/22
PA,37,Q,,82/23/121/84
PA,38,Q,,38/81/83/39
PA,39,Q,,90/38/39/91
PA,40,Q,,5/90/91/6
PA,41,Q,,66/20/108/69
PA,42,Q,,63/101/19/65
PA,43,Q,,32/62/67/37
PA,44,Q,,88/34/36/89
PA,45,Q,,3/88/89/4
PA,46,Q,,86/31/33/87
PA,47,Q,,1/86/87/2
END
2
1
GF,P1T47,,2/2,,,3501
END
2
2
CF,P1T5,QUAD,,13,3101
CF,P6T10,TRI,T1,13,3106
CF,P11T33,QUAD,,13,3111
CF,P34/35,TRI,T1,13,3134
CF,P36T47,QUAD,,13,3136
END
8
4
1
UPPER HEAT SHIELD --UPHESH--
N
5
```

4.5 THE INSULATION BLANKET

The surface panels between the leading edges and the 30% chord are insulated with a metallic blanket, made from 0.008 cm (0.003 inch) thick Inconel*-foil-encapsulated Microquartz* insulation. The thickness of the Microquartz is 0.3175 cm (0.125 in.). At first it was planned to represent the insulation like the construction pictured in Figures 4.11(a) and 4.11(b). Besides radiation heat transfer between the outside of the foil and the heat shield/surface, there is radiation between the top foil layer and the insulation blanket. Heat transfer by conduction is assumed to take place through the insulation material and the bottom foil layer. Because of obtaining unstable temperatures, which were attributed to the small thickness of the foil elements, this insulation model was modified. The internal radiation inside the insulation was deleted, as were the foil elements; and the properties of the remaining layer of insulation were adapted to take into account the changed model (see also Section 4.8). Figure 4.11(c) displays the final modeling of the insulation.

4.6 THE RADIATION ELEMENTS

To implement the contribution of radiation in the heat transfer within the structure, NASTRAN requires the use of a set of CHBDY cards, describing the location and orientation of the elements involved in the radiation, and the radiation exchange coefficient matrix or "radmatrix."

---

*Reference 4

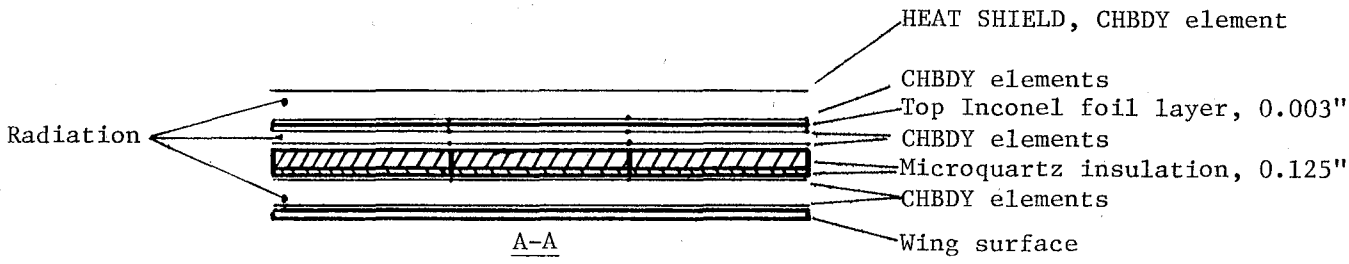

(a) First representation of insulation blanket

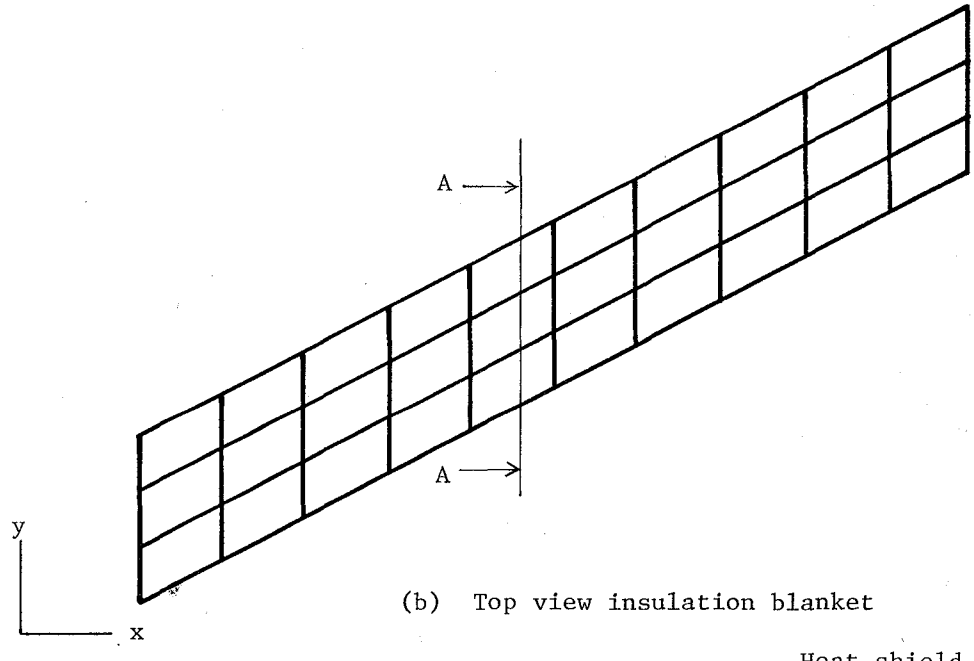

(b) Top view insulation blanket

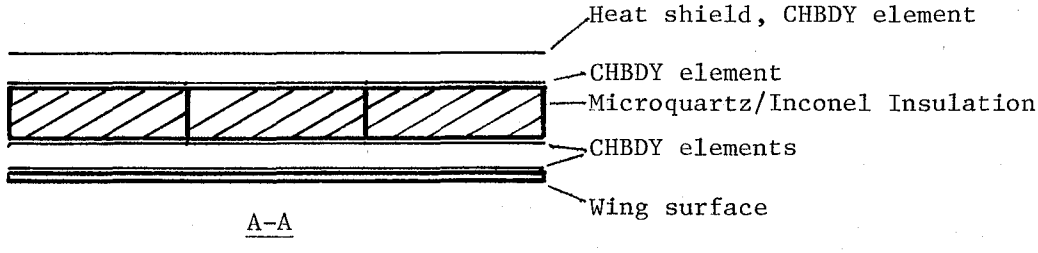

(c) Simplified representation of insulation blanket

Figure 4.11: Construction of Insulation Blanket.

This radmatrix, in combination with the elements listed on the RADLST card, defines the geometric view factors for each radiation element; and it will be discussed in more detail in Section 4.7. The size of each radiation (CHBDY) element was equal to the size of its corresponding plate element. The radiation elements on the heat shields have the size of the heat zones which they represent, except where it was necessary to split the elements due to presence of two different planes. Because PATRAN-G is not capable of generating CHBDY elements, it was necessary to obtain them by a conversion process from structural elements like the QUAD4 and TRIA3 elements. Existing plate elements in the wingbox were first copied and then converted with the help of a text editor and/or a simple Fortran program, CHANGE. In the case of the heat shields, the plate elements created by PATRAN-G were directly converted.

Besides the radiation within the bays of the wingbox, most of the radiation took place between the hot heat shields and the beaded panel surfaces or the insulation of the wingbox. During the tests the sides of the HWTS were closed with thermal curtains to keep the heat inside. To prevent the mathematical model's energy being lost to the surrounding space (with absolute zero temperature), special curtain elements were used. These curtain elements were CHBDY elements connected to the edges of the heat shields and wingbox (or between edges of insulation blanket and shield/surface). For simplification, a curtain element was also placed along the 30% chord line connecting the heat shield and wingbox for each side of the HWTS. It was assumed that no radiation would take place between the root part of the shield

before the 30% chord and the wingbox/insulation between leading edges and 30% chord line, and vice versa. The curtain elements have an emissivity value of zero and no mass, so that no heat from the shields would conduct to the wingbox.

In total, 1896 CHBDY elements were used for the radiation: 1185 for the internal wing bays, 348 for upper heat shield and upper surface of the wingbox, and 363 for the lower heat shield and lower surface of the wingbox radiation.

4.7 THE RADIATION EXCHANGE COEFFICIENT MATRIX, RADMTX

The coefficients in this matrix determine, for each element participating in the radiation exchange, how much of the area of another element will "see" that element. In other words, each term j of column i represents the view factor $F_{i \to j}$ (= percentage of area of element i that will see element j) from element i to element j multiplied by the area of element i, A_i. From the reciprocity theorem stating that $A_i F_{i \to j}$ is equal to $A_j F_{j \to i}$, it follows that the radmatrix in this form is a symmetric one. In NASTRAN the RADMTX cards represent the columns of the lower left triangle of the symmetric radiation exchange coefficient matrix. The RADLST cards list the identification numbers of all the CHBDY elements which participate in the radiation, in the order of the columns of the radmatrix.

The VIEW program has been developed especially for the computation of these view factors, and its output is directly compatible with the NASTRAN thermo analyzer program. The program permits computation of

the view factors between surfaces, taking into account the presence of any intermediate surfaces ("shading"). VIEW also computes these view factors either by contour intergration or by finite-difference (double summation) methods. The first method is more accurate, but the second method is faster. Either method may be selected; or a criterion based on the ratio of area and distance between the geometric center of the subelements may be specified, which causes the program to select the best method based upon the geometry of the problem. The user can define on $VIEW cards the desired mesh size of each element for the internal computation and can set flags to indicate whether the element can shade and/or can be shaded or not. A wise use of these flags can save computer time, but it is still possible with a control card to overwrite these flags or set the mesh size to 1 by 1 for a quick first check. The computed view factors are printed out on an element-to-element basis, along with the area of each element and the total sum of the view factors of all the elements seeing that element. The user can call for the program to produce output, punched or on file in the form of RADMTX and RADLST cards, that can be used directly as input for the NASTRAN program.

Although the user can specify the elements that can shade and/or can be shaded to save computer time, the process of determining which elements are shading and by how much will still result in very long CPU times for such a large and complex model as this. As it was not possible to run the VIEW program in one run within the available core size and time limits, the CHBDY elements were divided into separate groups. Figure 4.12 shows the various groups of the thermal elements.

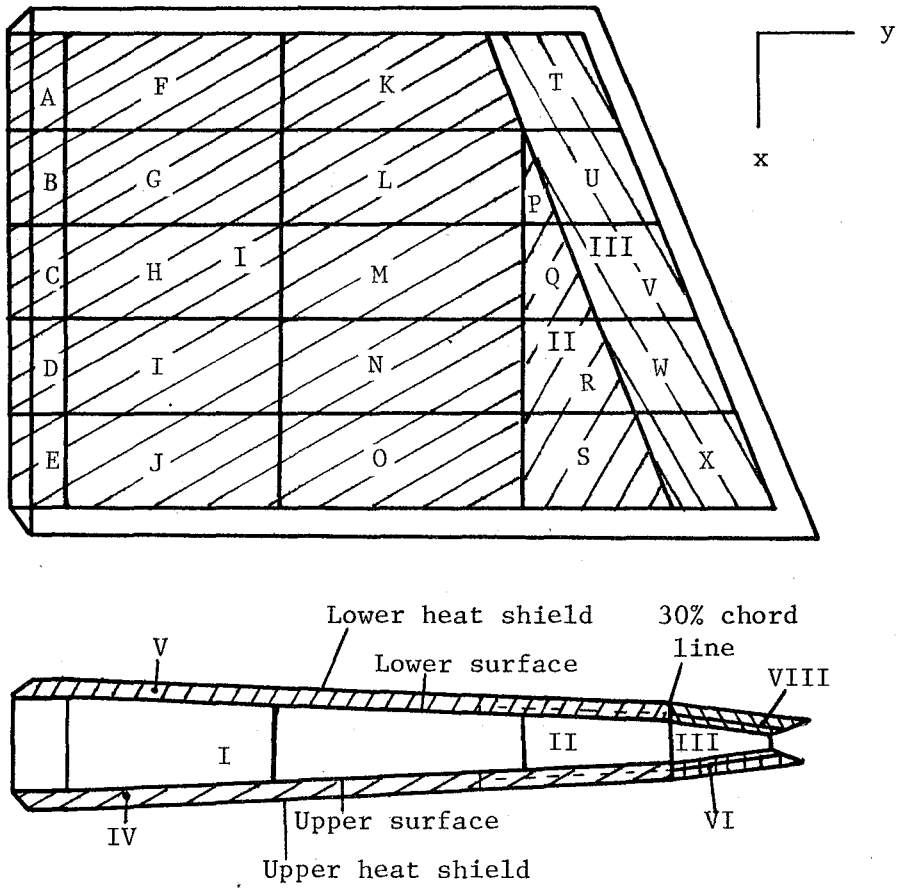

Figure 4.12: Subdivision of CHBDY Elements

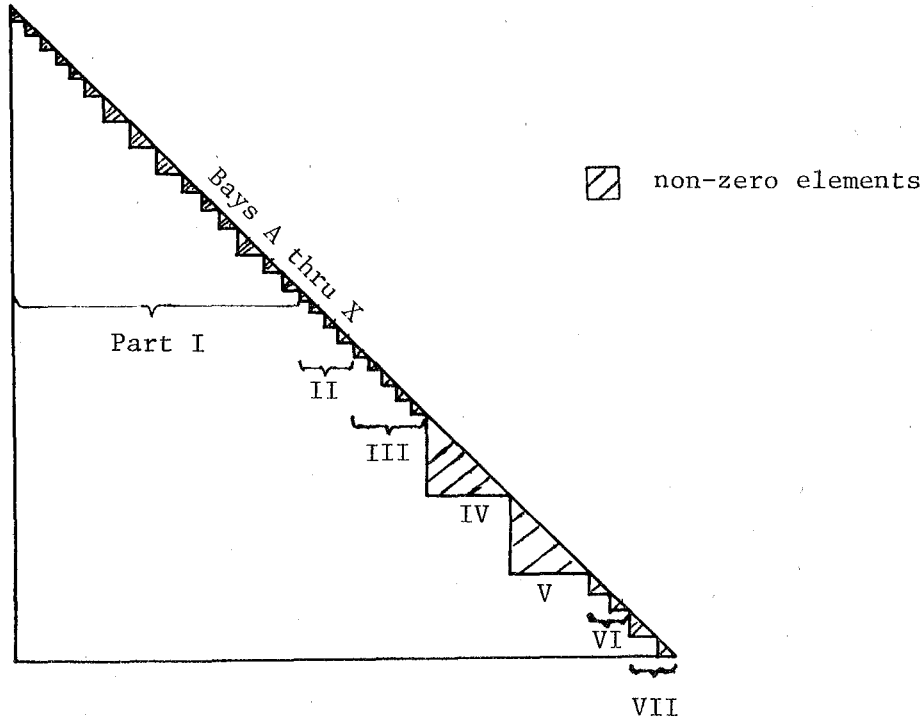

Figure 4.13: Lower Triangle of RADMATRIX, Position of Non-zero Viewfactors.

Groups one through three consist of the internal bays of the wingbox. For each unique bay of the wingbox (14 of the 24 total), a separate run of the VIEW program was made and used for the similar bays. Groups 4 and 5 contained the thermal elements of the upper and lower heat shield before the 30% chord line, respectively, and their corresponding elements on the wing surface. Groups 6 and 7 deal with the thermal elements of the heat shield, the insulation, and the surface between leading edge and the 30% chord line. Each group or subgroup consists of elements which cannot shade other elements, so that the VIEW program could run without the time-consuming and expensive shading calculations.

During the computations of the view factors, several discrepancies and problems were experienced with the VIEW program. These problems were related to the accuracy of the used approximation methods and the properties of the VIEW elements. They will be discussed in more detail together with some solutions in Chapter 6.

Two Fortran programs, MERGE and INVERT, were written to merge all the computed matrices into one large matrix called the radiation exchange coefficient matrix. To obtain the most efficient form of this matrix, the groups of CHBDY elements were chosen in such a way that most of the nonzero values of the matrix were located in the upper part of the lower matrix triangle. The program MERGE also deleted all of the last zeros at the end of each RADMTX card (see also Figure 4.13).

It was thought that a correction factor had to be applied to the view factors of the elements on heat shield and wing surface because of the representation of wing surface as flat elements instead of beaded or curved elements. Instead of applying the correction factor

to the view factors, it is much easier to apply it to the emissivity factor of the thermal elements involved. Figures 4.14 and 4.15 present the used test models RESURF and SISURF, successively, to determine the influence of the flat versus the beaded representation of the panel elements. In RESURF the beaded form of a half panel is simulated with flat elements, while in SISURF the flat panel model is represented. In both cases the heat shield is simulated by flat elements, although in reality the heat shield is slightly corrugated. From comparison of the computed view factors, it was found that almost the same amount of energy coming from the heat shield will be collected by the surface elements in each case. A comparison of the resulting temperature distribution over the surface elements was not very conclusive, due to a non-uniformity of the temperature distribution. It was, therefore, decided that no correction factor had to be applied.

4.8 MATERIAL PROPERTIES AND DIMENSIONS

Values for the temperature-dependent thermal conductivity, k, were derived from Reference 12 for René 41 and from Reference 13 for the insulation material. NASTRAN, however, does not update the conductivity and capacity values at each time step; and the time-dependent values provided for k are used only in combination with an estimated temperature, given at the start of the program.

From Reference 13 an emissivity value of $\varepsilon = 0.8$ was determined for René 41. The total emissivity (for parallel plates) then became definable according to the following equation:

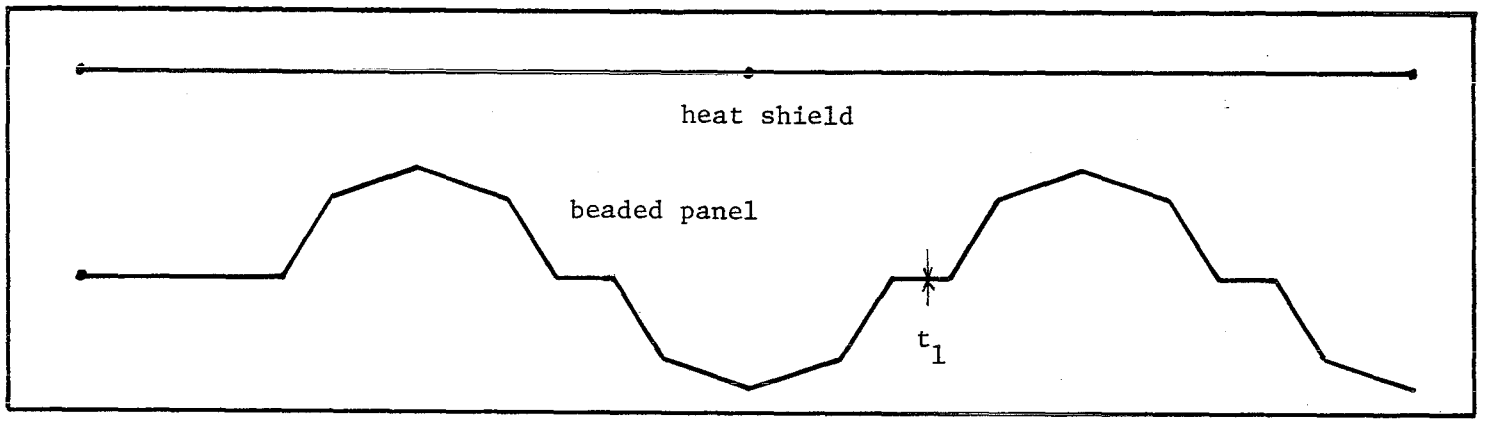

Figure 4.14: RESURF, NASTRAN Computer Model of a Half Size Beaded Panel and Heat Shield.

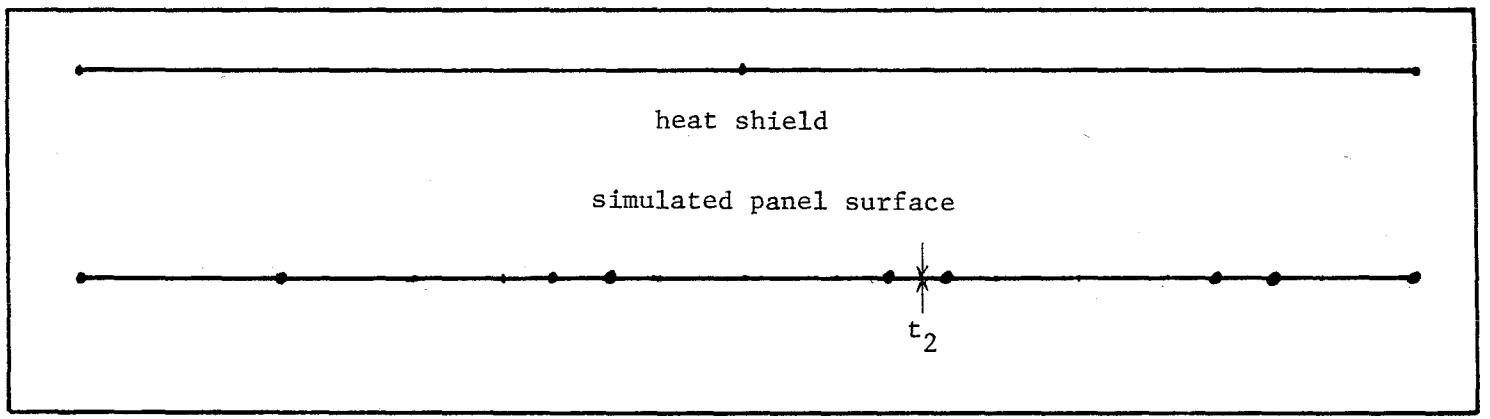

Figure 4.15: SISURF, NASTRAN Computer Model of Half Size Beaded Panel and Heat Shield, as Simulated in Thermal Model.

$$\varepsilon_t = \frac{1}{1/\varepsilon_1 + 1/\varepsilon_2 - 1} = 0.667,$$

where $\varepsilon_1 = \varepsilon_2 = 0.8$

Because of the change in the representation of the insulation blanket (see Figures 4.11[a] and 4.11[c]), the emissivity factor for the radiation elements at both sides of the insulation blanket was modified. A two-dimensional analysis using a Lockheed Thermo-Analyzer program indicated a new value for ε of 0.126 to compensate the loss of the radiation inside the insulation blanket. The dark discoloration of the foil as a result of the heat experienced was another reason for this low emissivity value.

Dimensions of the HWTS and the various parts of it were taken from the detailed drawings accompanying the HWTS. Direct measurements from the thickness of the webs, caps, and heat shields, and data determined for the beaded panel from Reference 4 indicated variations in the specified values up to ten percent. The measured values were used in all analyses of this project.

4.9 SUMMARY OF THE GENERATION OF THE THWTS MODEL

In the earlier sections, the generation of several components of the thermal model of the HWTS was described. Figure 4.16 shows the flowchart of the generation of this model. The individual components are

UPHESH: upper heat shield,

LOHESH: lower heat shield,

UPSURF: upper surface of wingbox,

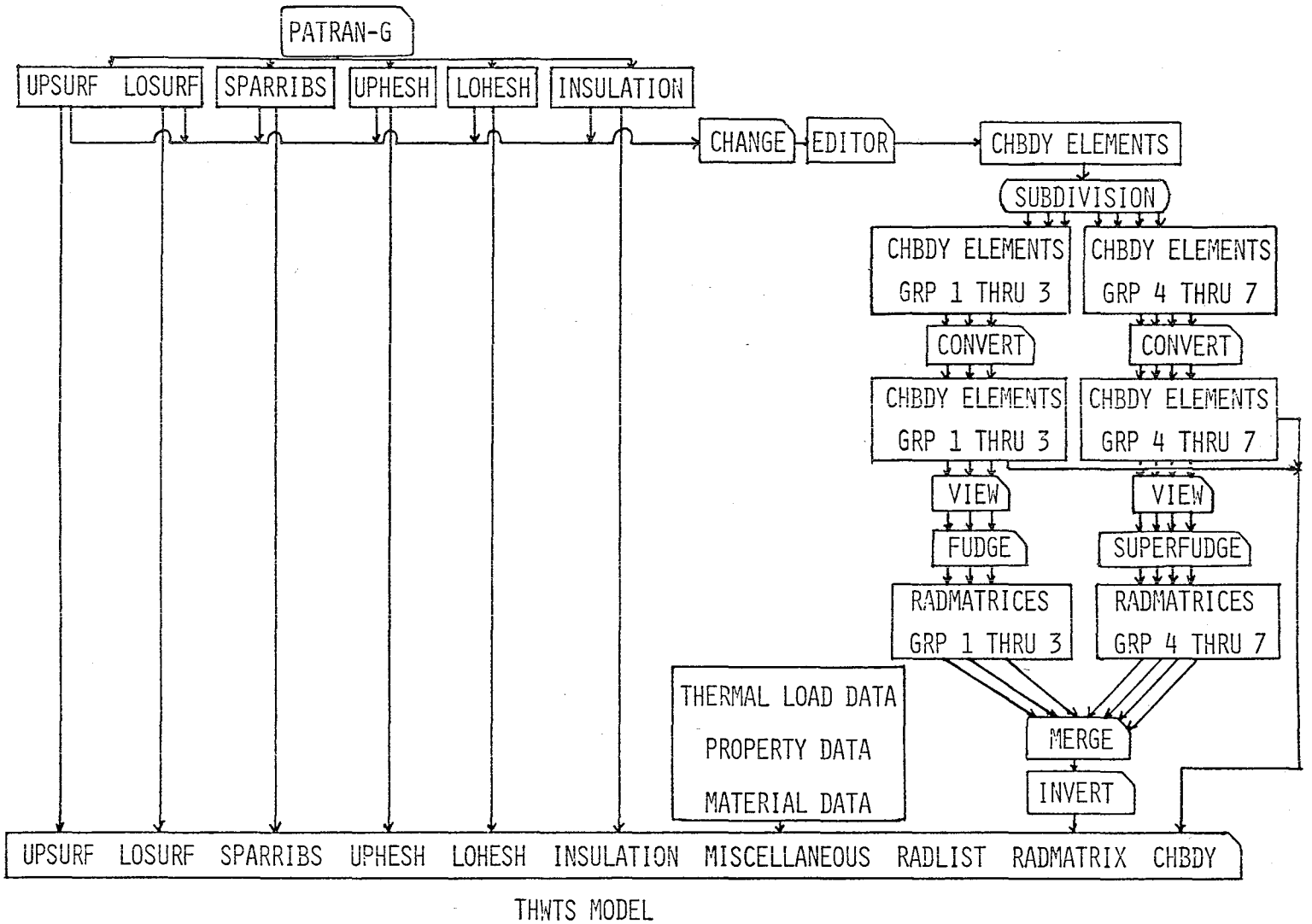

Figure 4.16: Flow Chart of the Generation of the THWTS Model.

LOSURF: lower surface of wingbox,

SPARRIBS: webs and caps of the spars and ribs in wingbox,

INSULATION: insulation blanket between 30% chord line and leading edge.

Each of these submodels could be generated by the PATRAN-G finite-element-generating program. The thermal radiation elements, CHBDY, could not be generated by this program but were converted with the help of the text editor from conventional plate elements, either specially generated (heat shields) or already existing (wingbox and insulation).

Thermal load, material, and property data were generated by a combination of PATRAN-G, small Fortran programs, and manual input.

The radiation exchange coefficient matrix was generated by the VIEW program in combination with several Fortran support programs. These programs--CONVERT, (SUPER)FUDGE, MERGE, and INVERT--were developed to cope with the deficiencies experienced in VIEW. They are discussed in more detail in Chapter 6 and are also listed in Appendix C.

4.10 THE THERMAL QUARTER BEADED PANEL MODEL, TBPQTR

It was necessary to use in the structural analysis a more detailed model of a quarter beaded panel. To include the thermal load in this SBPQTR model, an identical but thermal model of the quarter beaded panel called TBPQTR was developed. Figure 4.17 shows the view of this model. It consists of 433 plate and bar elements, and 433 grid points (433 degrees of freedom). The details of the beaded quarter panel model are discussed in Section 5.3. Enforced temperatures applied by

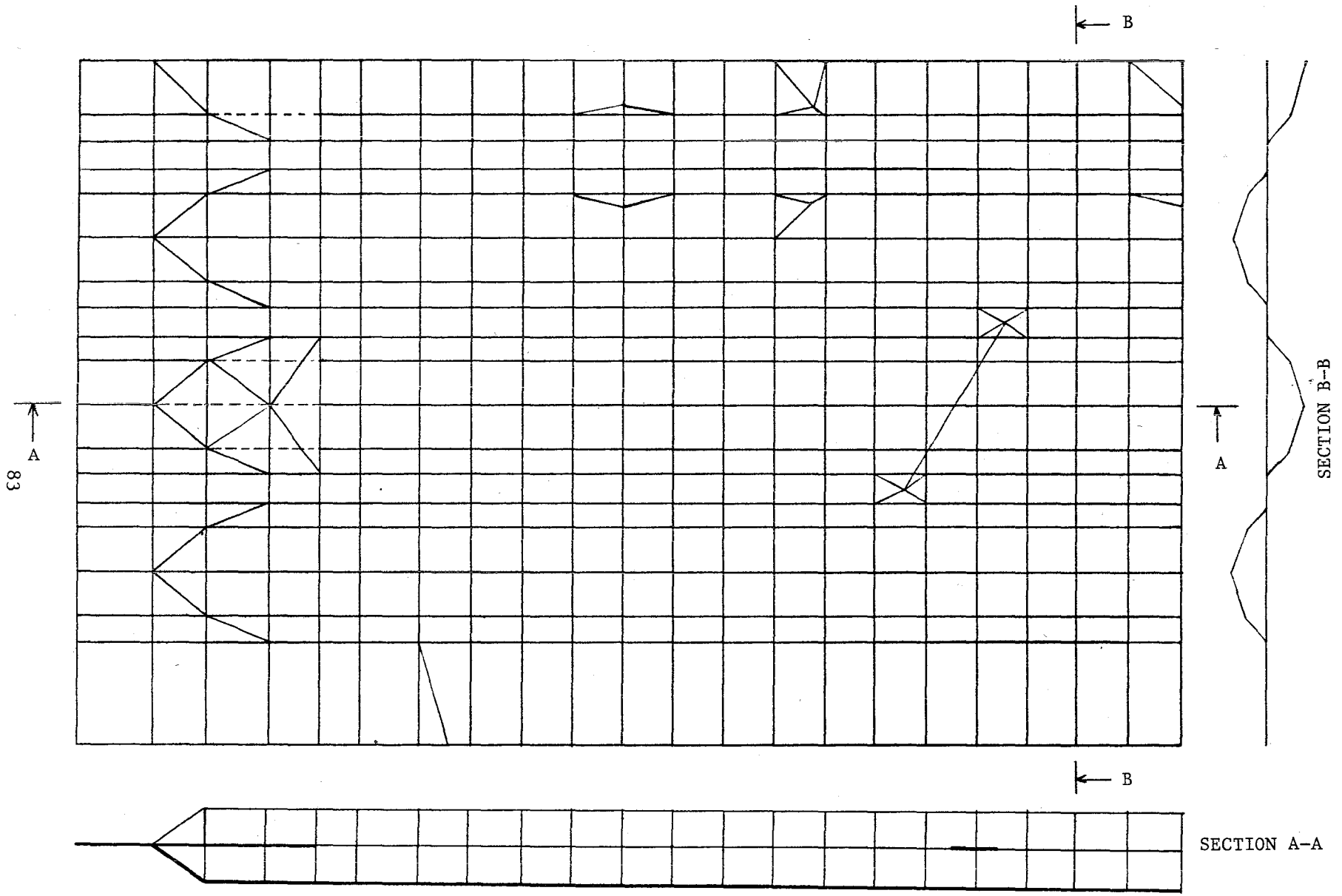

Figure 4.17: NASTRAN Thermal Quarter Beaded Panel Computer Model, TBPQTR.

the method described in Table 4.3 in this model will generate the rest of the temperature distribution in the panel. The temperatures from the grid points along the outward sides of the quarter panel and from unique points on the panel, corresponding with existing grid points in the THWTS model, are used as input for a Fortran program, TCHANGE, which converts these temperatures into temperature load data for each panel. The TBPQTR program included four subcases, each representing a quarter or one panel. To satisfy the boundary conditions at the cut edges of the panel, an equalizing process of the temperatures along these edges takes place after the first run of the program by the program TEQUIV. The second NASTRAN run of TBPQTR includes the enforced temperatures from along the four edges and from certain points in the model and generates the final temperature distribution in the panel.

CHAPTER 5

THE STRUCTURAL MODELS

5.1 INTRODUCTION

The structural modeling of the Hypersonic Wing Test Structure is based on two NASTRAN models of the structure: a simplified model of the whole structure, called SHWTS; and a more detailed model of a quarter beaded panel, called SBPQTR. The first model is derived from the NWML model from the Martin Marietta company and was used for the design of the structure (Reference 4). The second model is adapted from the model developed by Bill Siegel in his investigation of the buckling behavior of a beaded panel (Reference 6). This second model is used for the structural analysis of the beaded panels, as it was not possible to model these panels in the large NWML or SHWTS models within the limits of the available degrees of freedom. Fortran programs were written to support the different steps. As can be seen in Figure 3.5(b), the structural analysis follows almost the same procedure as the thermal analysis. There is a small difference in the execution of the several programs. In the structural analysis it is possible to run the SBPQTR programs for several panels at the same time. In the thermal analysis, each panel has to be run in separate cases.

5.2 THE SHWTS MODEL

For the development of the structural model of the HWTS structure, the basic plan of the THWTS model was used with reference to the numbering and sequencing of the grid points and elements. The main reasons

were the desired compatibility between the heat transfer and the structural models. The THWTS model referred to in this chapter is that of the first attempt. To implement the structural analysis as described in Chapters 3 and 5, a simple computer program has to be developed that correlates the output of the new thermal model with the input.data of the SHWTS and SBPQTR models.

Flat elements represent the corrugated/beaded parts of the structure because of the impractical number of degrees of freedom needed for a more explicit geometrical representation. However, the SHWTS model was improved, compared to the NWML model, by (1) representation by more elements closer to the actual dimensions, (2) representation by elements with better structural properties, and (3) a more accurate and more detailed input of the thermal load.

Actual thicknesses for the webs, the caps, and the various parts of the beaded panels were used. The data were obtained from the measurements of Siegel, Reference 6, and by the author. A total of 623 plate bending elements, 325 bar or rod elements, and 309 grid points were used for the main wing structure, compared to 143, 177, and 68, respectively, for the NWML model. The support structure was copied directly from the NWML model and consisted of rod elements.

In the NWML model, the beaded panels were modeled as four overlapping triangular membrane elements. Because the bending loads normally carried by the spars are carried by the beaded panels in the hypersonic research airplane, these panels were designed to handle local plate bending. The membrane elements from the NWML model are not designed for bending loads perpendicular to the plane. The SHWTS

model (and the SBPQTR model) uses QUAD2 or TRIA1 elements, which are developed for combined membrane and plate bending.

The thermal program THWTS provides the temperature load data for each grid point in the structural model. It was intended to use the interpolated values of the measured data as input for the NWML model. Obviously, this is a crude approximation due to the limited number and the location of the thermocouples (working in the whole range of temperatures).

The elements representing the webs of spars and ribs are modeled as membrane elements of the type QDMEM2 or TRMEM2, while the caps are represented by bar elements.

Values for the temperature-dependent properties of René 41 were derived from Reference 12 and implemented in the model by the use of MATT1 cards. The thermal load was applied through the use of TEMP cards. Application of thermal loads in the structural analysis in NASTRAN, however, is limited to static loading. This means that the structural analysis of the HWTS tests has to be executed for each time step. The mechanical load was introduced by the use of FORCE cards, defining the size and direction of the load at the grid points corresponding to the load points on the HWTS.

Figure 5.1 shows a three-dimensional view of the SWHTS model, while Figures 5.2 and 5.3 show a view of one of the surfaces and an isometric view of the spars and ribs, respectively.

The representation of the beaded panels by flat, coarse elements still did not lead to accurate, direct comparisons with the measured test data, although it was more accurate than the NWML model. The

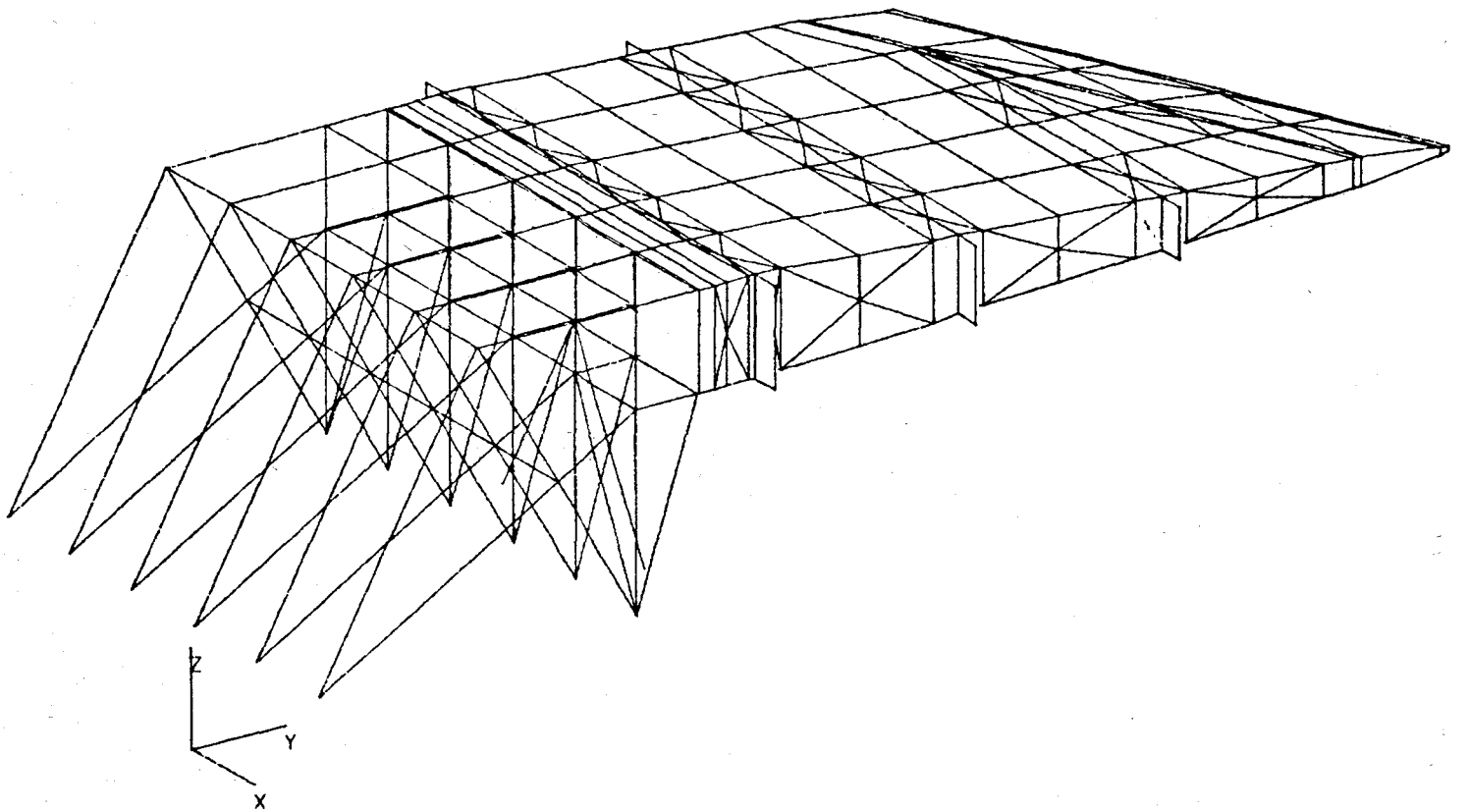

Figure 5.1: SHWTS NASTRAN Structural Model of the HWTS.

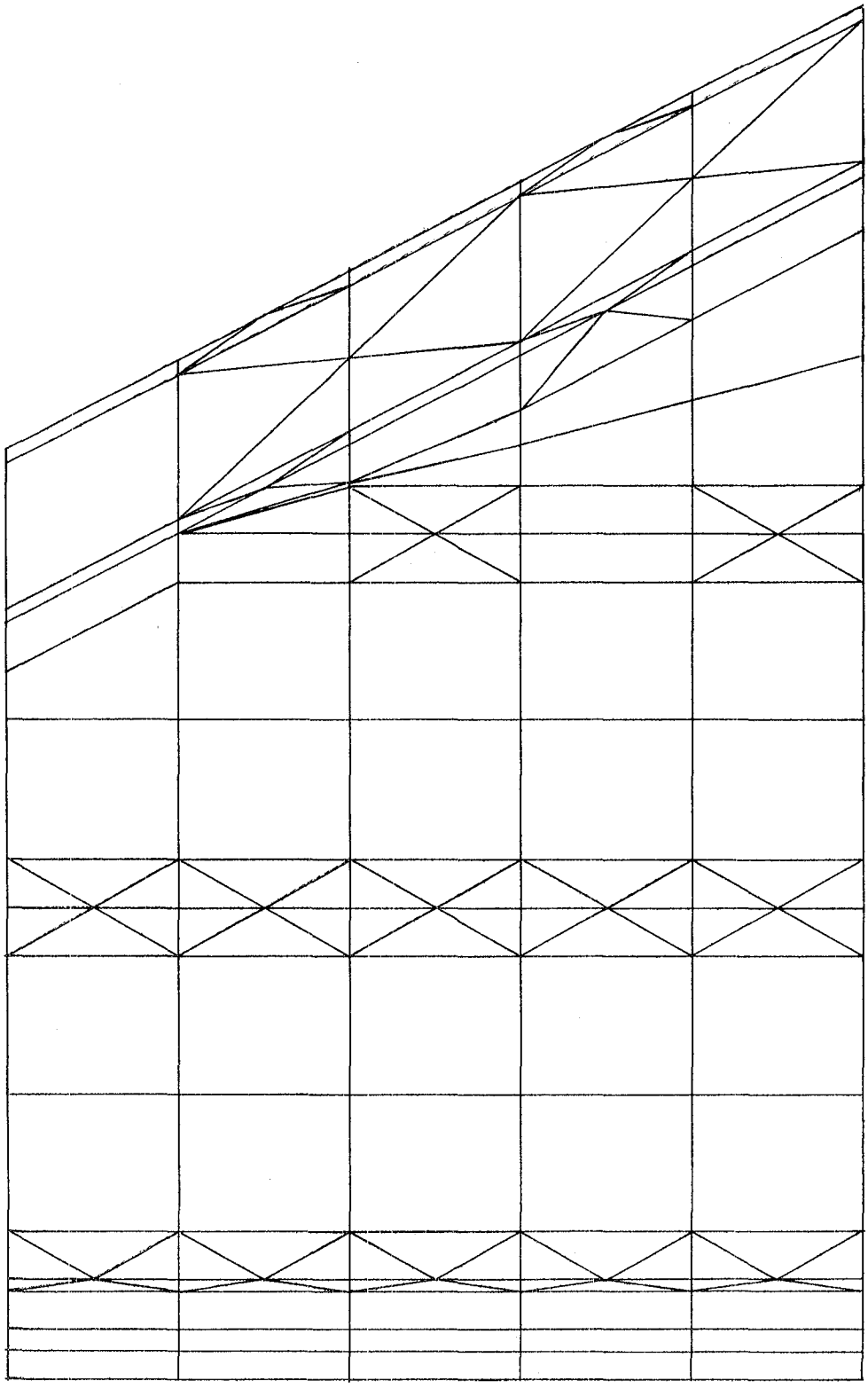

Figure 5.2: Top View of the SHWTS Model.

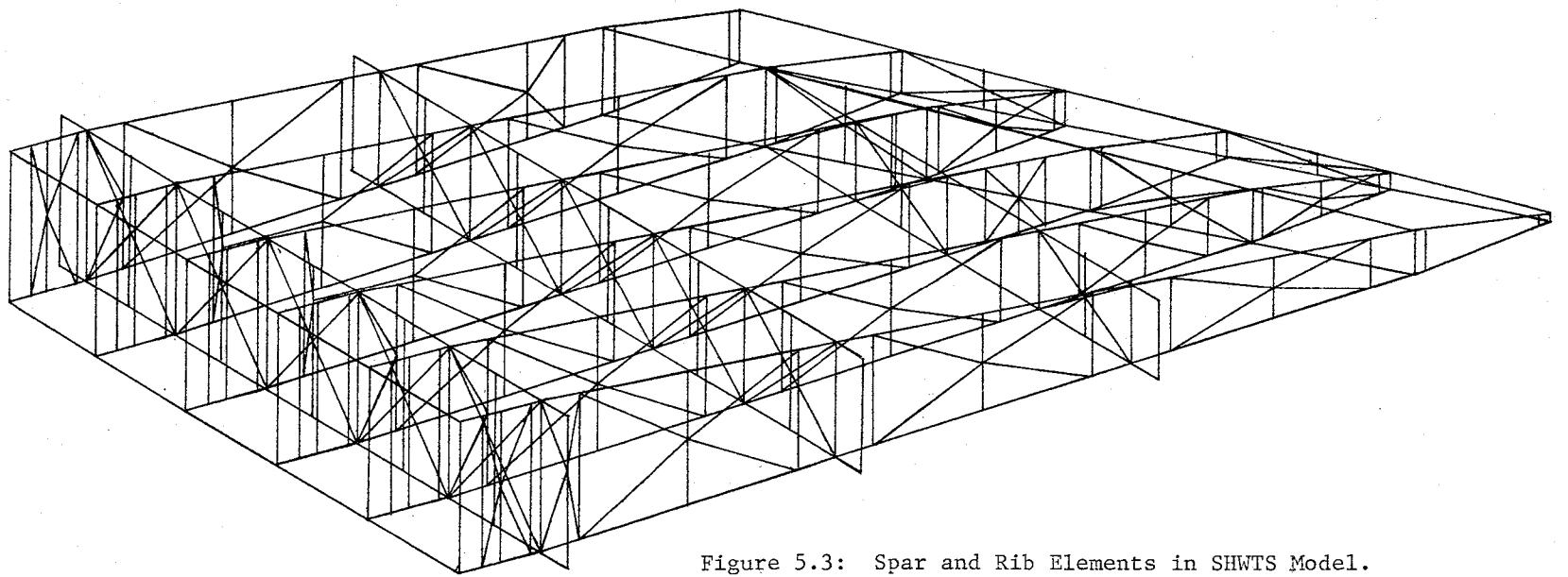

Figure 5.3: Spar and Rib Elements in SHWTS Model.

SBPQTR model was, therefore, developed for a more detailed representation of the beaded panel concept.

5.3 THE SBPQTR MODEL

Figure 5.4 shows a view of the SBPQTR model. It is a quarter panel model and takes advantage of the two lines of symmetry of the beaded panel. It consists of 433 elements, 433 grid points, and 2165 degrees of freedom. It was developed from the NASTR model (Chapter 3) and modified to include the locations of strain gages and thermocouples. Further, actual dimensions were used; and elements for the representation of the doubler plates and heat channels were added. By combining four subcases, the displacement/stress distribution of the whole panel could be obtained. Thermal loads were added using the TEMP cards generated by the TBPQTR model. This latter model is identical to the SBPQTR model and was described in Chapter 4.

For the enforcement of the mechanical load in the quarter beaded panel model, two methods were examined. The first one proceeded from the calculated element forces and the displacements at the common grid points of the edges of the beaded panel and the spar/rib structure in the SHWTS model. Elastic grounded spring elements connected to these grid points in the SBPQTR model simulated the surrounding structure. It was hoped that by applying the mechanical and thermal load for each grid point at the boundary with the proper derived elastic spring rate from the element forces and the displacement, a close approximation of the actual values of displacement and the element forces in the more

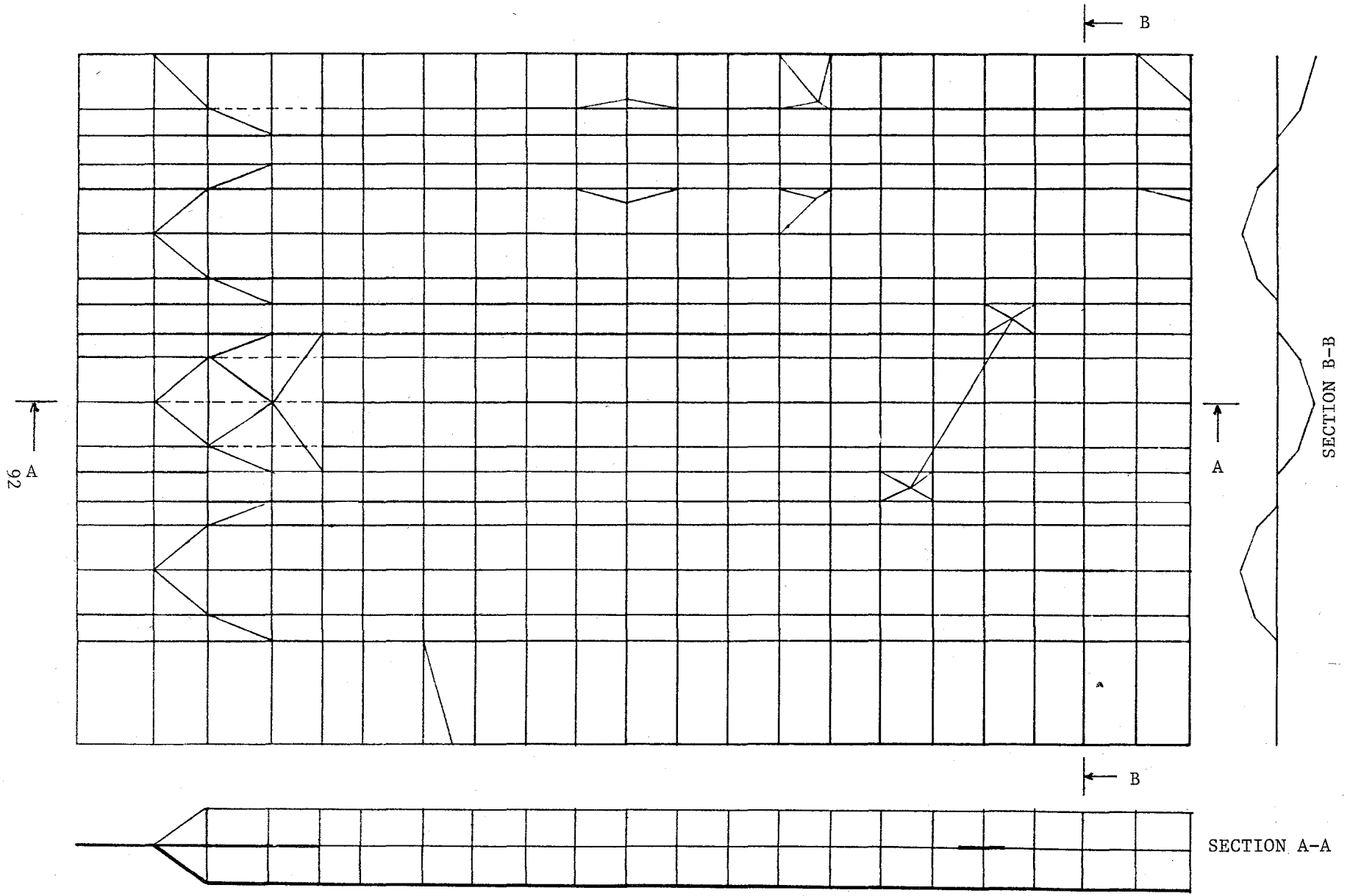

Figure 5.4: NASTRAN Structural Quarter Beaded Panel Computer Model, SBPQTR.

detailed SBPQTR model would be obtained. However, a satisfying correlation with the calculated data in the larger model was not found.

The second method was based on the calculated displacements of the grid points at the edge of the beaded panels in the SHWTS model. In the SBPQTR model, these displacements are enforced on the grid points by means of SPC (single point constraint) cards. This method is the simpler of the two and gave a closer agreement with the calculated element forces in the larger model.

A support computer program, called REDIST, was written to process the displacements from the SHWTS model according to the second method for each of the most critically loaded panels at the root of the wing.

The boundary conditions along the outside edges of the panel were relatively straightforward to define using the second approach, since the panel is attached to spar and rib caps at these boundaries. However, the boundary conditions along the cut edges (lines of symmetry) were not as easy to formulate. A relatively crude but simple solution was found to run the SBPQTR model in two steps. In the first run, the inner edges were free floating, and the displacements for all the grid points on these edges for the four quarter-panel models in the panel (the four subcases) were used as input for a support program. This program, called SEQUIV, equalizes these displacements for each common grid point by an averaging process and converts them into single point constraints. The second run of the SBPQTR program used these SPC cards as well as those derived from the REDIST program as the final boundary conditions for the computation of the stress distributions in the panel.

5.4 SUPPORTING PROGRAMS

As support in the structural analysis, three Fortran programs were developed: REDIST, SEQUIV, and ROSETTE. The first two were written especially for this project, while the ROSETTE program was borrowed from the earlier room temperature test analysis.

The REDIST program took the displacements from the SHWTS model and converted them into single-point constraints for the (outside) boundary conditions for each panel in the SBPQTR program. Before the conversion, it was necessary to transform the values of the displacements expressed in the coordinate system of the SHWTS model into that of the SBPQTR model, where the (quarter) panel lies in the horizontal plane.

SEQUIV processes the displacements at the inner sides of the quarter panels for the generation of the boundary conditions along these edges.

ROSETTE converts the computed stresses of the elements in the panel into strains for direct comparison with the test data. All of these support programs are listed in Appendix C.

CHAPTER 6

COMMENTS ON THE NASTRAN AND SUPPORT PROGRAMS

6.1 INTRODUCTION

During the development of the various models, several errors were discovered in the NASTRAN and VIEW programs. Most of the fatal errors experienced were related to the large size of the thermal model and the required core size for some of the routines in NASTRAN. Other errors were difficult to solve because of misleading messages given by the program. Some deficiencies were found in NASTRAN and in VIEW, and solutions for them were developed or obtained from consultants. This chapter describes the most significant experiences with these errors/deficiencies and their solutions, as well as some new thoughts about the modeling.

6.2 FATAL ERROR MESSAGES IN NASTRAN (COSMIC VERSION)

6.2.1 SYSTEM FATAL MESSAGE 3102, LOGIC ERROR EMA-1264

This error was experienced in the heat transfer application of NASTRAN, rigid format 9, in level 16.0. The functional module EMA stands for element matrix assembler and superimposes matrices corresponding to elements into a structural matrix corresponding to all degrees of freedom at all grid points (Reference 7). The error message was given when the number of elements connected to one particular degree of freedom exceeded the maximum of 19 recorded in this module for at least one grid point. Two grid points suffered this limitation due to their location at the center of five adjacent wing bays (bays K, L,

P, T, and U in Figure 2.14). The solution was to use a newer version of NASTRAN, level 17.6, which has a larger available core size.

6.2.2 SYSTEM FATAL MESSAGE 1159: ROW POSTIONS OF ELEMENTS FURNISHED TO ZBLPKI OR BLDPKI ARE NOT IN A MONOTONIC INCREASING SEQUENCE.

This error message is an example of a disguised data error resulting in a very obscure fatal error message. This error took place in the module GP4 (geometry processor, phase four), which deals with the various displacement sets. A keypunch error resulted in the same grid point ID for the dependent and the independent grid point on a multi-point constraint card.

6.2.3 USER FATAL MESSAGE 3031: UNABLE TO FIND SELECTED SET (11) IN TABLE (PLT) IN SUBROUTINE (TRL6).

This error message was found to be partly incorrect. The message was caused by unintentionally deleting a TLOAD1 card identified by set number 51, which was referred to at the DLOAD card. Set 11 was the first TLOAD1 ID referred to at the DLOAD card. The error message did not increase the set ID during the checking process. This message and the former one will be corrected in the next level of NASTRAN.

6.3 DEFICIENCIES IN (COSMIC) NASTRAN

During the analysis of the thermal model of the quarter beaded panel model, it was observed that the impossibility of using subcases in transient heat transfer analysis would set a limitation on the speed

of generating the temperature of the whole panel. A DMAP alter packet was received from Computer Science Corporation to include the use of subcases in rigid format 9 of the heat transfer application. Table 6.1 is a listing of the necessary cards.

Table 6.1: DMAP Alter Packet to Include Subcases in Transient Heat Analysis (Rigid Format 9)

```
ALTER 107,107 $
PARAM //C,N,MPY/V,N,REPEATT/C,N,1/C,N-1 $
JUMP LOOP $
LABEL LOOP $
CASE CASECC,/CASEXX/C,N,TRAN/V,N,REPEATT/V,N,NOLOOP $
SAVE REPEATT,NOLOOP $
CHKPNT CASEXX $
SDR2 CASEXX,CSTM,MPT,DIT,HEQDYN,HSILD,,,BGPDP,HTOL,HQP,HUPV,HEST,
     XYCDB,HPPO/HOPP1/HOQP1,HOUPV1,,HOEF1,HPUGV/C,N,TRANRESP $
ALTER 151 $
COND FINIS,REPEATT $
REPT LOOP,100$
ENDALTER $
```

However, caution is needed when a restart is used after a premature end of the checkpoint run in one of the modules in the loop. The checkpoint dictionary should include only the cards before the start of the loop (through DMAP sequence number 107).

A more severe deficiency of NASTRAN is that it is not possible to use temperature-dependent material properties directly in transient analysis. Due to the particular structure of the finite-element method used by NASTRAN, nonlinear heat conduction and heat capacity are not permitted. The computational effort required to recalculate the heat conduction and heat capacity matrices at each time step by this method is judged to be excessive. Also, the convective film coefficient, h, cannot be defined as a time-dependent function for the same reason. By using the general-purpose, nonlinear elements, a time-dependent behavior of h can be obtained.

The following procedure is offered to implement the temperature-dependent properties of materials in transient analysis. Based on the (estimated) time-history of the external load and the time steps defined in the program, the program should be divided into several steps. During each step, the reference temperature for the thermal properties should be defined as the best approximation for that time interval. The initial temperatures would be derived from the punched output of the last run. The same procedure can be followed with the coordinates. Based on the computed displacements of the last run of the structural model for the earlier time interval, the initial displacements of each time step could be updated with a simple program, such as NEWGD in Chapter 3. It is obvious that such a procedure will be time-consuming and expensive, especially for such a large and complex model as the HWTS.

Another deficiency in the COSMIC version of NASTRAN was detected during the thermal analysis of bay H, described in Chapter 7. It was found that the program did not compute correctly the capacitance of the

bar elements. For some reason not yet explained, bar elements did not contribute to the thermal capacitance of the grid points associated with these bar elements. When a zero capacitance value was assigned to the bar elements in the MSC NASTRAN bay model, identical temperature-time distributions were computed as in the COSMIC model. This discrepancy in the COSMIC version was reported to the COSMIC organization and will be corrected in the next release.

During the development of the THWTS model, it was found that it was possible to include inadvertently convection in the thermal analysis to scalar points with ambient temperature. This can occur when the property card belonging to the CHBDY elements used for the radiation also contain a reference to a material card with values that could be assumed as convection data. In NASTRAN the presence of this reference on a PHBDY (property card of a CHBDY element) is used as the sole flag for the existence of convection in the analysis. For radiation purposes, NASTRAN requires the absence of a reference to a material card; but this is not clearly stated.

6.4 THE VIEW PROGRAM

During the computation of the view factors, four important problem areas related to the VIEW program were detected. They will be discussed here in the order of sequence.

1. One of the first checks the VIEW program is executing is that of the coplanarity of the CHBDY elements. If the four grid points of a quadrilateral element are not in one plane, VIEW issues the following fatal error message:

Fatal error 10 **** Error in CHBDY card - ****
The four grid points must be in one plane.

It was observed that meeting this requirement in VIEW was more stringent than in NASTRAN. Elements that satisfied the NASTRAN requirements did not necessarily pass the VIEW test. In NASTRAN, the quadrilateral elements are internally composed of four triangular elements, which are obviously co-planar. Even some elements generated completely by the PATRAN-G program were affected by this problem. However, it was also observed that in several cases the fatal error in the VIEW program could be avoided by adding or subtracting 0.0005 inch to the z-coordinate of one of the four grid points.

A special program was written, QUAD, that corrects the z-coordinate of the fourth grid point determined as function of the other elements. Appendix C contains a listing of this HP program. This approach was more suited for the elements at the heat shields because of the lack of common grid points between elements. It was more time-consuming for the elements at the surfaces of the wingbox, where the consequences of each change had to be checked and corrected. Another approach would be to replace all the elements causing fatal error 10 with two triangular elements. In most cases, this will not create additional subelements for the VIEW program because these elements are nonrectangular AREA4 elements which will still be divided into two AREA3 elements by the program. It would, however, affect the efficiency of the NASTRAN program and its development. In the future, it would be wise to

change the value of the criterion in the VIEW program that checks the coplanarity of each AREA4 element.

2. It was observed that the contour integration method, which is considered the most accurate of both available algorithms, computed inconsistent view factors for identical geometrical pairs of elements. For instance, in the case of a simple rectangular box, each wall is modeled as one quadrilateral element. The sidewalls are longer than the top and bottom sides. Figure 6.1 shows the arrangement of this case. When the contour integration method was selected, a different view factor for element 2 to 3, $F_{2\to3}$, was computer than for element 4 to 3, $F_{4\to3}$. Theoretically, $F_{2\to3}$ should be equal to $F_{4\to3}$. This discrepancy could be tracked to an inaccurate computation for $F_{2\to3}$.

The VIEW program computes the view factors for only the lower left triangle of the radiation coefficient matrix. Values for the upper right triangle are derived from the lower triangle using the following relationship:

$$F_{i\to j} \cdot A_i = F_{j\to i} \cdot A_j$$

where $F_{i\to j}$ = view factor of element i to element j,

A_i = area of element i

$F_{j\to i}$ = view factor of element j to element i

A_j = area of element j.

This means, in practice, that only view factors from an element to elements with a higher ID number are computed.

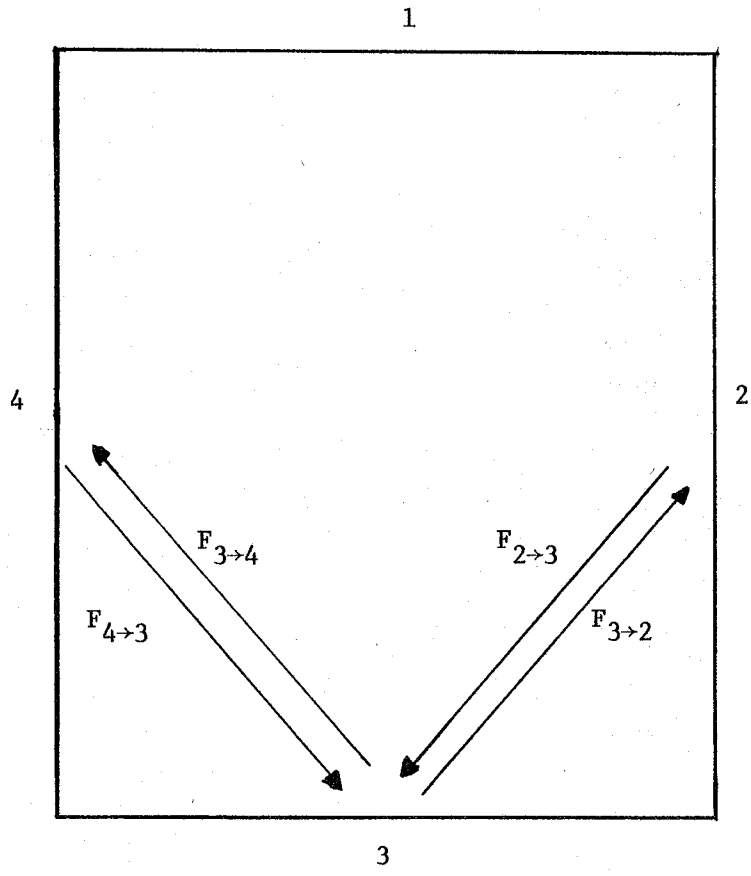

Figure 6.1: Arrangement of Test Case VIEW.

It was found that the contour integration method is not accurate when it has to compute view factors from large to small elements. The finite-difference method does not have this problem. This deficiency in the countour integral method could result in inaccuracies up to twenty percent. The solution was to write a program, CONVERT, that renumbered and resorted the CHBDY elements according to increasing area size. This program is listed in Appendix C. The resulting RADLIST from each run of the VIEW program starts with the smallest element and ends with the largest element, so all the computations are made for small elements to large sized; and all large-to-small view factors are derived from the computed values. An alternative approach would be to use the finite-difference method exclusively, but then inaccuracies would also be gotten due to this method.

3. Because the VIEW program is based on two approximation techniques, the total sum of view factors for an element is not necessarily equal to one. In the case that the computed element sum of view factors is less than zero, energy will be lost into space. In NASTRAN this means that energy will be radiated from an element with a high temperature (up to 1300K at the heat shields) to absolute zero environment. By using "curtain" elements with no conduction and zero emissivity in areas where the structure is open, as in the HWTS between the heat shields and wingbox, this energy loss can be prevented. Of course, a total sum of view factors of less than

one can indicate the existence of one or more elements not defined correctly or missing. The MSC version of NASTRAN on the VAX computer has a built-in feature that prevents this loss, but other versions do not have it.

For the same reason a total sum of the view factors larger than one is also possible. If this occurs, both versions of NASTRAN will issue a fatal error message and terminate the program. Observance of the computed view factor sum showed that in most of the cases the total sum of the view factors for an element with only a small value exceeded the limit value of 1.001 set by NASTRAN. This was primarily the case for the elements in the wingbays. Elements at the upper and lower side of the wingbox (groups IV through VI in Figure 4.10) showed more variance around 1.00. Two programs were written that made adjustments for this to the RADMTX. The first one, FUDGE, was very crude and was applied only to the radmatrices of the wingbays. It divided the elements of the radmatrix by the largest value found for the total sum of view factors. This value was provided by the fatal information message printed out by NASTRAN. FUDGE resulted in values of the total sum of the view factors being between 0.96 and 1.00. The other program, named SUPERFUDGE, was more accurate and also made adjustments upwards when the total sum of view factors was less than 0.97. It was more complex because the brute force approach used in FUDGE does not work well when several values of the sum are high (1.1

or higher). SUPERFUDGE is based on a column-by-column approach and applies a fudge factor, if needed, to each element in the lower part of the matrix while updating the remaining columns. SUPERFUDGE resulted in all the view factors for an element adding to a value between 0.97 and 1.00. Both programs are listed in Appendix C.

4. Inaccuracies in the view factors computed were observed primarily between elements, which were located in corners and at the edges of the structure. Improvements could be made by increasing the number of subelements used in the VIEW program for these elements.

The VIEW program itself is characterized by its requirements for a large core memory and long run times. Especially when shading is involved, the time required for computing view factors for a structure like the HWTS becomes critical. With 1896 elements, it was impossible to run the VIEW program in one trial without exceeding the core memory, time limits, or financial constraints. Despite the subdivision in non-shaded parts, it was still a cumbersome and time-consuming process. Because of the necessity of applying preventive and corrective manipulations to the CHBDY elements and to the output of the VIEW program, unavoidable inaccuracies are introduced; and the whole process of computation of view factors is made more cumbersome. It is recommended that, besides solving the problems encountered in the points described, time and effort also be spent to achieve a faster and more efficient solution method. The use of advanced hidden-line algorithms may be adapted for this purpose.

CHAPTER 7

RESULTS OF THE THERMAL ANALYSIS

7.1 INTRODUCTION

In Chapter 3 the general design for the thermal and structural analysis was described and compared to the existing analysis. As was mentioned in Chapter 4, the development of the thermal model of the wing structure, TWHTS, was done in two phases. As a result, no time was spent on the analysis of the thermal quarter beaded panel model or that of the structural model of the HWTS. This chapter will only discuss the results of the thermal analysis of the HWTS structure.

In Chapter 4, the development of this thermal model was described. Figure 7.1 shows the elements defining the wingbox and the insulation blanket in a hidden-line plot produced by the PATRAN-G program. Figure 7.2 shows the complete structure including the heat shields with the curtain elements. The next sections in this chapter will discuss the results of the different steps in the thermal analysis in more detail.

7.2 THE BAY H ANALYSIS

The first attempts to obtain temperature-time distributions with the THWTS model resulted in very low temperatures due to an unintentional existence of convection in the structure (see Section 6.3). During the process of locating the cause for this problem, a smaller NASTRAN model was derived from the main model. This model was named BAY H and represented the center bay, H, in the wingbox. Figure

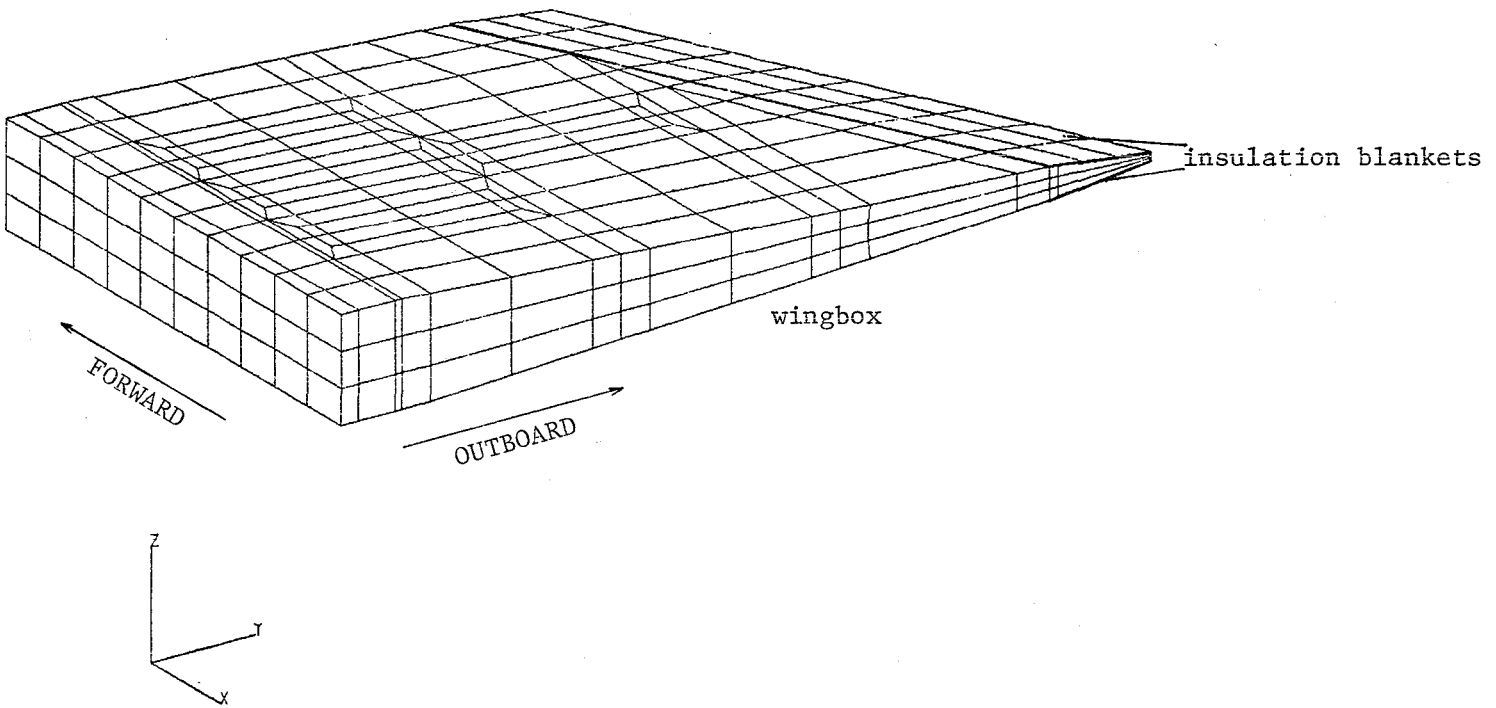

Figure 7.1: PATRAN-G Hidden Line Plot of Wingbox and Insulation Blanket of THWTS Model.

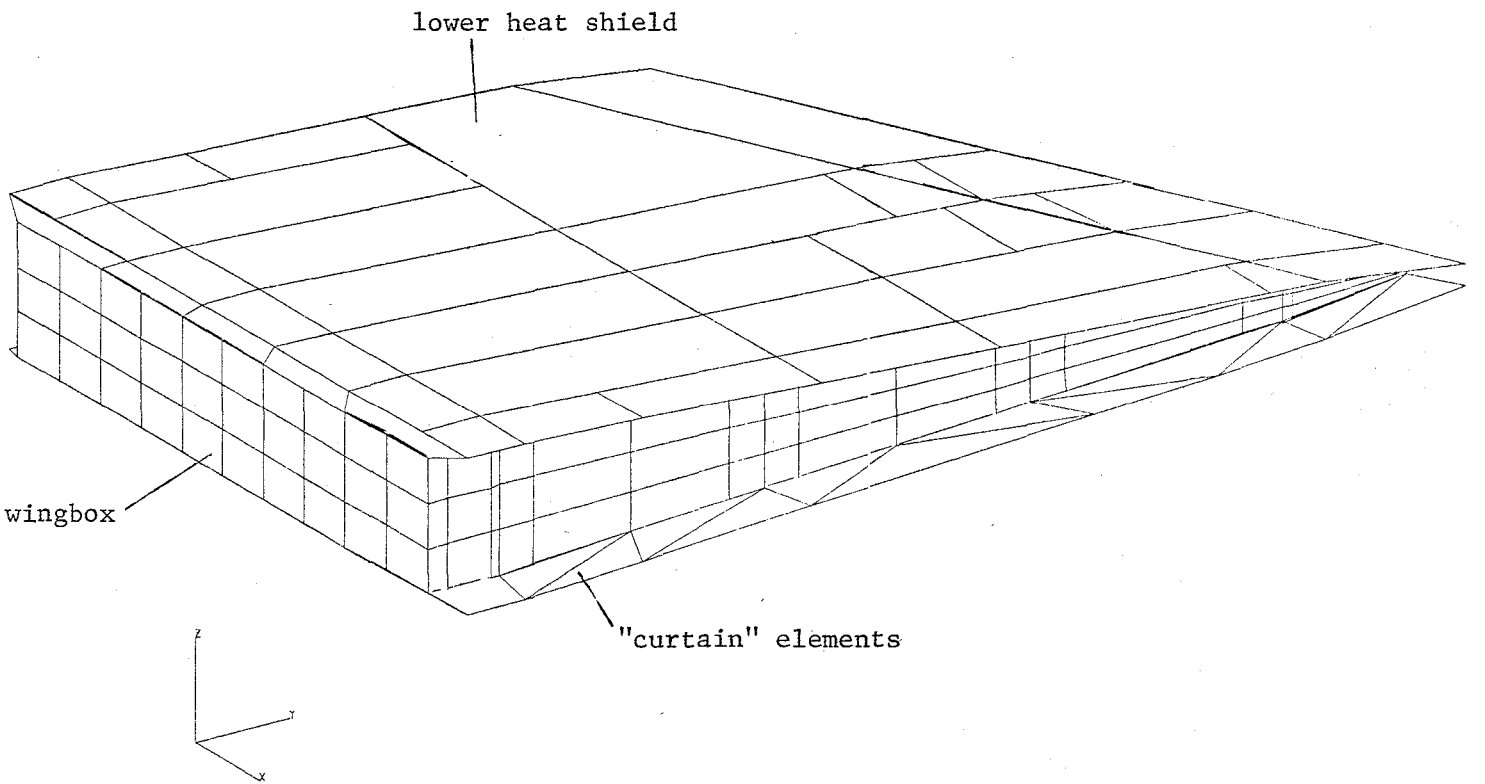

Figure 7.2: PATRAN-G Hidden Line Plot of THWTS Model Including Heat Shields and Curtain Elements.

7.3 shows this model including the heat shield elements taken from the main model, and the new curtain elements. All the data were directly borrowed without any changes from the THWTS model, except that the view factors between the heat shields and the curtain and surface elements had to be generated again. No compensations were made at that moment for the thickness of the webs and caps of the sidewall, which are shared by the surrounding elements. The opportunity was taken to use this model to compare both available versions of NASTRAN: the COSMIC version available on the Dryden computer, and the MSC version available at the Ames computers. As was explained in Chapter 3, the Ames computer system was used exclusively for the thermal analysis due to the core and CPU time requirements.

Figure 7.4 shows the temperature-time profiles as computed by the COSMIC version for four points at the rib at wing station 2.479 and fuselage station 24.384 (in the middle of the right rib wall of the bay). The temperatures computed in the web are lower at the beginning of the heating test than at the caps and, at the peak of the heating, approach the temperature of the upper cap, which is at the relatively cooler side of the structure. The measured temperatures indicate an initial higher midweb temperature, which at the time of the peak loading decreases compared to the lower cap temperature. The best agreement is found between measured and predicted temperature for the lower cap.

Figure 7.5 presents the comparison between measured and predicted temperatures as function of the time for the same location, when MSC NASTRAN is used. The predicted cap temperatures are much lower than the measured values or the values computed by the COSMIC version. The

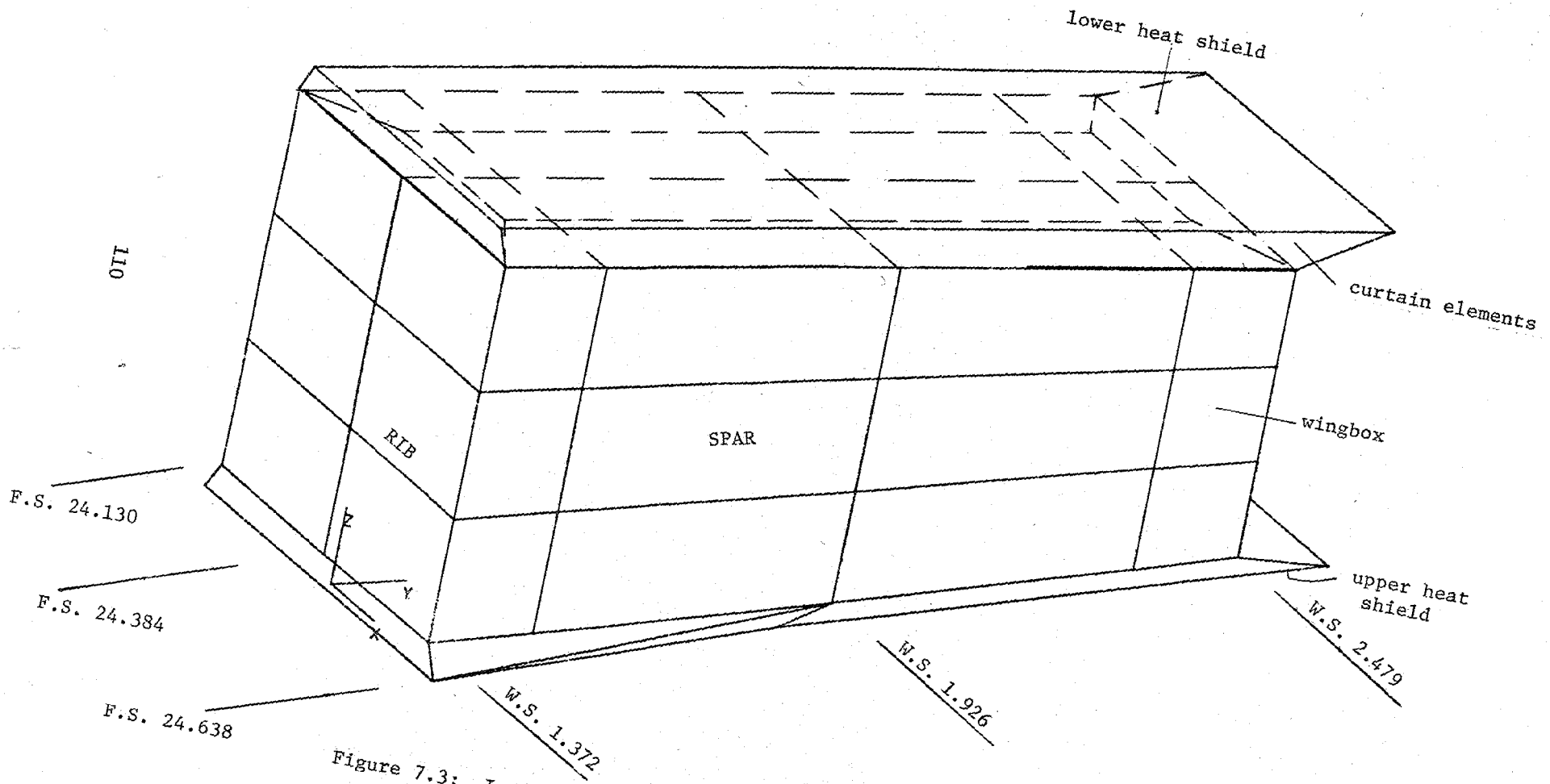

Figure 7.3: Isometric View of Thermal Model of Isolated Bay H, BAY H.

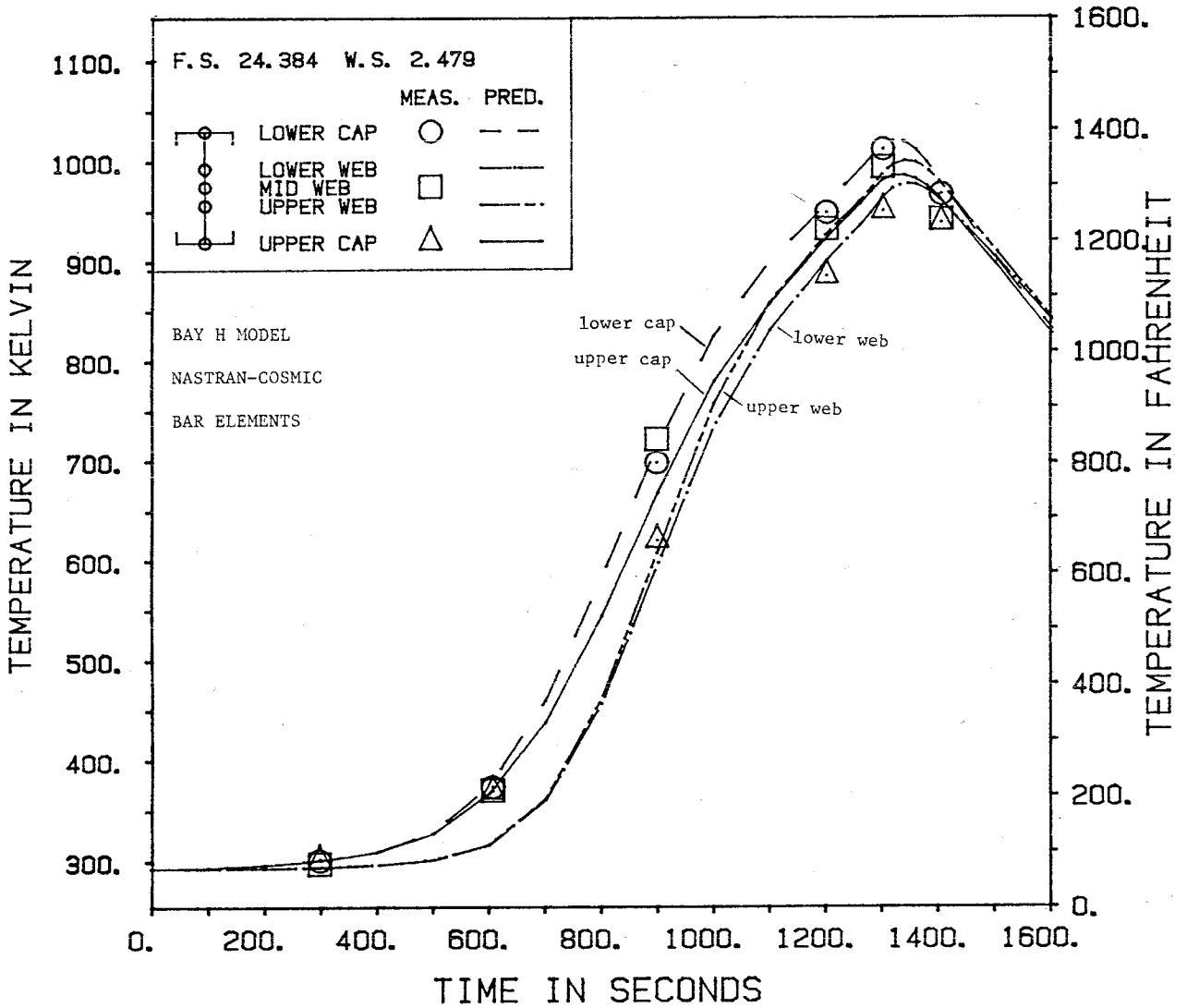

Figure 7.4: Results of NASTRAN COSMIC Analysis of BAY H Model, at F.S. 24.384 and W.S. 2.479.

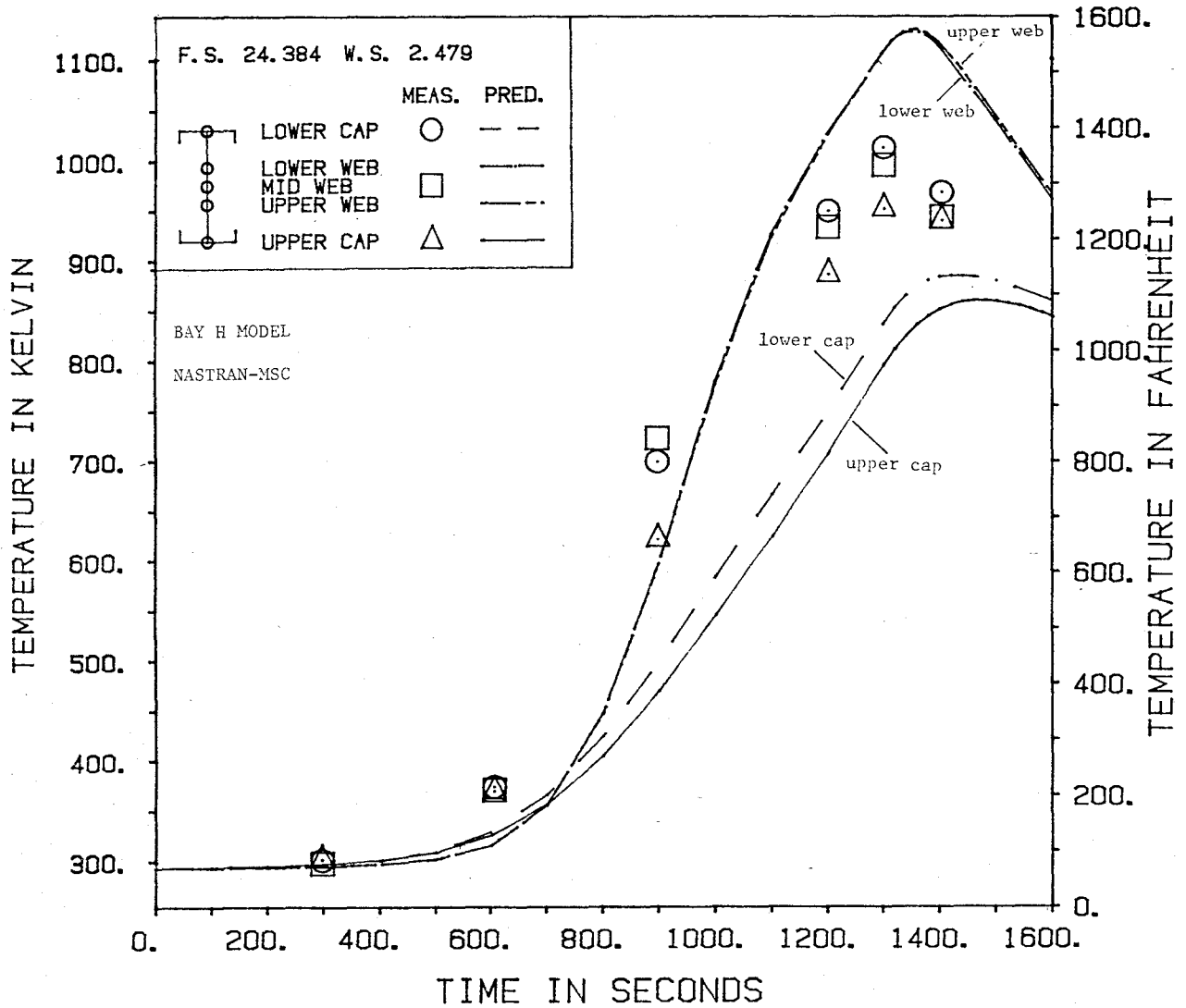

Figure 7.5: Results of NASTRAN/MSC Analysis of BAY H Model, at F.S. 24.384 and W.S. 2.479.

predicted upper and lower web temperatures are almost equal, but they are a lot higher than the cap temperatures. Both NASTRAN versions used the same time step sizes, reference temperature for the property values, and structural elements. The MSC model used only isoparametric QUAD4 elements versus the simpler QUAD2 elements in the COSMIC version. During the process of reviewing the internal computations of both versions, it was found that the COSMIC version of NASTRAN did not compute the contributions of the capacitance from the bar elements to the thermal load at the grid points connected to these bar elements. This was confirmed by running the MSC model and explicitly setting the capacitance of the bar elements equal to zero. Identical temperature values were obtained as with the COSMIC version. This deficiency in COSMIC (see also Section 6.3) involved only the bar elements. For thermal purposes, rod elements are identical to bar elements and are easier to define. The only reason why bars were used in the analysis was that PATRAN-G generates only bar elements.

Figure 7.6 shows the results of the COSMIC analysis of the same BAY H model but with rod elements instead of bar elements. When compared to the MSC analysis with bars (Figure 7.5), the cap temperatures of the COSMIC/rod model are slightly higher, while the web temperatures are lower than the web temperatures predicted by the MSC analysis. However, the most important phenomenon in both analyses is that the web temperatures are clearly too high after 1000 seconds. Figure 7.7 shows the predicted web temperatures of both the COSMIC/rod and MSC/bar models compared to the upper and lower heat shield temperature-time profiles. The web and skin temperatures should never be higher than

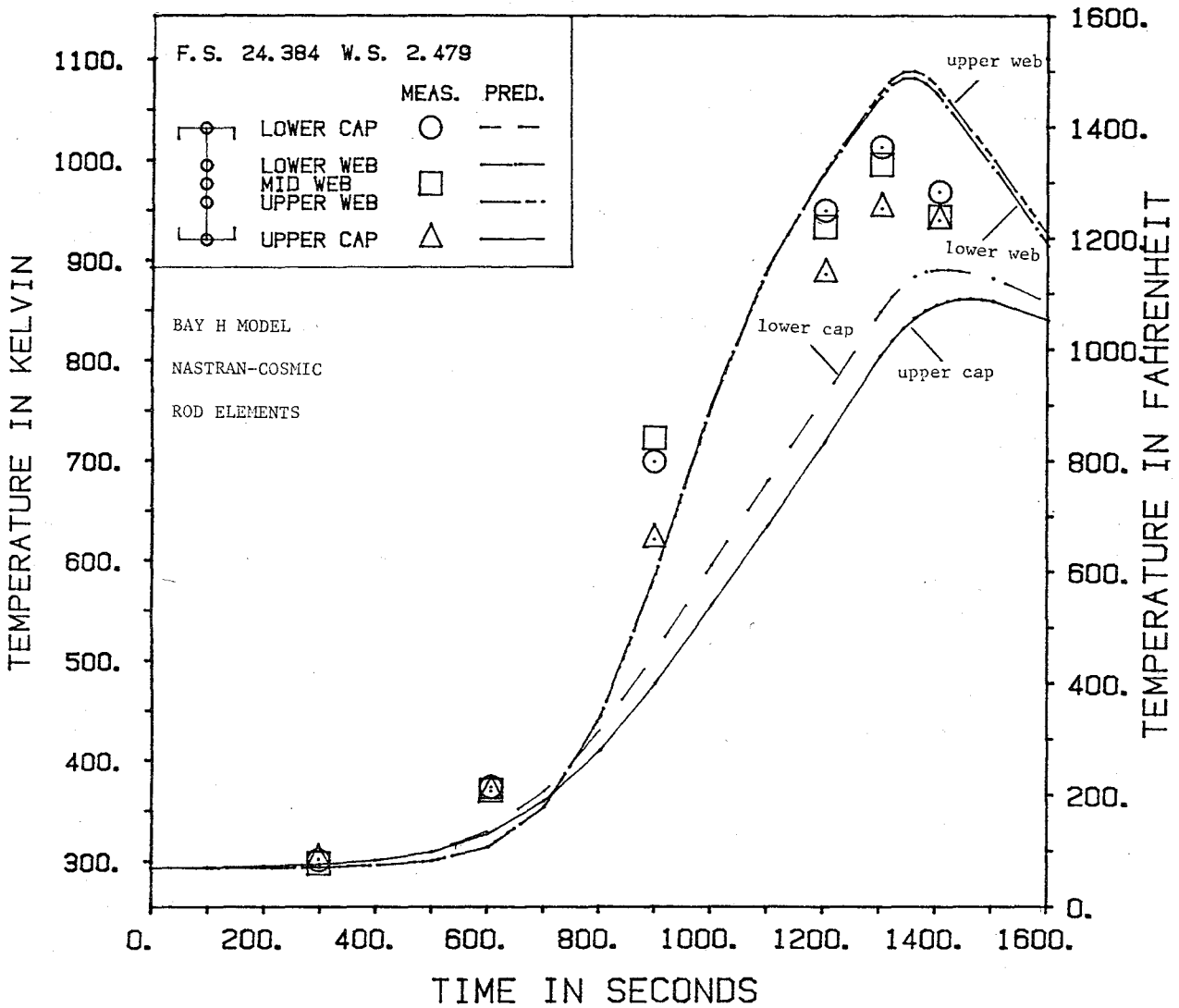

Figure 7.6: Results of NASTRAN-COSMIC Analysis of BAY H Model, with Rod Instead of Bar Elements, at F.S. 24.384 and W.S. 2.479.

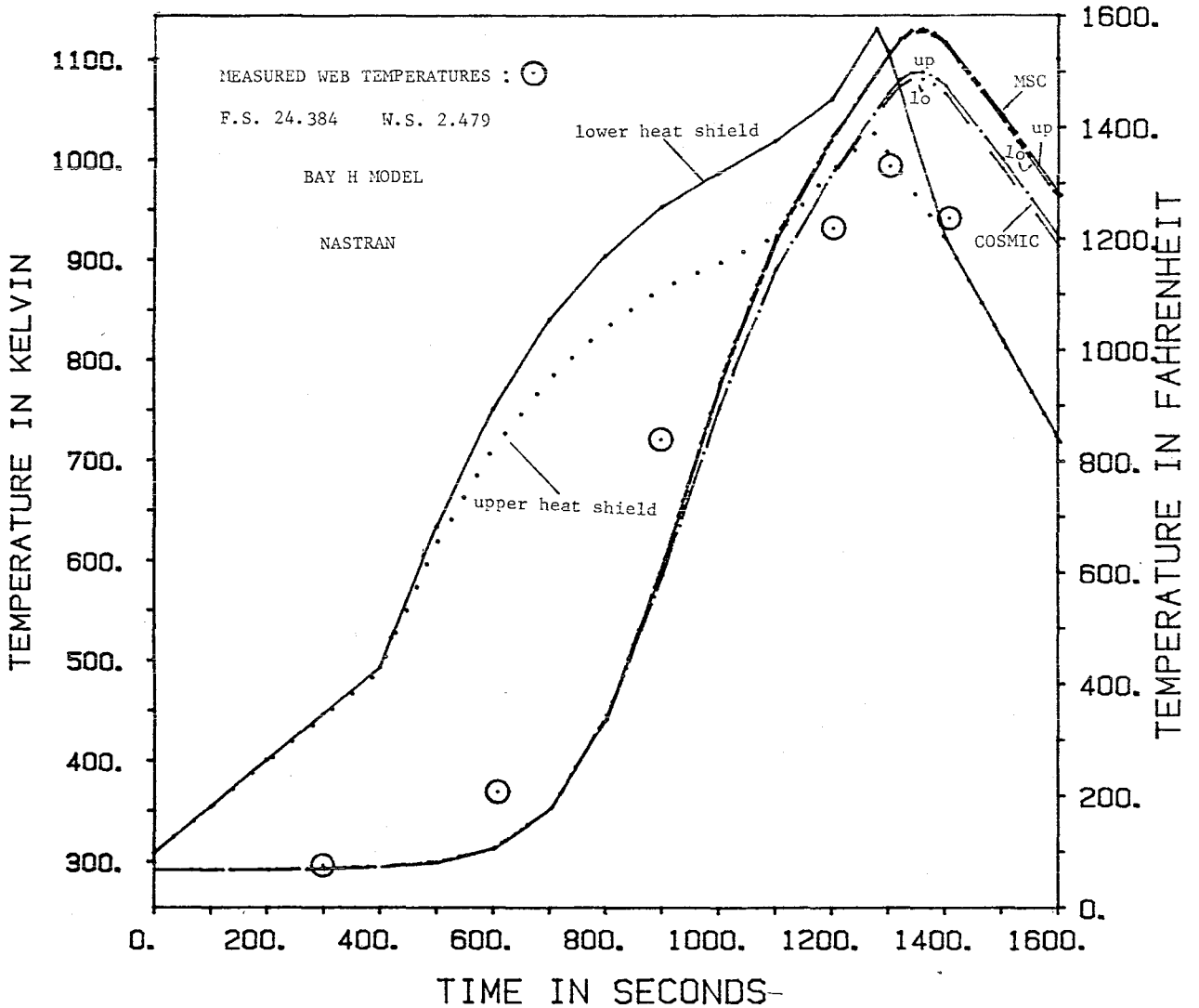

Figure 7.7: Comparison of MSC and COSMIC Versions of NASTRAN for the Web Temperatures in the BAY H Model at F.S. 24.384 and W.S. 2.479 with the Heat Shield Temperatures.

the temperatures of the hottest parts of the structure, the heat shields. It can be concluded from Figure 7.7 that the predictions made by both versions of NASTRAN are wrong.

In Figure 7.8 the measured temperatures of the centers of both surfaces are compared to the predicted temperature-time profiles by the three analysis methods. In addition the controlled temperatures of both heat shields are shown as function of time. After 700 seconds, the temperature profiles predicted by the MSC/bar and COSMIC/rod models rise at a decreased rate and follow the trend set by the heat shields. However, the measured temperatures are much higher and approach the temperatures of the upper heat shield.

7.3 THE BAY H* ANALYSIS

In additional analyses, the BAY H model was modified to investigate the different analysis methods in greater detail. To exclude the influence of the surrounding structure, the web thicknesses and areas of the caps of spars and ribs were divided by two; and the cross-sectional area of the vertical angles, connecting the spar and ribs, were divided by four. In addition to the two versions of NASTRAN, the new model, named BAY H*, was also analyzed with the finite-element program, SPAR (Reference 8). The input for this program was taken from the NASTRAN bulk data and converted into SPAR statements. Two runs were made using the SPAR program. The first run used constant material properties taken at 644 K (700°F) and was in this way identical with both NASTRAN analyses. In the second run, SPAR updated the material properties (thermal conductivity and capacitance) every 25 seconds.

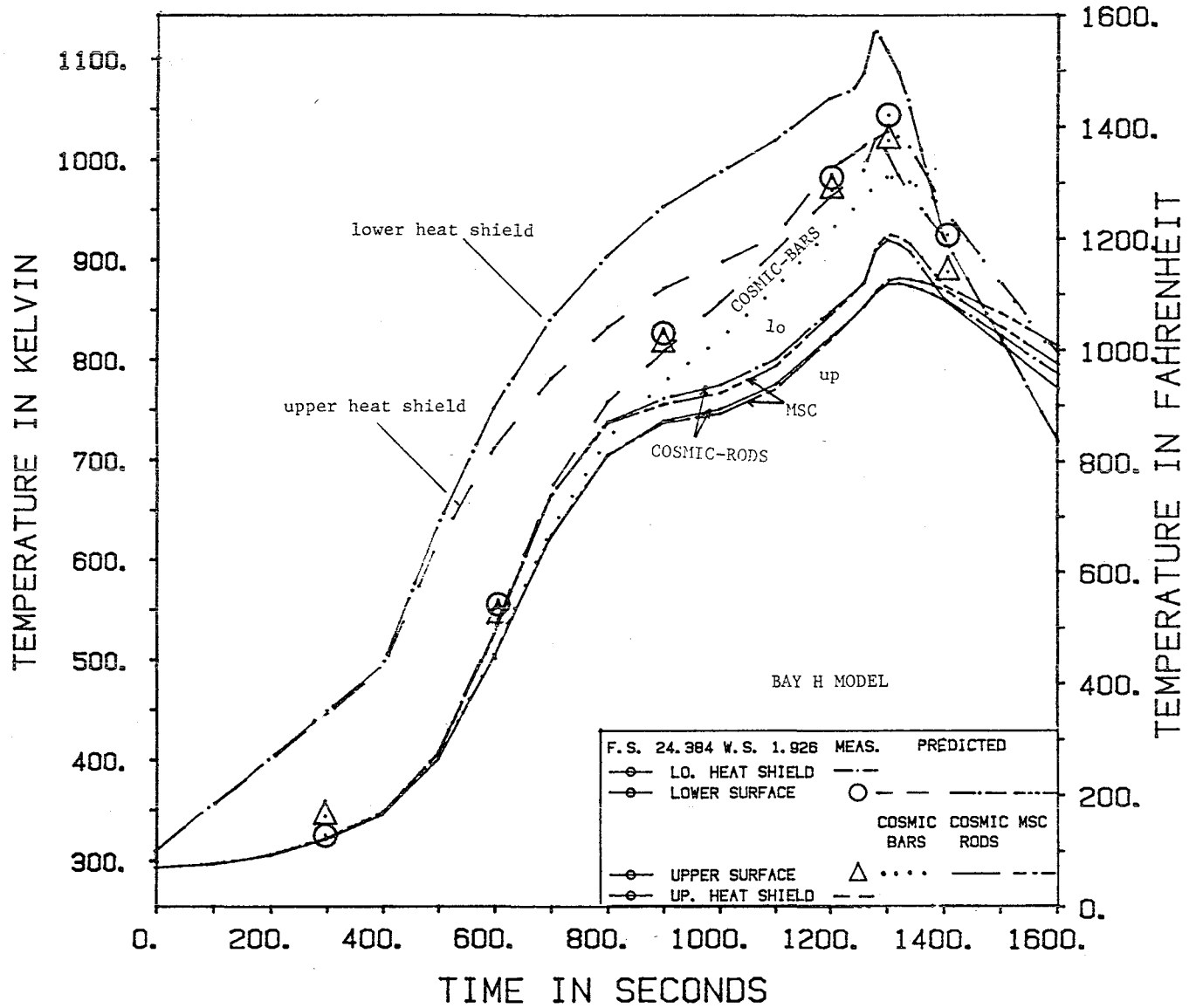

Figure 7.8: Comparison of MSC and COSMIC Versions of NASTRAN for the Center Temperatures of the Surface Panels in the BAY H Model (F.S. 24.384 and W.S. 1.926).

Figures 7.9 through 7.11 show the temperature-time distributions for the cross section at the center of the right wall (F.S. 24.384 and W.S. 2.479) of the BAY H* model for the NASTRAN (COSMIC) and the two SPAR analyses. Results of the MSC NASTRAN analysis are not given but were close to the results of the COSMIC version. The results of the NASTRAN analysis in Figure 7.9 have the same trend for the rib web and cap temperatures as in the BAY H analysis. The web temperatures after 900 seconds are too high, while the cap temperatures are consistently lower than the test data. Although an absolute comparison between the test data and the results of an isolated structure is not possible, the results of both SPAR analyses come close to the measured temperatures (see Figures 7.10 and 7.11). The SPAR analysis with constant material properties produces slightly lower temperatures than those measured, while updating the material properties each 25 seconds results in a close agreement between measured and predicted values. The upper cap temperature, however, is consistently too low or too high.

To study the predicted temperature distributions at different locations, several cross sections and surfaces were investigated in more detail. Tables 7.1 through 7.5 present the temperature distributions in a more comparative way. Figure 7.12 shows the temperature distributions along the lower surfaces at fuselage section 24.384. The predicted temperature distribution by the NASTRAN analysis stands out clearly from the two SPAR analyses by the irregularities at the edges of the surface panel. The SPAR distributions are, in general, smoother and in better agreement with the test data. An identical trend is shown in Figure 7.13, where results of the lower surface along wing

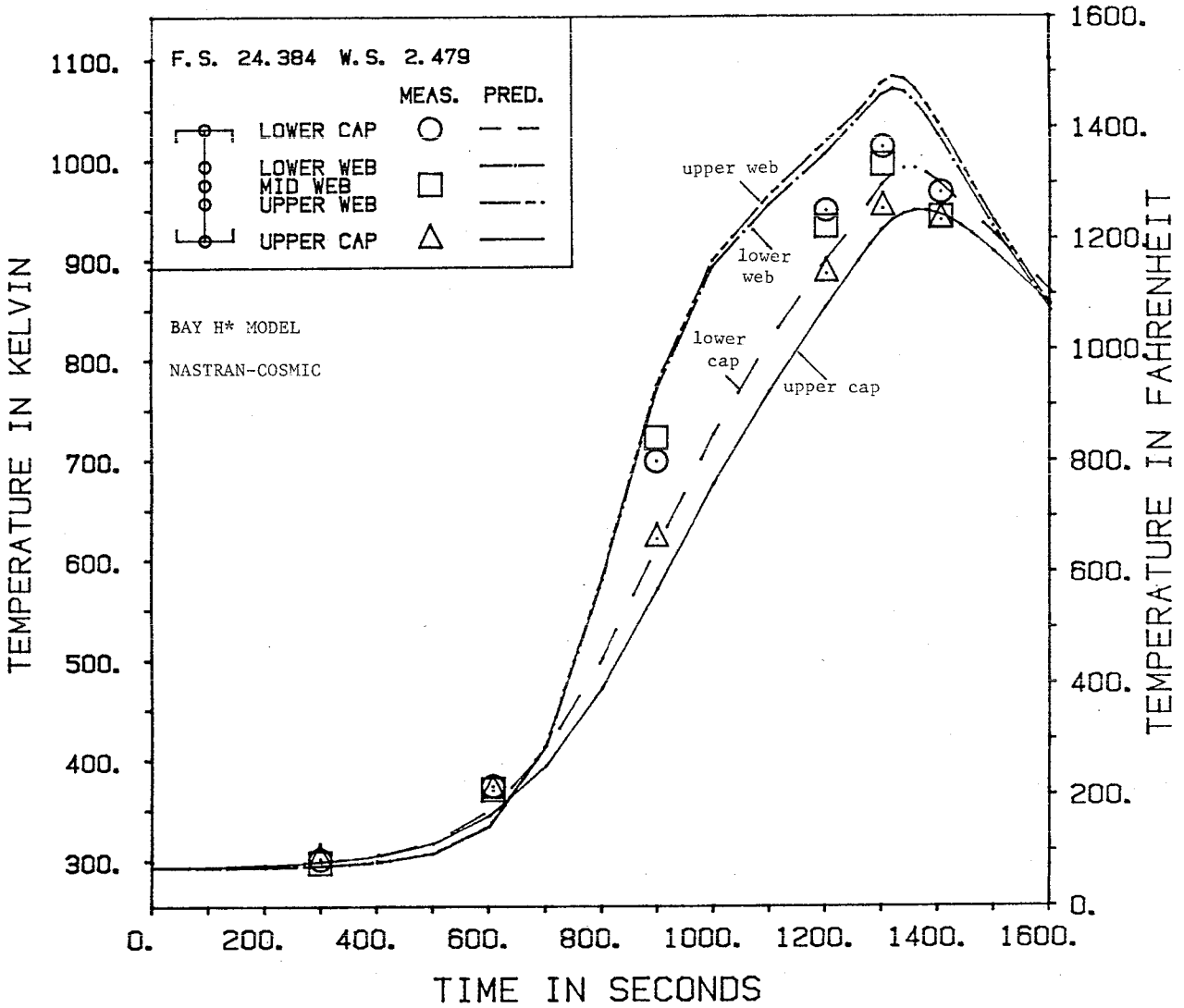

Figure 7.9: Results of the NASTRAN COSMIC Analysis of the BAY H* Model at F.S. 24.384 and W.S. 2.479.

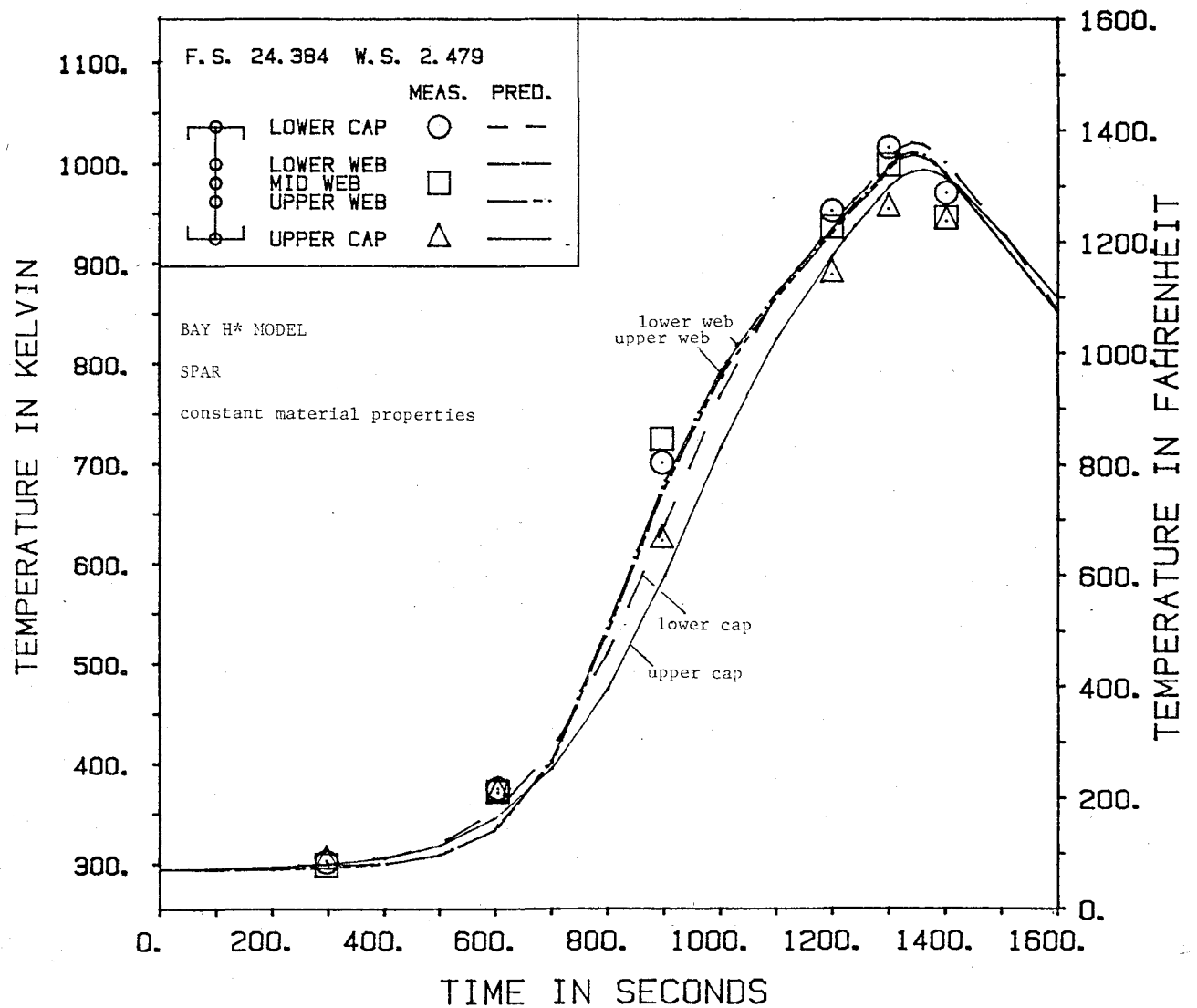

Figure 7.10: Results of the SPAR Analysis of the BAY H* Model with Constant Material Properties at F.S. 24.384 and W.S. 2.479.

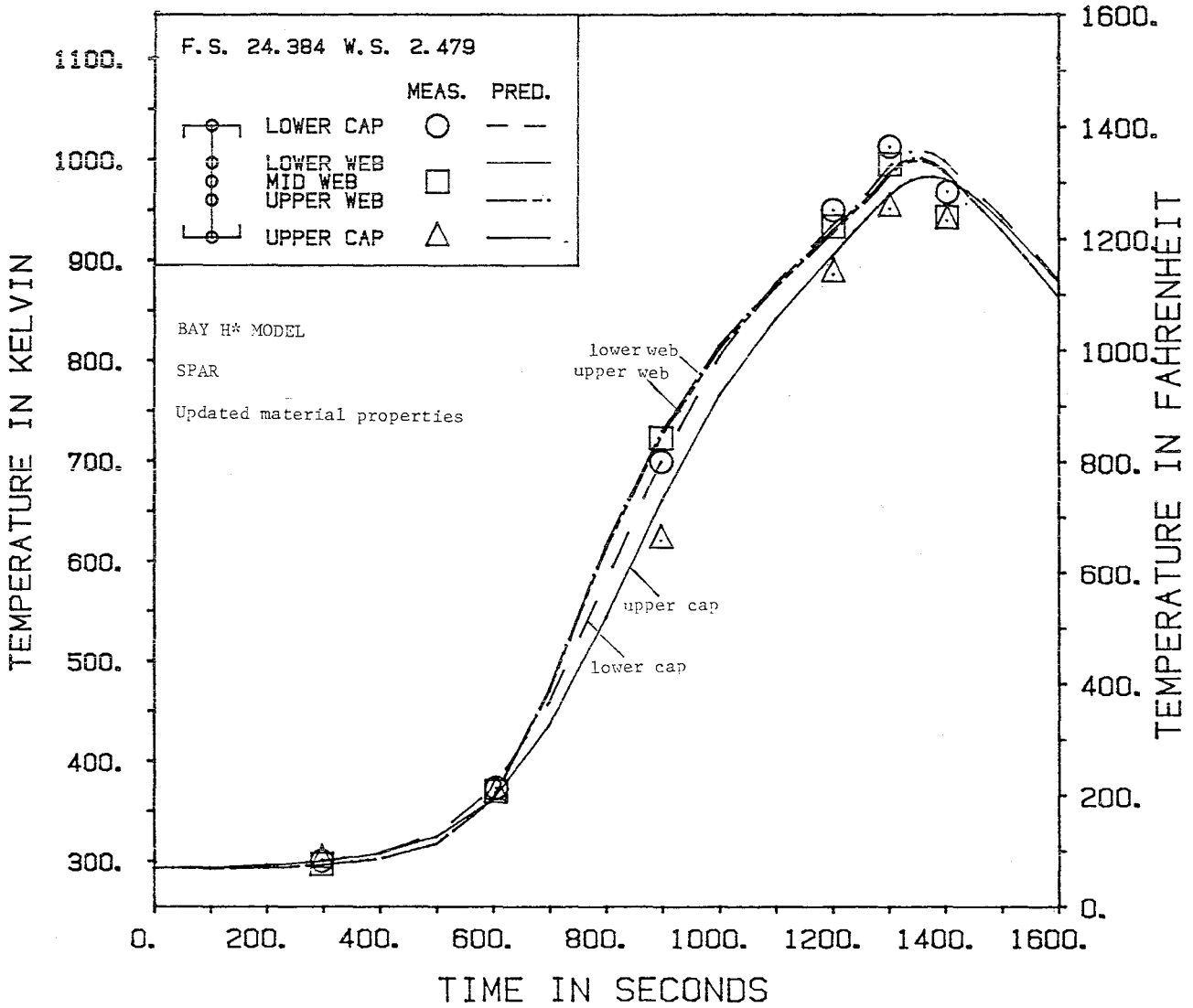

Figure 7.11: Results of the SPAR Analysis of the BAY H* Model with Variable Material Properties at F.S. 24.384 and W.S. 2.479.

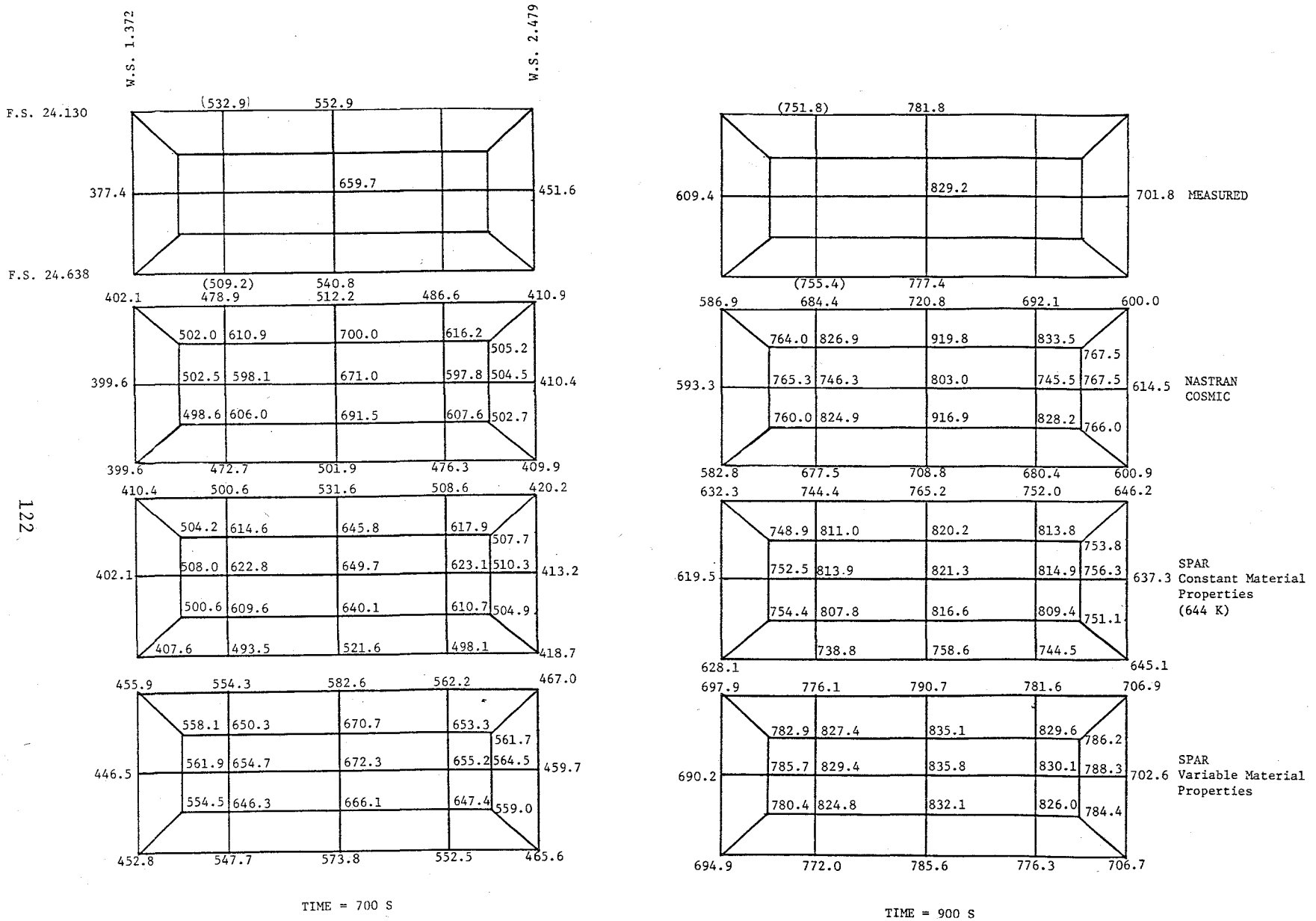

Table 7.1: BAY H* Results for the Three Analysis Methods at the Lower Surface. (Temperature in Kelvin)

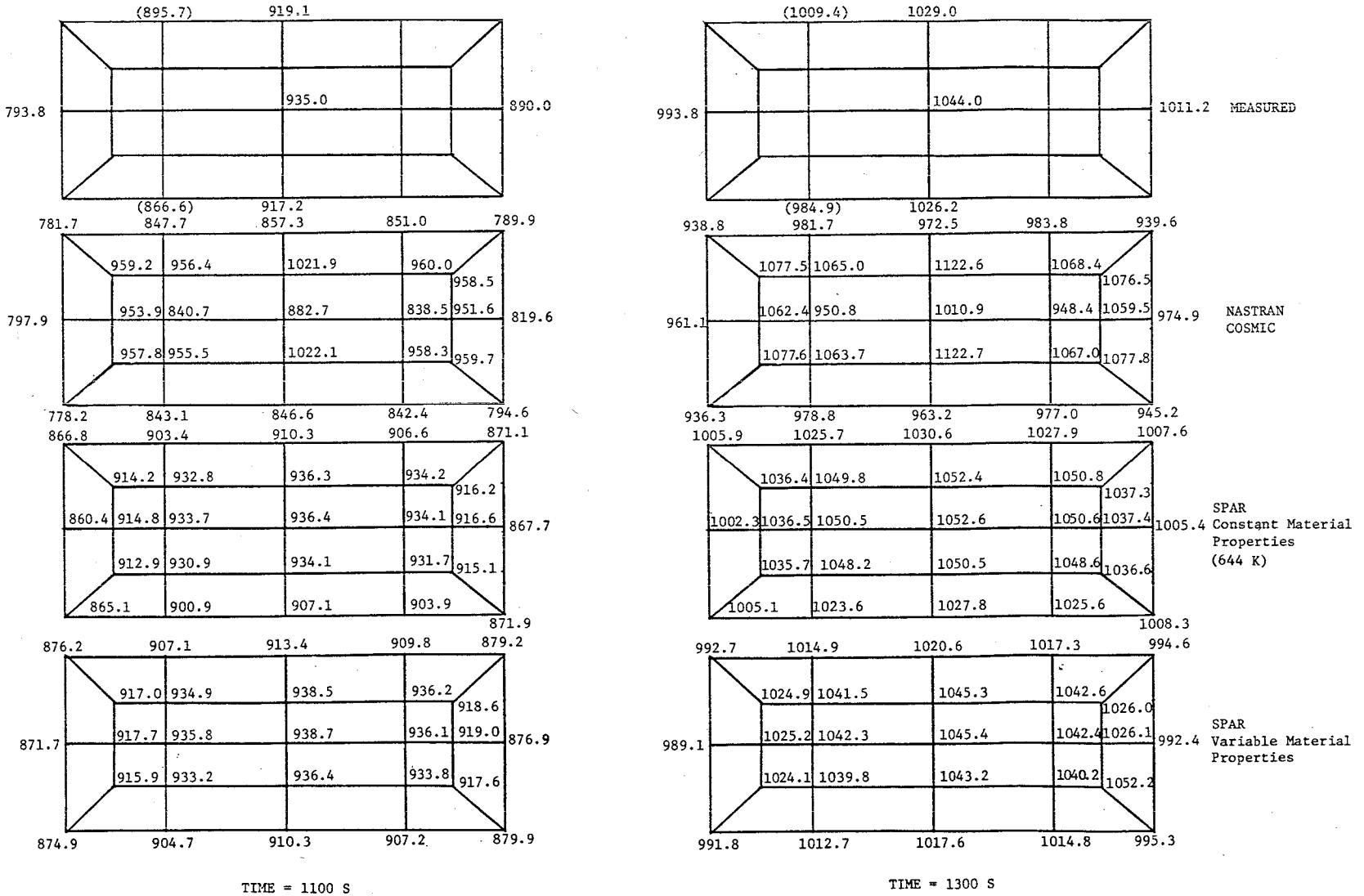

Table 7.1: Concluded.

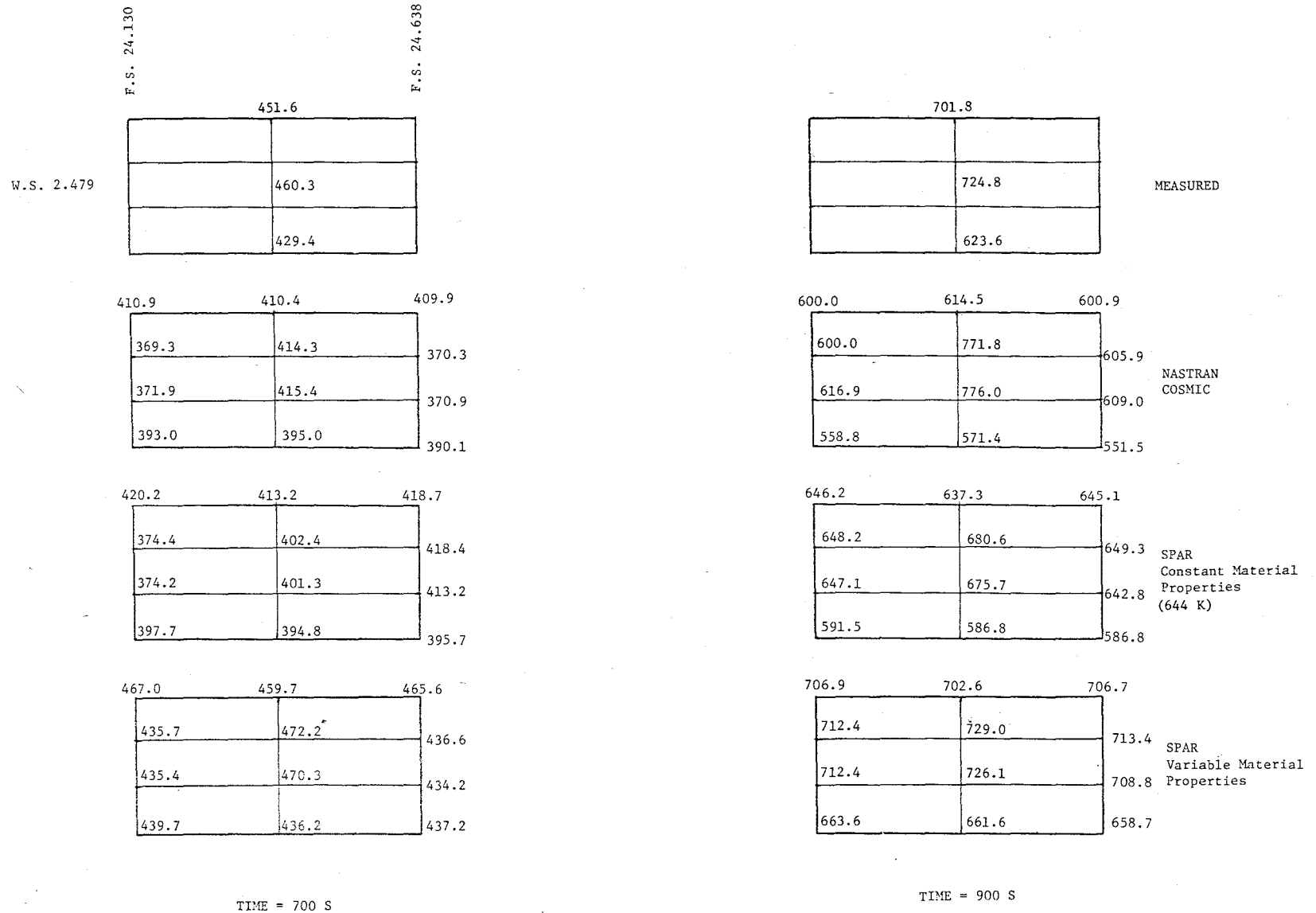

Table 7.2: BAY H* Results for the Three Analysis Methods at the Right Rib Surface. (Temperature in Kelvin)

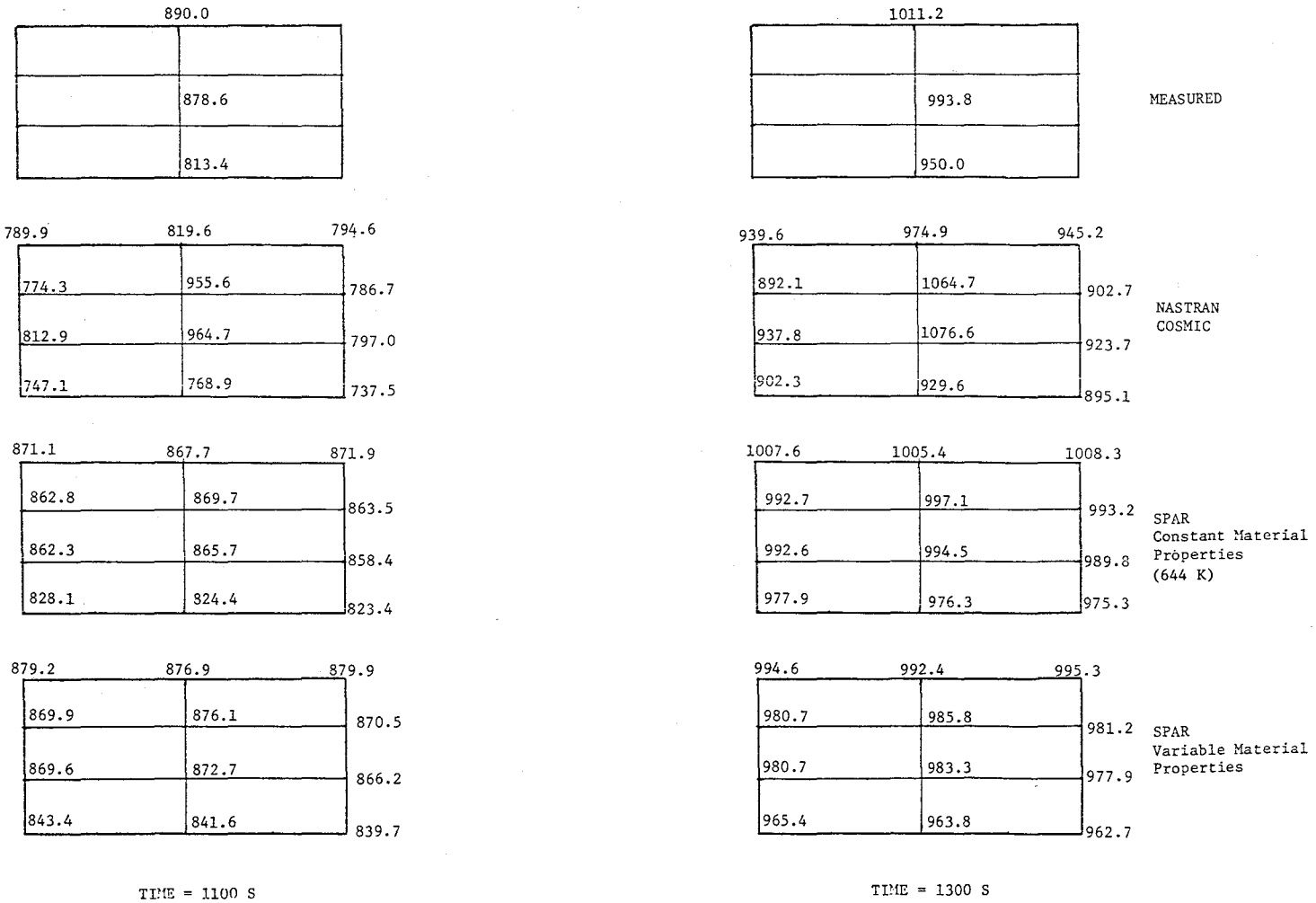

Table 7.2: Concluded.

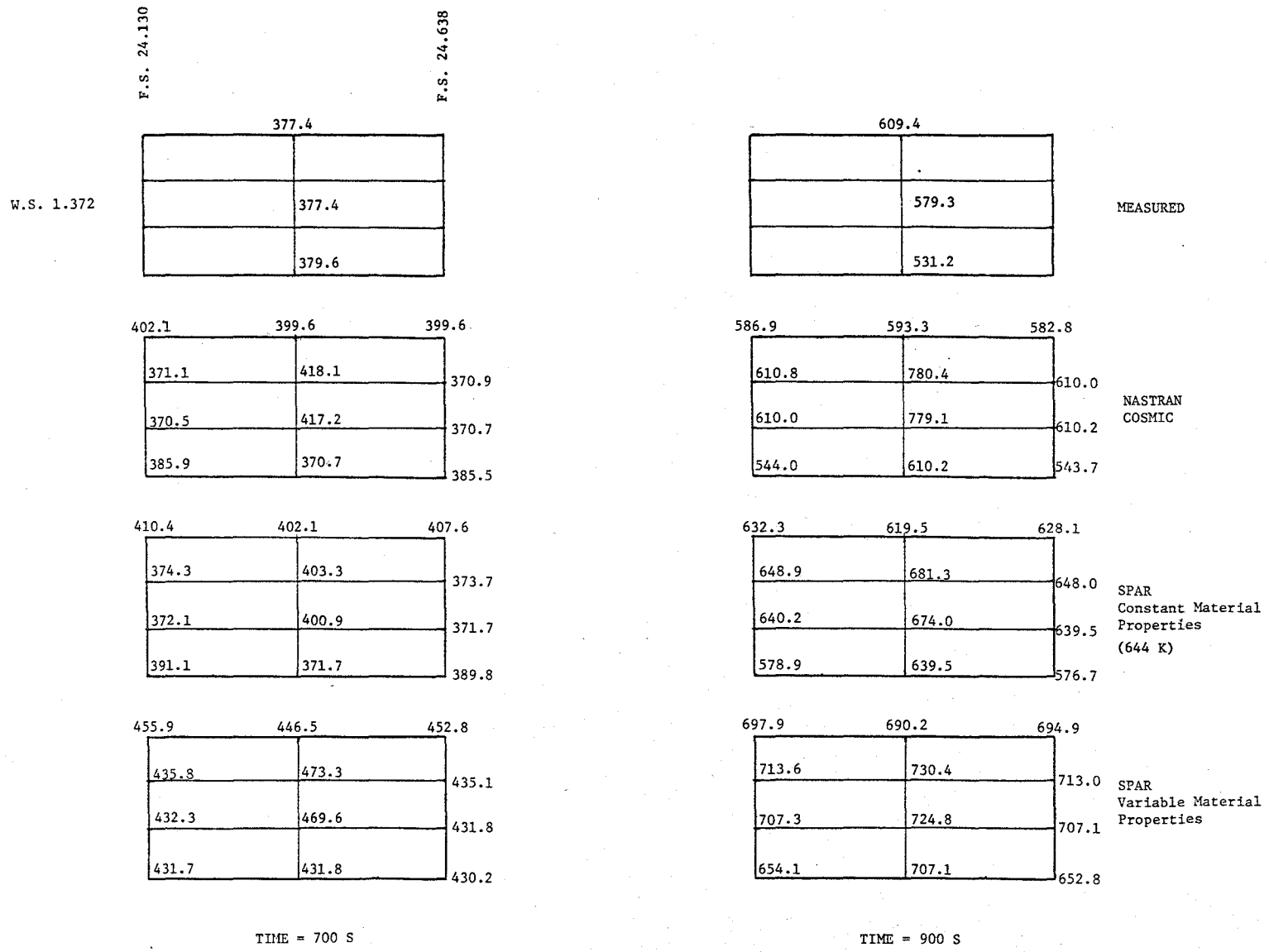

Table 7.3: BAY H* Results for the Three Analysis Methods at the Left Rib Surface. (Temperature in Kelvin)

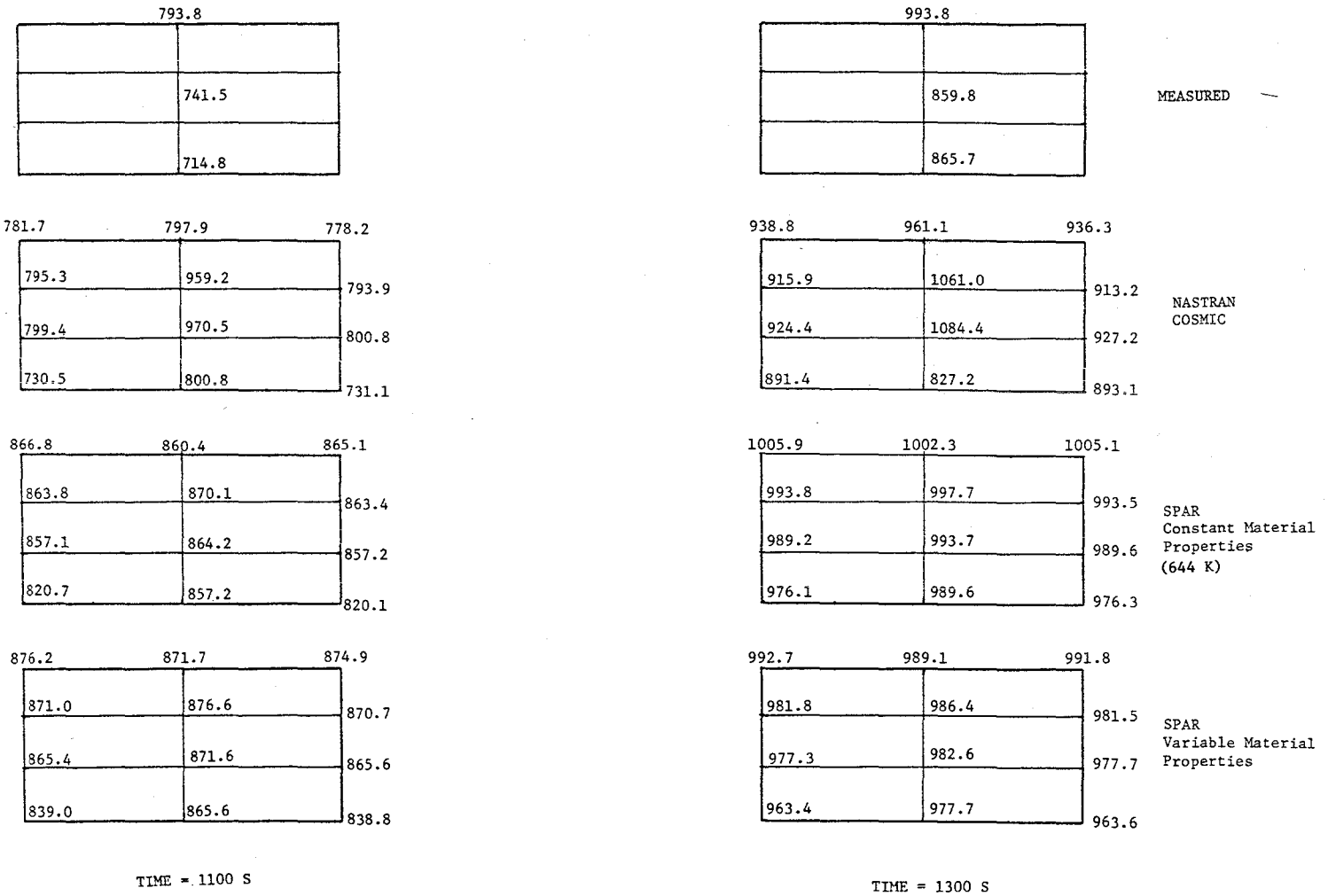

Table 7.3: Concluded.

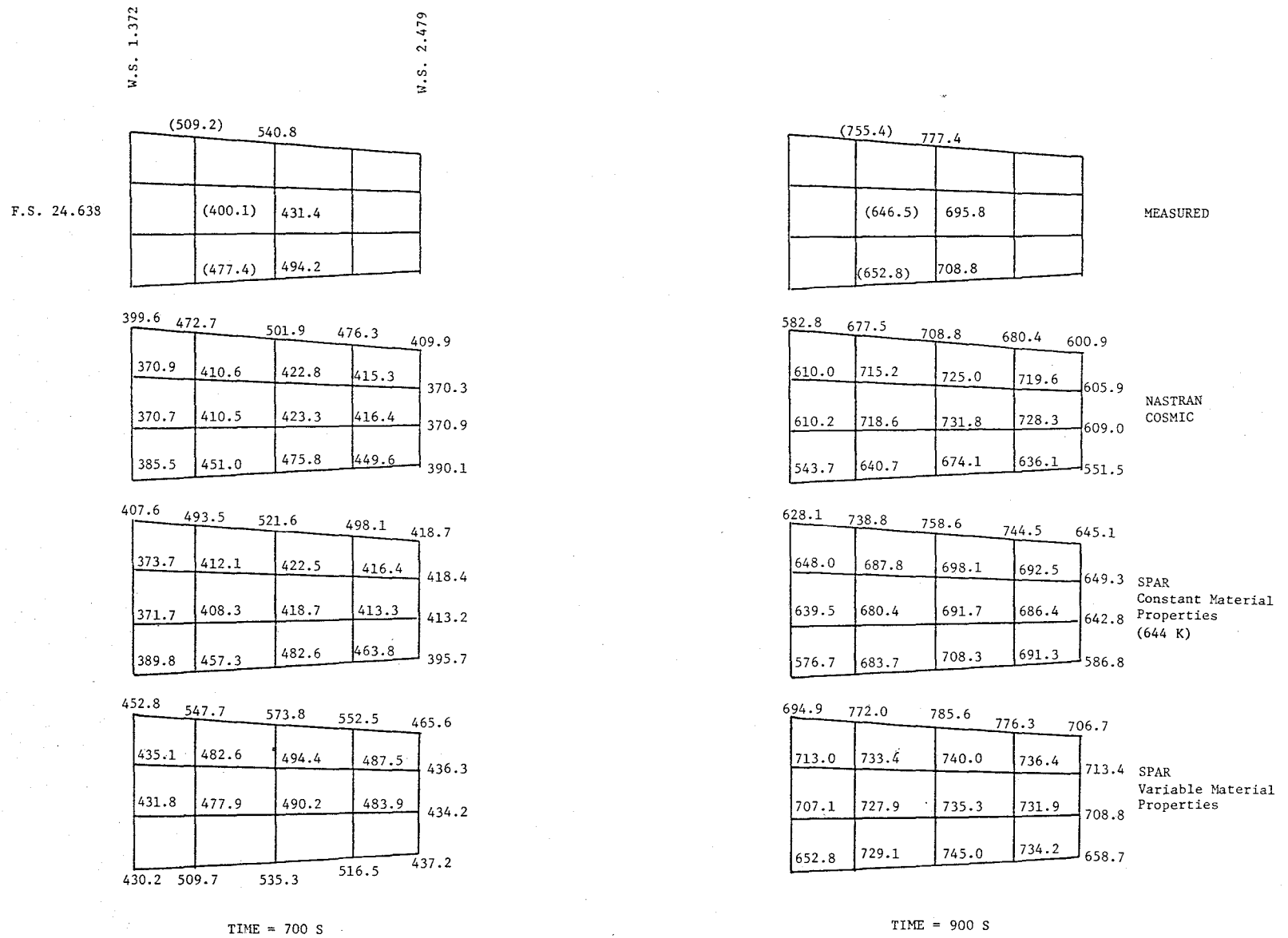

Table 7.4: BAY H* Results for the Three Analysis Methods at the Front Spar Surface. (Temperature in Kelvin)

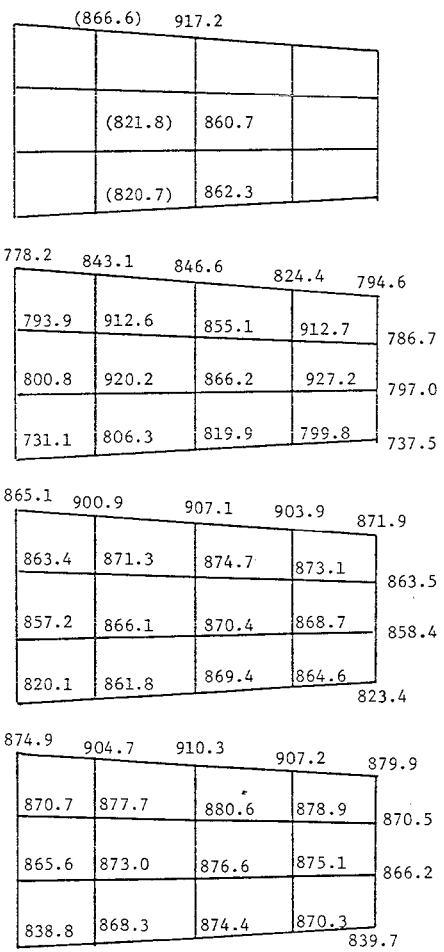

TIME = 1100 S

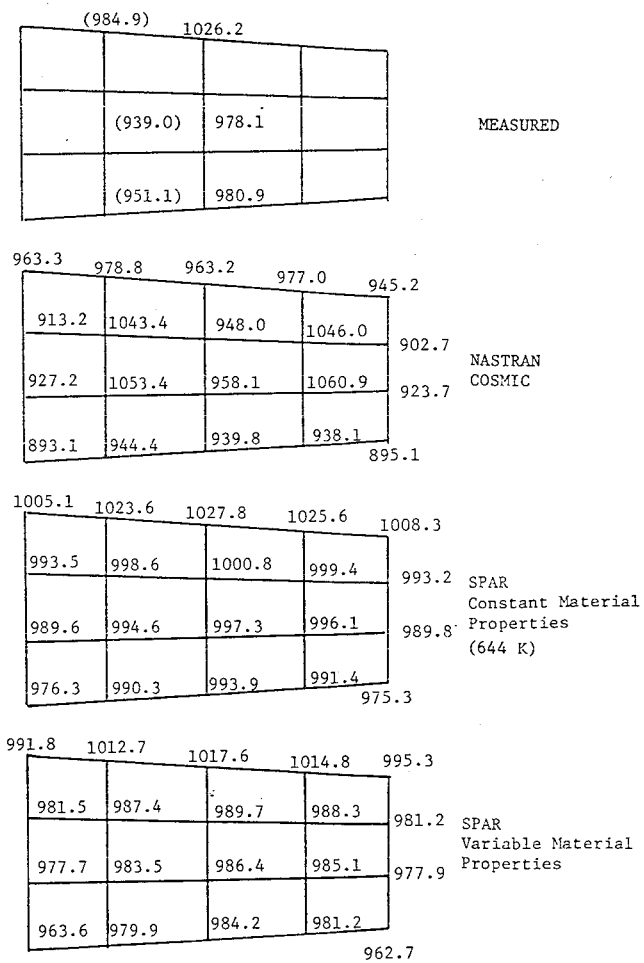

MEASURED

NASTRAN
COSMIC

SPAR
Constant Material
Properties
(644 K)

SPAR
Variable Material
Properties

TIME = 1300 S

Table 7.4: Concluded.

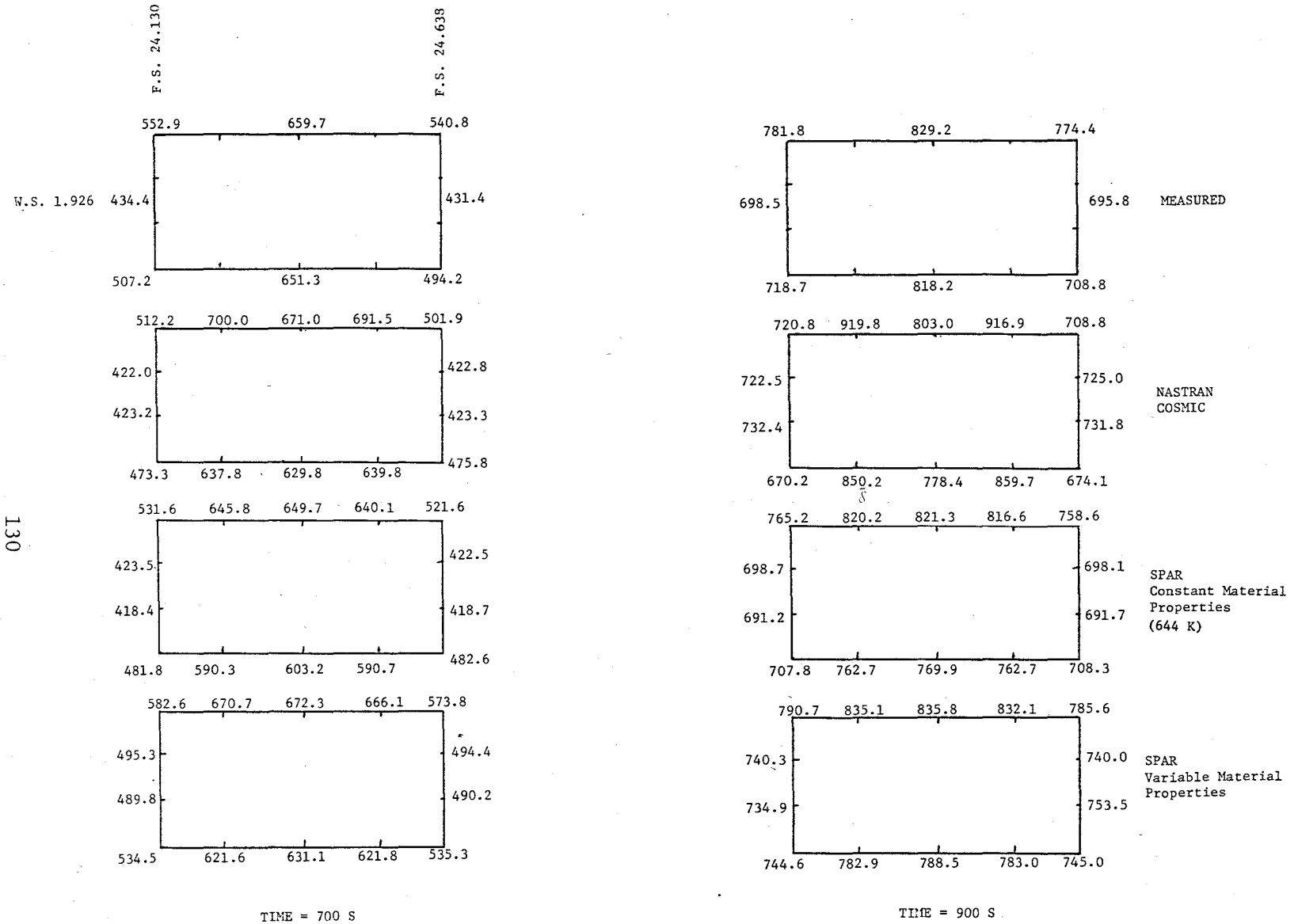

Table 7.5: BAY H* Results for the Three Analysis Methods at the Cross Section along W.S. 1.926. (Temperature in Kelvin)

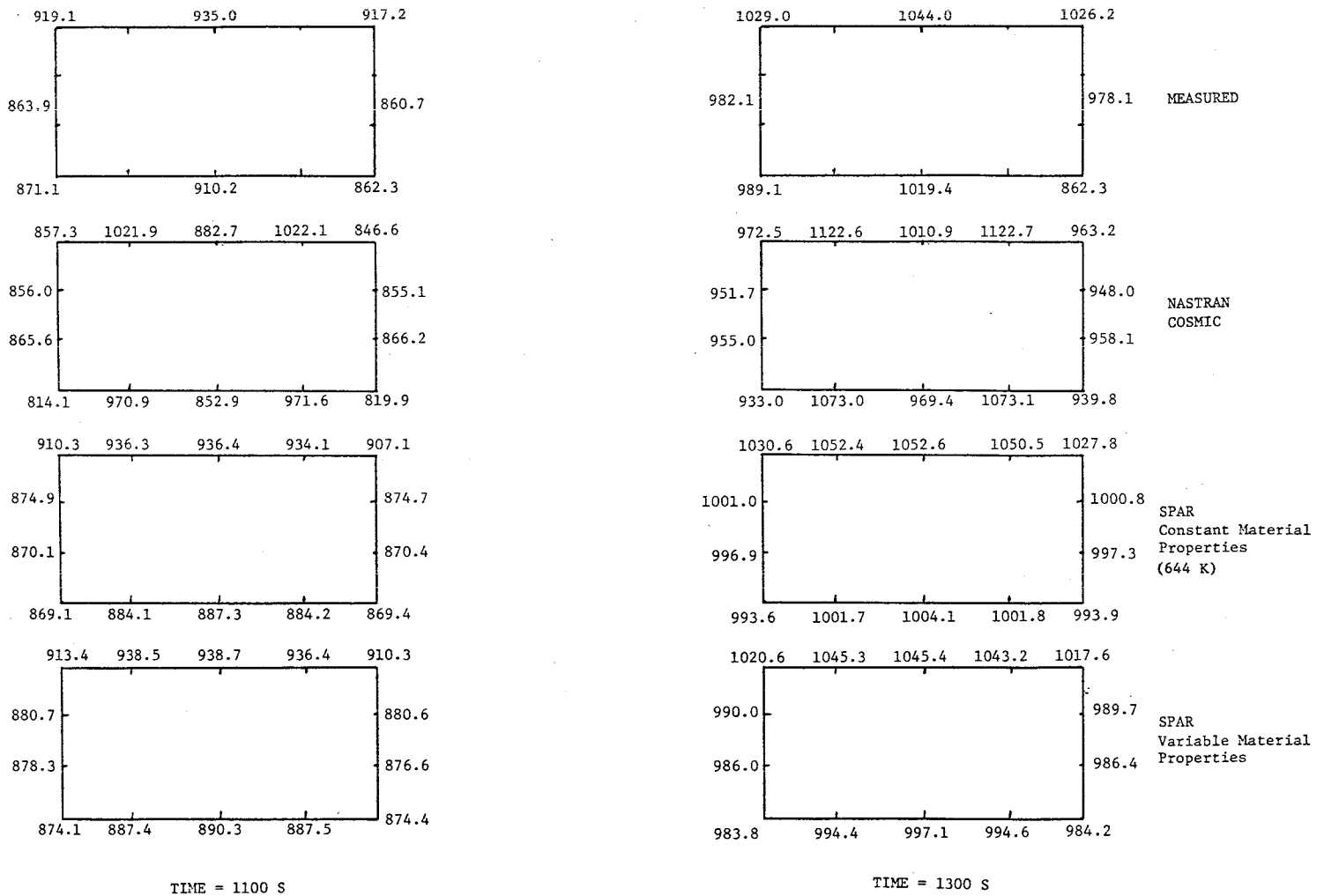

Table 7.5: Concluded.

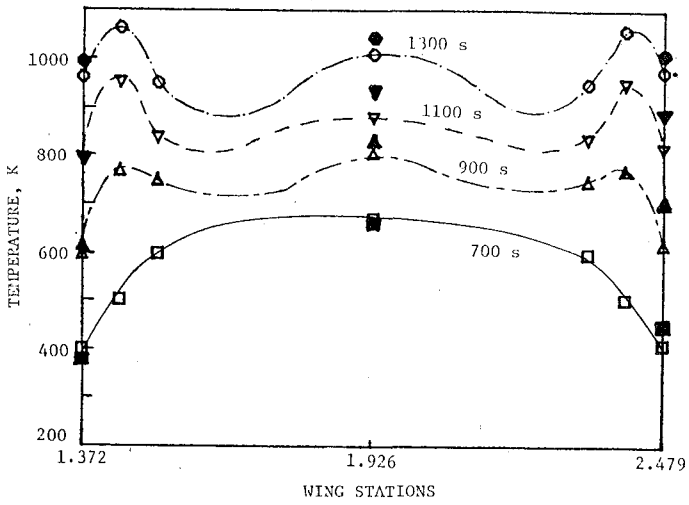

NASTRAN-COSMIC

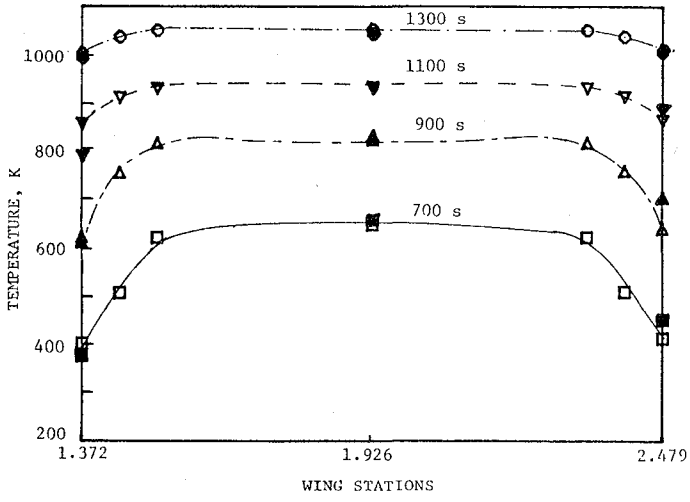

SPAR

constant material properties

at 644 K

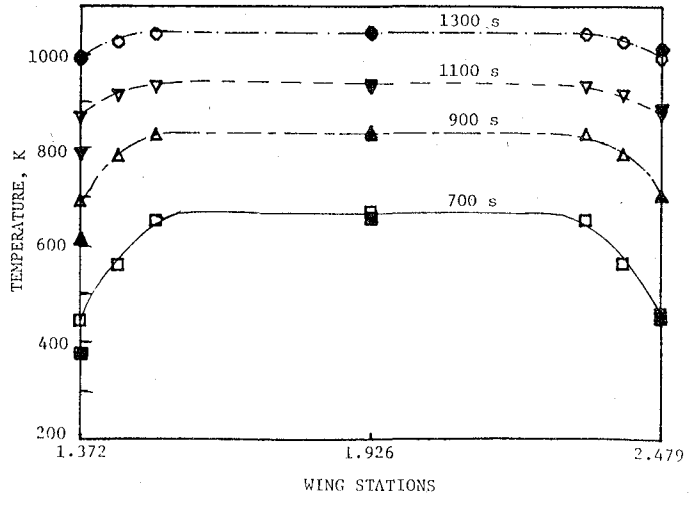

SPAR

variable material properties

Figure 7.12: BAY H* Results of Lower Surface along F.S. 24.334

(Test data given in solid symbols.)

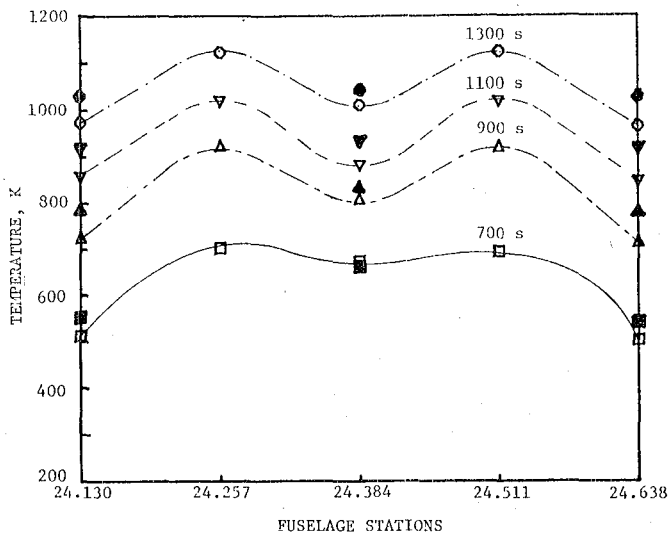

NASTRAN-COSMIC

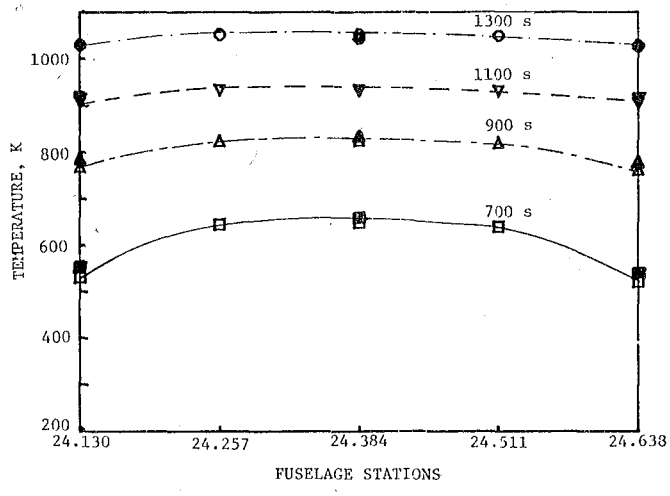

SPAR

constant material properties

at 644 K

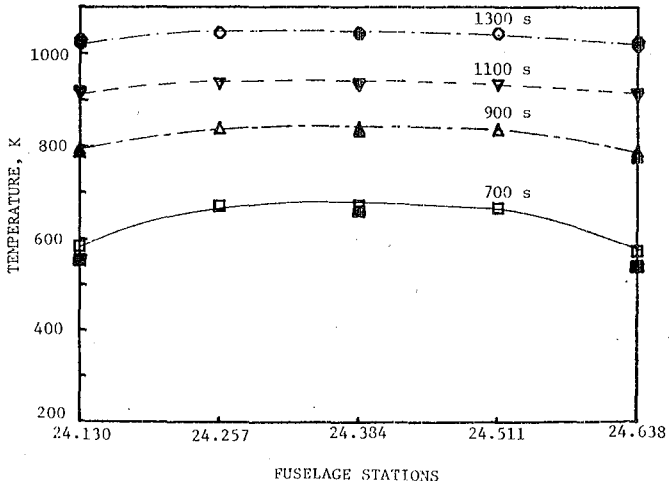

SPAR

variable material properties

Figure 7.13: BAY H* Results of Lower Surface along W.S. 1.926.

(Test data given in solid symbols.)

station 1.926 are presented. From both figures it can be noticed that the NASTRAN analysis consistently predicted temperatures too high for the grid points on the surface closest to, but not part of, the edge grid points. This is even more apparent in Figures 7.14, 7.15, and 7.16, where the temperature distributions along one spar and two rib cross sections are compared for the three analysis methods. The rib cross sections (W.S. 1.372 and W.S. 2.479 at F.S. 24.384) are different from the spar cross sections in that the center web grid points all have as neighbors grid points located at the edges, with the other center web grid point being the only exception (see Figure 7.17). The spar sections have in contrast to this some elements entirely within the web without having common grid points at the edges. The predicted NASTRAN temperature distributions in Figure 7.14 and 7.15 show elevated web temperatures compared to the NASTRAN predicted cap temperatures as well as to the predicted SPAR distributions in the corresponding cases. From these figures and tables, the suspicion arises that the NASTRAN computation of the temperatures at the "edge" elements is inaccurate.

7.4 DISCUSSION

Several runs were made to investigate this phenomenon in more detail. Variations in the conduction values indicated, as expected, that the heat transfer in the bay is predominantly by radiation. Heat transfer by conduction is minor due to the thin-walled structure and to the high temperature. The irregular high temperatures appear

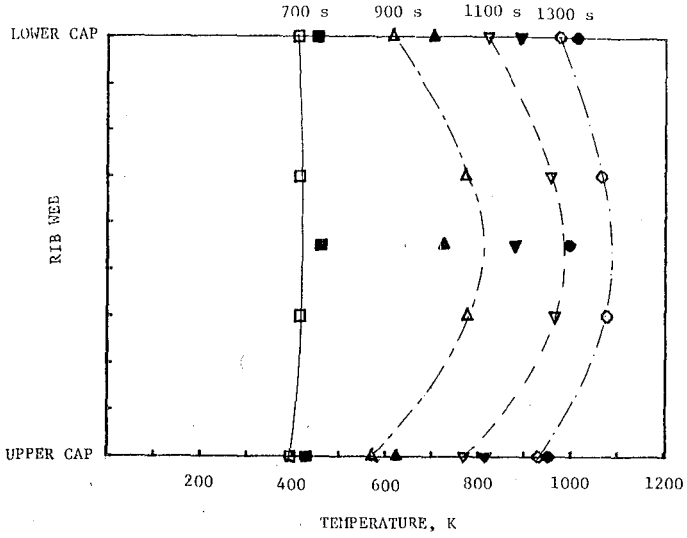

NASTRAN-COSMIC

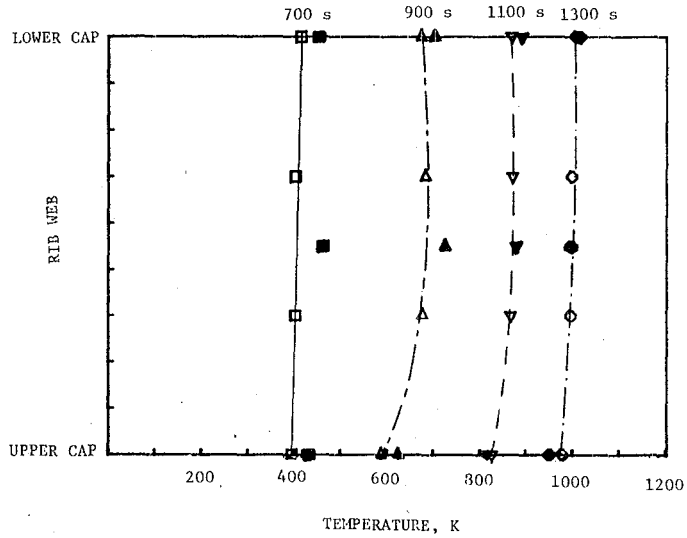

SPAR

constant material properties

at 644 K

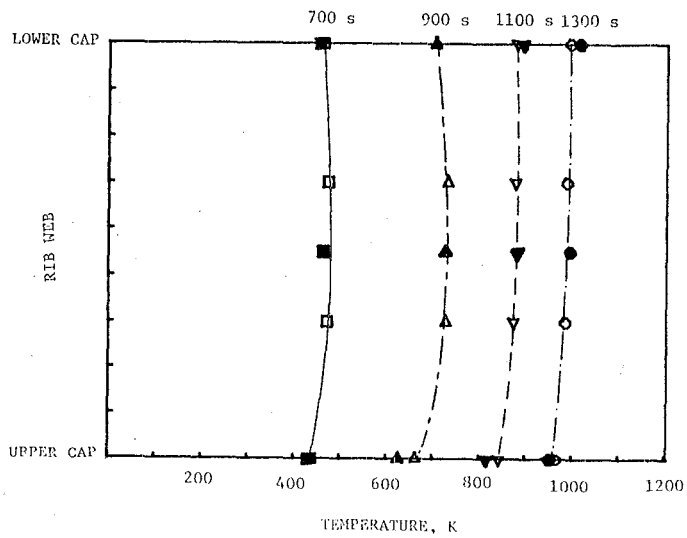

SPAR

variable material properties

Figure 7.14: BAY H* Results at W.S. 2.479 and F.S. 24.384 (Rib Cross Section). Test Data Given in Solid Symbols.

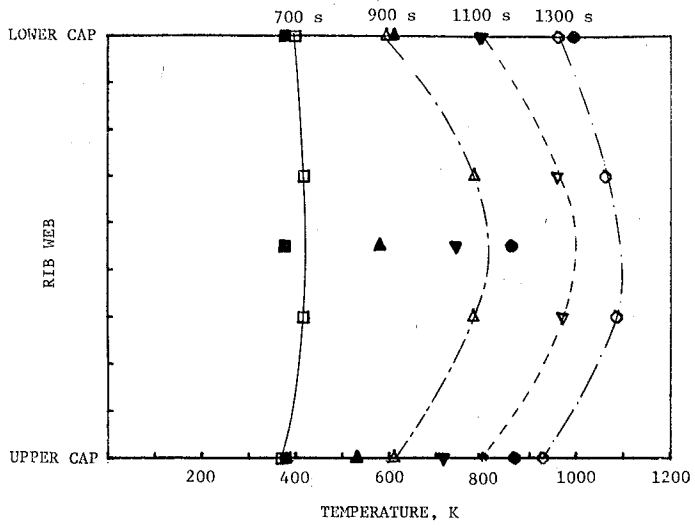

NASTRAN-COSMIC

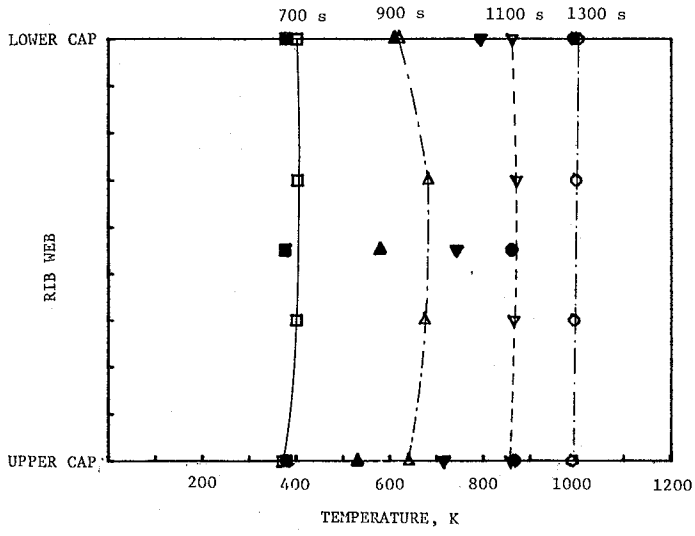

SPAR

constant material properties

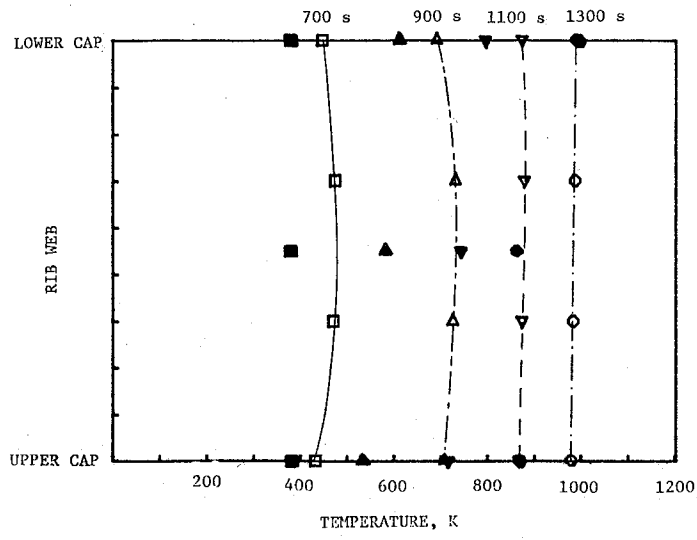

SPAR

variable material properties

Figure 7.15: BAY H* Results at W.S. 1.372 and F.S. 24.384 (Rib Cross Section).

(Test data given in solid symbols.)

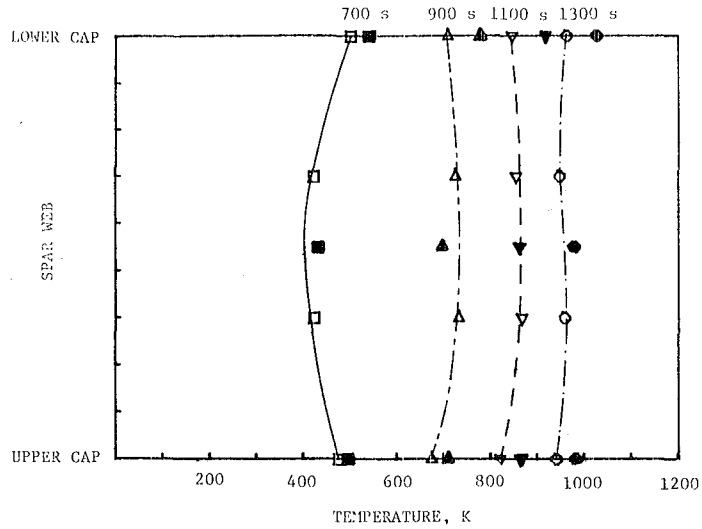

NASTRAN-COSMIC

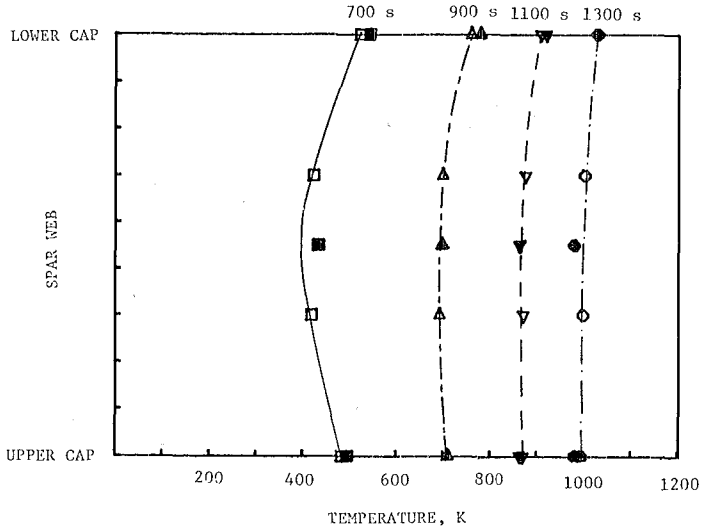

SPAR

constant material properties

at 644 K

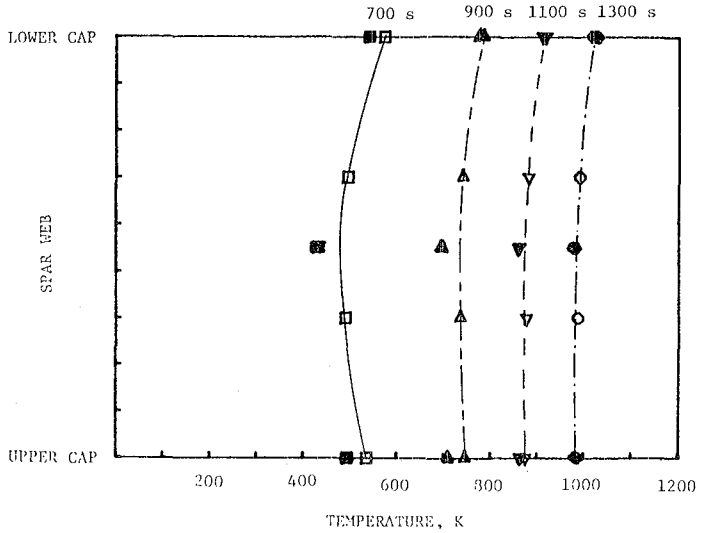

SPAR

variable material properties

Figure 7.16: BAY H* Results at W.S. 1.926 and F.S. 24.638 (Spar Cross Section).
(Test data given in solid symbols.)

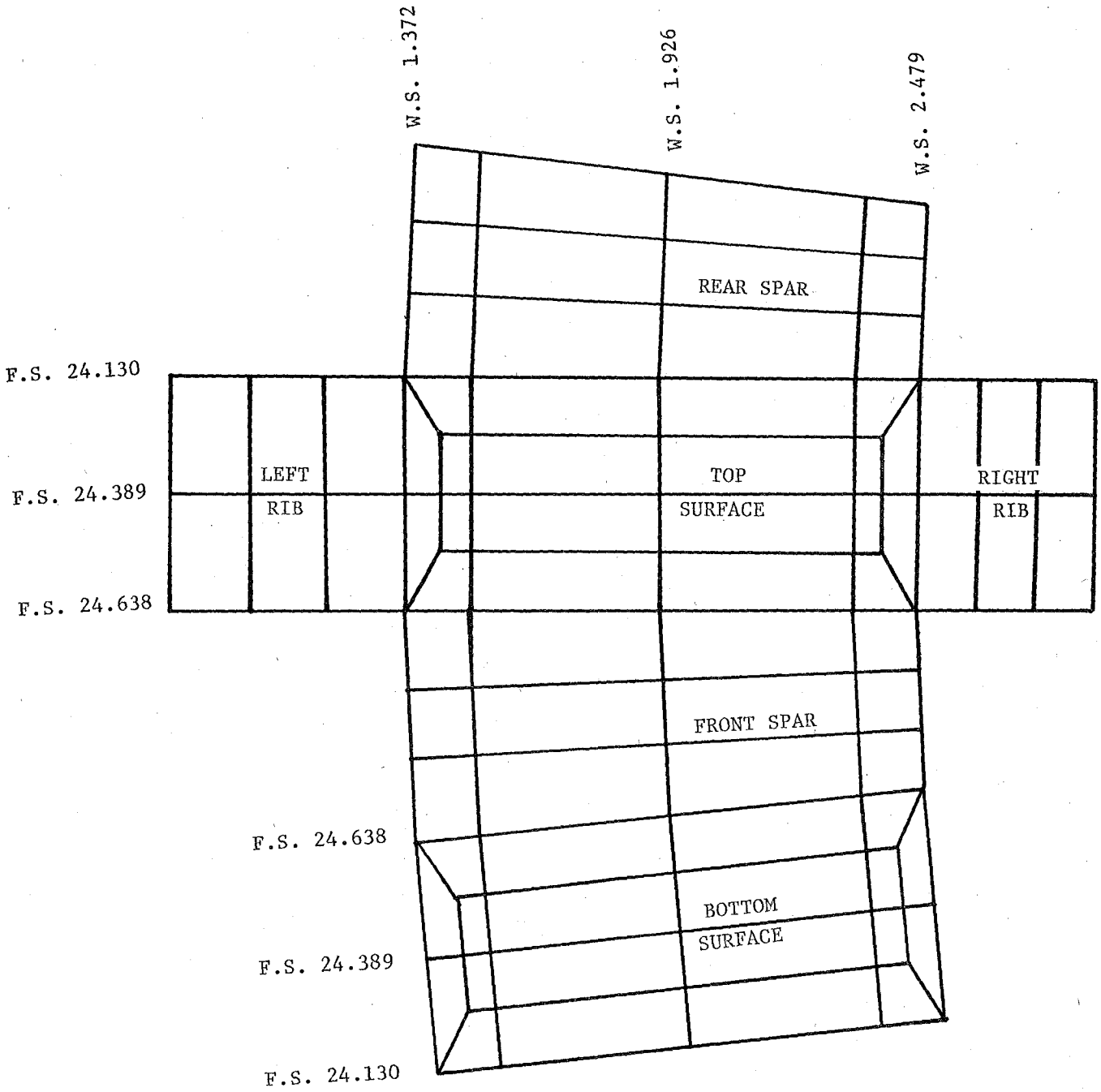

Figure 7.17: Unfolded Planform of BAY H(*) Models.

especially after 700 seconds in the heating cycle around the peak of the thermal loading, as was seen in the analysis shown earlier of the BAY H model (Figures 7.4 through 7.7). This appearance at high temperatures is another indication that this is related to radiation and not to conduction. In all the preceding analyses the time step used between computing temperatures was five seconds. Decreasing the time step to smaller values up to 0.25 seconds did not noticeably change the results.

Another important parameter in the solution method is the beta parameter that is considered a measure for the stability related to the time step used (Reference 14). A value of a half is normally sufficient to obtain stability with no limit on the time step. Tests with values of beta close to the maximum value of one did not noticeably change the results of the NASTRAN analysis. A possible deficiency in the view factor determination for elements close to corners or edges can, however, be excluded from the possibilities due to the fact that the SPAR analysis methods used the same view factors computed for the NASTRAN model.

To explain the experienced thermal behavior of the inner edge elements, several possible explanations can be sought. One of them is that in a finite-element analysis program, "element" temperatures are used for internal computation. These element temperatures are assumed to be the average of the temperatures of the connected node points. In the final stage of the heat transfer computations, a transformation matrix converts the element temperatures into separate grid point temperatures. For the elements at the outer edges of the

surface, rib, or spar web, the outer grid points are also connected to bar elements representing the caps. These grid points will possess a larger thermal capacitance due to their larger connected mass and will thus have a lower temperature than will the grid points connected to elements with less mass. The effect of ignoring the thermal capacitance of the bar elements was already observed in the NASTRAN COSMIC/bar and COSMIC/rod results (see Figures 7.4 and 7.6). The inclusion of the capacity of the bars to the edge grid points led to a (much too large) decrease in the heating rate of the cap temperatures directly from the start, and the web temperatures did increase but only after 1000 seconds. This leads to the suspicion not only that a deficiency exists in the transformation of the element-to-node temperatures but also that there is another unknown time-dependent effect. The results of the MSC-NASTRAN analysis of the BAY H model with no bar capacitance--or in that case the NASTRAN COSMIC analysis with bars--showed better agreement, although not perfect, with the available test data than did the NASTRAN analyses with the correct property values of the bar elements (see Figures 7.4 and 7.5). This would indicate that the distribution of mass or capacitance is also related to the problem.

Review of the results of the SPAR analyses will show that updating the material properties each 25 seconds resulted in higher temperatures compared to those in the analysis with constant material properties up to 1100 seconds, while at 1300 seconds a reverse effect existed in most cases (see Table 7.5). The updated SPAR analysis showed the worst agreement with the test data at the left side of the BAY H* model (W.S. 1.372).

It was felt that without knowledge of the reason behind the NASTRAN deficiency in predicting the edge element grid points, a more complete analysis of the whole structure of the HWTS would be irrelevant at this point. It was also thought that such large-scale analysis at this time would not produce indications that would lead to the explanations of the NASTRAN deficiency experienced.

The fact that both SPAR analyses, which used the same NASTRAN input data (element sizes, time steps, and view factors for the radiation), produced a good agreement, with expectations of more-or-less smooth temperature distributions as well with the test data, indicates that the physical modeling of the NASTRAN BAY H* model is basically sound.

It is also possible that the element size used in the models is the (primary) cause for the discrepancy experienced around the elements representing the caps. Despite the fact that the SPAR analyses with the same size elements agreed well with the test data and with the expected smooth temperature distribution, the accuracy of the NASTRAN program may be more dependent on the element sizes. It is intended that the possible influence of element size on the analysis be investigated using a simpler version of the BAY H model. Figure 7.18 presents possible candidates for this study: the KUBE and KUB2 models. Due to external reasons, the analysis of these models had to be postponed to a later date. This will be included in the documentation that will be submitted to the MSC and COSMIC organizations concerning this problem.

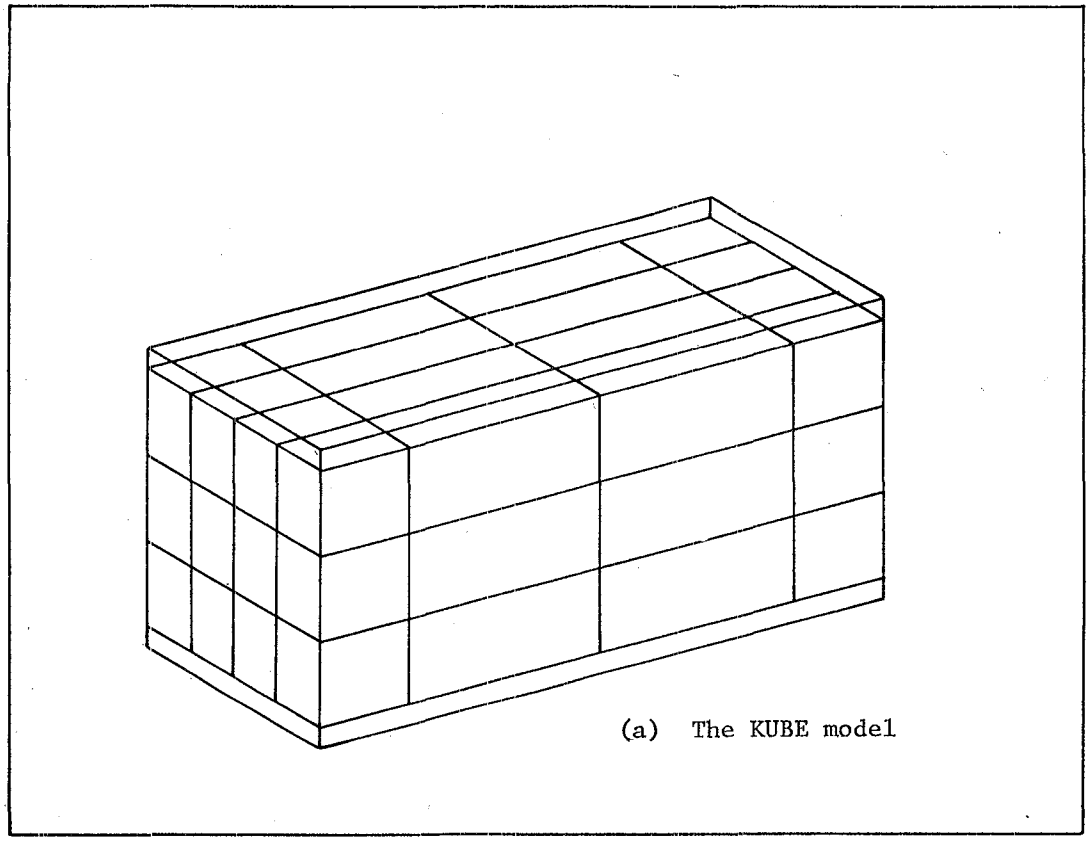

(a) The KUBE model

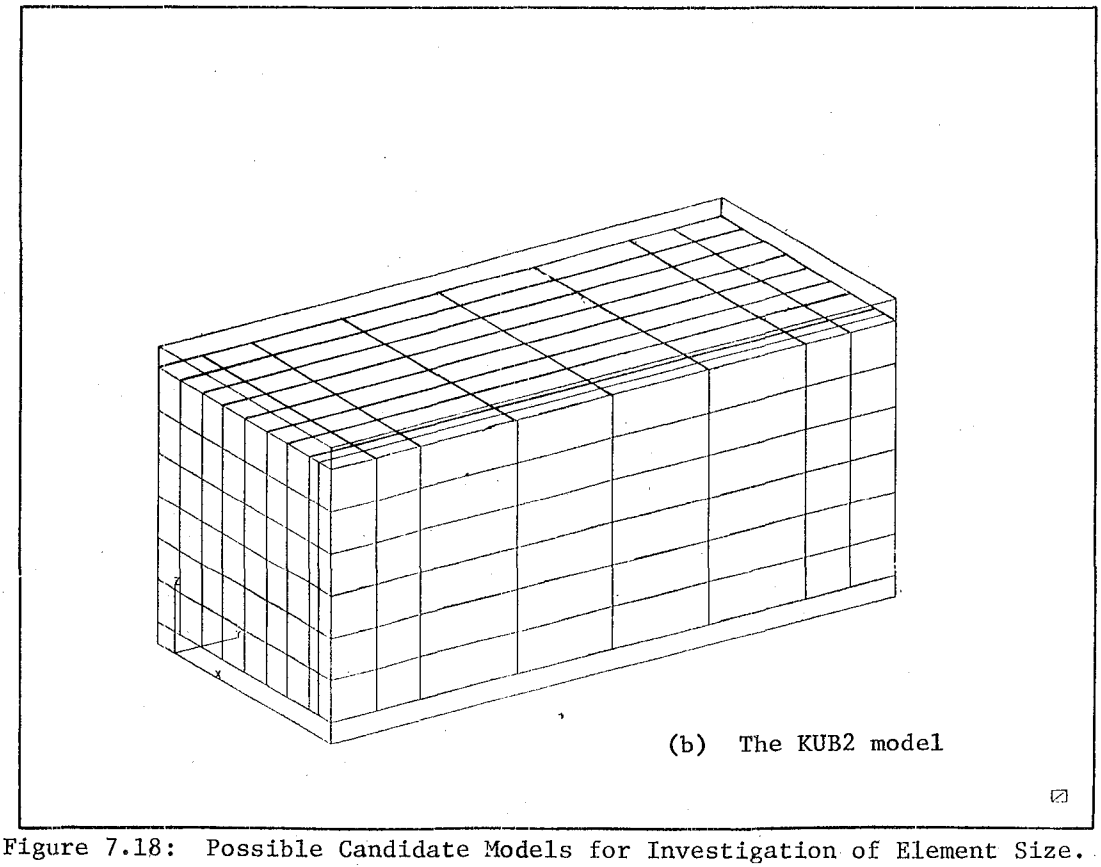

(b) The KUB2 model

Figure 7.18: Possible Candidate Models for Investigation of Element Size.

CHAPTER 8

DISCUSSION, CONCLUSIONS, AND RECOMMENDATIONS

8.1 INTRODUCTION

A finite-element analysis program, NASTRAN, was used to analyze the heat transfer in a wing section which was originally designed for a hypersonic research aircraft cruising at Mach 8. This 7.9 square meter planform semimonocoque wing structure consists of spanwise-stiffened beaded panels attached to orthogonal spars and ribs. Metallic heat shields with shallow chordwise corrugations cover the beaded panels and constitute the external surfaces. In heating tests simulating a Mach 8 maneuver environment, this structure was subjected to temperatures up to 1300 degrees Kelvin.

The major objectives set at the beginning of this program were (1) to investigate the feasibility of conducting a thermal and structural analysis of a medium-sized structure as one integral part, (2) to obtain experience with the thermal application of NASTRAN and supporting programs in handling this size and type of structure, and (3) to obtain accurate analytical thermal and structural data for evaluation of experimental data and test procedures.

In Chapter 3 the main design of an integral thermal and structural analysis was described. Using small Fortran support programs, the output of the thermal analysis was converted into input data for the structural model of the whole structure and in particular of the five upper and lower beaded panels of the important five root bays (bays F through J in Figure 2.14).

Due to delays in the development of the thermal model and the problems experienced with it, a structural analysis was not conducted. These delays were caused by deficiencies in the VIEW program and in the COSMIC version of NASTRAN. Finally a comparison of the analyses from two existing versions of NASTRAN and a SPAR analysis of a typical bay of the HWTS structure indicated that the present NASTRAN model does not produce an accurate temperature distribution around grid points connected with a large relative mass. Until the reasons are known and solutions are found for this problem, further analysis using the NASTRAN program will not produce the desired accurate temperature-time distributions.

8.2 DISCUSSION

During this program, two kinds of methods were used to generate a NASTRAN-based, finite-element model. In the first stage, element data were manually entered on cards; and the coordinates of each grid point had to be computed and entered. Checking out these input data could only be accomplished by visual inspection, NASTRAN runs, or the use of the plot capability of NASTRAN. As a result, this development was very time consuming and laborious. The second method consisted of using the PATRAN-G program and an interactive computer terminal with graphical capabilities. This PATRAN-G program enabled a fast and more efficient development of the model with real-time possibilities for checking and changing. The test editor features of the computer system also made modification and location of elements easier.

Generating the view factors for the radiation exchange coefficient matrix proved to be a major time-consuming part in the development of the NASTRAN model. Special requirements to the CHBDY elements, inaccuracies in the contour integral method used by the VIEW program, and approximation errors caused much delay. Ad hoc solutions in the form of support programs were developed for these problems, but they required many time-consuming manipulations of the data (see also programs QUAD, CONVERT, and [SUPER]FUDGE in Chapter 6). Running the VIEW program itself proved to be another major problem. Because of the presence of shading and the large number of radiation elements, the resulting core size and CPU time requirements for VIEW necessitated the subdivision of the input data into smaller units and running them separately.

Results of the first-phase thermal model indicated that the initial assumption--that besides radiation, conduction also plays an important role in the heat transfer in the HWTS--was wrong. Conduction played only a minor role. Unlike the earlier model, the current thermal model paid more attention to the size and number of the radiation elements than to the correct conduction path length in the corrugated parts, like the webs and panels.

During the development of the NASTRAN models, several error messages and deficiencies were encountered, for which solutions were obtained or which are in the process of being solved. One of the most prominent examples of these deficiencies was the problem associated with the bar elements in the thermal application of the COSMIC version of NASTRAN.

From the detailed analysis of one isolated bay model, BAY H*, it was observed that both NASTRAN versions used showed a severe discrepancy in the temperature distribution around the elements representing the caps. An exact cause for this phenomenon could not be found, but indications are that it is related to the transformation matrix that converts the element temperature to grid point temperatures and vice versa, and to the mass/thermal capacitance distribution of the elements. This problem is now being documented and will be submitted to both NASTRAN organizations.

The detailed SPAR analysis of the BAY H* model indicated that, at least for this bay, a model of an isolated bay and the corresponding parts of the heat shields is sufficient to predict temperature distributions that agree well with the measured data. It may be expected that this will also be true for the NASTRAN analysis if a solution for the problem experienced has been found.

From these observations the point can be made that an approach of using several isolated models, with or without the use of interpolation techniques, may be a better technique than using one large model. The disadvantages of such large model are (1) the requirements for large core size and CPU run times and (2) the necessity of making a compromise between, on the one hand, the desired mesh size and details and, on the other hand, what is possible under the restrictions set by the available number of grid points or degrees of freedom. Unlike a thermal analysis, a structural analysis requires a complete model to compute stress and strain distributions when asymmetrical or local (thermal) loads are applied. When additional structural analysis is

required, the use of a complete thermal model, preferably with identical node ID's, is much more desirable than extracting the necessary temperature data from a set of small models and using interpolation techniques where no model is available.

The use of a complete model would essentially change the results of an isolated bay in such a way that, through the thermal interaction between several surrounding bays, the heating rate in the spars and ribs would initially be slower, while the surface panels of each bay in the whole model would gain a little by the additional radiation from the heating zones at the peripheral areas of the bay. The size of these effects is dependent, among other things, upon the relative mass distribution of the surface, the web, and the cap elements and upon the relative location of the bay in the structure. A more complete study of two or more bays would possibly answer this.

From the flow charts for the integrated thermal/structural analysis of the HWTS in Chapter 3, as well as from the test procedure in Appendix B, it can be seen that data management of the model components and data files is extremely important. During the generation of the models and during the several steps in the thermal and structural analysis, numerous files were created and manipulated. The logistic problems involved in the isolated-bays approach would be even more complex.

Comparison between the SPAR runs with constant and variable material properties resulted in only slightly better agreement for the updated SPAR version. This is because of the minor role of the conduction in the heat transfer in the HWTS.

Although the PATRAN-G program is capable of modifying parts of a model stored in its data base in a relatively quick and efficient way, the flexibility in modification of parts of the thermal model is in general limited by the necessity to regenerate (large) parts of the radiation exchange coefficient matrix. This means that if more data points are desired in an area not before allocated as a prime area (in the current investigation bays G, H, I, and M), numerous changes have to be made.

Based on the experience with the conversion of the NASTRAN model of the BAY H* model, an alternative approach to meet the objective of obtaining an accurate temperature distribution could be the conversion of the complete NASTRAN THWTS model into a SPAR analysis model.

8.3 CONCLUSIONS

- The use of the PATRAN-G program has proven to be a very efficient way of generating a (thermal) finite-element model.
- Solutions for deficiencies in the VIEW program, related to the accuracy of input and output data and to the contour integral solution method, cause the computation of the view factors to be very tedious and time consuming.
- Due to these deficiencies and the large number of radiation elements required for such a large structure as the HWTS, the computation of the view factors for the radiation exchange coefficient matrix took up the most time of the development of the thermal model of the HWTS.

- In a high-temperature, thin-walled structure like the HWTS, radiation is the most important mode of heat transfer. Conduction does not play a major role in this structure.
- Updating the material properties during a transient thermal run did not improve noticeably the accuracy of the thermal (SPAR) analysis for this structure.
- The use of a medium-sized structure like the HWTS produced valuable information about the possibilities and deficiencies in the thermal application of NASTRAN.
- At the present time the NASTRAN thermal model of the HWTS is not capable of predicting accurate temperatures for grid points in the neighborhood of elements with a large relative mass. The exact reason is unknown at this moment but is probably related to the element-to-grid temperature transformation matrix.
- The use of a single bay (SPAR) model to study the local temperature-time distribution produced good agreement between measured and predicted data.

8.4 RECOMMENDATIONS

Concerning the VIEW program:

- The criterion for the planarity of quadrilateral CHBDY elements in the VIEW program should be softened.
- The contour integral solution method of this program should be modified to increase the accuracy of view factors from

large to small elements. One way to achieve this is to rearrange internally the sequence of the elements according to area size.

- Further study is required to investigate the possibility of reducing the overall computing time of the program when shading is involved. Application of newly developed, hidden-line algorithms is suggested as a possible way to achieve this.

Concerning NASTRAN:

- It is recommended to avoid at the present time the use of bar elements in the thermal application of the COSMIC version of NASTRAN. Rod elements are equivalent to bar elements in the thermal analysis.
- High priority should be given to finding the exact reason behind the deficiency experienced in both NASTRAN methods around the "cap" elements in the BAY H(*) models.
- If would be beneficial, in most of the thermal applications of NASTRAN, if the radiation energy that is lost because the overall sum of view factors for one or more elements is less than one, were directed to a scalar element with ambient temperature and not to absolute zero as in the current situation.
- A detailed study of the effect of element size around elements with a large relative mass, using the KUBE and KUB2 models is recommended.

Concerning the thermal analysis:

- To meet the immediate goal of obtaining an accurate thermal stress distribution in the HWTS, it is recommended to convert the existing NASTRAN THWTS model into a SPAR analysis model. The computed temperature-time distributions can be used for input in the existing NASTRAN structural analysis model, SHWTS.
- Based on the experiences of this study, the use of a small analytical pilot model is strongly recommended before modeling of a large and complex structure like the HWTS is begun.

REFERENCES

1. Plank, P. P.; Sakata, I. F.; Davis, G. W.; and Richie, C. C.: Hypersonic Cruise Vehicle Wing Structure Evaluation. NASA CR-1568, 1970.

2. Greene, Bruce E.: Advanced Beaded and Tubular Structural Panels, Volume 1, Design and Analysis. NASA CR-132460, 1974.

3. Kirkham, F. S.; Jackson, Robert L.; and Weidner, John P.: Study of a High-Speed Research Airplane. AIAA Paper 74-988, August 1974.

4. Plank, P. P.; and Penning, F. A.: Hypersonic Wing Test Structure Design, Analysis, and Fabrication. NASA CR-127490, 1973.

5. Fields, Roger A.; Reardon, Lawrence F.; and Siegel, William H.: Loading Tests of a Wing Structure for a Hypersonic Aircraft. NASA TP-1596, 1980.

6. Siegel, William H.: Experimental and Finite-Element Investigation of the Buckling Characteristics of a Beaded Skin Panel for a Hypersonic Aircraft. NASA CR-144863, 1978.

7A. NASA-COSMIC: NASTRAN Users Manual. NASA SP-221(05), 1978.

7B. McNeil-Schwindler Corporation: MSC-NASTRAN Application Manual, CDC-7600 ed., Nov. 1972.

8. Marlowe, M. B.: Moore, R. A.; and Whetstone, W. D.: SPAR Thermal Analysis Processors Reference Manual, System Level 16. NASA CR-159162, 1979.

9. Puccinelli, E. F.: VIEW Program User Manual, X-324-73-272. July 1973.

10. PDA Engineering: PDA/PATRAN-G Users Guide, Volumes I and II, 1980.

11. Herbener, D. G.; and Hanner, O. M.: Hypersonic Wing Test Structure: Preliminary Draft of a Portion of the Final Report, Part I--Design Task 2--Wing Temperatures. MCR-72-96, Issue 2, December 1972.

12. Defense Metals Information Center: Physical Properties of Some Nickel-Base Alloys. DMIC Report 129, May 1960.

13. Penning, F. A.; and Plank, P. P.: Hypersonic Wing Test Structure: Preliminary Draft of a Portion of the Final Report, Part I--Design Task 1--Assemble Data. MCR-72-96, Issue 1, May 1972.

14. NASA-COSMIC: NASTRAN Theoretical Manual. NASA SP-222(03), 1976.

APPENDIX A

DRAWINGS

In this appendix, detailed drawings of the generation of the thermal model of the HWTS (second phase) are given. Although PATRAN-G makes a distinction between grid points in the Phase-one, and node points in the Phase-two generation, the nominal name in NASTRAN used for these points is grid point. Therefore, the node point ID's of PATRAN-G are the grid point ID's in the NASTRAN analysis. The drawings are listed according to the functional components in the thermal model of the structure, THWTS:

A.1 Lower Surface of Wingbox

A.2 Upper Surface of Wingbox

A.3 Webs of Spars and Ribs

A.4 Caps and Vertical Angles of Spars and Ribs

A.5 Lower Heat Shield

A.6 Upper Heat Shield

A.7 Insulation Blanket

A.8 Curtain Elements

A.9 Radiation Elements.

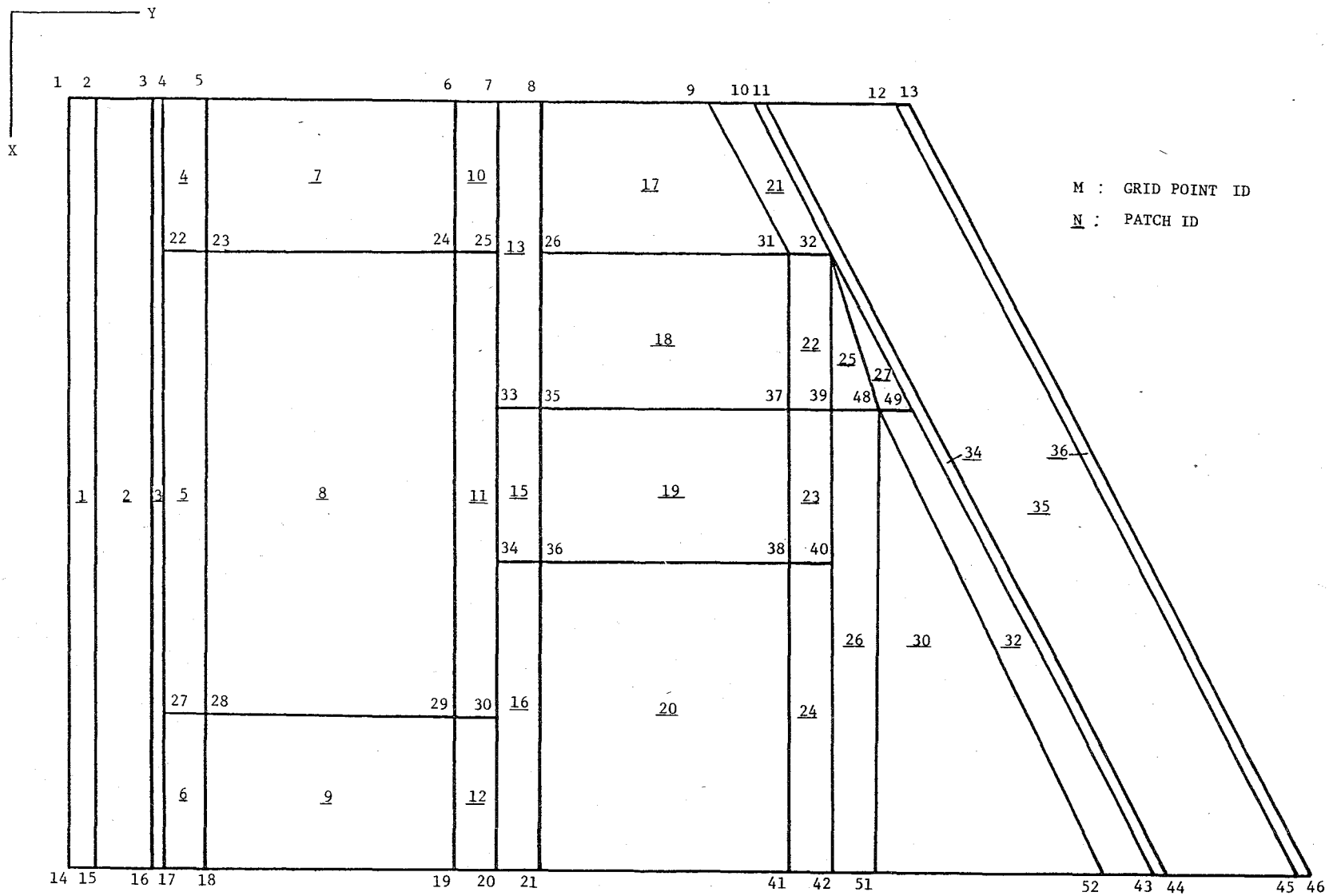

Figure A.1.1: Phase-one Plot of PATRAN-G Generation of Lower Surface of Wingbox. (Patch ID's underlined.)

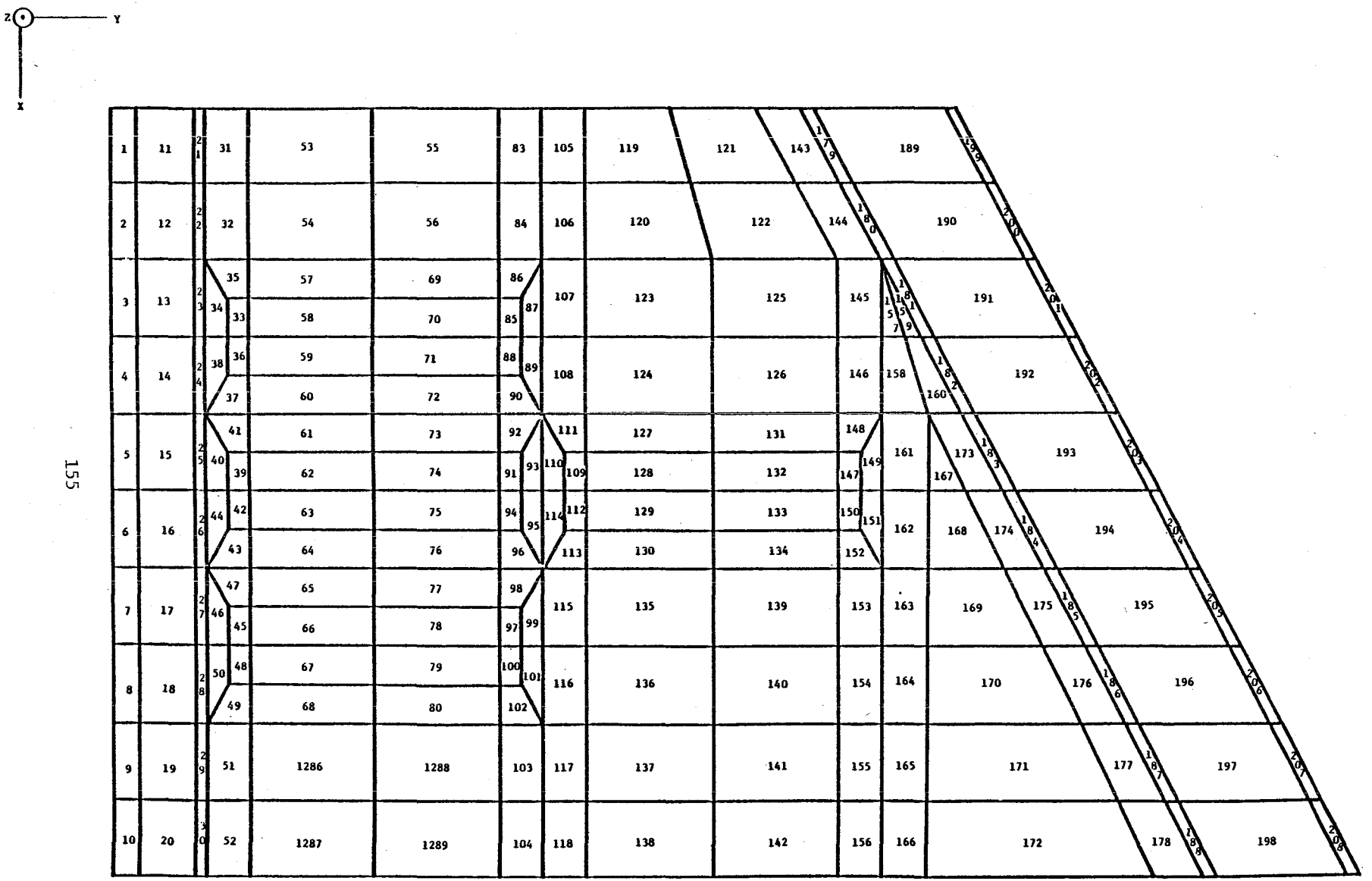

Figure A.1.2: Phase-two Plot of PATRAN-G Generation of Lower Surface of Wingbox. (Plate Elements.)

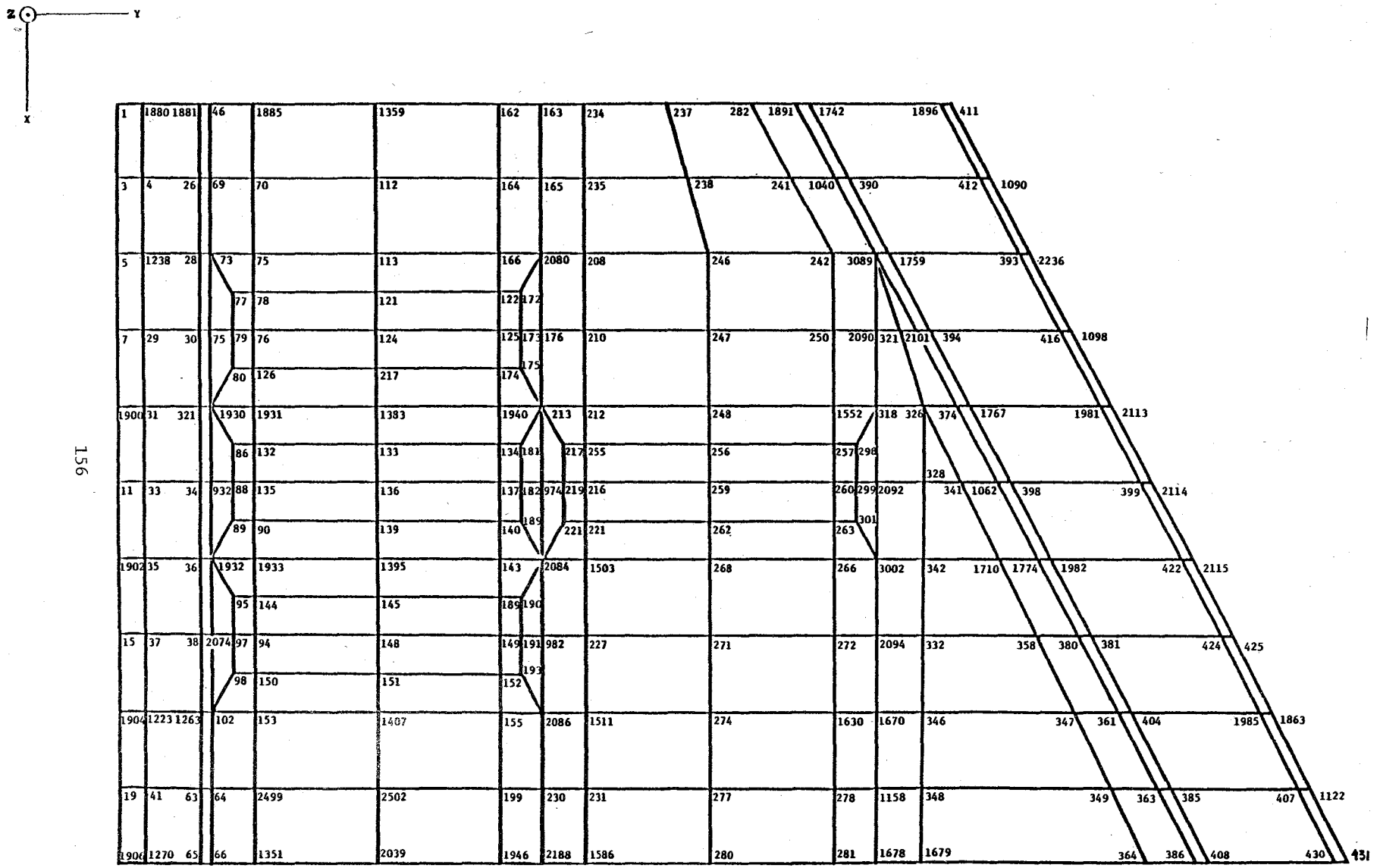

Figure A.1.3: Phase-two Plot of PATRAN-G Generation of Lower Surface of Wingbox. (Node points.)

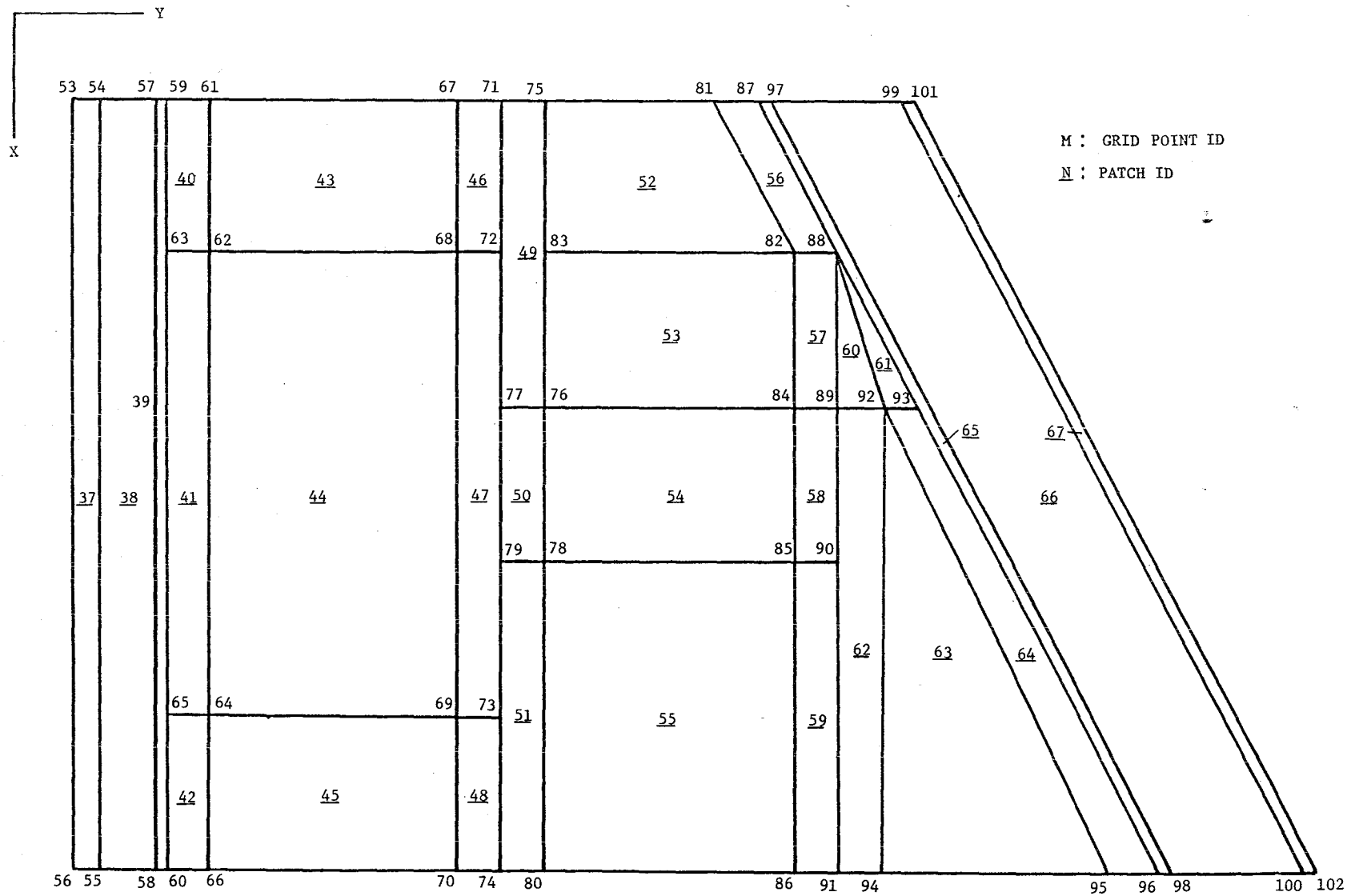

Figure A.2.1: Phase-one Plot of PATRAN-G Generation of Upper Surface of Wingbox. (Patch ID's underlined.)

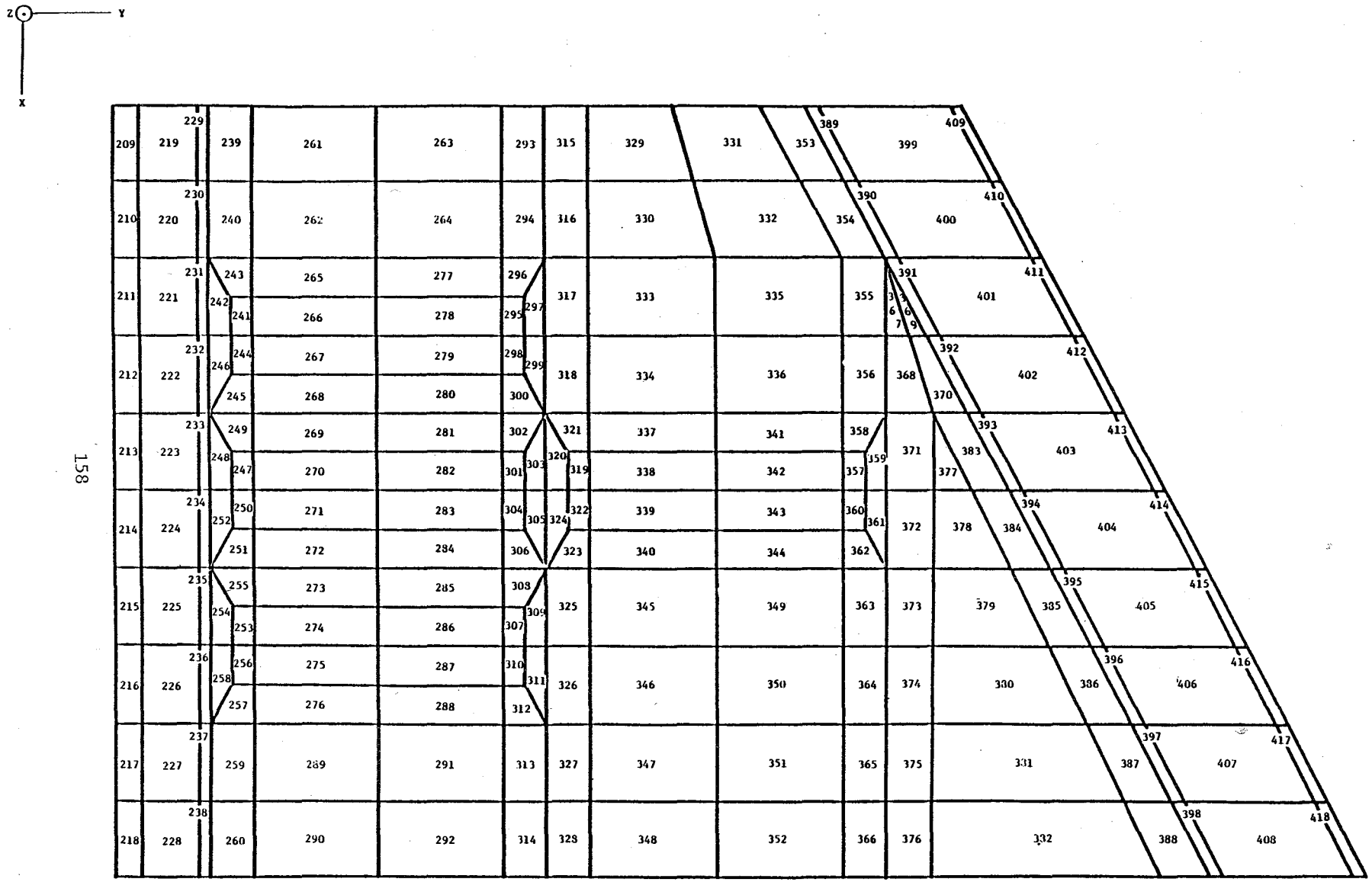

Figure A.2.2: Phase-two Plot of PATRAN-G Generation of Upper Surface of Wingbox. (Plate elements.)

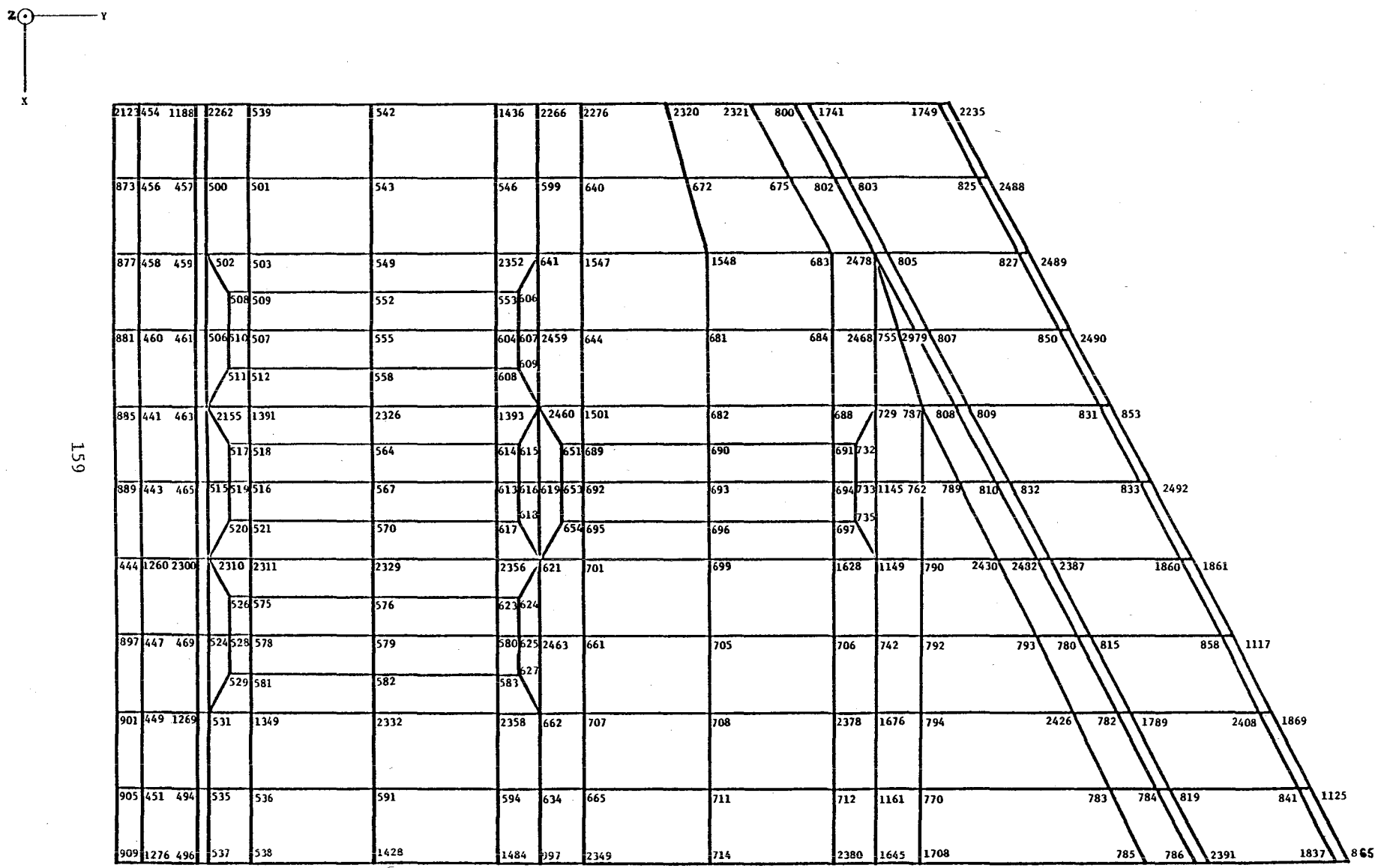

Figure A.2.3: Phase-two Plot of PATRAN-G Generation of Upper Surface of Wingbox. (Node points.)

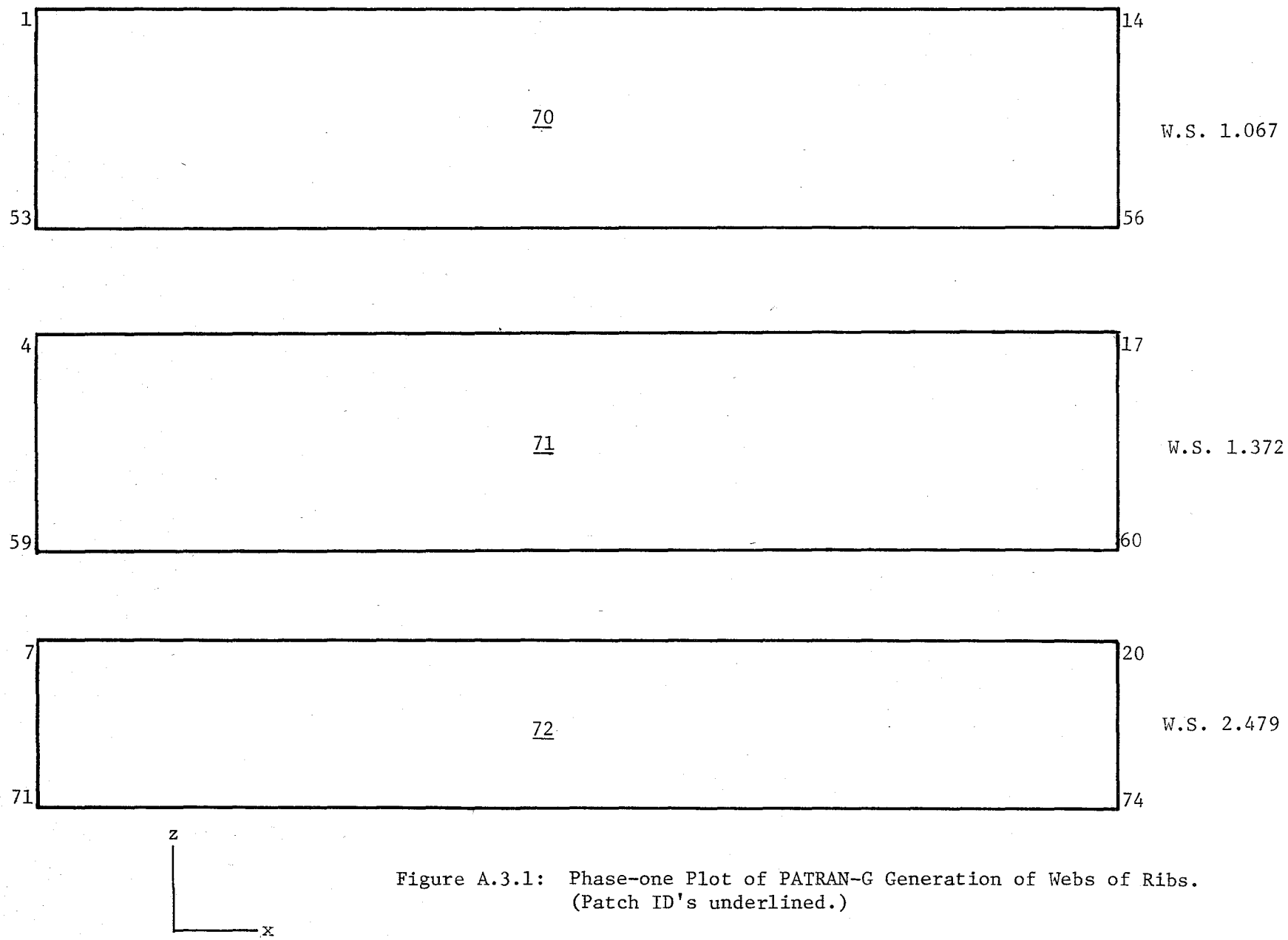

Figure A.3.1: Phase-one Plot of PATRAN-G Generation of Webs of Ribs. (Patch ID's underlined.)

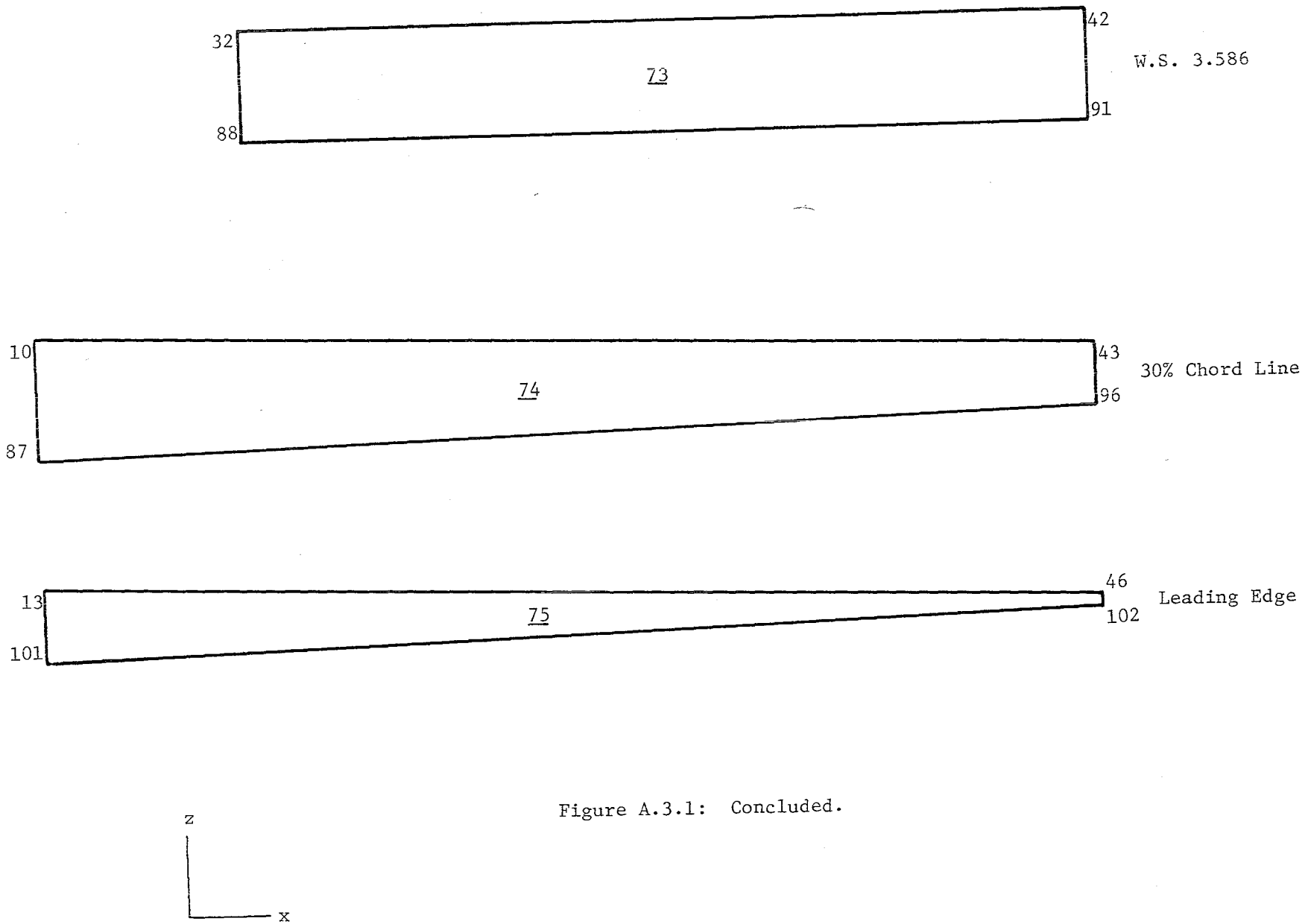

Figure A.3.1: Concluded.

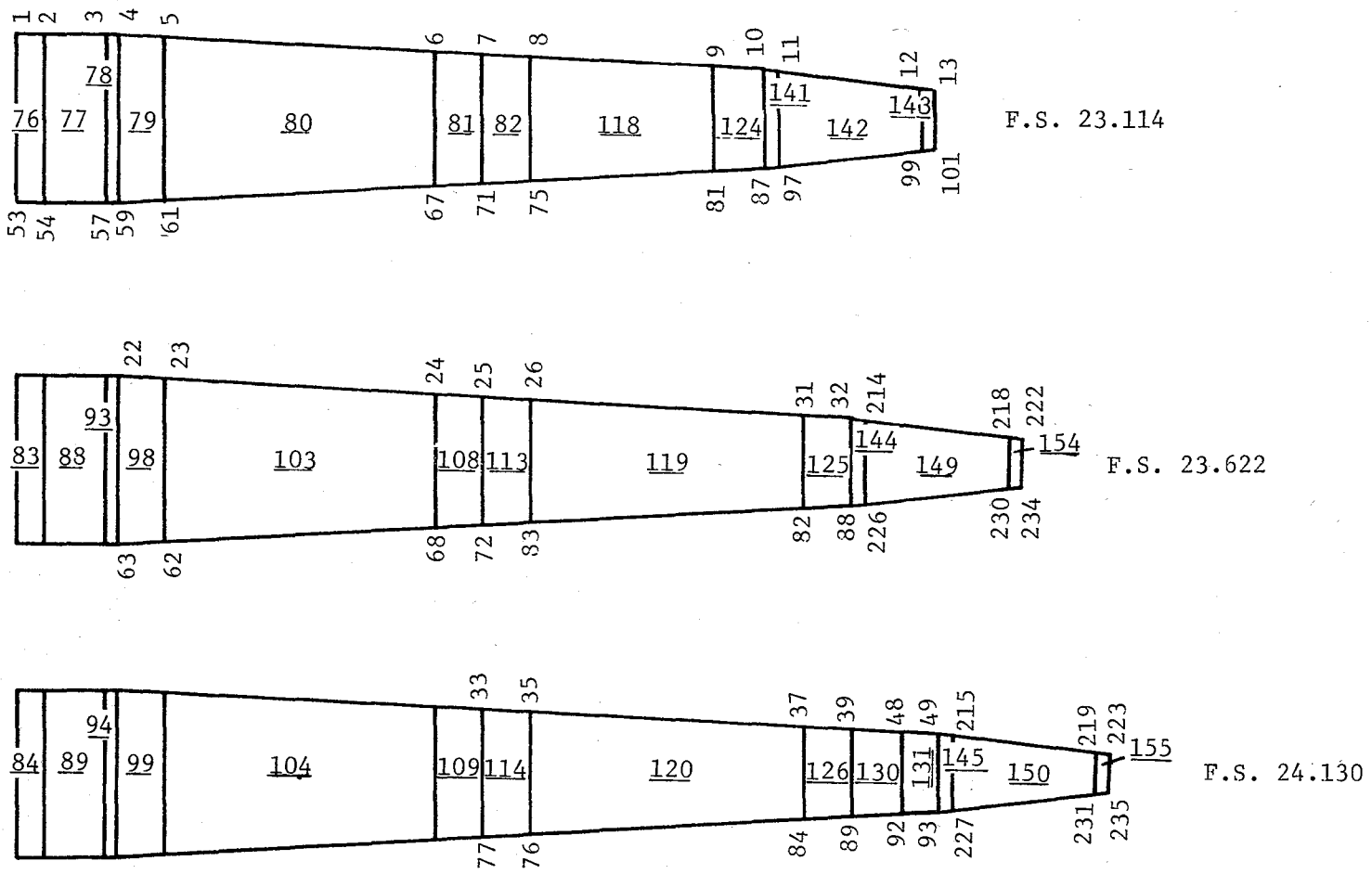

Figure A.3.2: Phase-one Plot of PATRAN-G Generation of Webs of Spars. (Patch ID's underlined.)

Figure A.3.2: Concluded

419	422	425	428	431	434	437	440	443	446
420	423	426	429	432	435	438	441	444	447
421	424	427	430	433	436	439	442	445	448

W.S. 1.067

449	452	455	458	461	464	467	470	473	476
450	453	456	459	462	465	468	471	474	477
451	454	457	460	463	466	469	472	475	478

W.S. 1.372

479	482	485	488	491	494	497	500	503	506
480	483	486	489	492	495	498	501	504	507
481	484	487	490	493	496	499	502	505	508

W.S. 2.479

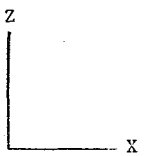

Figure A.3.3: Phase-two Plot of PATRAN-G Generation of Webs of Ribs. (Plate elements.)

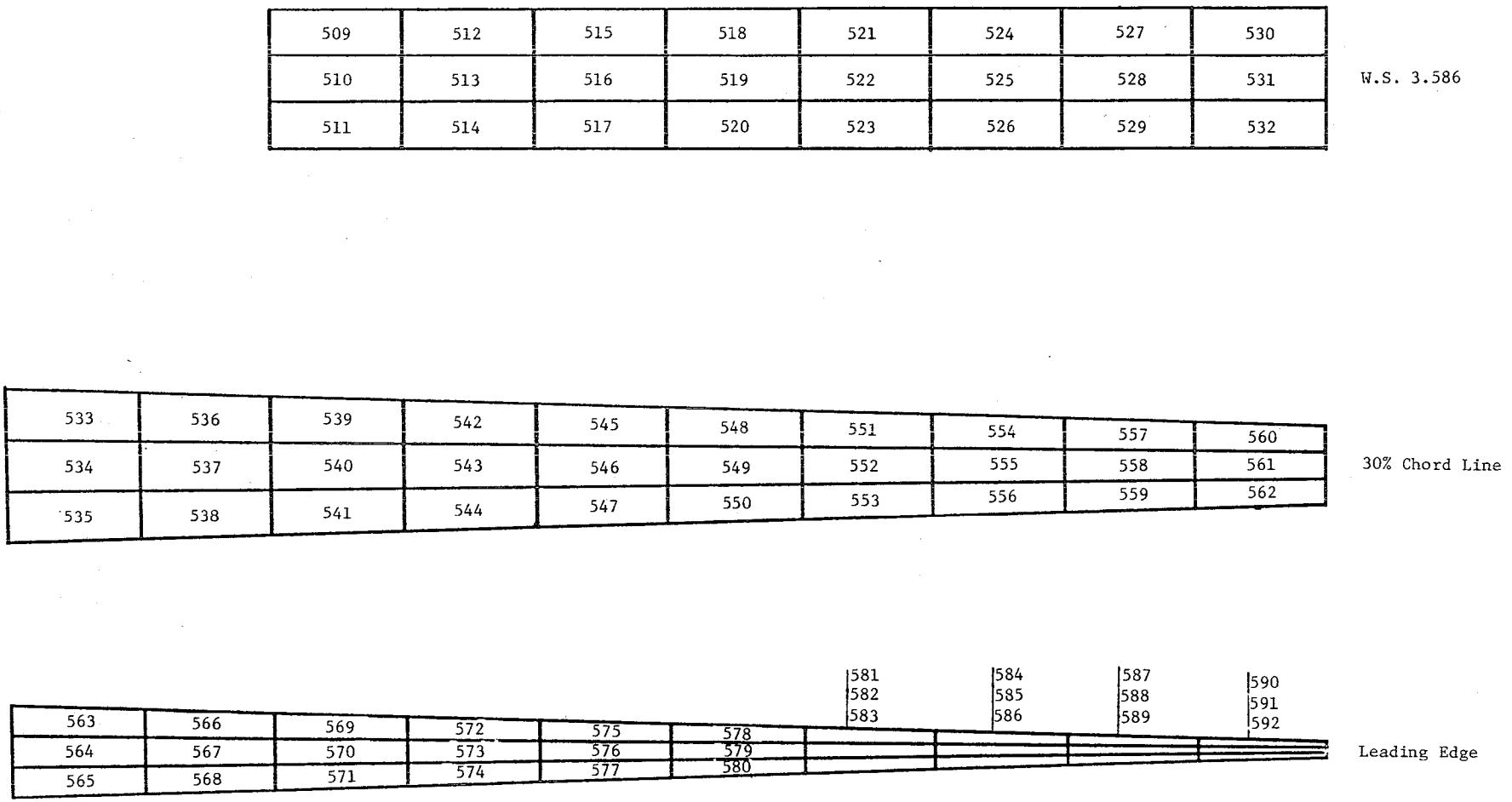

Figure A.3.3: Concluded.

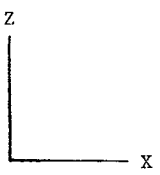

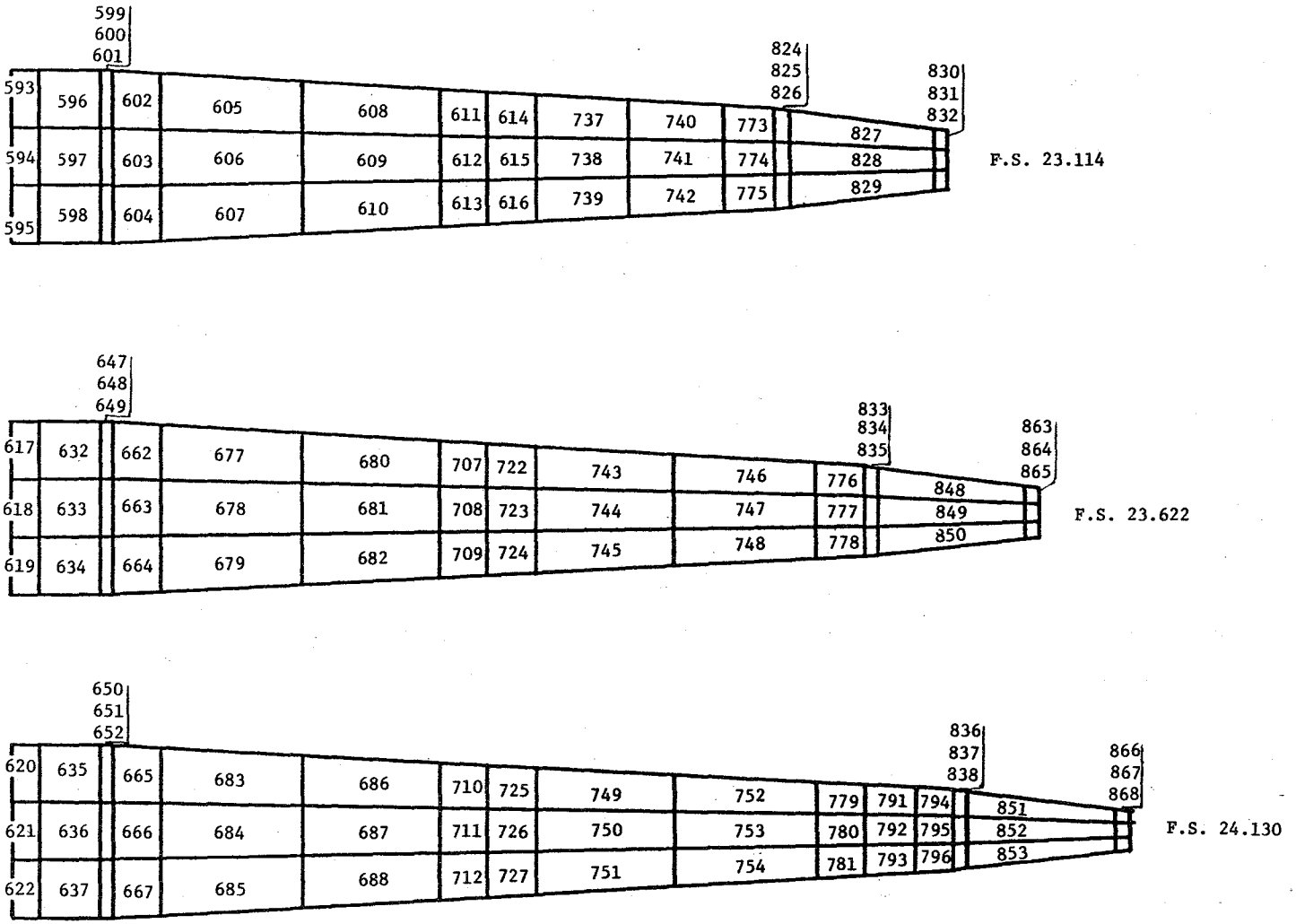

Figure A.3.4: Phase-two Plot of PATRAN-G Generation of Webs of Spars. (Plate elements.)

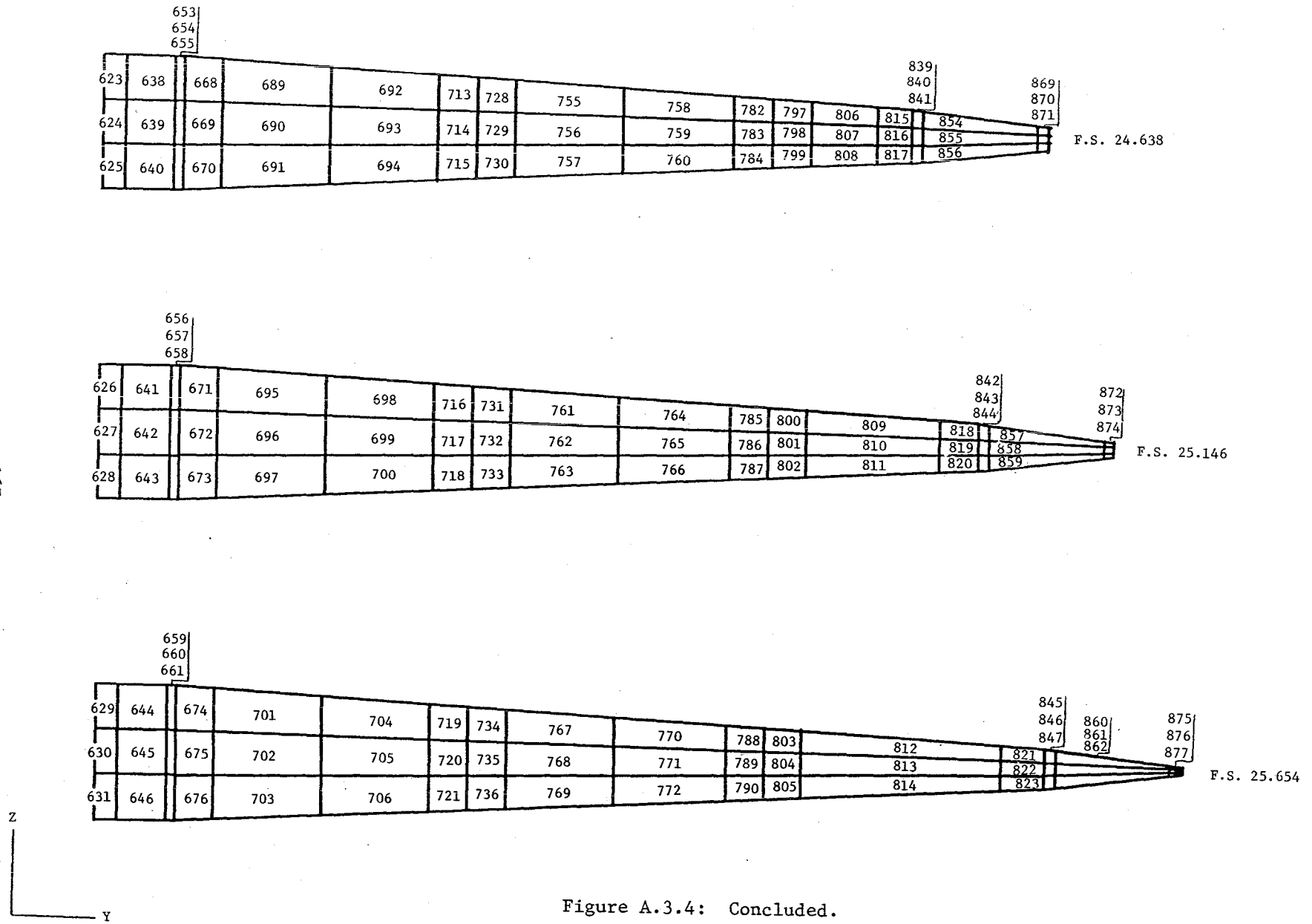

Figure A.3.4: Concluded.

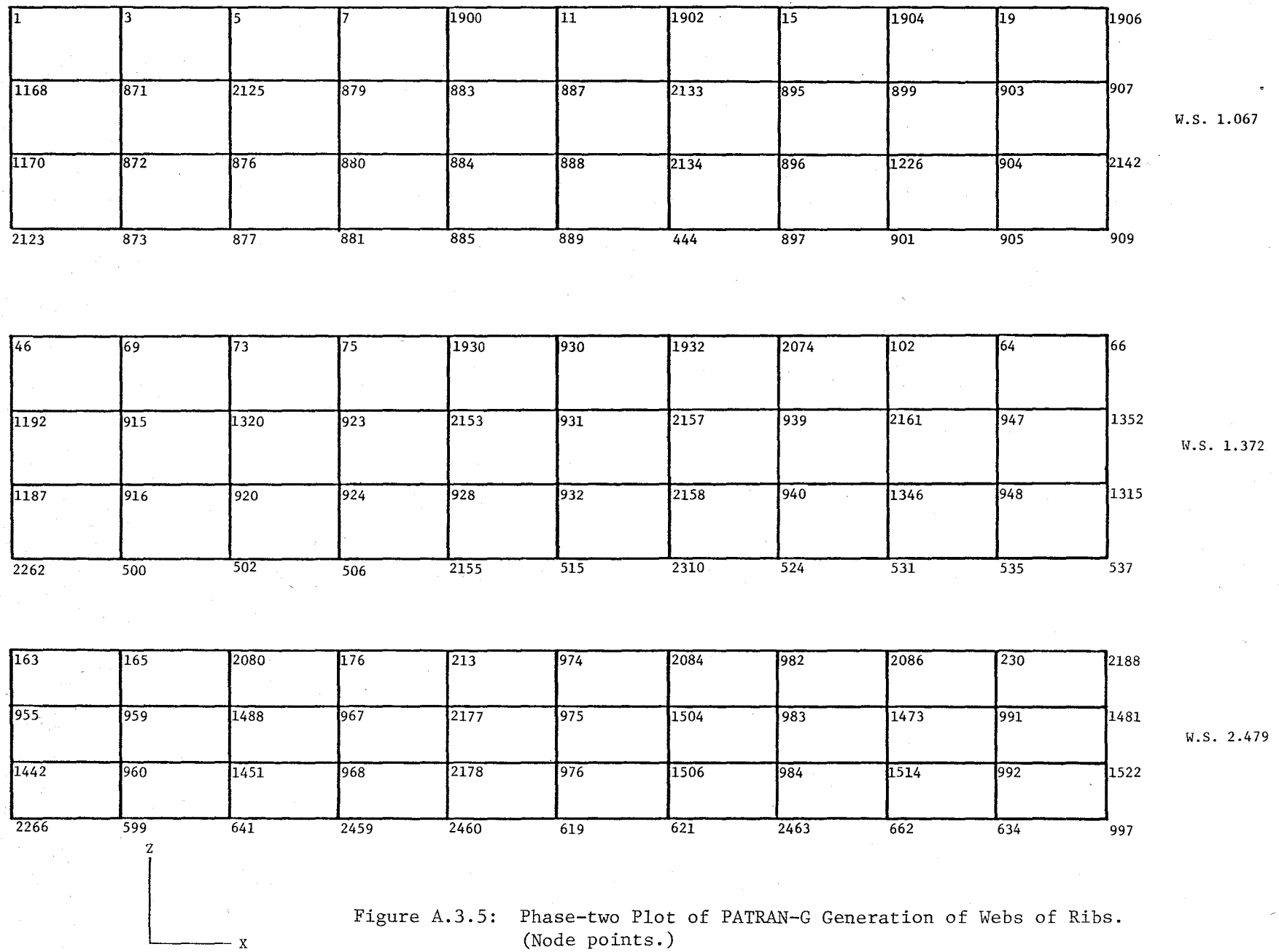

Figure A.3.5: Phase-two Plot of PATRAN-G Generation of Webs of Ribs. (Node points.)

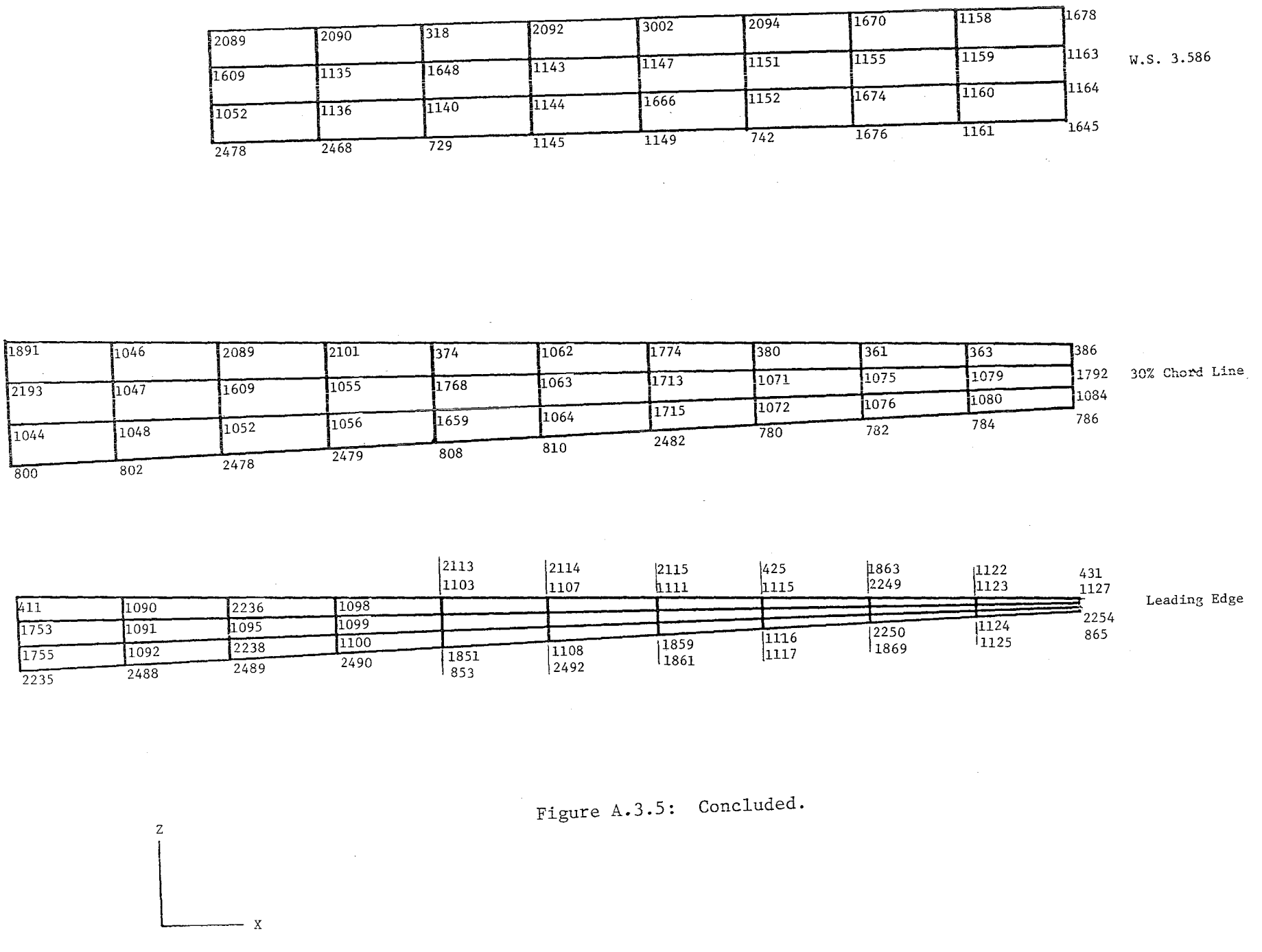

Figure A.3.5: Concluded.

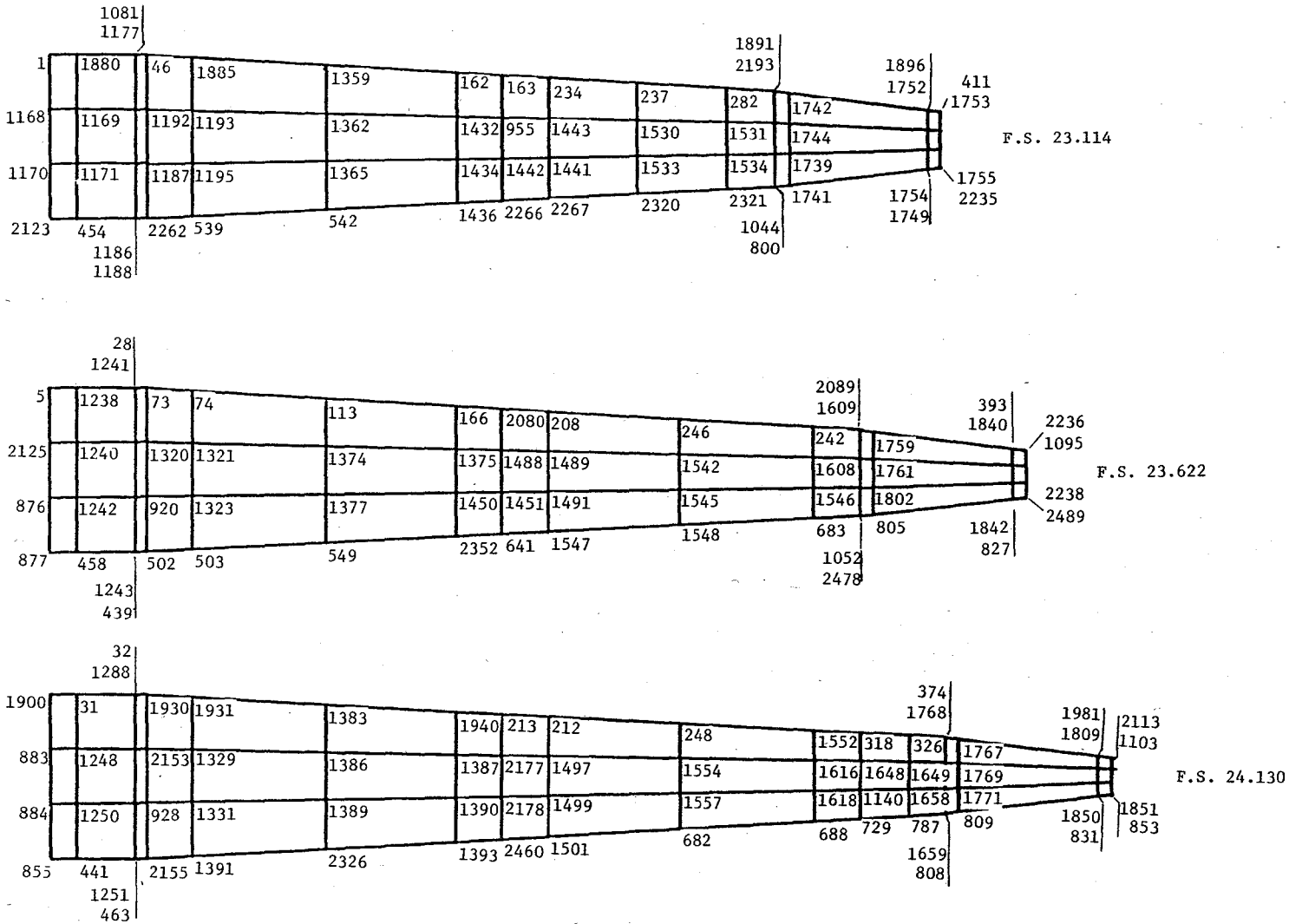

Figure A.3.6: Phase-two Plot of PATRAN-G Generation of Webs of Spars. (Node points.)

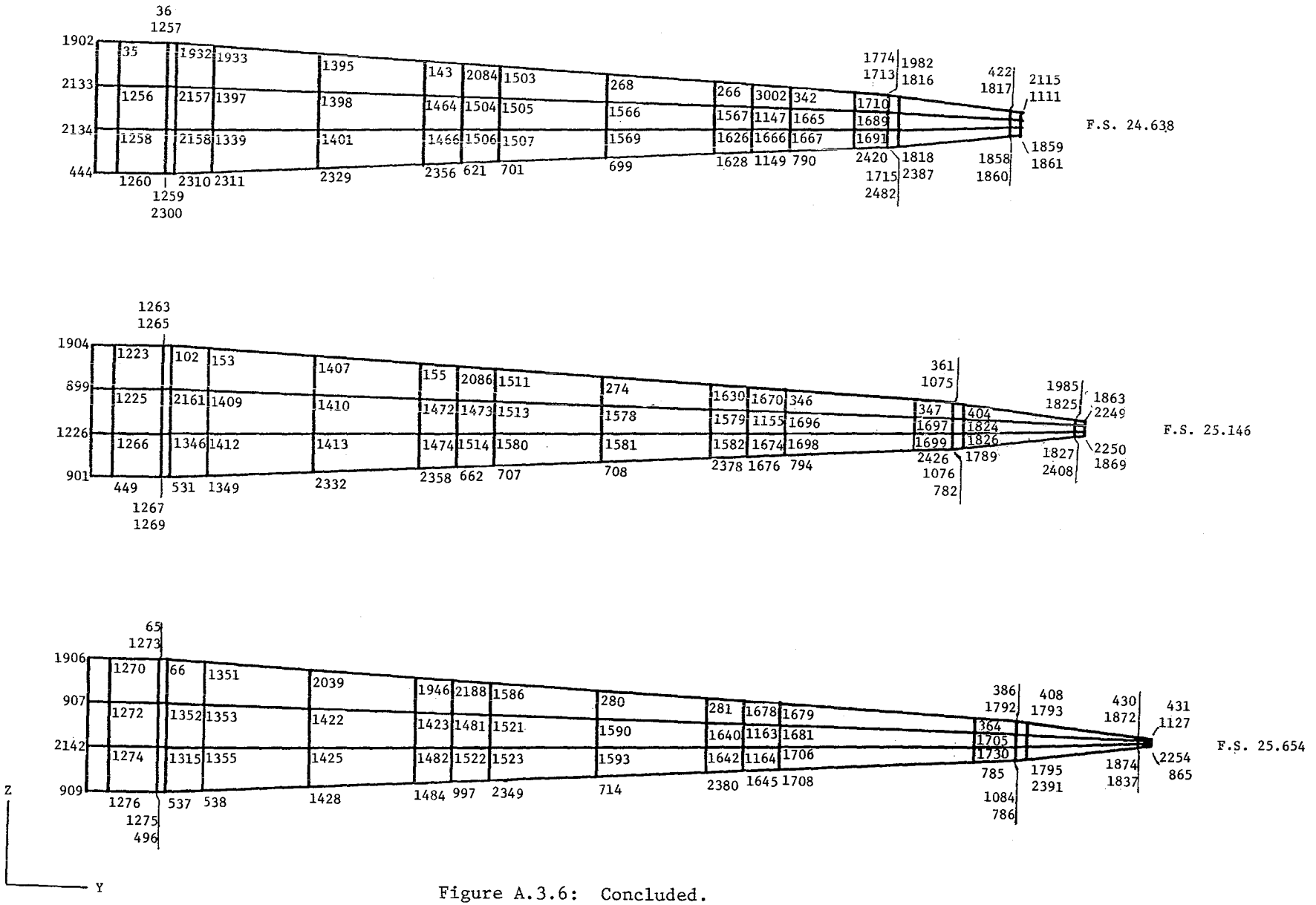

Figure A.3.6: Concluded.

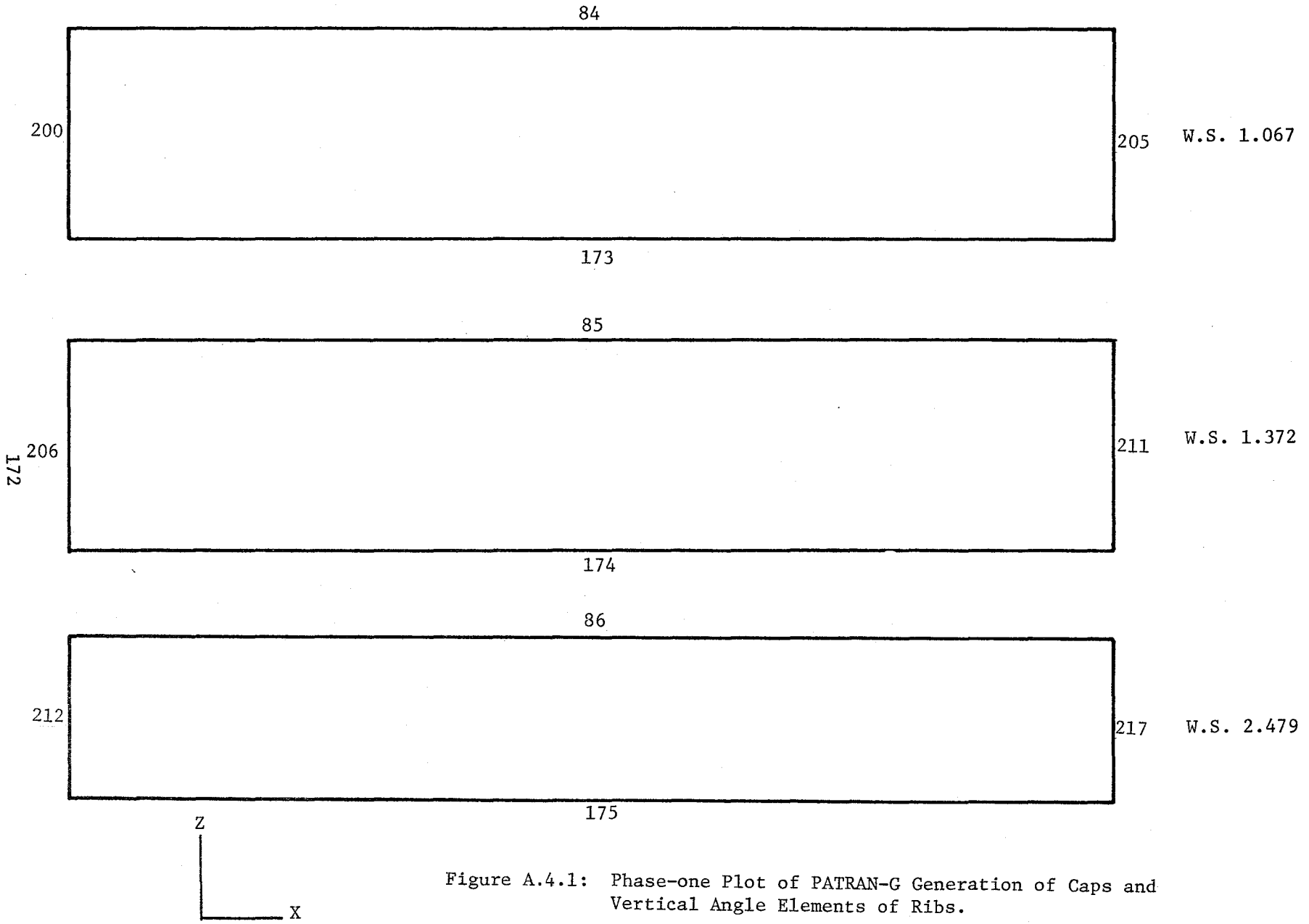

Figure A.4.1: Phase-one Plot of PATRAN-G Generation of Caps and Vertical Angle Elements of Ribs.

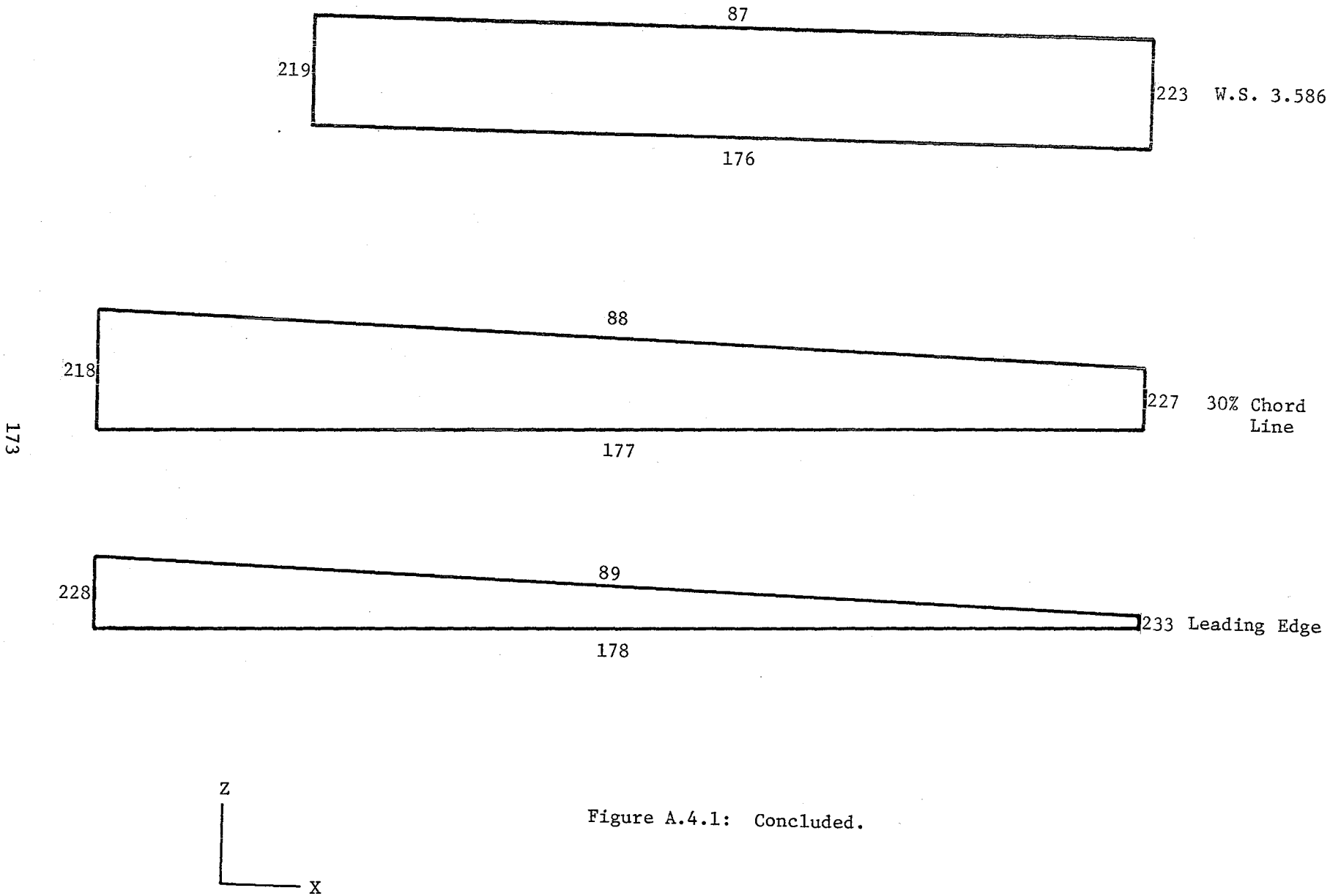

Figure A.4.1: Concluded.

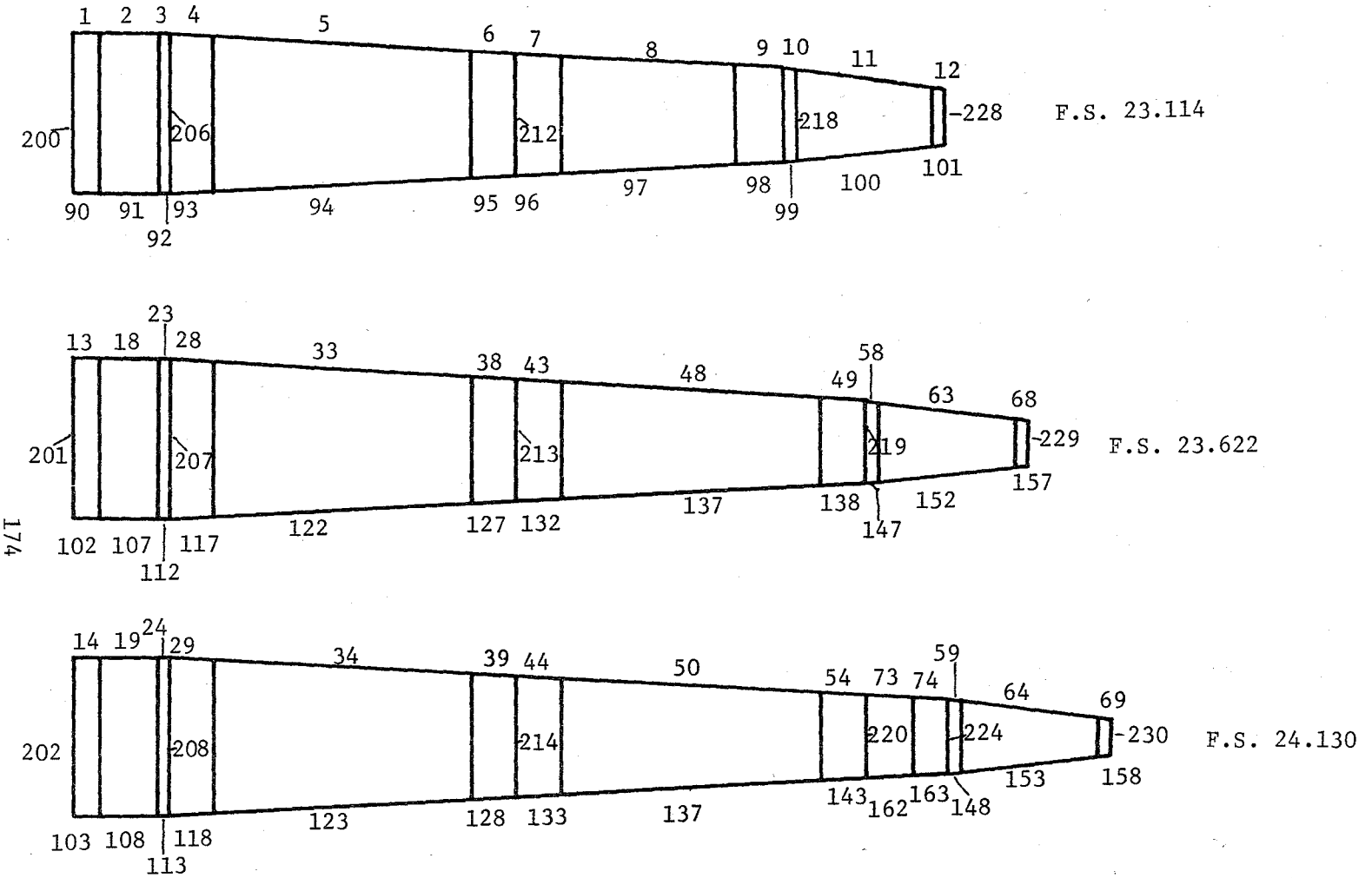

Figure A.4.2: Phase-one Plot of PATRAN-G Generation of Caps and Vertical Angle Elements of Spars.

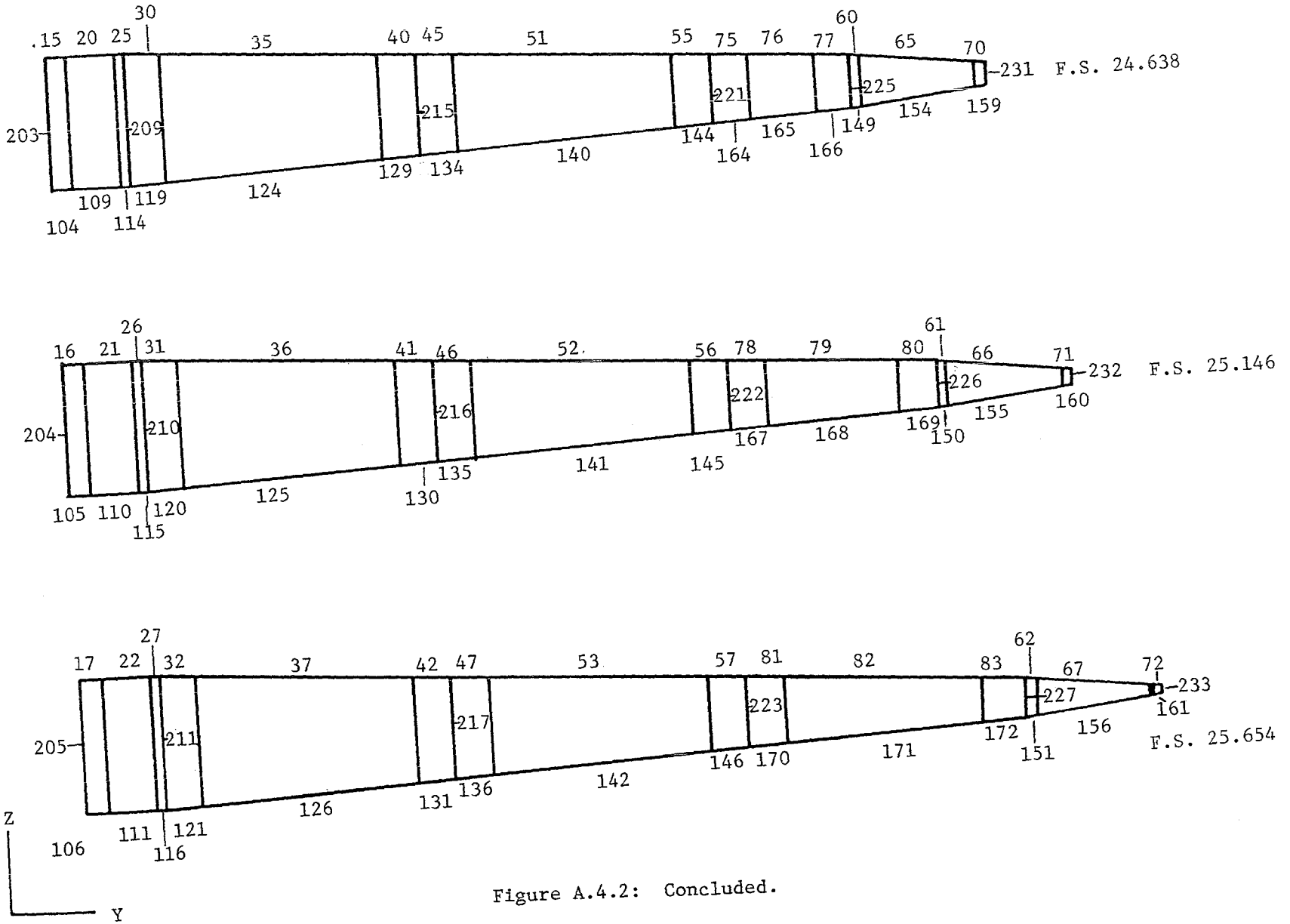

Figure A.4.2: Concluded.

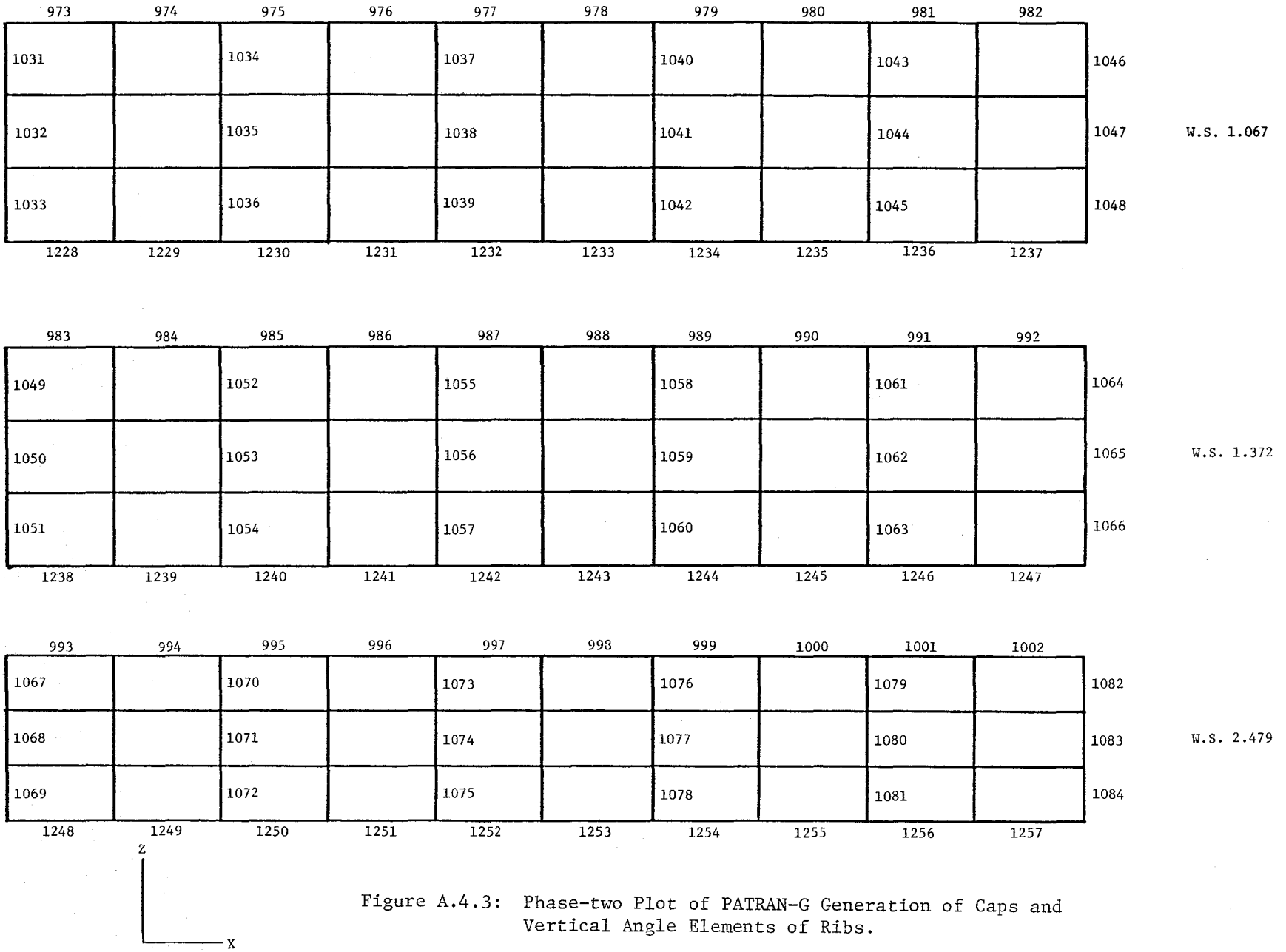

Figure A.4.3: Phase-two Plot of PATRAN-G Generation of Caps and Vertical Angle Elements of Ribs.

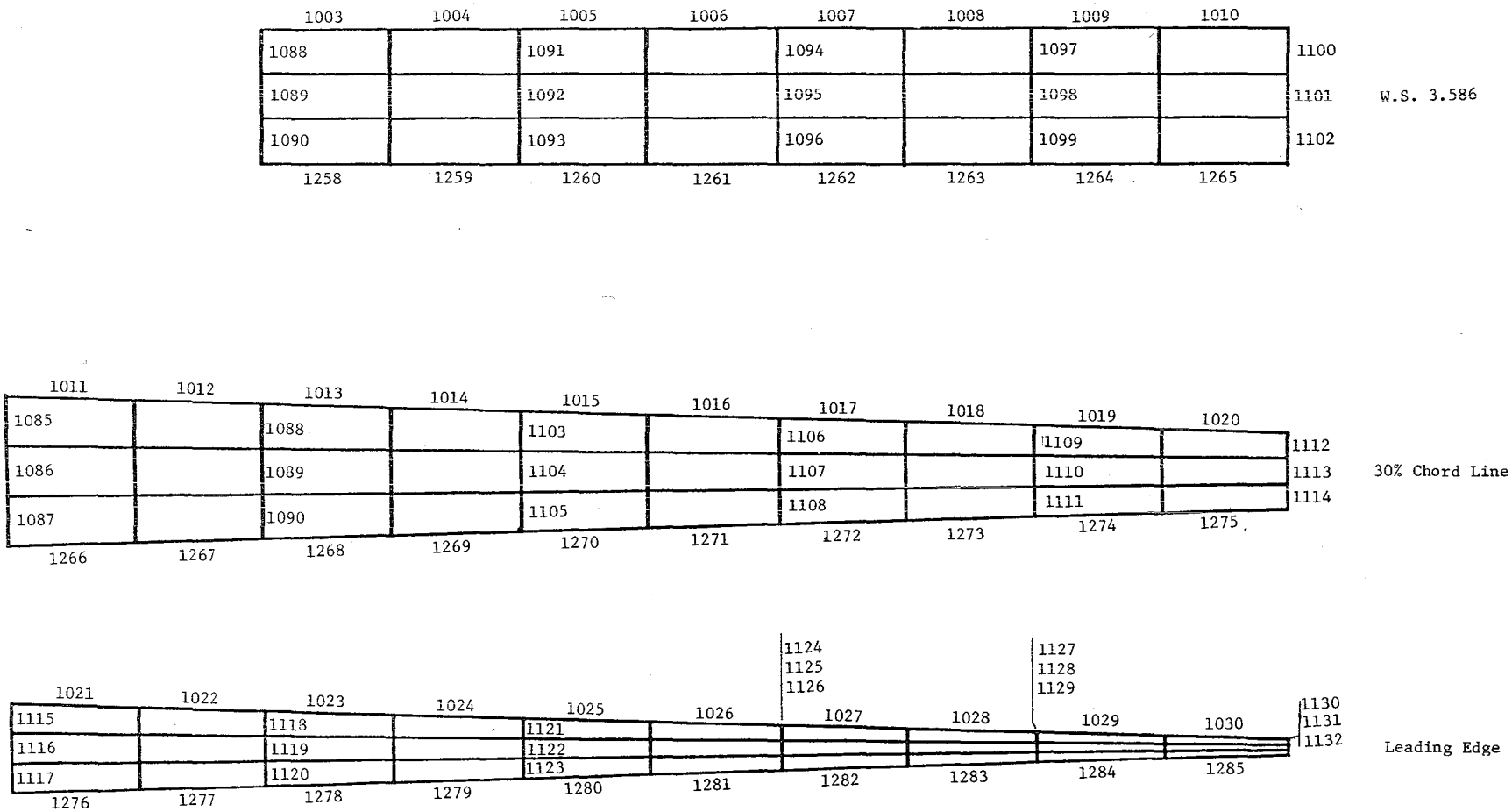

Figure A.4.3: Concluded.

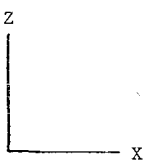

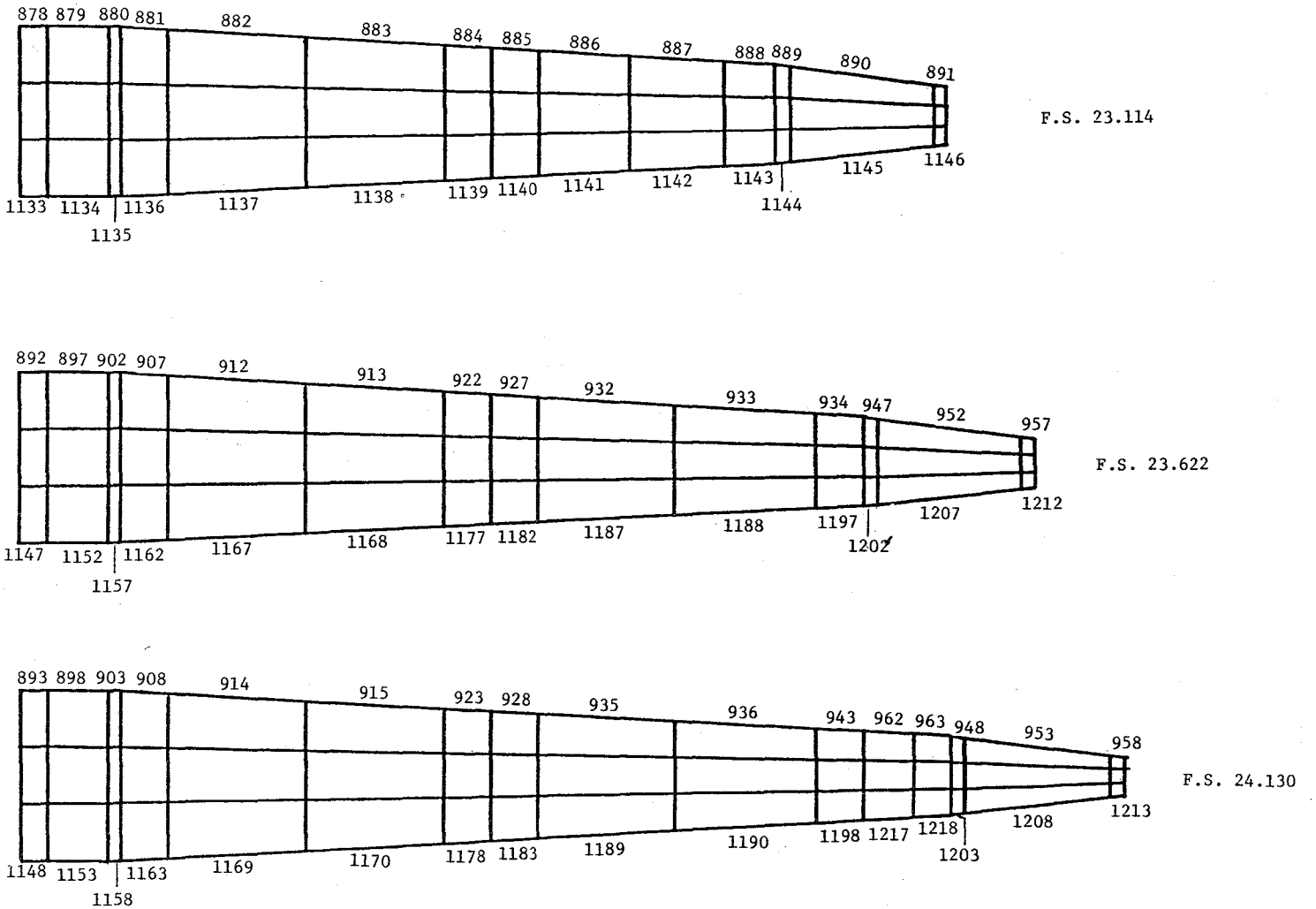

Figure A.4.4: Phase-two Plot of PATRAN-G Generation of Caps and Vertical Angle Elements of Spars.

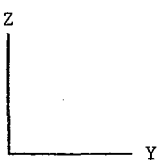

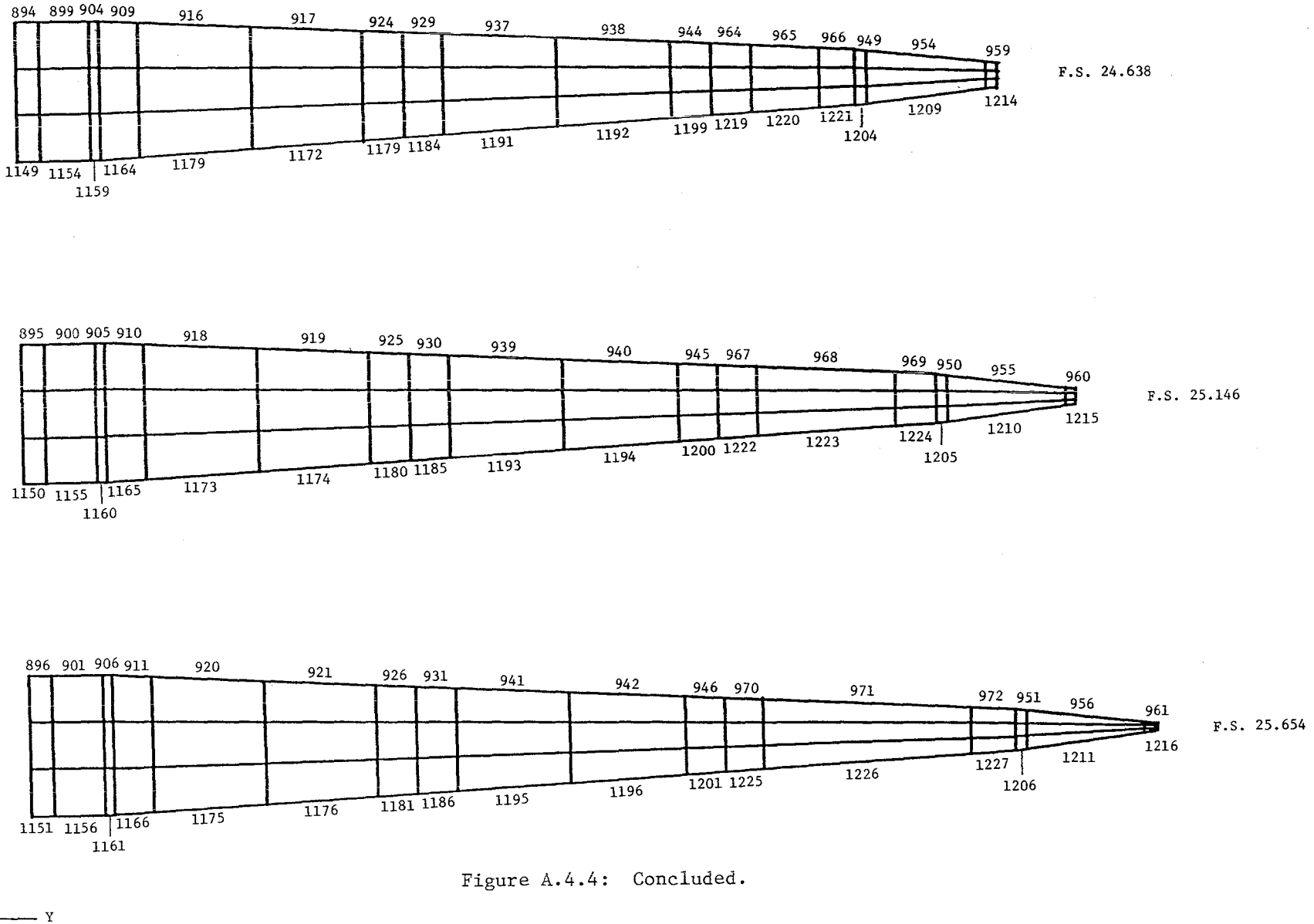

Figure A.4.4: Concluded.

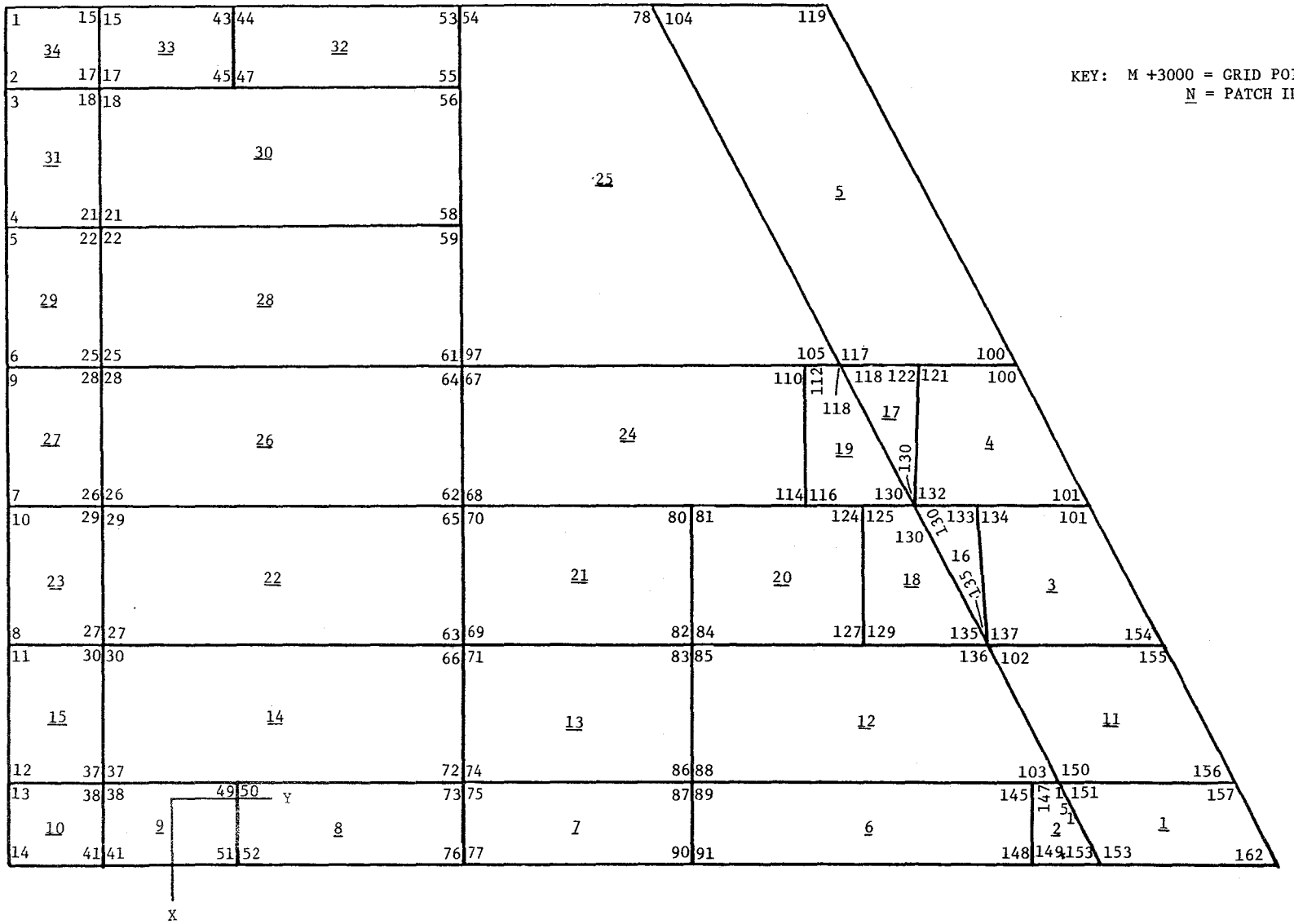

Figure A.5.1: Phase-one Plot of PATRAN-G Generation of Lower Heat Shield. (Patch ID's underlined, add 3000 to grid point ID.)

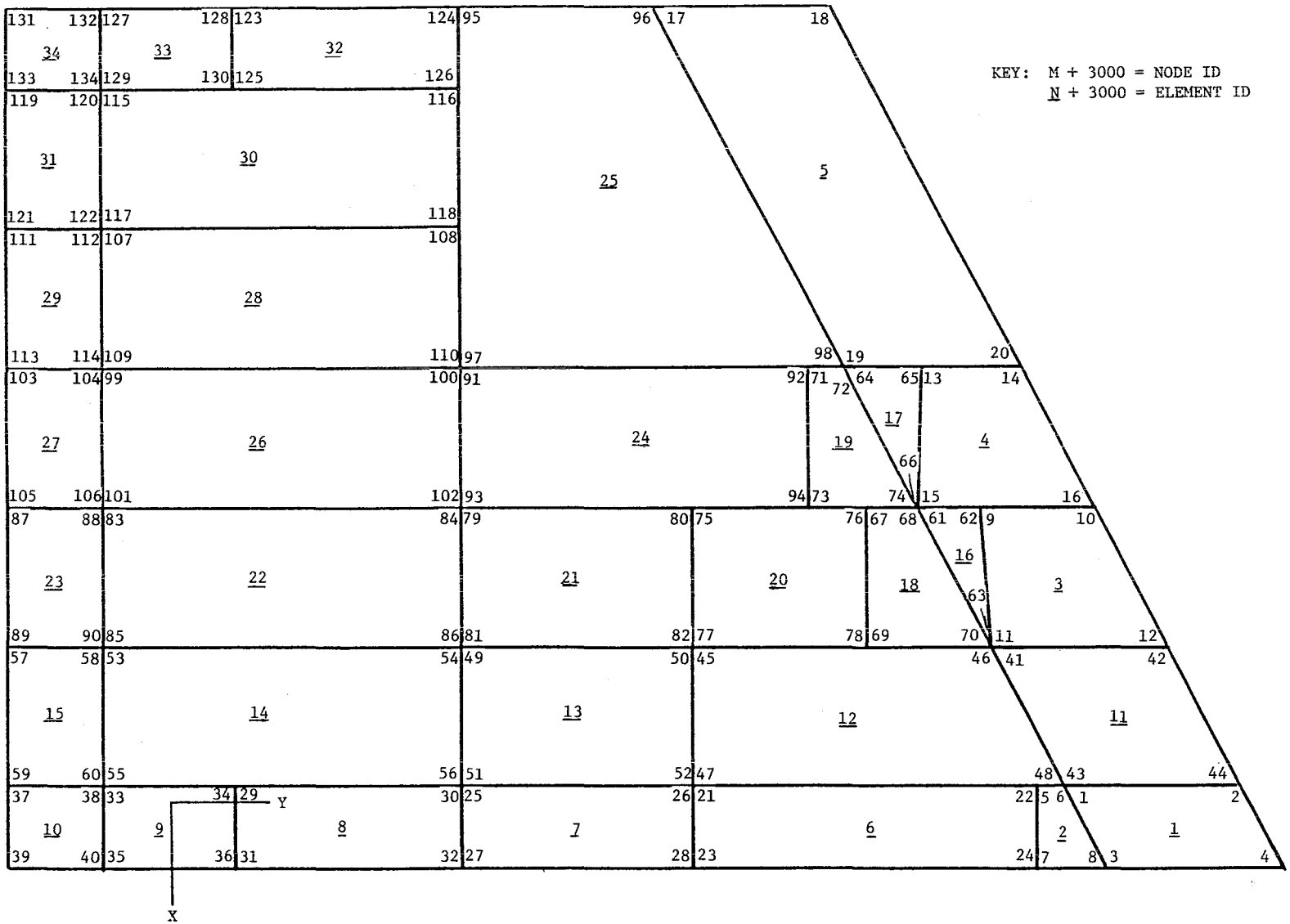

Figure A.5.2: Phase-two Plot of PATRAN-G Generation of Lower Heat Shield. (Add 3000 to underlined plate element ID's and to node point ID's.)

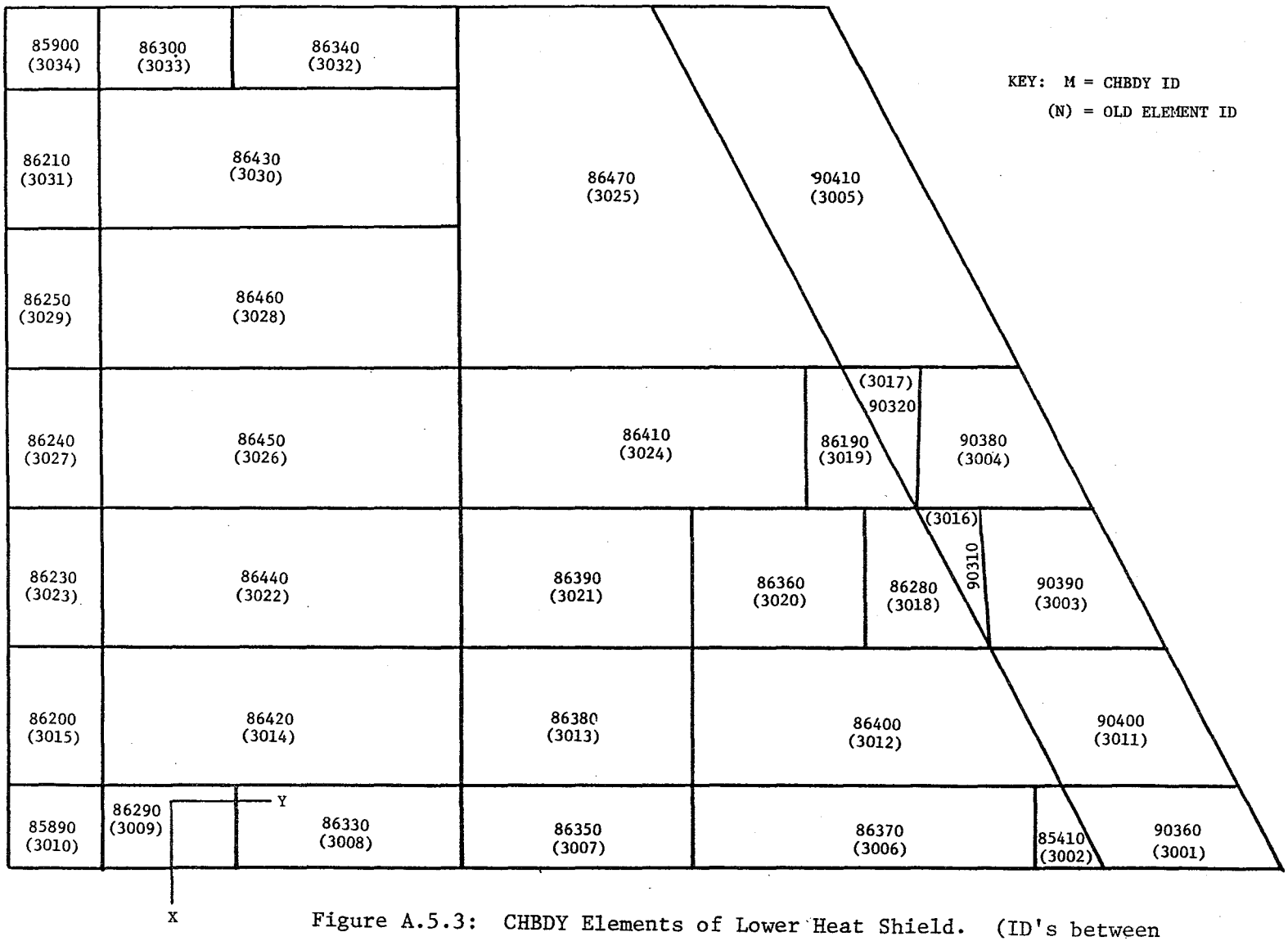

Figure A.5.3: CHBDY Elements of Lower Heat Shield. (ID's between parentheses are original plate element ID's.)

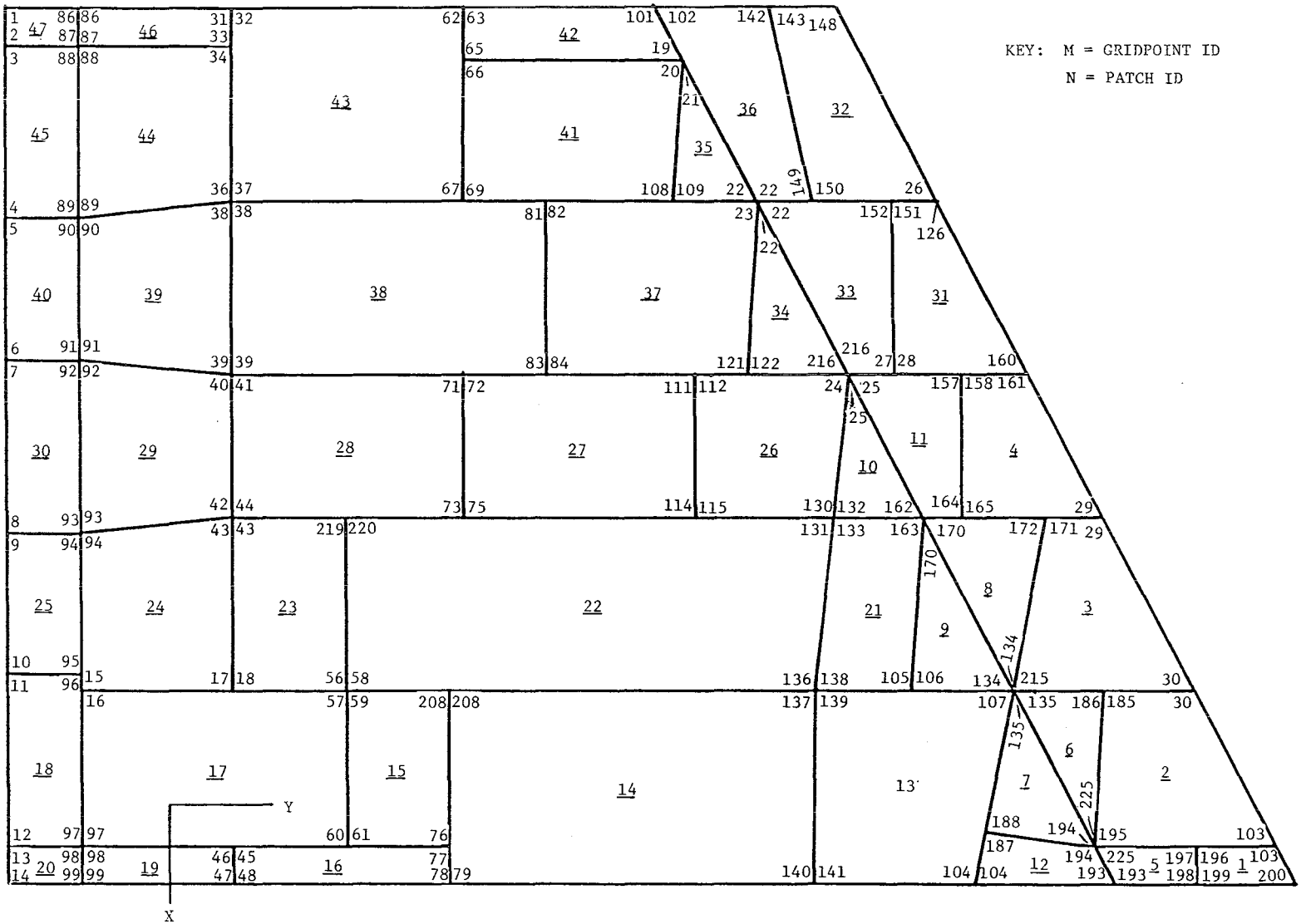

Figure A.6.1: Phase-one Plot of PATRAN-G Generation of Upper Heat Shield. (Patch ID's underlined.)

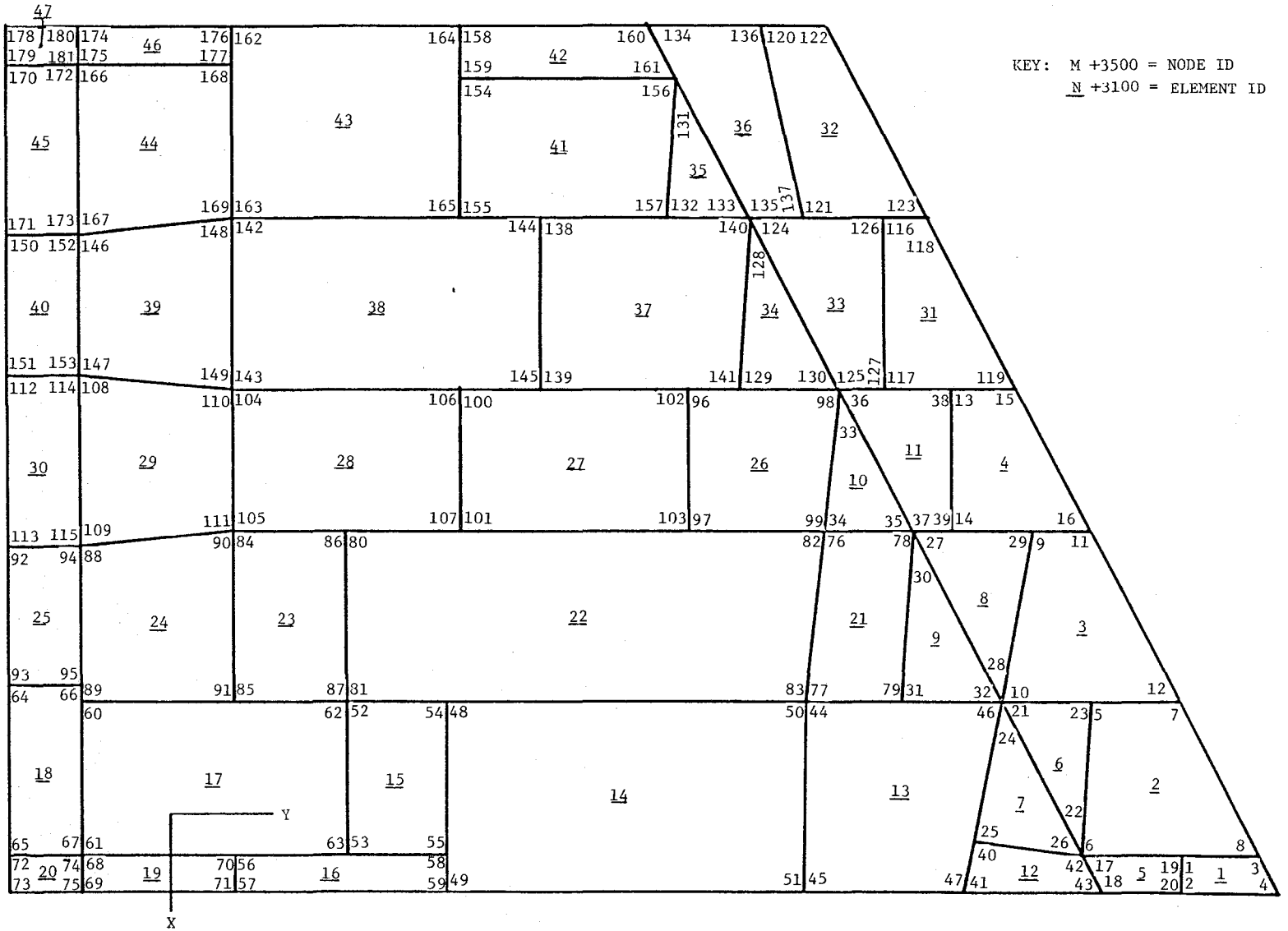

Figure A.6.2: Phase-two Plot of PATRAN-G Generation of Upper Heat Shield. (Add 3100 to underlined ID's of plate elements and 3500 to node point ID's.)

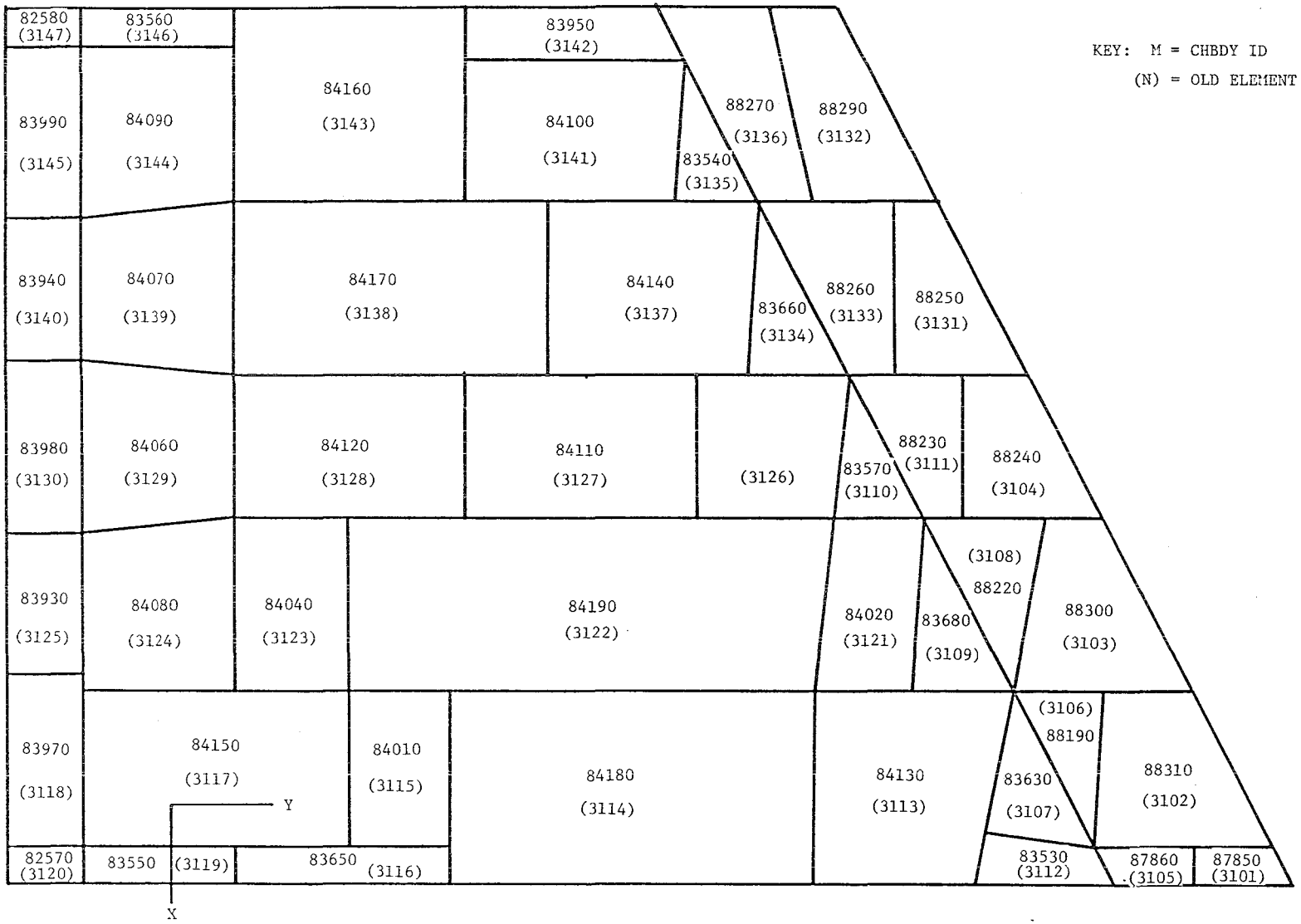

Figure A.6.3: CHBDY Elements of Upper Heat Shield. (ID's between parentheses are original plate elements ID's.)

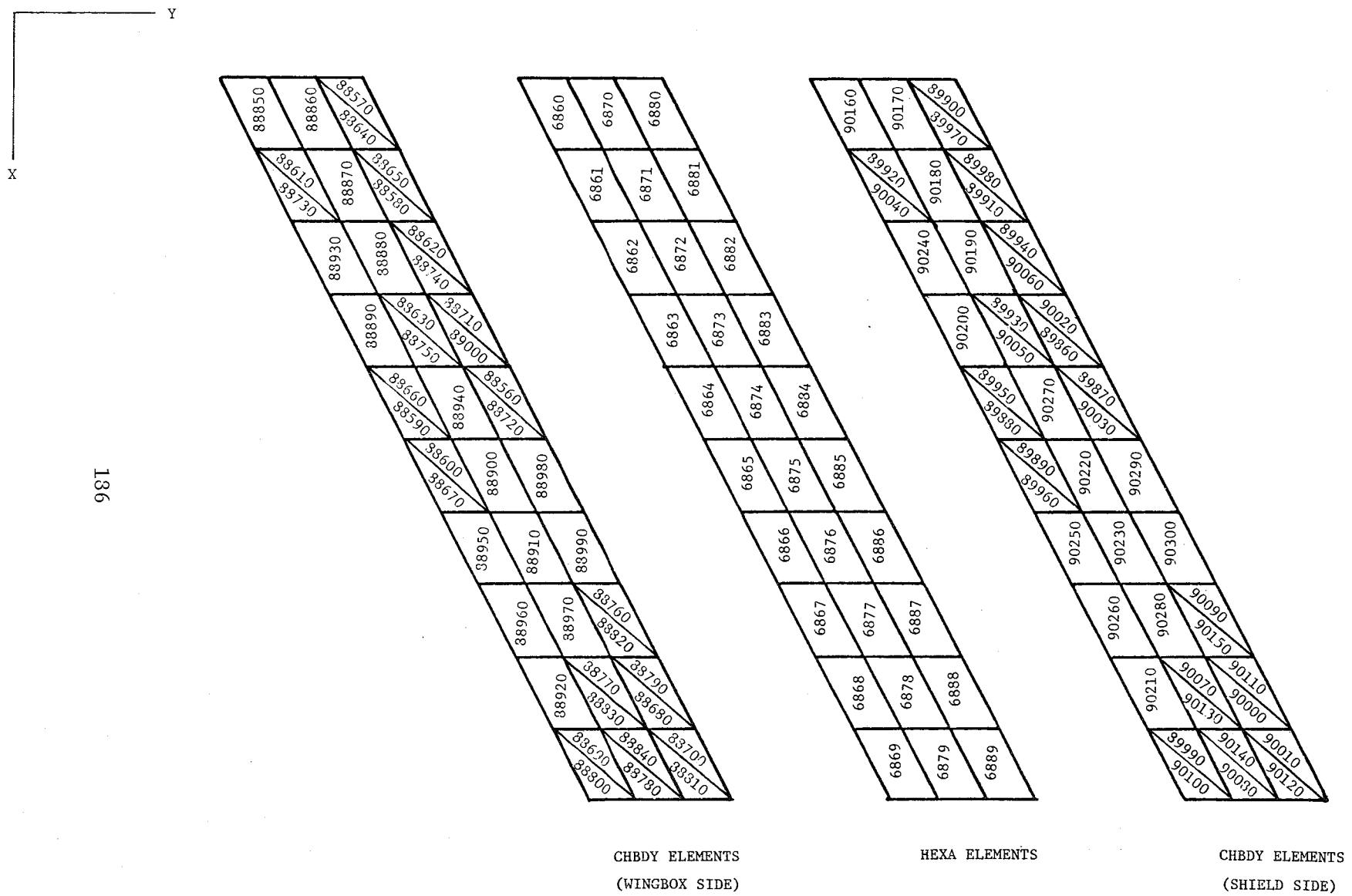

Figure A.7.1: CHBDY and HEXA Elements of Lower Insulation Blanket.

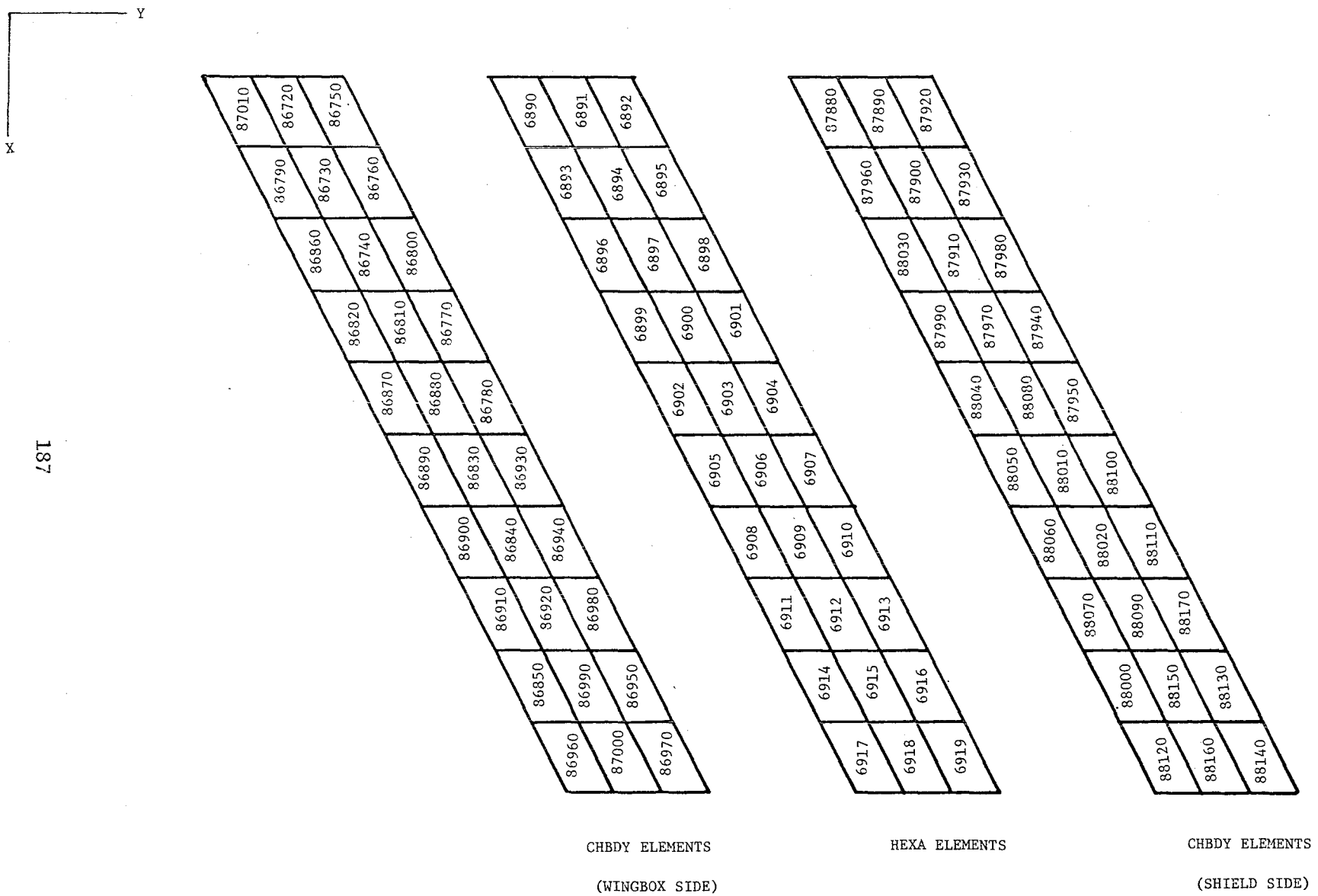

Figure A.7.2: CHBDY and HEXA Elements of Upper Insulation Blanket.

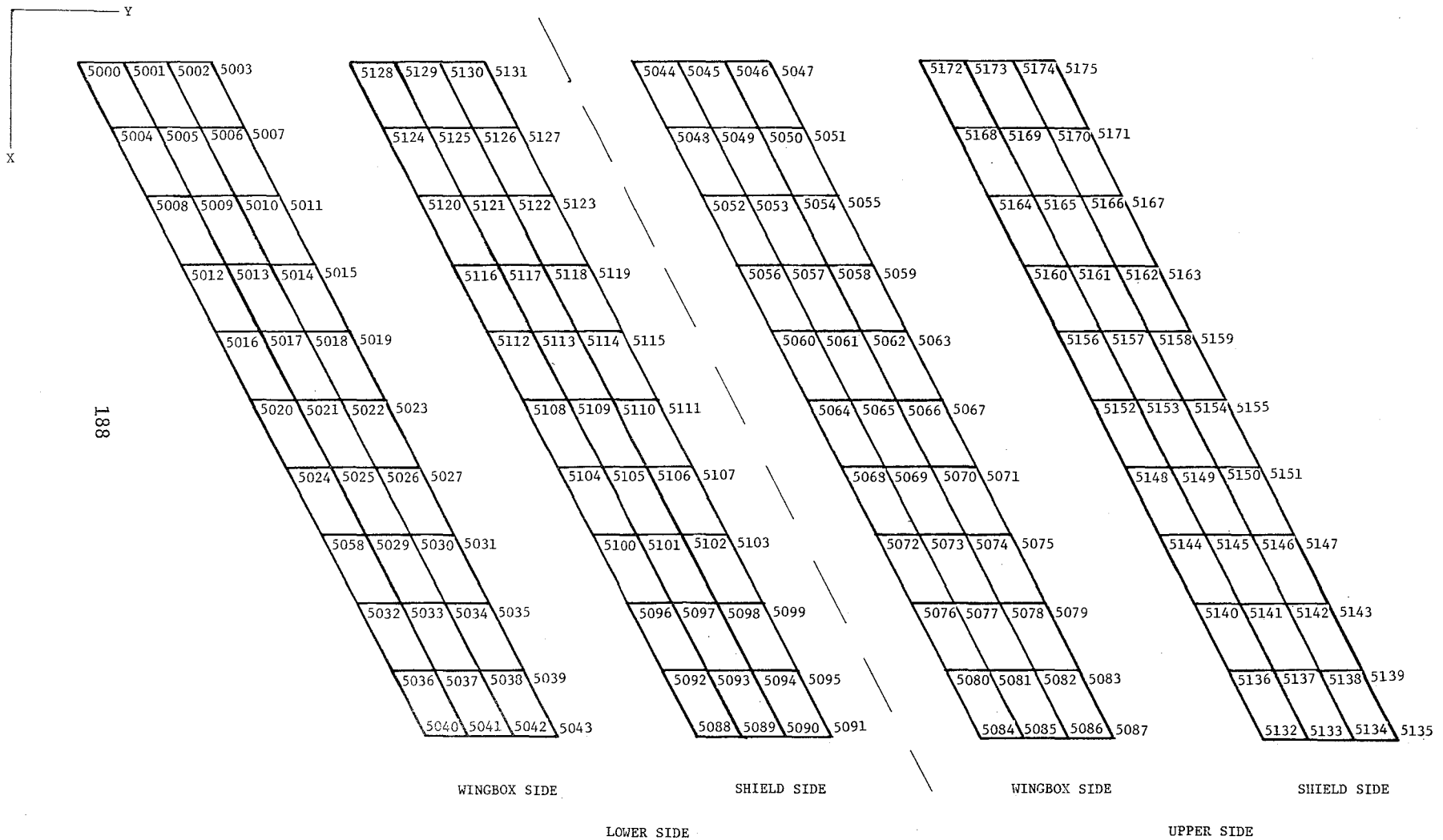

Figure A.7.3: Grid Points of Insulation Blanket at Lower and Upper Sides of Wingbox.

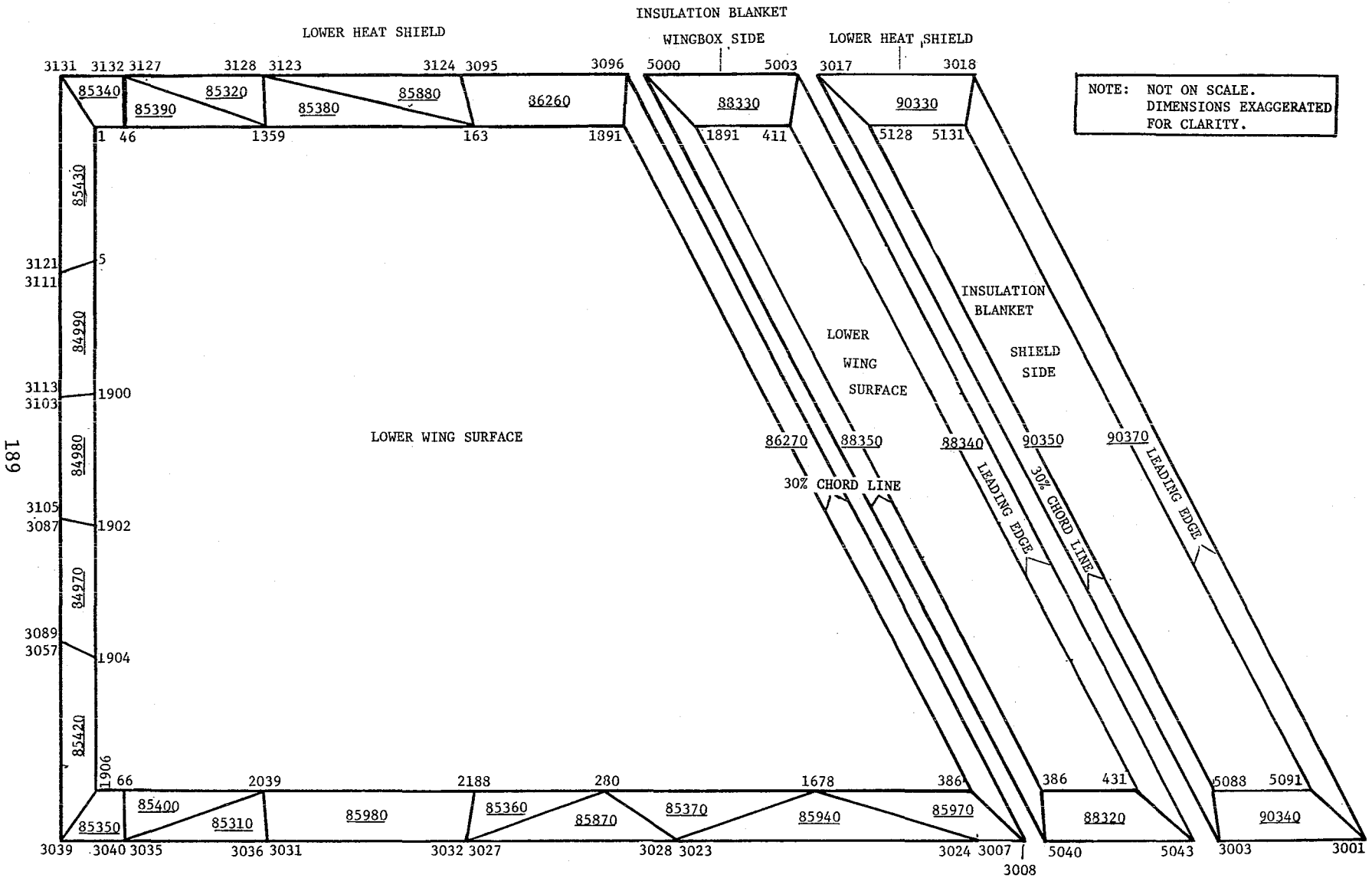

Figure A.8.1: CHBDY Elements of Curtain Elements between Lower Heat Shield, Insulation and Lower Surface of Wingbox. (CHBDY elements underlined.)

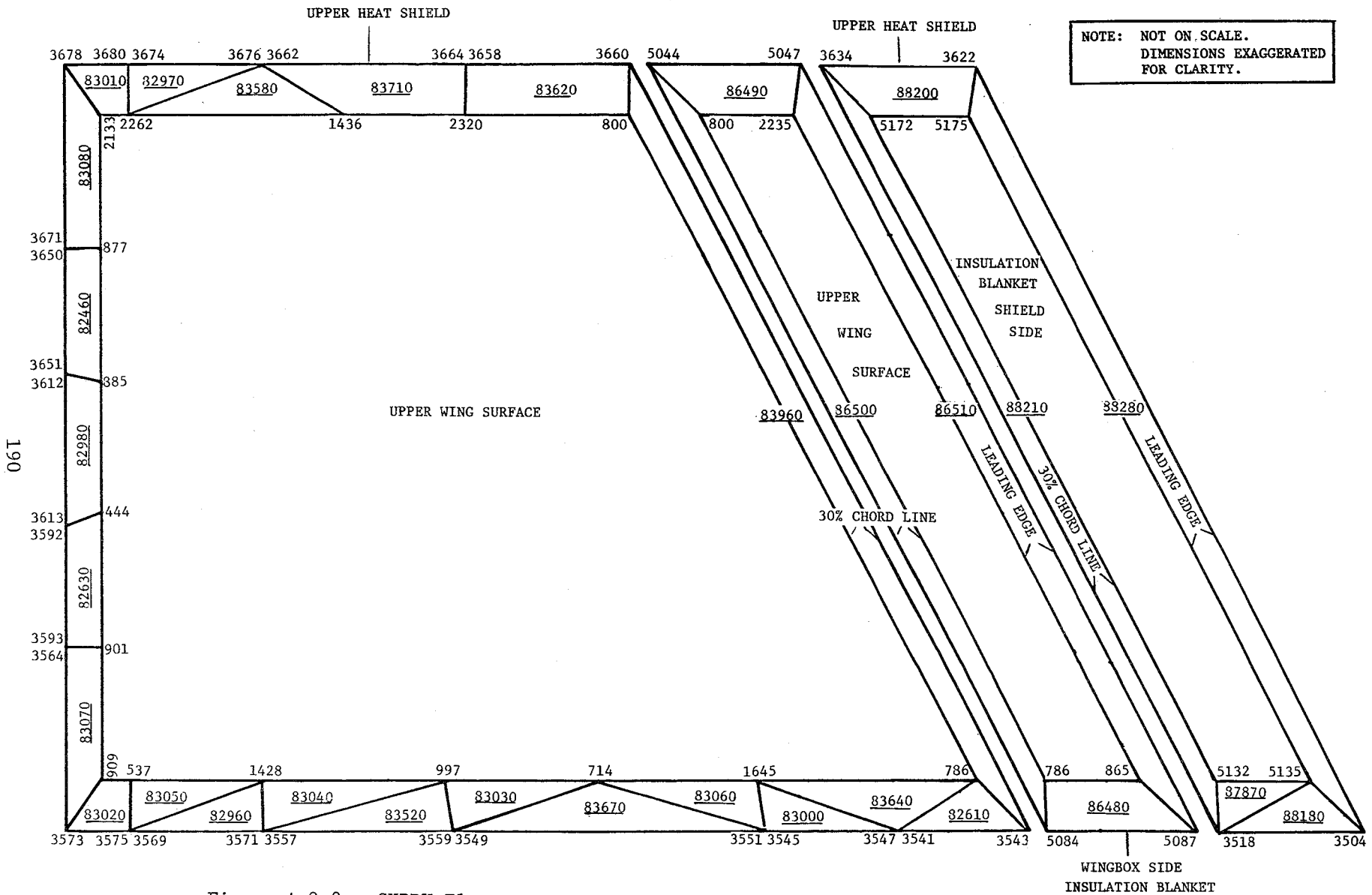

Figure A.8.2: CHBDY Elements of Curtain Elements between Upper Heat Shield, Insulation and Upper Surface of Wingbox. (CHBDY elements underlined.)

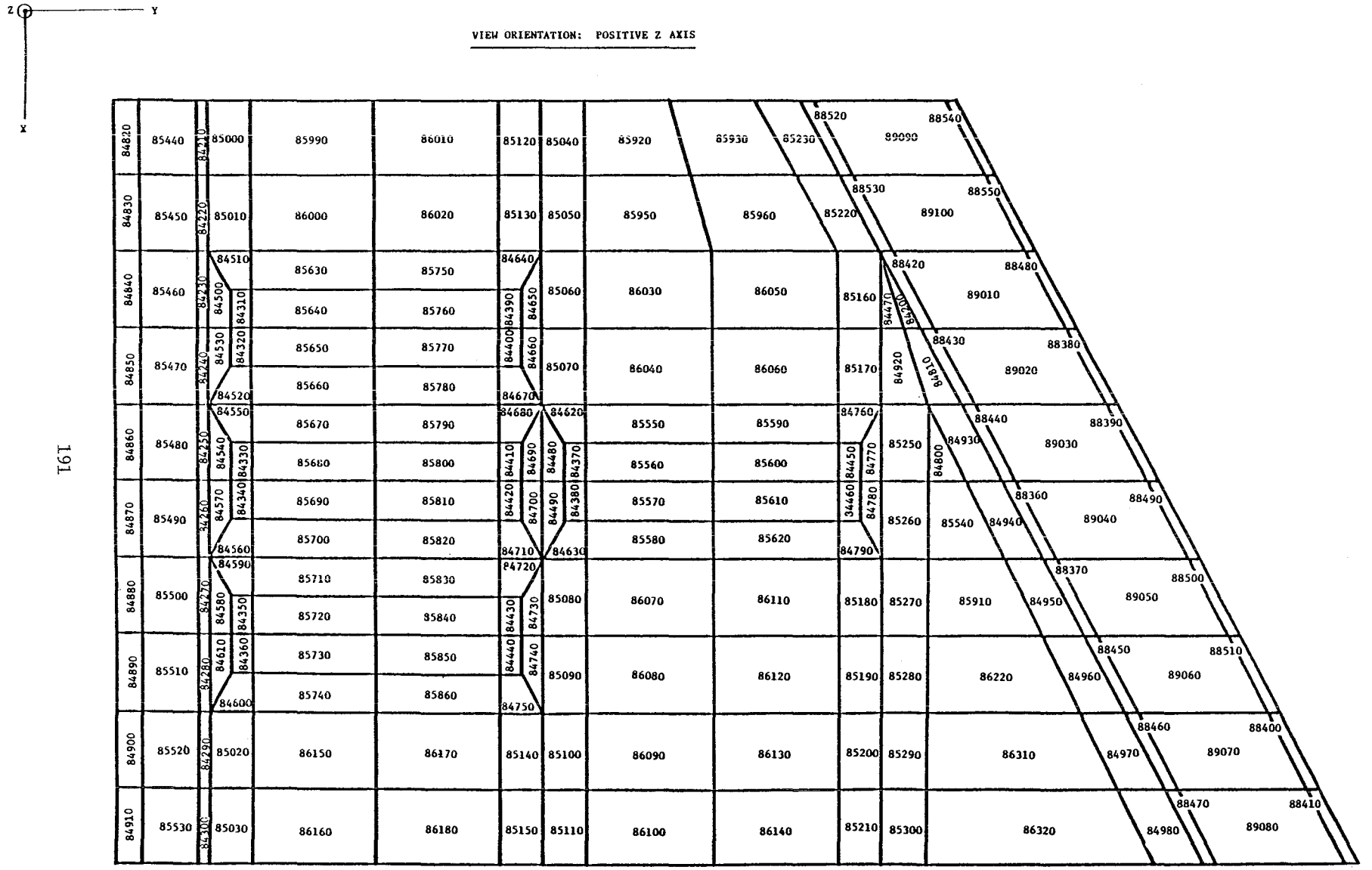

Figure A.9.1: CHBDY Elements of Lower Surface of Wingbox. (View orientation to lower heat shield, positive Z axis.)

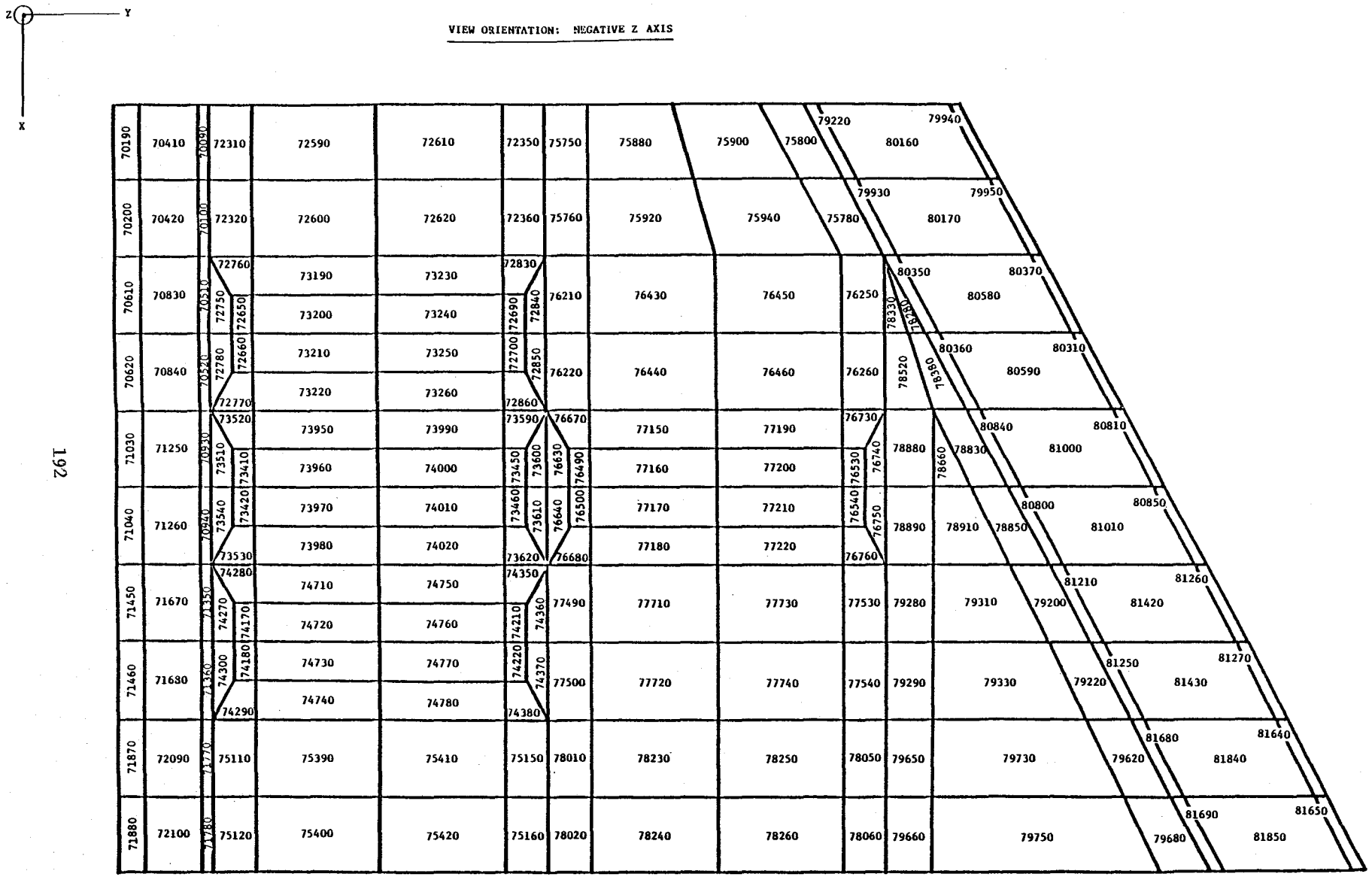

Figure A.9.2: CHBDY Elements of Lower Surface of Wingbox. (View orientation to internal bays, negative Z axis.)

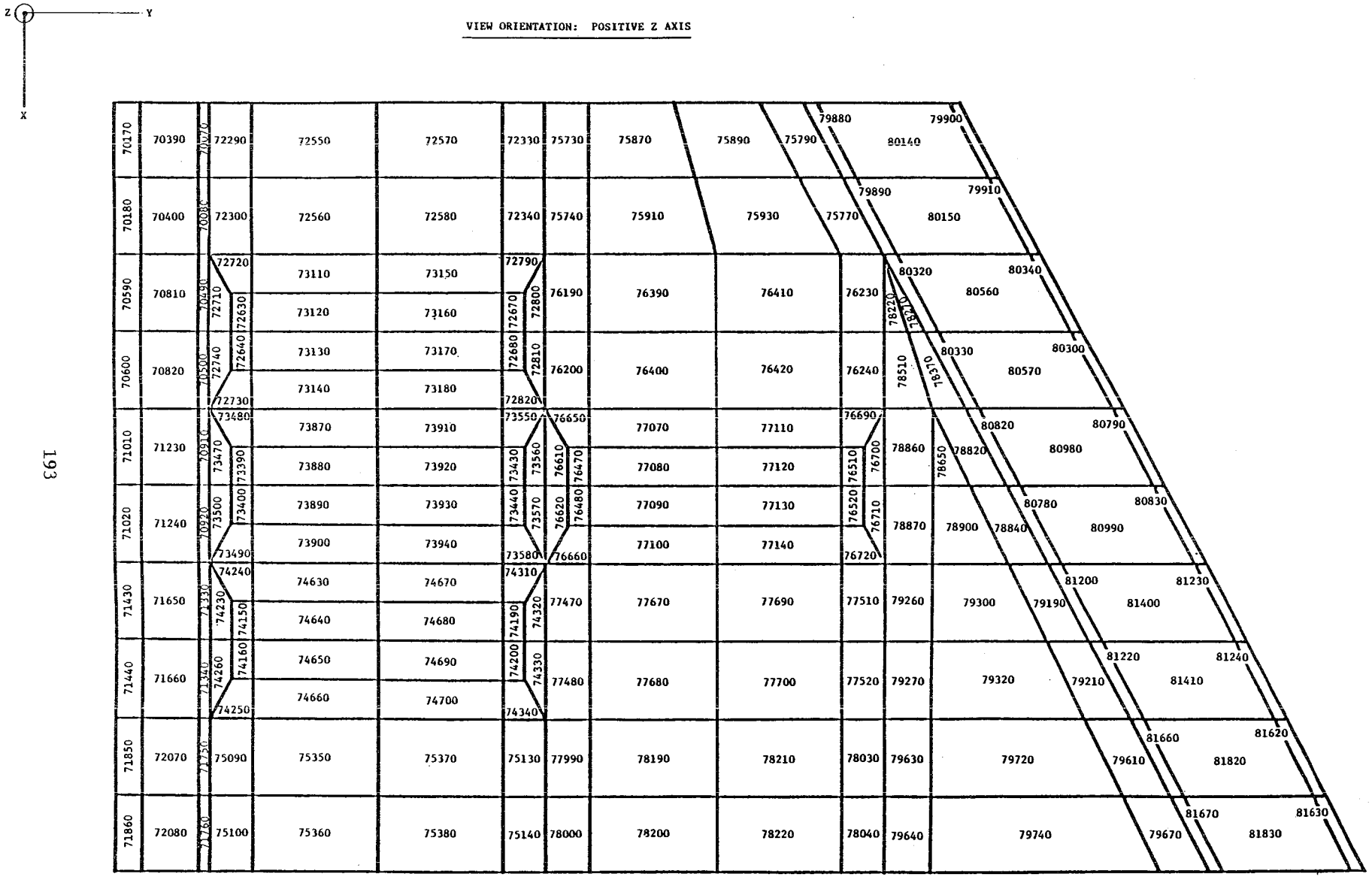

Figure A.9.3: CHBDY Elements of Upper Surface of Wingbox. (View orientation to internal bays, positive Z axis.)

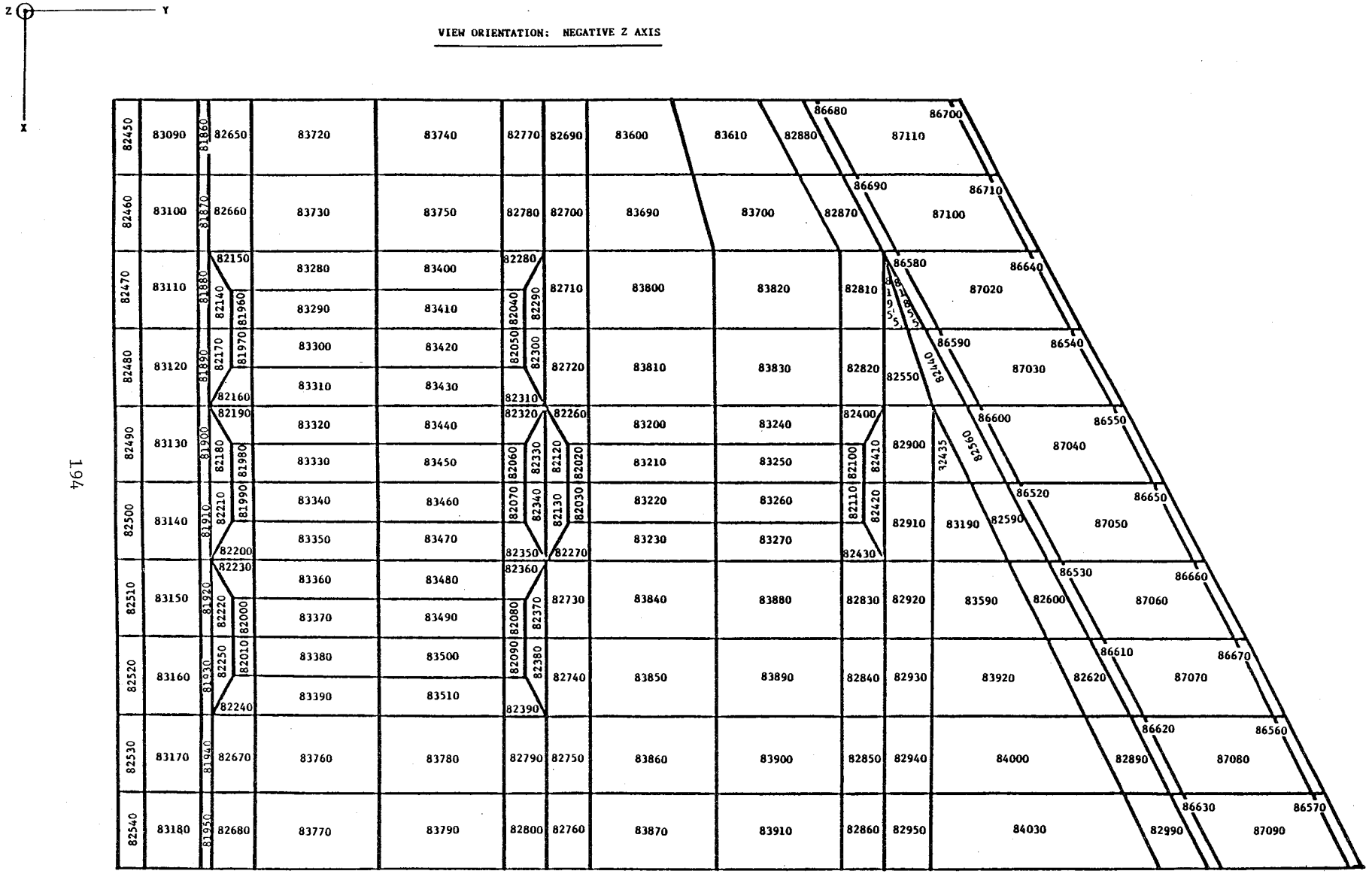

Figure A.9.4: CHBDY Elements of Upper Surface of Wingbox. (View orientation to upper heat shield, negative Z axis.)

70310	70330	70730	70750	71150	71170	71560	71580	71970	71990
70370	70380	70790	70800	71210	71220	71630	71640	72050	72060
70320	70340	70740	70760	71160	71180	71570	71590	71980	72000

W.S. 1.067

VIEW ORIENTATION: POSITIVE Y AXIS

72370	72390	73050	73070	73810	73830	74570	74610	75190	75210
72410	72420	73090	73100	73850	73860	74600	74620	75200	75220
72380	72400	73060	73080	73820	73840	74580	74590	75170	75180

W.S. 1.372

75660	75680	76150	76170	76910	76930	77430	77450	77950	77970
75640	75650	76130	76140	76890	76900	77410	77420	77930	77940
75670	75690	76160	76180	76920	76940	77440	77460	77960	77980

W.S. 2.479

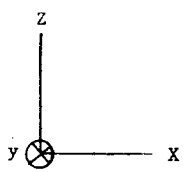

Figure A.9.5: CHBDY Elements of Ribs in Wingbox. (View orientation to positive Y axis.)

78390	78420	78760	78790	79130	79160	79520	79550
78400	78430	78770	78800	79140	79170	79530	79560
78410	78440	78780	78810	79150	79180	79540	79570

VIEW ORIENTATION: POSITIVE Y AXIS

80050	80020	80470	80440	80930	80860	83140	81310	81760	81730
80070	80040	80490	80450	80920	80870	81350	81320	81770	81740
80060	80030	80480	80460	80940	80880	81360	81330	81780	81750

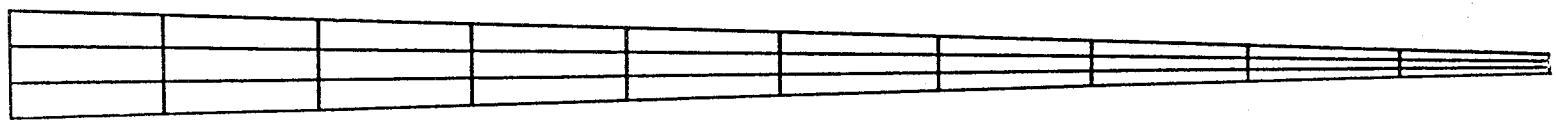

Figure A.9.5: Concluded.

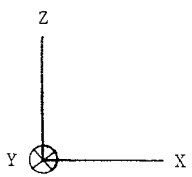

W.S. 1.076

VIEW ORIENTATION: NEGATIVE Y AXIS

70270	70290	70690	70710	71110	71130	71530	71610	72010	72030
70350	70360	70770	70780	71190	71200	71600	71620	72020	72040
70280	70300	70700	70720	71120	71140	71540	71550	71950	71960

W.S. 1.372

72250	72270	73010	73030	73770	73790	74530	74550	75050	75070
72230	72240	72990	73000	73750	73760	74510	74520	75030	75040
72260	72280	73020	73040	73780	73800	74540	74560	75060	75080

W.S. 2.479

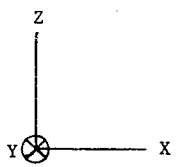

Figure A.9.6: CHBDY Elements of Ribs in Wingbox. (View orientation: negative Y axis.)

76070	76100	76830	76860	77350	77380	77870	77900
76080	76110	76840	76870	77360	77390	77880	77910
76090	76120	76850	76880	77370	77400	77890	77920

VIEW ORIENTATION: NEGATIVE Y AXIS

75580	75550	78480	78450	78740	78700	79070	79040	79490	79460
75600	75570	78500	78460	78730	78710	79080	79050	79500	79470
75590	75560	78490	78470	78750	78720	79090	79060	79510	79480

						81170 81180 81190	81150 81140 81160	81590 81610 81600	81560 81570 81580
79990	79960	80410	80380	80760	80720				
80010	79980	80430	80390	80750	80730				
80000	79970	80420	80400	80770	80740				

Figure A.9.6: Concluded.

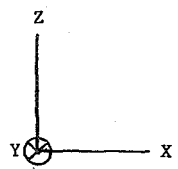

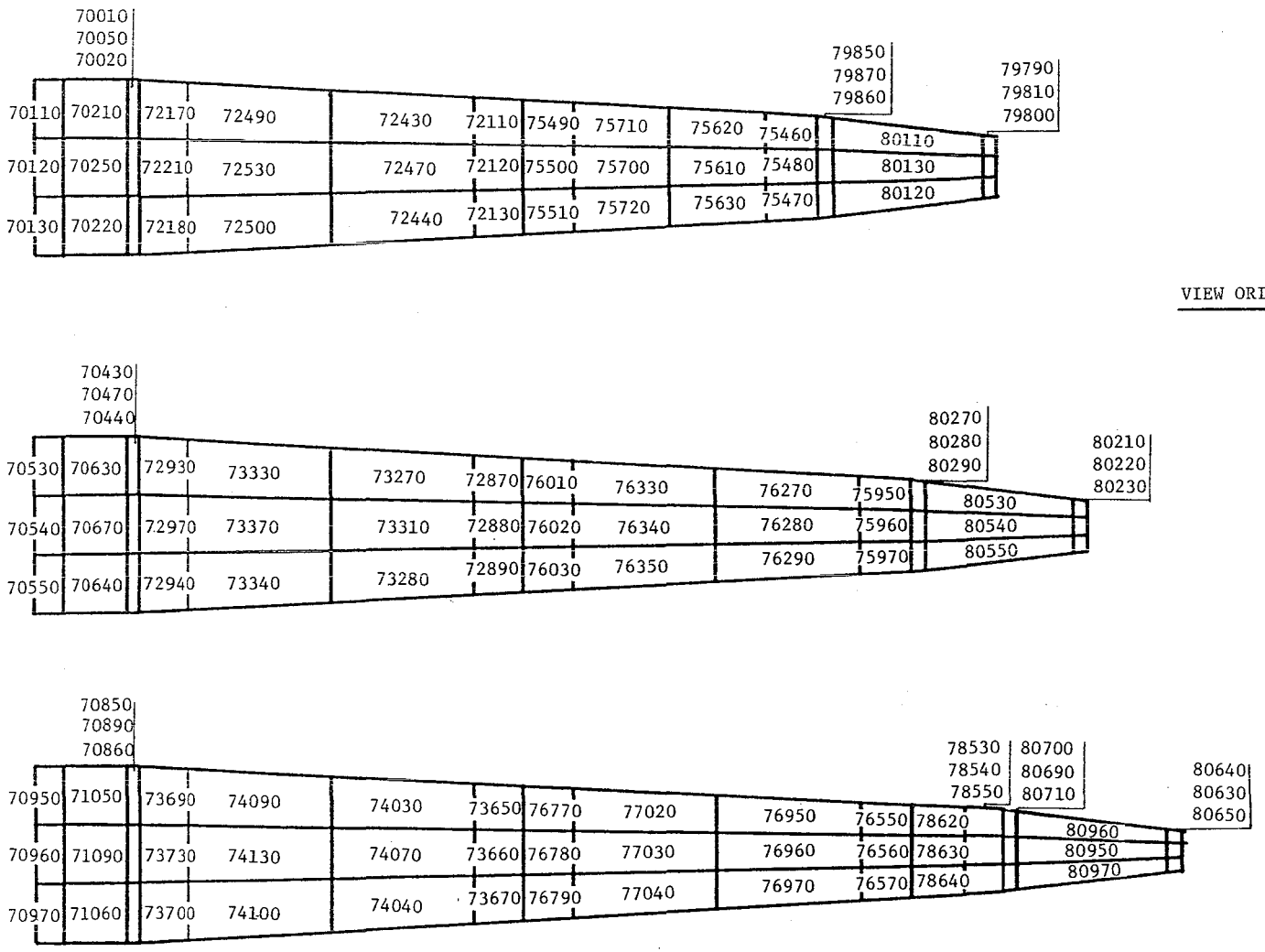

Figure A.9.7: CHBDY Elements of Spars in Wingbox.
(View orientation: positive X axis.)

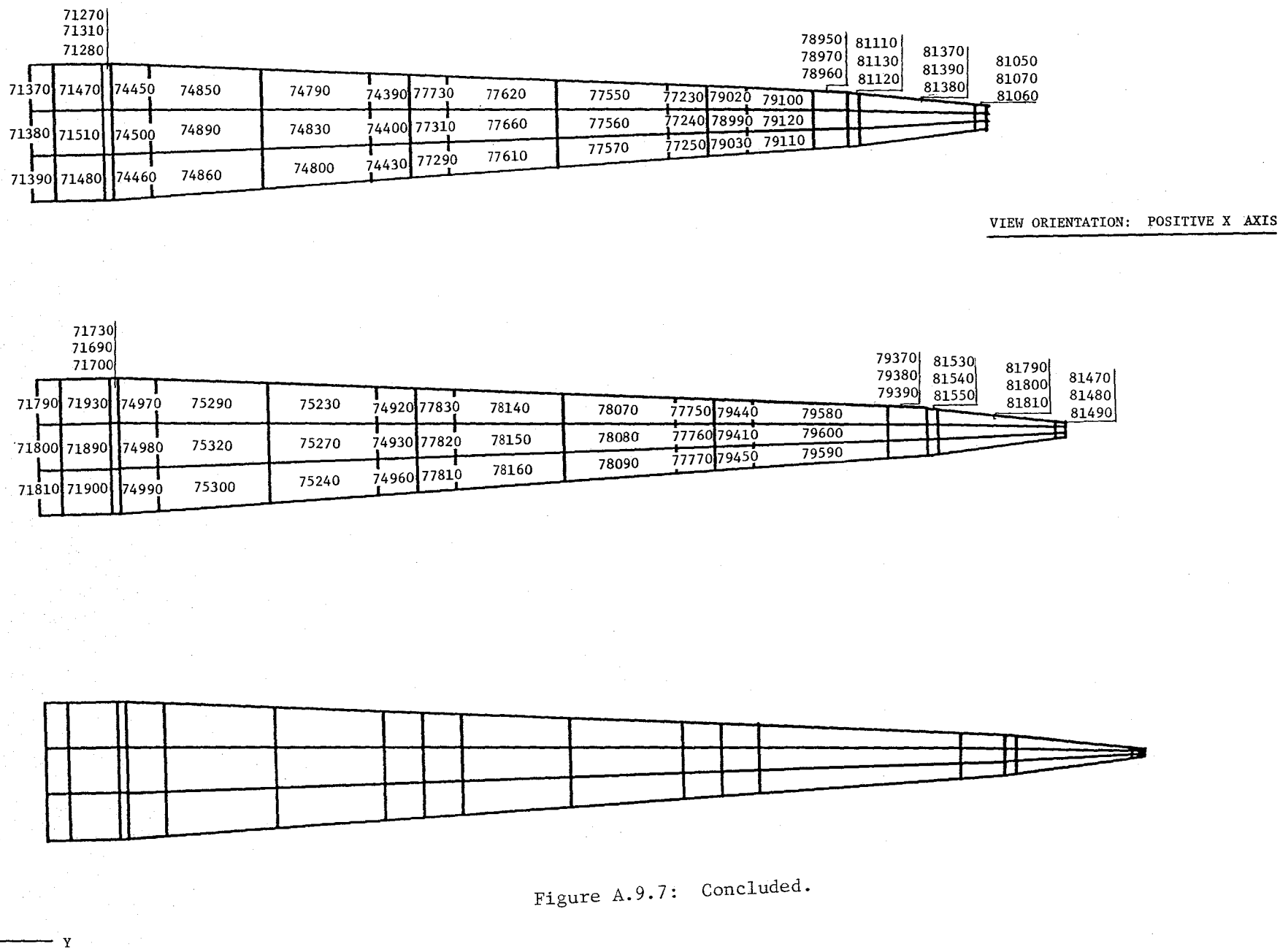

Figure A.9.7: Concluded.

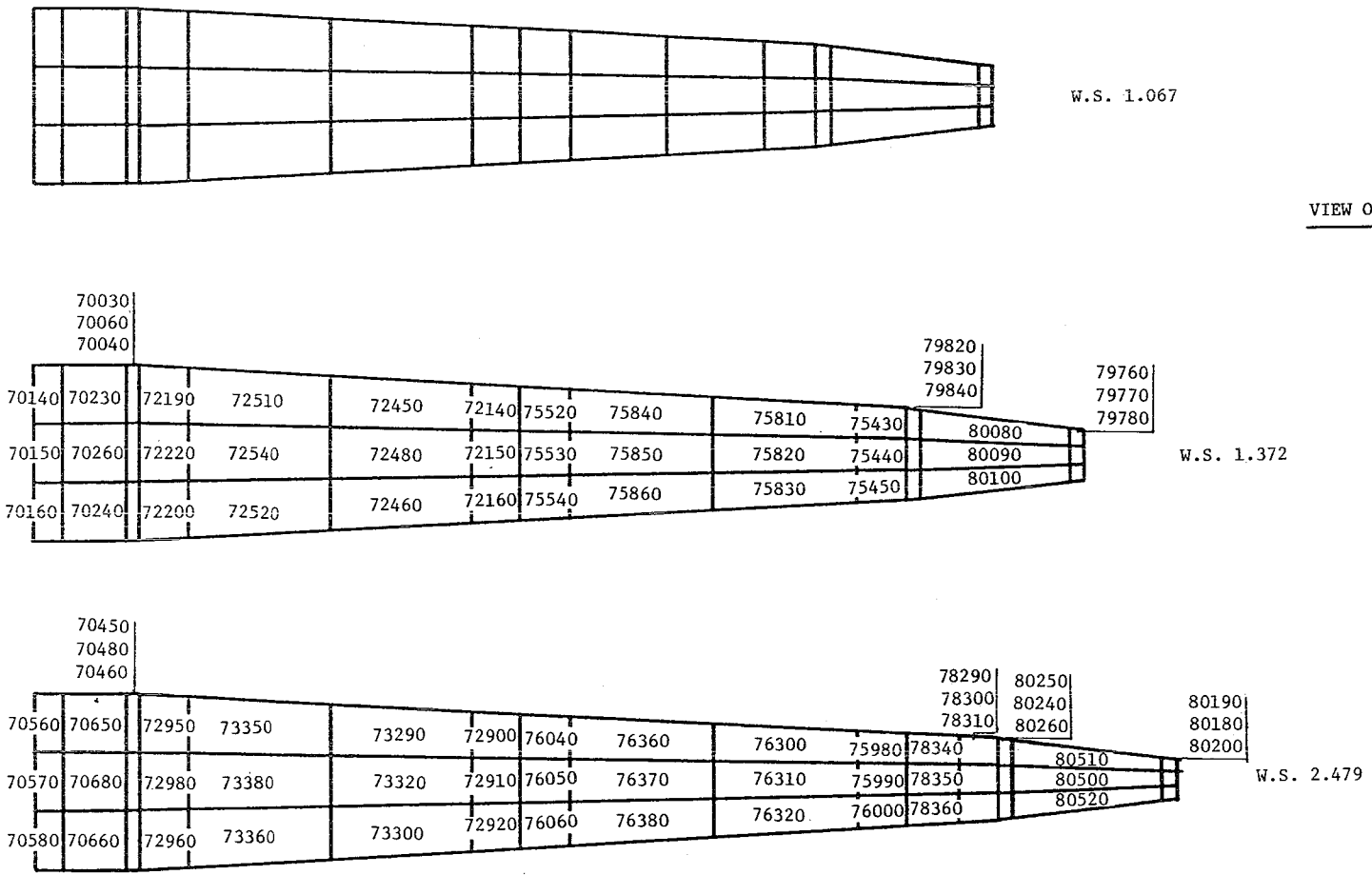

Figure A.9.8: CHBDY Elements of Spars in Wingbox.
(View orientation: negative X axis.)

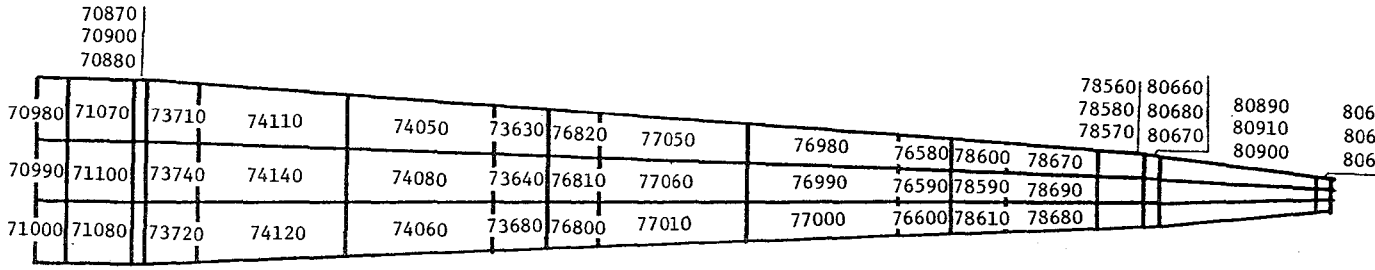

F.S. 24.638

VIEW ORIENTATION: NEGATIVE X AXIS

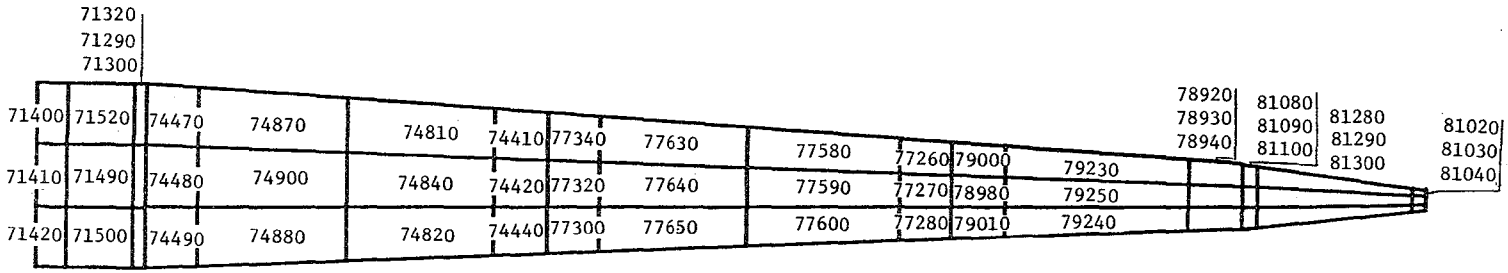

F.S. 25.146

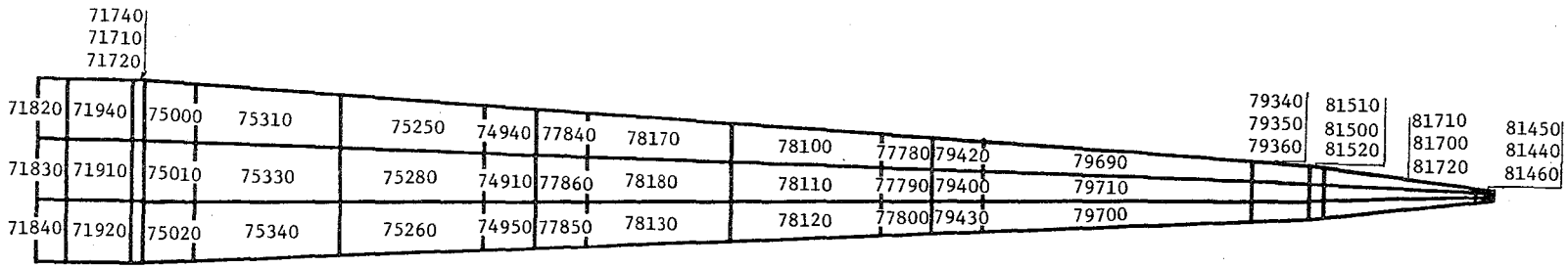

F.S. 25.654

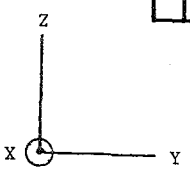

Figure A.9.8: Concluded.

APPENDIX B

PROCEDURE OF THERMAL AND STRUCTURAL ANALYSIS OF THE HYPERSONIC WING TEST STRUCTURE

This procedure has been written to describe the different steps in the thermal and structural analysis of the HWTS. In addition to the whole structure, this analysis studies the five upper and lower surface panels of bays F through J in more detail. Figure B.1 shows the flow chart with the names of the update files and the files for temporary storage of the data. Table B lists the different files and explains the names of the files. A more detailed expanation of the working is given in Chapters 4 and 5. Although this procedure was developed initially for the first phase development, it is still valid for the current analysis.

A. THERMAL ANALYSIS

1. Run program "THWTS".

   Input: Update file UTHWTS
   Purpose: Computation of temperature distribution in HWTS
   Output: on file TDATA:
   - checkpoint dictionary
   - sets of temperature cards for each subcase in THWTS.
   Comment: Contents of TDATA will be printed in the listing.
   Figure B.2 relates the subcase number with the ID and location of the matching panel.

2. Run program "SORT".

   Input: File TDATA
   Purpose: Sort and punch the checkpoint dictionary of THWTS
   Output: On cards: checkpoint dictionary
   On file TDATA
   - sets of temperature cards for each subcase in THWTS.

3. Run program "TCHANGE".

   Input: File TDATA2
   Purpose: Sort temperature cards for input SHWTS and TBPAxxx models; convert temperature cards into thermal load tables for input in the TBPAxxx models
   Output: On file RDA:
   - temperature cards for input in SHWTS model on files RDA1 thru RADA10:
   - TABLED1 cards for input in TBPAxxx models.

4. Run NASTRAN program "TBPA206" thru "TBPA210," group I.

   Input: Files RDA1 thru RDA5
   Update file UTBP1.
   Purpose: Computation of temperature distribution in each upper root panel
   Output: On files TBDP1 thru TBPD5:
   - temperature cards for grid points along internal edges of each panel
   Comment: Insert after the following card in the deck
   * D TBP.935
   the next card:
   TEMPD 15 YYYYY
   1 2
   12345678901234567890123 45
   where YYYYY is a real number representing an average temperature of the panel. This card is referenced by the temp (material) card in case control deck. This temperature can be determined from the printed listing of TDATA in program THWTS for the matching subcase.

5. Run program "TEQUIV".

   Input: Files TBPD1 thru TBPD5
   Purpose: Equalize temperatures at common internal edges of the four submodels for each panel.
   Output: On files TBPDS1 thru TBPDS5:
   - TABLED1 cards for input in TBPBxxxx models.

6. Run NASTRAN models "TBPB206" thru "TBPB210" group I.

   Input: Files TBPDS1 thru TBPDS2
   Files RDA1 thru RDA5
   Update file UTBP2
   Purpose: Computation of final temperature distribution in each upper lower root panel.
   Output: On files TBPDA1 thru TBPDA5:
   - temperature cards for each grid point and time step
   Comment: Insert same TEMPD card at the same location as in step 4.

7. NASTRAN programs "TBPA106" thru TPBA110", group II.

Input: Files RDA6 thru RDA10
Update file UTBP1.
Purpose: Computation of temperature distribution in each lower root panel
Output: On files TBPD1 thru TBPD5:
- temperature cards for grid points along internal edges of each panel.
Comment: Insert after the following card in the deck
*DTBP.935
the next card:

```
TEMPD    15   YYYYY
         1         2
12345678901234567890123 45
```

where YYYYY is a real number representing an average temperature of the panel. This card is referenced by the temp (material) card in the case control deck. This temperature can be determined from the printed listing of TDATA in program THWTS for the matching sub-case.

8. Run program "TEQUIV".

Input: Files TBPD1 thru TBPD2
Purpose: Equalize temperatures at common internal edges of the four submodels for each panel
Output: On files TBPDS1 thru TBPDS5:
- TABLED1 cards for input in TBPBxxx models.

9. Run NASTRAN models "TBPB106" thru "TBPB110," group II.

Input: Files TBPDS1 thru TPBDS5.
Files RDA6 thru RDA10.
Update file UTBP2.
Purpose: Computation of final temperature distribution in each lower root panel
Output: On files TBPDA6 thru TBPDA10:
- temperature cards for each grid point and time step
Comment: Insert same TEMPD card at the same location as in step 7.

10. Run program "REDUCE".

Input: Files TBPDA1 thru TBPDA10
File RDA
Purpose: Sort and reduce the output of each temperature set to only time step, 700 seconds
Output: Files RDA, RDAN1, and RDAN2
Comment: For another time step replace last card in deck with the new time step, 14 format.

B. STRUCTURAL ANALYSIS

1. Run NATRAN program "SHWTS".

   Input: Update file USHWTS.
   File RDAN
   Purpose: Computation of stress distribution at spars and ribs of the HWTS
   Output: Printed: Stresses for spar and rib locations. On file SDATA:
   - displacements sets for each root panel.

2. Run program "REDIST".

   Input: File SDATA
   Purpose: Convert displacements in spc cards for input in structural models of the beaded panels
   Output: On file SPCDATA:
   - spc cards.

3. Run NASTRAN program "SBPU1".

   Input: Update file USBPQTR.
   File SPCDATA
   File RDAN1
   Purpose: Generation stress data for each upper root panel
   Output: On file SDATA1
   - displacements for grid points along internal edges of each panel
   Comment: Insert after the following card in the deck,
   *D SBP.1027 the next card:

```
TEMPD    20        xxxxx
          1         2
12345678901234567890123456789
```

   where xxxx is an average temperature of the upper panels at the time step.

4. Run program "SEQUIVA".

   Input: File SDATA1
   Purpose: Equalize displacements along internal edges of each panel and convert them into spc cards
   Output: On file SDATA2:
   - spc cards.

5. Run NASTRAN program "SBPU2".

   Input: File SDATA2
   File RDAN1
   File SPCDATA
   Update file SPBQTR.

Purpose: Compute final stress distribution at each upper root panel
Output: Printed:
Stresses and displacements for each root panel
Comment: Insert same TEMPD card at the same location as in step 3.

6. Run NASTRAN program "SPBL1".

Input: Update file USBPQTR.
File SPCDATA.
File RDAN2.
Purpose: Generation stress data for each lower root panel
Output: On file SDATA3:
- displacements for grid points along internal edges of each panel
Comment: Insert after the following card in the deck,

```
*D SVPQTR.          The next card:
TEMPD    20         xxxxx
         1         2
12345678901234567890123456789
```

where xxxxx is an average temperature of the lower panels.
Comment: Insert after the following card in the deck,

```
*D SBPQTR.          The next card:
TEMPD   20          xxxxx
         1         2
12345678901234567890123456789
```

where xxxx is an average temperature of the lower panels at the time step.

7. Run program "SEQUIVB".

Input: File SDATA3
Purpose: Equalize displacements along internal edges of each panel and convert them into spc cards.
Output: On file SDATA4:
- spc cards.

8. Run NASTRAN program "SBPL2".

Input: File SDATA
File RDAN2
File SPCDATA
Update file SBPQTR.
Purpose: Compute final stress distribution at each lower root panel.
Output: Printed:
- stress and displacements for each root panel
Comment: Insert same TEMPD card at the same location as in step 5.

9. Prepare from printed output (stresses) of SHWTS, SBPU2, and SBPL2 programs, and the listed temperature values for σ_x, σ_y, τ_{xy}, ψ, and E(T). Punch cards for input in ROSETTE.

10. Run program "ROSETTE" for conversion of stresses into strains.

TABLE B.1: LIST OF PROGRAMS AND FILES

PROGRAMS:

FORTRAN:

SORT	REDIST
TCHANGE	SEQUIVA
TEQUIV	SEQUIVB
REDUCE	ROSETTE

NASTRAN:

THWTS	Thermal analysis program, HWTS
TBPxyyy	Thermal analysis program, beaded panels where, x = A x = B yyy = panel number (106-110 lower panels) (206-210 upper panels) See Figure B.2.
SHWTS	Structural analysis program, HWTS
SBPxy	Structural analysis program, beaded panels where, x = U upper panels x = L lower panels y = 1 first run y = 2 second run

FILES

UPDATE FILES:

UTHWTS	Thermal model of HWTS
UTBP1	Thermal model of beaded panel, phase one
UTBP2	Thermal model of beaded panel, phase two
USHWTS	Structural model of HWTS
USBPQTR	Structural model of beaded panels

TABLE B.1: (continued)

DATA FILES:

TDATA	Data output of program THWTS
TDATA2	Data output of program SORT
RDA	Temperature cards for input in SHWTS
RDA 1	Temperature tables for input in TBPx206
RDA 2	Temperature tables for input in TBPx207
RDA 3	Temperature tables for input in TBPx208
RDA 4	Temperature tables for input in TBPx209
RDA 5	Temperature tables for input in TBPx210
RDA 6	Temperature tables for input in TBPx106
RDA 7	Temperature tables for input in TBPx108
RDA 8	Temperature tables for input in TBPx108
RDA 9	Temperature tables for input in TBPx109
RDA10	Temperature tables for input in TBPx110
TBPD1	Panel x06
TBPD2	Panel x07
TBPD3	Panel x08
TBPD4	Panel x09
TBPD5	Panel x10

temperature cards for gridpoints along internal edges.

TBPDS1	Temperature tables for input in TBPBy06
TBPDS2	Temperature tables for input in TBPBy07
TBPDS3	Temperature tables for input in TBPBy08
TBPDS4	Temperature tables for input in TBPBy09
TBPDS5	Temperature tables for input in TBPBy10

TABLE B.1: (continued)

TBPDA 1	Temperature cards for each gridpoint in panel 206
TBPDA 2	" " " " " " " 207
TBPDA 3	" " " " " " " 208
TBPDA 4	" " " " " " " 209
TBPDA 5	" " " " " " " 210
TBPDA 6	" " " " " " " 106
TBPDA 7	" " " " " " " 107
TBPDA 8	" " " " " " " 108
TBPDA 9	" " " " " " " 109
TBPDA10	" " " " " " " 110
RDAN	Reduced temperature input in program SHWTS
RDAN1	Reduced and renumbered temperature cards for input in SBPUx
RDAN2	Reduced and renumbered temperature cards for input in SBPLx
SDATA	Displacements cards from program SWHTS
SPCDATA	Spc cards for input in structural models of beaded panels
SDATA1	Displacements cards for gridpoints along upper internal edges
SDATA2	Spc cards for gridpoints along upper internal edges
SDATA3	Displacements cards for gridpoints along lower internal edges
SDATA4	Spc cards for gridpoints along upper internal edges

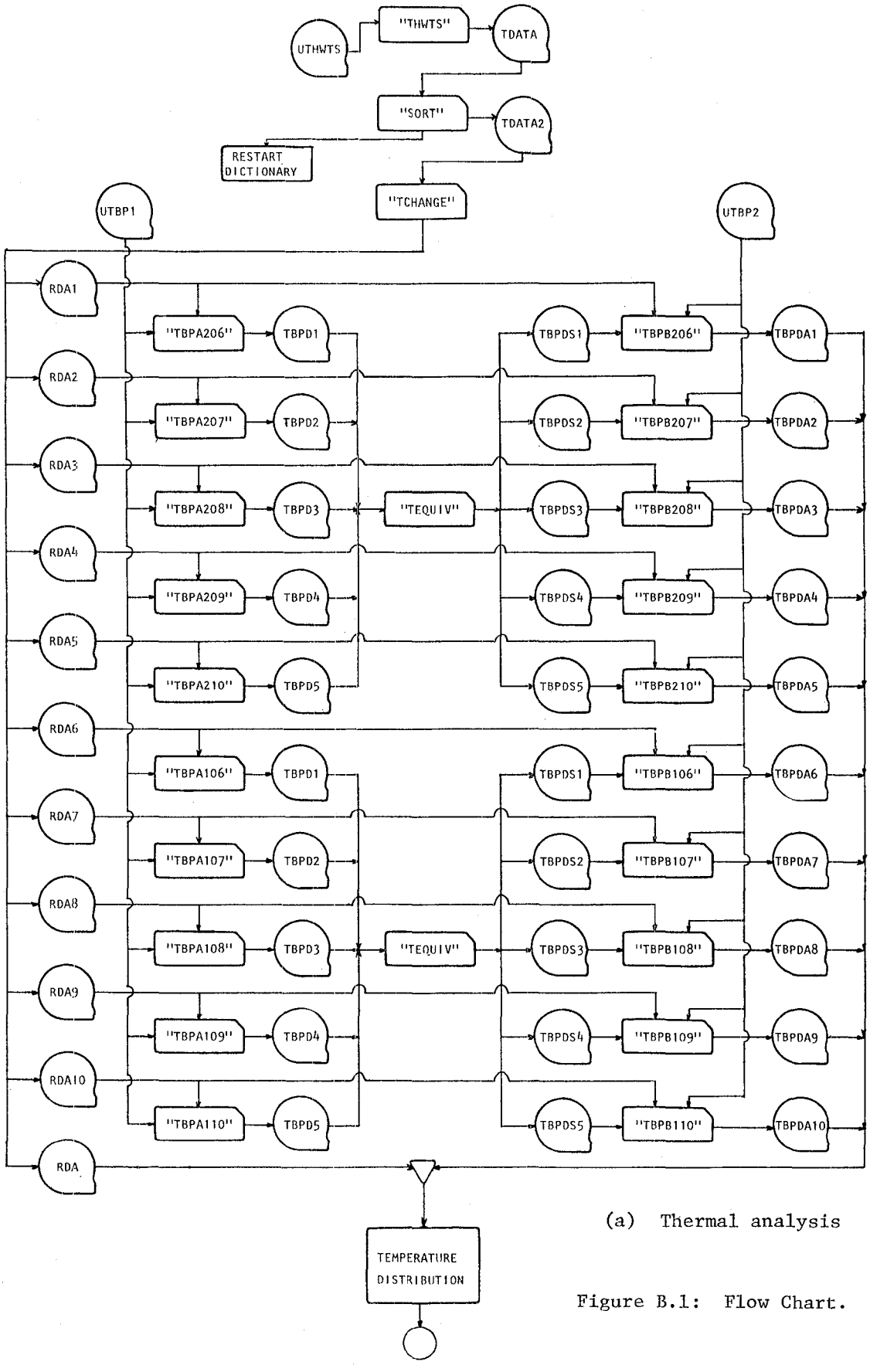

(a) Thermal analysis

Figure B.1: Flow Chart.

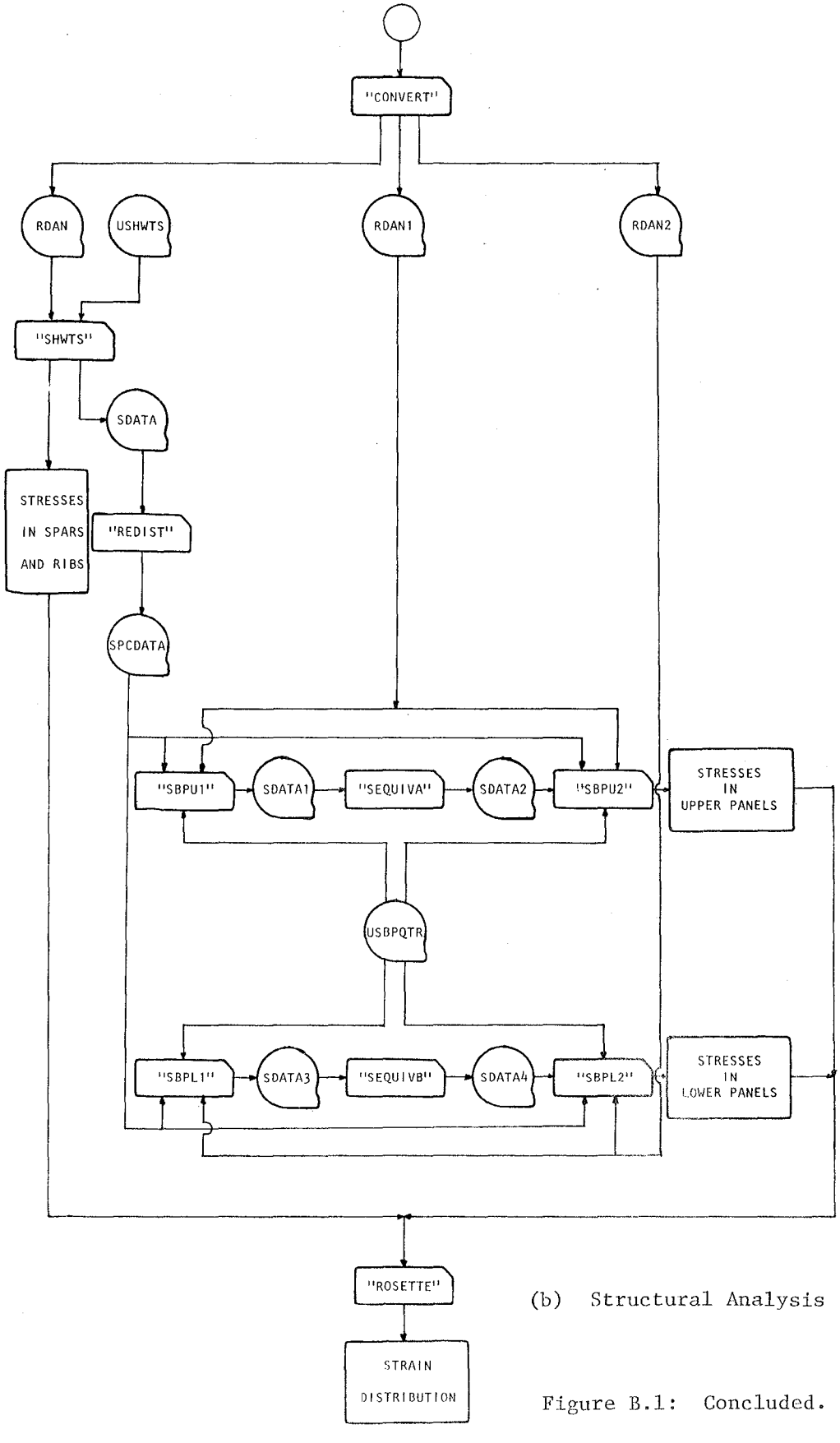

(b) Structural Analysis

Figure B.1: Concluded.

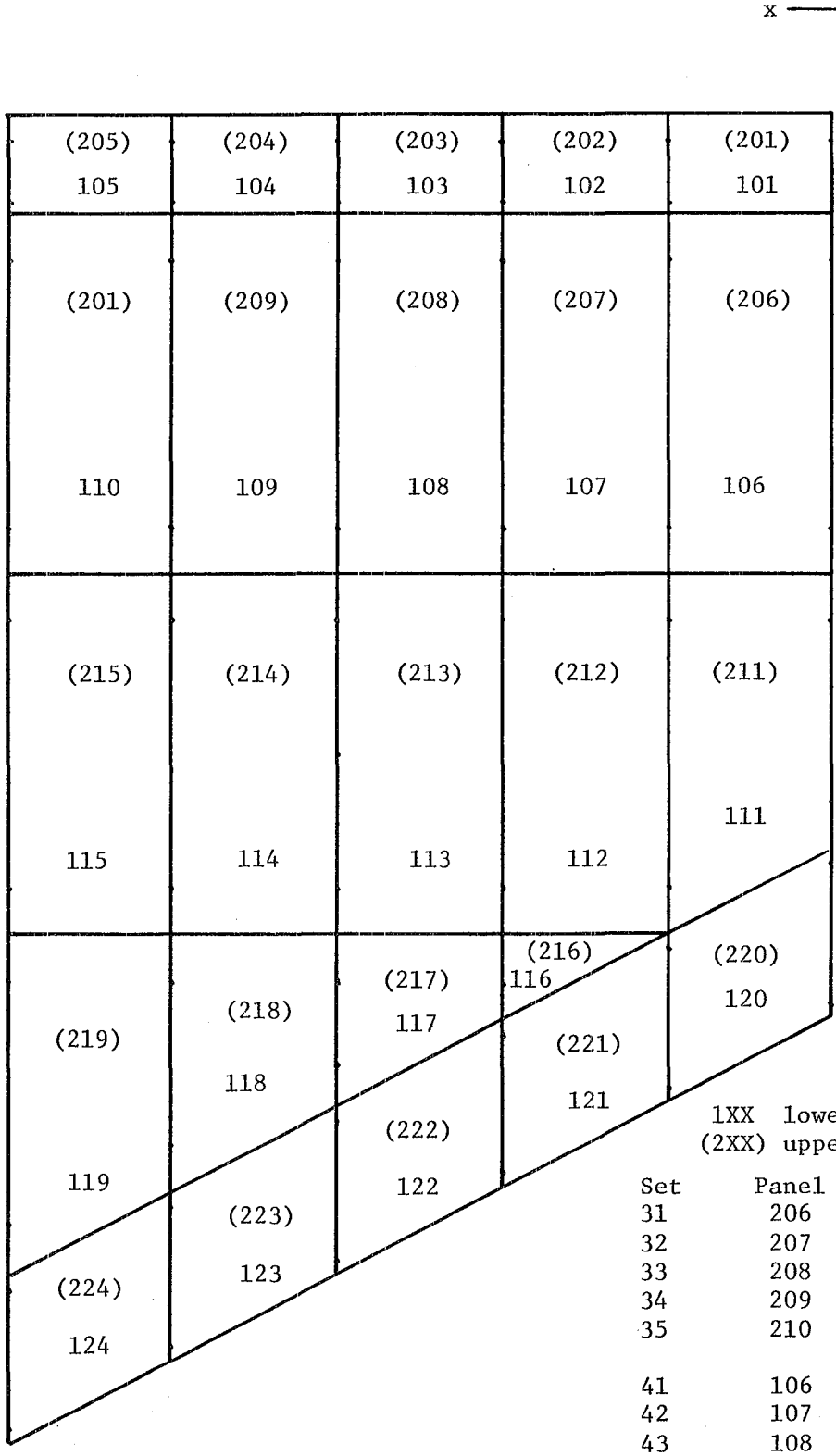

1XX lower surface panels
(2XX) upper surface panels

Set	Panel
31	206
32	207
33	208
34	209
35	210
41	106
42	107
43	108
44	109
45	110

Figure B.2: Panel Identification Numbers.

APPENDIX C

COMPUTER PROGRAMS

C.1 Listing of Main Computer Programs Used in the Generation of the Thermal Model

C.1.1: QUAD
C.1.2: CONVERT
C.1.3: FUDGE
C.1.4: SUPERFUDGE
C.1.5: MERGE
C.1.6: INVERT

C.2 Listing of Main Computer Programs Used in the Thermal* and Structural Analysis (See also Appendix B)

C.2.1: TCHANGE
C.2.2: TEQUIV
C.2.3: REDUCE
C.2.4: REDIST
C.2.5: SEQUIV
C.2.6: ROSETTE

---

*Although these programs were written for the first phase development of the thermal model, they are still applicable in the current analysis with only minor changes in some cases.

C.1.1 QUAD

Purpose: Determine correct z coordinate of fourth gridpoint of CHBDY element to ensure planarity of the gridpoints.

System: HP-41

Input:

$X_1\uparrow Y_1\uparrow Z_1$	(XEQ)	A
$X_2\uparrow Y_2\uparrow Z_2$		B
$X_3\uparrow Y_3\uparrow Z_3$		C
determinant:		D
$X_4\uparrow Y_4$		E → Z_4

```
01*LBL "AA"
02 STO 03
03 RDN
04 STO 02
05 RDN
06 STO 01
07 RTN
08 LBL "BB"
09 STO 06
10 RDN
11 STO 05
12 RDN
13 STO 04
14 RTN
15 LBL "CC"
16 STO 09
17 RDN
18 STO 08
19 RDN
20 STO 07
21 RTN
22 LBL "DD"
23 RCL 01
24 RCL 05
25 RCL 09
26 *
27 RCL 08
28 RCL 06
29 *
30 -
31 *
32 RCL 02
33 RCL 09
34 *
35 RCL 08
36 RCL 03
37 *
38 -
39 RCL 04
40 *
41 -
42 RCL 02
43 RCL 06
44 *
45 RCL 05
46 RCL 03
47 *
48 -
49 RCL 07
50 *
51 +
52 STO 23
53 RCL 05
54 RCL 09
55 *
56 RCL 08
57 RCL 06
58 *
59 -
60 RCL 02
61 RCL 09
62 *
63 RCL 08
64 RCL 03
65 *
66 -
67 -
68 RCL 02
69 RCL 06
70 *
71 RCL 05
72 RCL 03
73 *
74 -
75 +
76 RCL 23
77 /
78 STO 20
79 RCL 04
80 RCL 09
81 *
82 RCL 07
83 RCL 06
84 *
85 -
86 CHS
87 RCL 01
88 RCL 09
89 *
90 RCL 07
92 RCL 03
92 *
93 -
94 +
95 RCL 01
96 RCL 06
97 *
98 RCL 04
99 RCL 03
100 *
101 -
102 -
103 RCL 23
104 /
105 STO 21
106 RCL 04
107 RCL 08
108 *
109 RCL 07
110 RCL 05
111 *
112 -
113 RCL 01
114 RCL 08
115 *
116 RCL 07
117 RCL 02
118 *
119 -
120 -
121 RCL 01
122 RCL 05
123 *
124 RCL 04
125 RCL 02
126 *
127 -
128 +
129 RCL 23
130 /
131 STO 22
132 RTN
133 LBL "EE"
134 RCL 21
135 CHS
136 *
137 X<>Y
138 RCL 20
139 *
140 -
```

```
141 1
142 +
143 RCL 22
144 /
145 RTN
146 STOP
147 END
```

C.1.2 CONVERT

Purpose: Resort and renumber radiation elements according to increasing area size.

System: VAX-11

```
      PROGRAM CONVERT
C
      DIMENSION ID(900),ID1(900,A(900),NID(900),NO(900),KID(900)
      DIMENSION NI(900),W(14),IDD(900),CARD(900,14),CARDT(14)
C
C     READ NUMBER OF ELEMENTS N
C
      TYPE *,'N?'
      ACCEPT 5,N
 5    FORMAT(I4)
C
C     READ AREA AND ID FOR EACH ELEMENT
C
      OPEN (UNIT=1,FILE='INPUT',STATUS='OLD")
      READ (1,10) (ID(I),A(I),I=1,N)
 10   FORMAT(5(I12,F13.4))
C
      EQUIVALENT ID(I) WITH  ID1(1)
C
      DO 20 I=1,N
      ID1(I)=ID(I)
 20   CONTINUE
C
C     GENERATE NEW ID ARRAY
C     TYPE *,'ENTER STARTING ID : XXXX0 '
      ACCEPT *,KL
      NID(1)=KL
      DO 25 I=2,N
      NID(I)=NID(I-1)+10
 25   CONTINUE
C
C     SORT ARRAY A(I) WITH INCREASING SIZE ACCORDING BUBBLE SORT METHOD
C
      NN=N-1
      DO 35 K=1,NN
            JJ=N-K
            DO 30 L=1,JJ
                  IF(A(L).LE.A(L+1)) GO TO 30
                  TEMPA=A(L)
                  ID1TEMP=ID1(L)
                  A(L)=A(L+1)
                  ID1(L)=ID1(L+1)
                  A(L+1)=TEMPA
                  ID1(L+1)=ID1TEMP
 30           CONTINUE
```

```
 35       CONTINUE
C
C      CALCULATE RELATIONSHIPS BETWEEN SORTED AND UNSORTED ARRAYS
C
         M2=1
         DO 50 M1=1,N
 40      IF(ID(M1).EQ.ID1(M2)) GO TO 45
         M2=M2+1
         GO TO 40
 45      NI(M1)=M2
         NO(M2)=M1
         M2=1
 50      CONTINUE
C
C      PRINT OLD ID, AREA , NEW ID AND RELATIONSHIP BETWEEN BOTH ID'S
         OPEN (UNIT =3,FILE='PRINT',STATUS='NEW')
         WRITE (3,55)
 55    FORMAT('1',10X,6HOLD ID,4X,4HAREA,5X,6HNEW ID,9X6HOLD ID,2X,'= ',
     1     6HNEW ID,///)
         DO 65 I=1,N
         K1=NI(I)
         K2=NO(I)
         WRITE (3,60),ID1(I),A(I),NID(I),ID(I),NID(K1)
 60      FORMAT(11X,I5,3X,E10.4,3X,I5,10X,I5,5X,I5)
 65      CONTINUE
         CLOSE (UNIT3)
C
C         READ OLD CHBDY CARDS AND WRITE NEW CARDS WITH NEW ID'S
C
         OPEN (UNIT=2,FILE='OUTPUT',STATUS='NEW')
         DO 85 I=1,N
         READ (1,70),KID(I),(W(J),J=1,14)
 70      FORMAT(8X,I8,14A4)
        M3=1
 75     IF(KID(I).EQ.ID1(M3)) GO TO 80
        M3=M3+1
        GO TO 75
 80     IDD(I)=NID(M3)
        DO  85 J=1,14
            CARD(I,J)=W(J)
 85     CONTINUE
C
C     SORT CHBDY CARDS WITH INCREASING ID ACCORDING TO BUBBLE SORT METHOD
C
           NN=N-1
           DO 110 K=1,NN
           JJ=N-K
           DO 105 L=1,JJ
              IF(IDD(L).LE.IDD(L+1)) GO TO 105
              IDDT=IDD(L)
              IDD(L)=IDD(L+1)
```

```
                IDD(L+1)=IDDT
                DO 100 J=1,14
                   CARDT(J)=CARD(L,J)
                   CARD(L,J)=CARD(L+1,J)
                   CARD(L+1,J)=CARDT(J)
 100            CONTINUE
 105         CONTINUE
 110         CONTINUE
C        DO 125 I=1,N
            WRITE (2,120),IDD(I),(CARD(I,J),J=1,14)
 120        FORMAT('CHBDY   ',I8,14A4)
 125     CONTINUE
C
C
          CLOSE (UNIT1)
          CLOSE (UNIT2)
          STOP
          END
```

C.1.3 FUDGE

Purpose: Readjust radmatrix to obtain total sum of view factors for each element equal to or less than one.

System: VAX-11

```
        PROGRAM FUDGE
C
      DIMENSION CARD(8),CARDN(8),W(18),VALUE(8)
C
      OPEN (UNIT=1,FILE='INPUT',STATUS='OLD')
      OPEN (UNIT=2,FILE='OUTPUT',STATUS='NEW')
C
 1    TYPE *,' ENTER COLUMN NUMBER,( 0 = END OF JOB)'
      ACCEPT *,N
      IF (N.LE.0) GO TO 200
C
 5    READ (1,10) A,B,(CARD(I),I=1,8),C,D
 10   FORMAT(2A4,8E8.3,2A4)
C
      IF(A.EQ.'RADM') GO TO 15
      GO TO 150
C
 15   CC=CARD(1)*1000.
      KID=IIFIX(CC)
      CKID=KID
      IF((CC-CKID).GT..5) KID=KID+1
      TYPE *,CARD(1),CC,CKID,KIE
      IF(KID.EQ.N) GO TO 20
      GO TO 100
C
 20   TYPE 25,N
 25   FORMAT(5X,'ENTER TOTAL SUM OF VIEWFACTORS ',
     1  'OF ELEMENT IN COLUMN: ',I5)
      ACCEPT *,F
 30   DO 35 I=1,8
         CARDN(I)=CARD(I)/F
 35   CONTINUE
C
     IF(A.EQ.'RADM') GO TO 37
      WRITE (2,10) A,B,(CARDN(I),I=1,8),C,D
      GO TO 38
 37   WRITE (2,110) A,B,KID,(CARDN(I),I=2,8),C,D
 110  FORMAT(2A4,I8,7E8.3,2A4)
 38   IF(C.EQ.'    ') GO TO 40
      READ (1,10) A,B,(CARD(I),I=1,8),C,D
      GO TO 30
C
 40   GO TO 1
```

```
C
C
 100    WRITE (2,110) A,B,KID,(CARD(I),I=2,8),C,D
        GO TO 5
C
 150    WRITE (2,10) A,B,(CARD(I),I=1,8),C,D
        GO TO 5
 200    READ (1,210,ERR=250) (W(K),K=1,18)
 210    FORMAT(18A4)
        WRITE (2,210) (W(K),K=1,18)
        GO TO 200

C
 250    CLOSE (UNIT1)
        CLOSE (UNIT2)
        STOP
        END
```

C.1.4 SUPERFUDGE

Purpose: Adjust elements of rad matrix in order to obtain total sum of new factors for each element between 0.97 and 1.00.

System: VAX-11

```
      PROGRAM SUPERFUDGE
C
      DIMENSION F(300,300),ID(300),A(300),SF(300),FI(300,300),SFU(300)
      DIMENSION SVF(300),FUD(300),SVFN(300),KK(300),FA(300,300),SFL(300)
      DIMENSION FB(300,300),DD(300),FF(300),S(300)
C
      OPEN (UNIT=1,FILE='IN',STATUS='OLD')
      OPEN (UNIT=2,FILE='PRINT',STATUS='NEW')
      OPEN (UNIT=3,FILE='OUT',STATUS='NEW')
C
      TYPE *,'ENTER DEBUGGING CODE, 1=YES 2=NO'
      ACCEPT *,II
      TYPE *,'ENTER # OF RADMATRIX CARDS'
      ACCEPT *,N
C
C     READ ELEMENT ID,SUM OF VIEWFACTORS AND AREA
C
      DO 10 I=1,N
      READ (1,5) ID(I),SF(I),A(I)
 5    FORMAT(T17,I5,T26,E13.6,T53,E12.5)
 10   CONTINUE
C
C     READ VIEW FACTORS
C
      DO 30 I=1,N
C
      J1=I+6
      IF(J1.GE.N) J1=N
      READ (1,15,ERR=300) (FA(I,J),J=I,J1)
 15   FORMAT(16X,7E8.3)
      IF (J1.GE.N) GO TO 30
      J3=J1
 20   J2=J3+1
      J3=J3+8
      IF (J3.GE.N) J3=N
      READ (1,25,ERR=300) (FA(I,K),K=J2,J3)
 25   FORMAT(8X,8E8.3)
      IF (J3.EQ.N) GO TO 30
      GO TO 20
 30   CONTINUE
C
C     GENERATE UPPER TRIANGLE OF MATRIX
C
```

```
      IF(II.NE.1) GO TO 32
      DO 31 I=1,N
      WRITE (2,320) (FA,(I,J),J=I,N)
 31   CONTINUE
C
 32   CALL ASSEM(N,FA,FB,II)
      DO 34 I=1,N
      DO 33 J=1,N
      FA(I,J)=FB(I,J)
 33   CONTINUE
 34   CONTINUE
C
C     FUDGE FIRST COLUMN
C
      SUM = 0
      DO 45 J=1,N
      SUM = SUM + FA(1,J)
 45   CONTINUE
      SVF(1) = SUM
      IF ((SVF(1).LT.A(1)).AND.(SVF(1).GT.(A(1)*0.97))) GO TO 51
      FUD(1)=(SVF(1)/A(1)) * 1.01
      IF(SVF(1).LT.(A(1)*0.97)) FUD(1)=FUD(1)/1.00
      DO 50 J=1,N
      FA(1,J)=FA(1,J)/FUD(1)
 50   CONTINUE
      IF(II.EQ.1) WRITE (2,330) FUD(1)
C
C     REASSEMBLAGE VIEW MATRIX
C
 51   CALL ASSEM(N,FA,FI,II)
C
C     CHECK IF SFU(I) IS LARGER THAN A(I)
C
      DO 500 I=1,N
      SUM = 0.
        DO 510 J=1,I
        SUM = SUM +FA(I,J)
 510  CONTINUE
      S(I)=SUM
      IF (S(I).GT.A(I)) WRITE (2,520) I,S(I),A(I)
 520  FORMAT(2X,'WARNING COMUMN:',I3,' SFU=',E10.5,
     1       ' IS LARGER THAN A(I):',E10.5)
 500  CONTINUE
C
C     FUDGE COLUMNS 2 THRU N-1
C
 52   DO 75 I=2,N-1
C
C     COMPUTE SUM OF VIEW FACTORS IN UPPER TRIANGLE
C
      SUM = 0
      DO 55,J=1,I
```

```
       SUM = SUM + FI(I,J)
 55    CONTINUE
       SFU(I) = SUM
C
C     COMPUTE SUM OF VIEW FACTORS IN LOWER TRIANGLE
C
       SUM = 0
       DO 60 J=I,N
       SUM = SUM + FI(I,J)
 60    CONTINUE
       SFL(I)=SUM
C
C     COMPUTE FUDGE FACTOR FUD(I)
C
       SVF(I) = SFU(I) + SFL(I)
       IF((SVF(I).GT.(A(I)*0.97)).AND.(SVF(I).LT.A(I))) GO TO 70
                IF(SFL(I).EQ.0.)GO TO 66
                IF(SFU(I).GE.A(I)) GO TO 66
       FUD(I) = 1.01 * ( SFL(I)  ) / (A(I) - SFU(I))
       IF(SVF(I).LT.(A(I)*0.97)) FUD(I)=FUD(I)/1.0
C
C     APPLY FUDGE FACTOR ON COLUMN 1
C
       DO 65 J=I,N
       FI(I,J) = FI(I,J) / FUD(I)
 65    CONTINUE
       GO TO 67
C
C     IF SFU(I) LARGER THAN A(I),
C
C                OR
C
C     IF SFL(I) IS A ZERO COLUMN, APPLY FUDGE FACTOR ON FI(I,I)
C
 66    FI(I,I) = A(I) - SFU(I) -SFL(I)
       WRITE (2,661) I,ID(I)
 661   FORMAT(2X,'WARNING COLUMN:',I5,' (ID:',I7,')',
     1        'FA(I,I) HAS BEEN ASSIGNED A NEGATIVE VALUE')
       FUD(I) = 0.000
C
C
C     REASSEMBLAGE VIEW MATRIX
C
 67     CALL ASSEM(N,FI,FA,II)
C
       DO 69 IJ=1,N
       DO 68 J=1,N
       FI(IJ,J)=FA(IJ,J)
 68    CONTINUE
 69    CONTINUE
C
```

```
 70     CONTINUE
        IF(II.EQ.1) WRITE (2,340) I,SFU(I),SFL(I),SVF(I),FUD(I)
 75     CONTINUE
C
C      FUDGE LAST COLUMN
C
        SUM = 0
        DO 80 J=1,N
        SUM = SUM + FA(N,J)
 80     CONTINUE
        SVF(N) = SUM
        IF (SVF(N).GT.A(N)) FA(N,N)=A(N)-SVF(N)
        IF(II.EQ.1) WRITE (2,350) I,SVF(N),FA(N,N)
C
C      COMPUTE NEW SUM OF VIEW FACTORS
C
        SUM = 0
        DO 90 I=1,N
        DO 85 J=1,N
        SUM = SUM + FA(I,J)
 85     CONTINUE
        SVFN(I) = SUM
        SUM = 0
 90     CONTINUE
C
C      PRINT RESULTS
C
        DO 104 I=1,N
        FF(I)=SVFN(I)/A(I)
        DD(I)= (SF(I)-FF(I))*100 /SF(I)
 104    CONTINUE
C
        WRITE (2,105)
 105    FORMAT(//,7X,'ID,7X,'OLD SUM',6X,'NEW SUM',6X,'FUDGE FACTOR',
     1         6X,'CHANGE %',//)
        DO 115 I=1,N
        WRITE (2,110) ID(I),SF(I),FF(I),FUD(I),DD(I)
 110    FORMAT(4X,I6,6X,F7.5,6X,F7.5,8X,F8.5,6X,F8.2)
 115    CONTINUE
C
C      WRITE NEW RADMATRIX CARDS
C
        DO 155 I=1,N
        KK(I) = I * 100
        J1 = I+6
        IF (J1.GE.N) GO TO 145
        WRITE (3,120,ERR=400) I,(FA(I,J),J=I,J1),KK(I)
 120    FORMAT('RADMTX  ',I8,E8.2,6E8.3,'+',I7)
        KL = KK(I) + 1
 125    J1 = J1 + 1
        J2 = J1+7
```

```
      IF (J2.GE.N) GO TO 135
      WRITE (3,130,ERR=400) KK(I),(FA(I,J),J=J1,J2),KL
 130  FORMAT('+',I7,8E8.3,'+',I7
      KK(I) = KL
      KL = KK(I) + 1
      J1 = J2
      GO TO 125
 135  WRITE (3,140,ERR=400) KK(I),(FA(I,J),J=J1,N)
 140  FORMAT('+',I7,8E8.3)
      GO TO 155
 145  IF(I.EQ.N) GO TO 152
      WRITE (3,150,ERR=400) I,(FA(I,J),J=I,N)
 150  FORMAT('RADMTX  ',I8,E8.2,6E8.3)
      GO TO 155
 152  WRITE (3,153) I,FA(N,N)
 153  FORMAT('RADMTX  ',I8,E8.2)
C
      GO TO 155
 400  WRITE (2,410) I,(FA(I,J),J=I,N)
 410  FORMAT(5X,' I =:',I8,//,'FA :',(/,4(E12.5,4X)))
 155  CONTINUE
C
      GO TO 170
 300  TYPE 310,I,K,N,Z,ID(1)
 310  FORMAT(3(5X,I5),5X,'Z:',A1,5X,I5)
 320  FORMAT(2X,'FA::',5(5X,E9.4))
 330  FORMAT(5X,'FUD(1)=',F8.6)
 340  FORMAT(5X,'I=',I3,' SFU(I)= ',F8.5,' SFL(I)= ',F8.5,'SVF(I)= ',
     1       F8.5,' FUD(I)= ',F8.5)
 350  FORMAT(5X,'N= ',I3,' SVF(N)= ',F8.5,' FA(N,N)= ',E10.4)
C
 170  STOP
      END
C
C
C
C
C
      SUBROUTINE ASSEM(N,F,F2,II)
C
      DIMENSION F(300,1),F1(300,300),F2(300,300)
C
 60   DO 10 I=1,N
      DO 5  J=I,N
      F1(I,J)=F(I,J)
 5    CONTINUE
 10   CONTINUE
C
      DO 20 I=1,N
      DO I5 J=I,N
      F2(J,I)=F(I,J)
```

```
 15     CONTINUE
 20     CONTINUE
C
        DO 40 I=1,N
        DO 35 J=I,N
        F2(I,J)=F1(I,J)
 35     CONTINUE
 40     CONTINUE
C
        IF(II.NE.1) GO TO 65
        WRITE (2,2)
 2      FORMAT(3X,'MATRIX2')
        DO 90 J=1,N
        WRITE (2,95) (F2(I,J),I=1,N)
 95     FORMAT(10(2X,F10.7))
 90     CONTINUE
C
C
 65     RETURN
        END
```

C.1.5 MERGE

Purpose: Merge output of up to eight viewfactor programs into one large radiation exchange coefficient matrix.

System: VAX-11

```
        PROGRAM MERGE
C
       DIMENSION CARD(20)
C
C
CCCCCCCCCCCCCCCCCCCCCCCCCCCCCCCCCCCCCCCCCCCCCCCCCCCCCCCCCCCCCCCCCCCC
C
C    THIS PROGRAM MERGES THE OUTPUT OF EIGHT SEPARATE VIEW
C
C    PROGRAMS INTO ONE LARGE RADMATRIX, WITH THE FITTING
C
C                    CONTINUATION STATEMENTS.
C
CCCCCCCCCCCCCCCCCCCCCCCCCCCCCCCCCCCCCCCCCCCCCCCCCCCCCCCCCCCCCCCCCCCC
C
       OPEN (UNIT=1,FILE='INP1',STATUS='OLD')
       OPEN (UNIT=2,FILE='INP2',STATUS='OLD')
       OPEN (UNIT=3,FILE='INP3',STATUS='OLD')
       OPEN (UNIT=4,FILE='INP4',STATUS='OLD')
       OPEN (UNIT=5,FILE='INP5',STATUS='OLD')
       OPEN (UNIT=6,FILE='INP6',STATUS='OLD')
       OPEN (UNIT=7,FILE='INP7',STATUS='OLD')
       OPEN (UNIT=8,FILE='INP8',STATUS='OLD')
       OPEN (UNIT=9,FILE='OUT',STATUS='NEW')

       CALL PRINT(1,826,1)
       CALL PRINT(827,975,2)
       CALL PRINT(976,1185,3)
       CALL PRINT(1186,1419,4)
       CALL PRINT(1470,1647,5)
       CALL PRINT(1648,1831,6)
       CALL PRINT(1832,1892,7)
       CALL PRINT(1893,2041,8)
C
       CLOSE (UNIT1)
       CLOSE (UNIT2)
       CLOSE (UNIT3)
       CLOSE (UNIT4)
       CLOSE (UNIT5)
       CLOSE (UNIT6)
       CLOSE (UNIT7)
       CLOSE (UNIT8)
       CLOSE (UNIT9)
C
       STOP
       END
C
```

```
C
      SUBROUTINE PRINT(L1,L2,N)
      DIMENSION W(45,8),NK(45),KA(45)
C
      DO 80 K=L1,L2
C
      READ (N,5) (W(1,L),L=1,7),KA(1)
 5    FORMAT(T17,7E8.3,1X,I7)
      J=1
      IF(KA(1).EQ.0) GO TO 20
 10   J=J+1
      READ (N,15) (W(J,L),L=1,8),KA(J)
 15   FORMAT(T9,8E8.3,1X,I7)
      IF(KA(J).EQ.0) GO TO 20
      GO TO 10
 20   DO 40 I=1,J
      NK(I)=K*100+1-1
 40   CONTINUE
 21   IF(W(J,8).NE.0.0) GO TO 30
 25   IF(W(J,7).NE.0.0) GO TO 31
      IF(W(J,6).NE.0.0) GO TO 32
      IF(W(J,5).NE.0.0) GO TO 33
      IF(W(J,4).NE.0.0) GO TO 34
      IF(W(J,3).NE.0.0) GO TO 35
      IF(W(J,2).NE.0.0) GO TO 36
      IF(W(J,1).NE.0.0) GO TO 37
      IF(J.EQ.1) GO TO 80
      J=J-1
      IF(J.EQ.1) GO TO 25
      GO TO 21
C
 30   IF(J.EQ.1) GO TO 80
C
      WRITE (9,45) NK(J),(W(J,L),L=1,8)
 45   FORMAT(1H+,I7,8E8.3)
      GO TO 50
 31   IF(J.EQ.1) GO TO 71
      WRITE (9,45) NK(J),(W(J,L),L=1,7)
      GO TO 50
 32   IF(J.EQ.1) GO TO 72
      WRITE (9,45) NK(J),(W(J,L),L=1,6)
      GO TO 50
 33   IF(J.EQ.1) GO TO 73
      WRITE (9,45) NK(J),(W(J,L),L=1,5)
      GO TO 50
 34   IF(J.EQ.1) GO TO 74
      WRITE (9,45) NK(J),(W(J,L),L=1,4)
      GO TO 50
 35   IF(J.EQ.1) GO TO 75
      WRITE (9,45) NK(J),(W(J,L),L=1,3)
      GO TO 50
```

```
 36     IF(J.EQ.1) GO TO 76
        WRITE (9,45) NK(J),(W(J,L),L=1,2)
        GO TO 50
 37     IF(J.EQ.1) GO TO 77
        WRITE (9,45) NK(J),W(J,1)
 50     J=J-1
        IF(J.EQ.1) GO TO 60
        WRITE (9,55) NK(J),(W(J,L),L=1,8),NK(J+1)
 55     FORMAT(1H+,I7,8E8.3,1H+,I7)
        GO TO 50
C
 60     WRITE (9,65) K,(W(1,L),L=1,7),NK(2)
 65     FORMAT(8HRADMTX  ,I8,E8.2,6E8.3,1H+,I7)
        GO TO 80
 71     WRITE (9,79) K,(W(1,L),L=1,7)
 79     FORMAT(8HRADMTX  ,I8,E8.2,6E8.3)
        GO TO 80
 72     WRITE (9,79) K,(W(1,L),L=1,6)
        GO TO 80
 73     WRITE (9,79) K,(W(1,L),L=1,5)
        GO TO 80
 74     WRITE (9,79) K,(W(1,L),L=1,4)
 75     WRITE (9,79) K,(W(1,L),L=1,3)
        GO TO 80
 76     WRITE (9,79) K,(W(1,L),L=1,2)
        GO TO 80
 77     WRITE (9,79) K,W(1,1)
C
 80     CONTINUE
C
C
C
        RETURN
        END
```

C.1.6 INVERT

Purpose: Readjust output of MERGE program for aesthetic reasons.

System: VAX-11

```
        PROGRAM INVERT
       DIMENSION CARD(45,19),Z(45),Y(45)
C
       OPEN (UNIT=1,FILE='INPUT',STATUS='OLD')
       OPEN (UNIT=2,FILE='OUTPUT',STATUS='NEW')
C
       TYPE *,'ENTER NUMBER OF ELEMENTS'
       ACCEPT *,N
C
       DO 30 I=1,N
         J=0
 1       J=J+1
         READ (1,5,ERR=40) Z(J),(CARD(J,K),K=1,19),Y(J)
 5       FORMAT(A1,19A4,A3)
         IF  (Z(J).EQ.'R') GO TO 10
         GO TO 1
 10      DO 20 II=J,1,-1
          WRITE (2,5) Z(II),(CARD(II,K),K=1,19),Y(II)
 20      CONTINUE
C
 30    CONTINUE
C
       GO TO 50
 40    TYPE *,'PROGRAM HAS DETECTED LESS ELEMENTS THAN SPECIFIED'
 50    CLOSE (UNIT1)
       CLOSE (UNIT2)
       STOP
       END
```

C.2.1 TCHANGE

Purpose: Converts temperature output data from THWTS program into input data for SHWTS and TBPQTR programs.

System: CYBER 73

```
TCHANGE(T7777)
USER(LAMERIS,JAAP)
CHARGE(14,60,FTN)
FTN(A)
ATTACH(TAPE1=TDATA2)
LGO.
REWIND(TAPE2)
REWIND(TAPE3)
REWIND(TAPE4)
REWIND(TAPE5)
REWIND(TAPE6)
REWIND(TAPE7)
REWIND(TAPE8)
REWIND(TAPE9)
REWIND(TAPE10)
REWIND(TAPE11)
REWIND(TAPE12)
PURGE(RDA 1/NA)
PURGE(RDA 2/NA)
PURGE(RDA 3/NA)
PURGE(RDA 4/NA)
PURGE(RDA 5/NA)
PURGE(RDA 6/NA)
PURGE(RDA 7/NA)
PURGE(RDA 8/NA)
PURGE(RDA 9/NA)
PURGE(RDA10/NA)
PURGE(RDA/NA)
DEFINE(RDA=TAPE2)
DEFINE(RDA 1=TAPE3)
DEFINE(RDA 2=TAPE4)
DEFINE(RDA 3=TAPE5)
DEFINE(RDA 4=TAPE6)
DEFINE(RDA 5=TAPE7)
DEFINE(RDA 6=TAPE8)
DEFINE(RDA 7=TAPE9)
DEFINE(RDA 8=TAPE10)
DEFINE(RDA 9=TAPE11)
DEFINE(RDA10=TAPE12)
COPY(TAPE2,RDA)
COPY(TAPE3,RDA 1)
COPY(TAPE4,RDA 2)
COPY(TAPE5,RDA 3)
```

```
COPY(TAPE6,RDA 4)
COPY(TAPE7,RDA 5)
COPY(TAPE8,RDA 6)
COPY(TAPE9,RDA 7)
COPY(TAPE10,RDA 8)
COPY(TAPE11,RDA 9)
COPY(TAPE12,RDA10)

7/8/9

      PROGRAM TCHANGE(INPUT,OUTPUT,PUNCH,TAPE1,TAPE2,TAPE3,TAPE4,TAPE5,
     1TAPE6,TAPE7,TAPE8,1TAPE9,TAPE10,TAPE11,TAPE12)
      DIMENSION CARD(8),ID(10,400),TI(11),NID(51),W(11,350,14),S(8)
      DIMENSION N(51,10)
      DATA TI/0.,175.,350.,525.,700.,875.,1050.,1225.,1270.,1315.,1360./
      DATA NID/11,12,13,14,21,23,31,32,33,34,41,42,43,44,51,52,53,54,61,
     162,63,64,71,72,73,74,81,82,91,92,101,102,103,104,111,112,113,114,
     1121,122,123,124,131,132,142,151,162,172,182,191,192/
C
C
C     CCCCCCCCCCCCCCCCCCCCCCCCCCCCCCCCCCCCCCCCCCCCCCCCCCCCCCCCCCCCCCCCC
C     C                                                               C
C     C                                                               C
C     C            THIS PROGRAM PLACES THE TEMPERATURE CARDS          C
C     C            OF SUBCASE 1 OF PROGRAM THWTS ON A FILE RDA        C
C     C            FOR INPUT IN SHWTS.  IT WILL CONVERT THE           C
C     C            TEMPERATURE CARDS OF THE OTHER SUBCASES            C
C     C            INTO TABLED1 CARDS FOR INPUT IN THE THERMAL        C
C     C            BEADED PANEL MODELS.                               C
C     C                                                               C
C     C            INPUT IS NSK, REPRESENTING THE NUMBER OF CARDS     C
C     C            IN SUBCASE 1 OF THWTS, FORMAT I5.  SEE LISTING     C
C     C            OF TDATA IN PROGRAM THWTS.                         C
C     C                                                               C
C     CCCCCCCCCCCCCCCCCCCCCCCCCCCCCCCCCCCCCCCCCCCCCCCCCCCCCCCCCCCCCCCCC

C
      READ 1,NSK
      FORMAT(I5)
      DO 20 J=1,NSK
      READ (1,15) K,(S(I),I=1,6)
 15   FORMAT(A1,6A10)
      IF(K.EQ.1HT) GO TO 20
      GO TO 25
 20   PUNCH (2,15) K,(S(I),I=1,6)
 25   CONTINUE
C
```

```
C
C     CONVERSION TEMP CARDS IN TABLED1 CARDS
      J=0
 30   J=J+1
      I=0
      IT=1
 35   I=I+1
 37   READ (1,40) CARD
 40   FORMAT(8A10)
      DECODE(1,45,CARD(1)) K
 45   FORMAT(A1)
      IF(EOF(1)) 125,50
 50   IF(K.EQ.1H$) GO TO 37
 65   DECODE(60,70,CARD(1)) ID(J,I),W(J,I,IT)
 70   FORMAT(T37,I4,T45,E12.6)
      DO 80 IT=2,11
      READ (1,75) W(J,I,IT)
 75   FORMAT(T45,E12.6)
 80   CONTINUE
C
C     DETERMINATION ID OF TABLED1 CARDS
C
 85   DO 90 KL=1,51
        IF(ID(J,I).EQ.N(KL,J)) GO TO 95
 90   CONTINUE
C
 95   L=NID(KL)
      M=J+2
      PUNCH (M,100) L,L
 100  FORMAT(8HTABLED1 ,T12,I4,T73,*+*,I4,*1*)
      PUNCH (M,105) L,TI(1),(W(J,I,1),TI(2),W(J,I,2),TI(3),W(J,I,3),
     1TI(4),W(J,I,4),L
 105  FORMAT(*+*,I4,*1 *,8F8.2,*+*,I4,*2*)
      PUNCH (M,110) L,TI(5),W(J,I,5),TI(6),W(J,I,6),TI(7),W(J,I,7),
     1TI(8),W(J,I,8),L
 110  FORMAT(*+*,I4,*2 *,8F8.2,*+*,I4,*3*)
      PUNCH (M,115) L,TI(9),W(J,I,9),TI(10),W(J,I,10),TI(11),W(J,I,11)
 115  FORMAT(*+*,I4,*3 *,6F8.2,*ENDT*)
C
C
      IF(J.LE.5) GO TO 117
 116  MM= 43
      GO TO 118
 117  MM= 49
 118  IF(I.EQ.MM) GO TO 120
      GO TO 35
C
 120  GO TO 30
C
C
 125  CONTINUE
C
      STOP
      END
```

C.2.2 TEQUIV

Purpose: Equalize temperatures at common internal edges of the four submodels of TBPQTR for each panel.

System: CYBER 73

```
TEQUIV(T7777)
USER(LAMERIS,JAAP)
CHARGE(14,60,FTN)
FTN(A)
ATTACH(TAPE1=TBPD1)
ATTACH(TAPE2=TBPD2)
ATTACH(TAPE3=TBPD3)
ATTACH(TAPE4=TBPD4)
ATTACH(TAPE5=TBPD5)
LGO.
REWIND(TAPE6)
REWIND(TAPE7)
REWIND(TAPE8)
REWIND(TAPE9)
REWIND(TAPE10)
PURGE(TBPDS1/NA)
PURGE(TBPDS2/NA)
PURGE(TBPDS3/NA)
PURGE(TBPDS4/NA)
PURGE(TBPDS5/NA)
DEFINE(TBPDS1)
DEFINE(TBPDS2)
DEFINE(TBPDS3)
DEFINE(TBPDS4)
DEFINE(TBPDS5)
COPY(TAPE6,TBPSD1)
COPY(TAPE7,TBPDS2)
COPY(TAPE8,TBPDS3)
COPY(TAPE9,TBPDS4)
COPY(TAPE10,TBPDS5)

7/8/9

      PROGRAM TEQUIV(INPUT,OUTPUT,TAPE1,TAPE2,TAPE3,TAPE4,TAPE5,TAPE6,
     1 TAPE7,TAPE8,TAPE9,TAPE10)
C
C
      CALL SUBR(1,6)
      CALL SUBR(2,7)
      CALL SUBR(3,8)
      CALL SUBR(4,9)
      CALL SUBR(5,10)
C
C
      STOP
      END
```

```
      SUBROUTINE SUBR(LA,LB)
      DIMENSION NIDA(45),NIDB(45)
      DIMENSION TI(11),NTD(41),W(4,14,45),R(14,45),S(14,45)
      DIMENSION CARD(8)
      DATA TI/0.,175.,350.,525.,700.,875.,1050.,1225.,1270.,1315.,1360./
      DATA NTD/38,57,76,95,114,133,152,171,190,209,228,247,266,285,304,
     1 323,342,361,380,399,401,402,403,404,405,406,407,408,409,410,411,
     1 412,413,414,415,416,417,1057,1076,1095,1114/
C
      DO 25 IS=1,4
         DO 20 ID=1,41
 2    READ (LA,4) CARD
 4    FORMAT(8A10)
      DECODE(1,6,CARD(1)) K
 6    FORMAT(A1)
      IF(K.EQ.1H$) GO TO 2
      DECODE(60,10,CARD(1)) (W(IS,IT,ID),IT=1,11)
 10   FORMAT(145,E12.6)
 20          CONTINUE
 25   CONTINUE
      DO 35 ID=1,20
         DO 30 IT=1,11
      R(IT,ID)= (W(1,IT,ID)+W(2,IT,ID))/2
      S(IT,ID)=(W(3,IT,ID)+W(4,IT,ID))/2
 30          CONTINUE
 35   CONTINUE
      DO 45 ID=21,37
         DO 45 IT=1,11
      R(IT,ID)= (W,(1,IT,ID)+ W(3,IT,ID))/2
      S(IT,ID)= (W,(2,IT,ID)+ W(4,IT,ID))/2
 40          CONTINUE
 45   CONTINUE
      DO 55 ID=38,41
         DO 50 IT=1,11
      R(IT,ID)=(W(1,IT,ID)+W(3,IT,ID))/2
      S(IT,ID)= (W(3,IT,ID)+W(4,IT,ID))/2
 50          CONTINUE
 55   CONTINUE
      DO 60 I=1,41
      NIDA(I)=NID(I)*10+1
      NIDB(I)=NID(I)*10+3
 60   CONTINUE
C
      DO 85 J=1,41
      PUNCH (LB,65) NIDA(J),NIDA(J)
 65   FORMAT(8HTABLED1 ,18,T73,*+*,I5,*1*)
      PUNCH(LB,70) NIDA(J),TI(1),R(I,J),TI(2),R(2,J),TI(3),R(3,J),TI(4),
     1 R(4,J),NIDA(J)
 70   FORMAT(*+*,I5,*1 *,8F8.2,*+*,I5,*2*)
      PUNCH(LB,75) NIDA(J),TI(5),R(5,J),TI(6),R(6,J),TI(7),R(7,J),TI(8)
     1 R(8,J),NIDA(J)
```

```
75    FORMAT(*+*),I5,*2 *,8F8.2,*+*,I5,*3*)
      PUNCH(LB,80) NIDA(J),TI(9),R(9,J),TI(10),R(10,J),TI(11),R(11,J)
80    FORMAT(*+*,I5,*3 *,6F8.2,* ENDT*)
85    CONTINUE
      DO 90  J=1,41
      PUNCH (LB,65) NIDB(J),NIDB(J)
      PUNCH(LB,70) NIDB(J),TI(1),S(1,J),TI(2),S(2,J),TI(3),S(3,J),TI(4),
     1 S(4,J),NIDB(J)
      PUNCH(LB,75) NIDB(J),TI(5),S(5,J),TI(6),S(6,J),TI(7),S(7,J),TI(8),
     2 S(8,J),NIDB(J)
      PUNCH(LB,80) NIDB(J),TI(9),S(9,J),TI(10),S(10,J),TI(11),S(11,J)
90    CONTINUE
      RETURN
      END
```

C.2.3 REDUCE

Purpose: Sort and reduce the output of each temperature set to only one time stop.

System: CYBER 73

```
REDUCE (T777)
USER(LAMERIS,JAAP)
CHARGE(14,60,FTN)
FTN(A)
ATTACH(TAPE1=TBPDA1)
ATTACH(TAPE2=TBPDA2)
ATTACH(TAPE3=TBPDA3)
ATTACH(TAPE4=TBPDA4)
ATTACH(TAPE5=TBPDA5)
ATTACH(TAPE6=TBPDA6)
ATTACH(TAPE7=TBPDA7)
ATTACH(TAPE8=TBPDA8)
ATTACH(TAPE9=TBPDA9)
ATTACH(TAPE10=TBPDA10)
ATTACH(TAPE11=RDA)
LGO.
REWIND(TAPE12)
REWIND(TAPE13)
REWIND(TAPE14)
PURGE(RDAN/NA)
PURGE(RDAN1/NA)
PURGE(RDAN2/NA)
DEFINE(RDAN)
DEFINE(RDAN1)
DEFINE(RDAN2)
COPY(TAPE12,RDAN2)
COPY(TAPE13,RDAN)
COPY(TAPE14,RDAN1)

7/8/9/      END OF RECORD

      PROGRAM CONVERT(INPUT,OUTPUT, TAPE1,TAPE2,TAPE3,TAPE4,TAPE5,TAPE6,
     1 TAPE7,TAPE8,TAPE9,TAPE10,TAPE11,TAPE12,TAPE13,TAPE14,TAPE15)
C
C     CCCCCCCCCCCCCCCCCCCCCCCCCCCCCCCCCCCCCCCCCCCCCCCCCCCCCCCCCCCCCCCCCCCCCCC

      THIS PROGRAM RENUMBERS THE TEMPERATURE CARDS FOR EACH PANEL
      FOR INPUT IN THE STRUCTURAL ANALYSIS AND REDUCES THE OUTPUT
      TO ONLY ONE TIME STEP.
C
C     CALL PUNCH(A,B,C,N1)
C     CALL PUNCH2(A,C,N1)
C
```

```
C
C       A = NUMBER OF INPUT FILE
C       B = PANEL NUMBER
C       C = NUMBER OF OUTPUT FILE
C
C       N1 = NUMBER OF DESIRED TIME STEP
C
C
C
C       CCCCCCCCCCCCCCCCCCCCCCCCCCCCCCCCCCCCCCCCCCCCCCCCCCCCCCCCCCCCCCCCCCCCCCC
C
C
        READ 1,N1
 1      FORMAT(I4)
C
        CALL PUNCH(1,106,12,N1)
        CALL PUNCH(2,107,12,N1)
        CALL PUNCH(3,108,12,N1)
        CALL PUNCH(4,109,12,N1)
        CALL PUNCH(5,110,12,N1)
        CALL PUNCH(6,206,14,N1)
        CALL PUNCH(7,207,14,N1)
        CALL PUNCH(8,208,14,N1)
        CALL PUNCH(9,209,14,N1)
        CALL PUNCH(10,210,14,N1)
C
        CALL PUNCH2(11,13,N1)
C
C
        STOP
        END
C
        SUBROUTINE PUNCH(LB,LC,LD,N1)
        DIMENSION CARD(8)
C
 6      DO 28 J=1,4
        DO 18 I=1,433
        DO 16 M=1,11
 7      READ (LB,8) CARD
 8      FORMAT(8A10)
        DECODE(1,10,CARD(1)) K
 10     FORMAT(A1)
        IF(K.NE.1HT) GO TO 7
        DECODE(80,12,CARD(1)) ID,IDGP,TEMP
 12     FORMAT(T23,I2,T36,I5,T44,F13.6)
        NID=LC*1000+J*100+ID
        PUNCH (11,14) NID,IDGP,TEMP
 14     FORMAT(5HTEMP*,T19,I6,T36,I5,T44,F13.6)
        IF(ID.EQ.N1) GO TO 20
        GO TO 16
 20     PUNCH (LD,14) NID,IDGP,TEMP
 16     CONTINUE
 18     CONTINUE
```

```
 28     CONTINUE
        RETURN
        END
        SUBROUTINE PUNCH2(LA,LB,N1)
        DIMENSION CARD(8)
C
 3      READ (LA,5) CARD
 5      FORMAT(8A10)
        IF(EOF(LA).EQ.0) GO TO 25
        DECODE(1,10,CARD(1)) K
 10     FORMAT(A1)
        IF(K.NE.1HT) GO TO 3
        DECODE(80,15,CARD(1)) ID,IDGP,TEMP
 15     FORMAT(T23,I2,T36,I5,T44,F13.6)
        IF(ID.EQ.NI) GO TO 20
        GO TO 3
 20     PUNCH(LB,5) CARD
        GO TO 3
 25     RETURN
        END
```

7/8/9

C.2.4 REDIST

Purpose: Convert displacements in spc cards for input in structural models of the beaded panels.

System: CYBER 73

```
REDIST,T777.
USER(LAMERIS,JAAP)
CHARGE(14,60,FTN)
ATTACH(TAPE9=SDATA)
FTN(A)
LDSET(PRESET=ZERO)
LGO.
REWIND(PUNCH)
PURGE(SPCDATA/NA)
DEFINE(TAPE=SPCDATA)
COPY(PUNCH,TAPE)
ROUTE(PUNCH,DC=SC)

7/8/9       END OF RECORD

      PROGRAM REDIST  (INPUT,OUTPUT,PUNCH,TAPE9)
      DIMENSION CARD(8),ID(10,12),NID(40),N(12,10),NA(10),NB(12)
      DIMENSION W(10,12,6),Z(10,12,6),CARD1(9)
      DATA NA/106,107,108,109,110,206,207,208,209,210/
      DATA NB/1,1,1,1,19,19,96,96,96,96,400,400/
C
C     PUNCH RESTART DICTIONARY
C
      DO 3 T=1,109
 1    READ (9,2) CARD1
 2    FORMAT(A1,7A10,A9)
 3    CONTINUE
C
C     READ GRID POINT IDENTIFICATION NUMBERS
C
C
 4    READ 5,N
 5    FORMAT(12(I4,1X))
C
C
 10   DO 150 J=1,10
      I=0
      KP=0
 15   I=I+1
 20   READ (9,25) CARD
 25   FORMAT(8A10)
      IF(EOF(9)) 160,26
```

```
 26     DECODE(1,30,CARD(1)) K
 30     FORMAT(A1)
        IF(K.EQ.1H$) GO TO 20
        DECODE(80,35,CARD(1)) ID(J,I),(W(J,I,IS),IS=1,3)
 35     FORMAT(T7,I4,T24,E13.6,T42,E13.6,T60,E13.6)
        READ (9,40) (W(J,I,IS),IS=4,6)
 40     FORMAT(T24,E13.6,T42,E13.6,T60,E13.6)
C
C       TRANSFORMATION DISPLACEMENTS INTO OTHER COORDINATE SYSTEM
C
        IF(J.LE.5) GO TO 42
        A=ATAN(.05495)
        GO TO 44
 42     A=ATAN(-.05495)
 44     Z(J,I,1)=W(J,I,2)*COS(A)-W(J,I,3)*SIN(A)
        Z(J,I,2)=-W(J,I,1)
        Z(J,I,3)= W(J,I,2)*SIN(A)+W(J,I,3)*COS(A)
        Z(J,I,4)= W(J,I,5)*COS(A)-W(J,I,6)*SIN(A)
        Z(J,I,5)=-W(J,I,4)
        Z(J,I,6)= W(J,I,5)*SIN(A)+W(J,I,6)*COS(A)
C
C       DETERMINATION OF ID OF SPC CARDS
C
 45     DO 50 KL=1,12
              IF(ID(J,I).EQ.N(KL,J)) GO TO 55
        50 CONTINUE
C
C
 55     LA=NA(J)
        IF(KL.EQ.1) GO TO 80
        IF(KL.EQ.2) GO TO 85
        IF(KL.EQ.3) GO TO 90
        IF(KL.EQ.4) GO TO 95
        IF(KL.EQ.5) GO TO 75
        IF(KL.EQ.6) GO TO 70
        IF(KL.EQ.7) GO TO 80
        IF(KL.EQ.8) GO TO 85
        IF(KL.EQ.9) GO TO 90
        IF(KL.EQ.10) GO TO 95
        IF(KL.EQ.11) GO TO 65
 60     LB=LA*10+2
        LC=LA*10+4
        GO TO 120
 65     LG=LA*10+1
        LC=LA*10+3
        GO TO 120
 70     LB=LA*10+3
        LC=LA*10+4
        GO TO 120
 75     LB=LA*10+1
        LC=LA*10+2
        GO TO 120
```

```
 80     LD=LA*10+1
        GO TO 100
 85     LD=LA*10+2
        GO TO 100
 90     LD=LA*10+3
        GO TO 100
 95     LD=LA*10+4
C
C       PUNCH SPC CARDS
C
 100    PUNCH 105,LD,NB(KL),Z(J,I,1),NB(KL),Z(J,I,2)
        PUNCH 110,LD,NB(KL),Z(J,T,3),NB(KL),Z(J,I,4)
        PUNCH 115,LD,NB(KL),Z(J,I,5),NB(KL),Z(J,I,6)
 105    FORMAT(3HSPC,T9,I4,T17,I4,T25,*1*,T33,F8.5,T41,I4,T49,*2*,T57,
     6 F8.5)
 110    FORMAT(3HSPC,T9,I4,T17,I4,T25,*3*,T33,F8.5,T41,I4,T49,*4*,T57,
     7 F8.5)
 115    FORMAT(3HSPC,T9,I4,T17,I4,T25,*5*,T33,F8.5,T41,I4,T49,*6*,T57,
     8 F8.5)
        IF(KP-2) 135,130,135
C
C
 120    LD=LB
        KP=2
        GO TO 100
 130    LD=LC
        KP=4
        GO TO 100
C
C
 135    IF(I.EQ.12) GO TO 145
        GO TO 15
 145    IF(J.EO.10) GO TO 160
 150    CONTINUE
C
C
 160    CONTINUE
        STOP
        END

7/8/9

1009,1000,1809,1800,1004,1804,1146,1120,1606,1580,1409,1398
1018,1009 1818 1809 1013 1813 1172 1146 1632 1606 1420 1409
1027 1018 1827 1818 1022 1822 1198 1172 1658 1632 1431 1420
1036 1027 1836 1827 1031 1831 1224 1198 1684 1658 1442 1431
1045 1036 1845 1836 1040 1840 1250 1224 1710 1684 1453 1442
1011 1002 1811 1802 1007 1807 1149 1123 1609 1583 1413 1402
1020 1011 1820 1811 1016 1816 1175 1149 1635 1609 1424 1413
1029 1020 1829 1820 1025 1825 1201 1175 1661 1635 1435 1424
1038 1029 1838 1829 1034 1834 1227 1201 1687 1661 1446 1435
1047 1038 1847 1838 1043 1843 1253 1227 1713 1687 1457 1446
```

C.2.5 SEQUIV (or SEQUIVA, SEQUIVB)

Purpose: Equalize displacements along material edges of each panel and convert them into spc cards.

System: CYBER 73

```
      PROGRAM SEQUIV (INPUT,OUTPUT,PUNCH,TAPE9)
      DIMENSION CARD(8)
      DIMENSION KN(10)
      DIMENSION NID(41),W(4,6,41),R(4,6,41),S(4,6,41),ID(4,41),M(4)
      DATA KN/106,107,108,109,110,206,207,208,209,210/
      DATA NID/38,57,76,95,114,133,152,171,190,209,228,247,266,285,304,
     1 323,342,361,380,399,401,402,403,404,405,406,407,408,409,410,411,
     2 412,413,414,415,416,417,1057,1076,1095,1114/
C
C     CCCCCCCCCCCCCCCCCCCCCCCCCCCCCCCCCCCCCCCCCCCCCCCCCCCCCCCCCCCCCCCCCCC
C     C                                                                  C
C     C  THIS PROGRAM EQUALIZES THE DISPLACEMENTS ALONG THE INTERNAL     C
C     C  EDGES OF THE FOUR QUARTER MODELS OF THE BEADED PANEL FOR EACH   C
C     C  PANEL.                                                          C
C     C  AFTER THIS, IT CONVERTS THESE CARDS INTO SPC CARDS.             C
C     C                                                                  C
C     C                                                                  C
C     C  INPUT : L = 0  NO RESTART                                       C
C     C          L = XXXX  NUMBER OF CARDS OF THE CHECKPOINT DICTIONARY  C
C     C                                                                  C
C     C  L IS PUNCHED IN THE FIRST 4 COLUMNS  (I4 FORMAT)                C
C     C                                                                  C
C     C                                                                  C
C     C                                                                  C
C     CCCCCCCCCCCCCCCCCCCCCCCCCCCCCCCCCCCCCCCCCCCCCCCCCCCCCCCCCCCCCCCCCCC
C
      READ 1,L
 1    FORMAT(I4)
      IF(L.EQ.0) GO TO 4
      DO 3 I=1,L
      READ (9,10) CARD
 3    CONTINUE
 4    DO 110 NN=6,10
      N=KN(NN)
C
C
      M(1)=N*10+1
      M(2)=N*10+2
      M(3)=N*10+3
      M(4)=N*10+4
C
C
```

```
      DO 20 J=1,4
C
C
      DO 20 J=1,4
         DO 15 L=1,41
 5    READ (9,10) CARD
 10   FORMAT(8A10)
      DECODE (1,11,CARD(1)) K
 11   FORMAT(A1)
      IF(K.EQ.1H$) GO TO 5
 8    DECODE (80,12,CARD(1)) ID(J,L),(W(J,L,1),I=1,3)
 12   FORMAT(T7,I4,T24,E13.6,T42,E13.6,T60,E13.6)
      READ (9,14) (W(J,L,I),I=4,6)
 14   FORMAT(T24,E13.6,T42,E13.6,T60,E13.6)
 15      CONTINUE
 20   CONTINUE
C
C
      DO  51 J =1,4
      DO 30 L=1,20
         DO 25 I=1,6
         R(J,L,I)=(W(1,L,I)+W(2,L,I))/2
         S(J,L,I)=(W(3,L,I)+W(4,L,I))/2
 25      CONTINUE
 30   CONTINUE
      DO 40 L=21,37
         DO 35 I=1,6
         R(J,L,I)=(W(1,L,I)+W(3,L,I))/2
         S(J,L,I)=(W(2,L,I)+W(4,L,I))/2
 35      CONTINUE
 40   CONTINUE
      DO 50 L=38,41
         DO 45 1=1,6
         R(J,L,I)=(W(1,L,I)+W(2,L,I))/2
         S(J,L,I)=(W(3,L,I)+W(4,L,I))/2
 45      CONTINUE
 50   CONTINUE
 51   CONTINUE
C
C
      DO 70 I=1,41
         PUNCH 55,M(1),ID(1,I),R(1,I,1),ID(1,I),R(1,I,2)
 55      FORMAT(*SPC*,T9,I4,T17,I4,T25,*1*,T33,F8.5,T41,I4,T49,*2*,T57,
     3 F8.5)
         PUNCH 60,M(1),ID(1,I),R(1,I,3),ID(1,I),R(1,I,4)
 60      FORMAT(*SPC),T9,I4,T17,I4,T25,*3*,T33,F8.5,T41,I4,T49,*4*,T57,
     4 F8.5)
         PUNCH 65,M(1),ID(1,I),R(1,I,5),ID(1,I),R(1,I,6)
 65    FORMAT(*SPC*,T9,I4,T17,I4,T25,*5*,T33,F8.5,T41,I4,T49,*6*,T57,
     5 F8.5)
C
C
```

```
C
C
 70     CONTINUE
        DO 75 I=1,20
        PUNCH 55,M(2),ID(2,I),R(2,I,1),ID(2,I),R(2,I,2)
        PUNCH 60,M(2),ID(2,I),R(2,I,3),ID(2,I),R(2,I,4)
        PUNCH 65,M(2),ID(2,I),R(2,I,5),ID(2,I),R(2,I,6)
 75     CONTINUE
C
C
        DO 80 I=21,37
        PUNCH 55,M(2),ID(2,I),S(2,I,1),ID(2,I),S(2,I,2)
        PUNCH 60,M(2),ID(2,I),S(2,I,3),ID(2,I),S(2,I,4)
        PUNCH 65,M(2),ID(2,I),S(2,I,5),ID(2,I),S(2,I,6)
 80     CONTINUE
C
C
        DO 85 I=38,41
        PUNCH 55,M(2),ID(2,I),R(2,I,1),ID(2,I),R(2,I,2)
        PUNCH 60,M(2),ID(2,I),R(2,I,3),ID(2,I),R(2,I,4)
        PUNCH 65,M(2),ID(2,I),R(2,I,5),ID(2,I),R(2,I,6)
 85     CONTINUE
C
C
C
C
        DO 90 I=1,20
        PUNCH 55,M(3),ID(3,I),S(3,I,1),ID(3,I),S(3,I,2)
        PUNCH 60,M(3),ID(3,I),S(3,I,3),ID(3,I),S(3,I,4)
        PUNCH 65,M(3),ID(3,I),S(3,I,5),ID(3,I),S(3,I,6)
 90     CONTINUE
C
C
        DO 95 I=21,37
        PUNCH 55,M(3),ID(3,I),R(3,I,1),ID(3,I),R(3,I,2)
        PUNCH 60,M(3),ID(3,I),R(3,I,3),ID(3,I),R(3,I,4)
        PUNCH 65,M(3),ID(3,I),R(3,I,5),ID(3,I),R(3,I,6)
 95     CONTINUE
C
C
        DO 100 I=38,41
        PUNCH 55,M(3),ID(3,I),S(3,I,1),ID(3,I),S(3,I,2)
        PUNCH 60,M(3),ID(3,I),S(3,I,3),ID(3,I),S(3,I,4)
        PUNCH 65,M(3),ID(3,I),S(3,I,5),ID(3,I),S(3,I,6)
 100    CONTINUE
C
C
C
        DO 105 I=1,41
        PUNCH 55,M(4),ID(4,I),S(4,I,1),ID(4,I),S(4,I,2)
        PUNCH 60,M(4),ID(4,I),S(4,I,3),ID(4,I),S(4,I,4)
        PUNCH 65,M(4),ID(4,I),S(4,I,5),ID(4,I),S(4,I,6)
 105    CONTINUE
```

```
C
C
C
 110    CONTINUE
C
C
       STOP
       END

7/8/9
```

C.2.6 ROSETTE

Purpose: Conversion of stresses into strains.

System: CYBER 73

```
      PROGRAM ROSETTE(INPUT,OUTPUT,TAPE1=OUTPUT,TAPE3=INPUT)
C     ROSETTE-2 STRAIN GAGE ANALYSIS PROGRAM
C
C       INPUT CARDS
C       AS MANY CASES AS DESIRED MAY BE RUN WITH ONE PROGRAM
C       EXECUTION.  DATA IS TO BE IN A F FORMAT UNLESS SPECIFIED
C       OTHERWISE.  THE FOLLOWING DATA CARDS ARE NECESSARY TO RUN THE
C       PROGRAM.
C
C*------*-------*-------------------------------------------------------*
C* CARD *  COL  *                    EXPLANATION                        *
C*------*-------*-------------------------------------------------------*
C*   1  *  1-80 * TITLE INFORMATION.                                     *
C*   2  *  1-80 * GENERAL INFORMATION RELATED TO THE PROBLEM.           *
C*------*-------*-------------------------------------------------------*
C*   3  *  1-10 * YOUNGS MODULUS                                        *
C*      * 11-20 * POISSONS RATIO.                                       *
C*      * 21-30 * THE SHEAR MODULUS.                                    *
C*      *       * NOTE-ONLY TWO OF THE ABOVE THREE MATERIAL PROPERTIES  *
C*      *       * MUST BE SPECIFIED IN WHICH CASE THE THIRD IS          *
C*      *       * CALCULATED BY THE RELATIONSHIP G=E/2(1 + NU).  ALL    *
C*      *       * THREE MAY BE SPECIFIED AT USER OPTION.  E OR F FORMAT.*
C*------*-------*-------------------------------------------------------*
C* 4-N  *  1-8  * GAGE ID.  UP TO 8 ALPHANUMERIC CHARACTERS.            *
C*      *  9-18 * THE X COMPONENT OF STRESS.  MAY BE LEFT BLANK IF ZERO.*
C*      * 19-28 * THE Y COMPONENT OF STRESS.  MAY BE LEFT BLANK IF ZERO.*
C*      * 29-38 * THE SHEAR COMPONENT OF STRESS.  MAY BE LEFT BLANK IF  *
C*      *       * ZERO.                                                 *
C*      * 39-48 * THE ANGLE BETWEEN GAGE A AND THE X AXIS (ANGLE A) IN  *
C*      *       * DEGREES.  MAY BE LEFT BLANK IF ZERO.                  *
C*      * 49-58 * THE GAGE B-FACTOR.  MAY BE LEFT BLANK IF ZERO.        *
C*      *       * NOTE-IF NO B-FACTOR IS SPECIFIED NO TRANSVERSE        *
C*      *       * SENSITIVITY IS ACCOUNTED FOR.                         *
C*      * 59-61 * GAGE TYPE.  SEE EXPLANATION BELOW.                    *
C*      *       *                                                       *
C*      *       *            EXPLANATION OF GAGE TYPES                  *
C*      *       *            -------------------------                  *
C*      *       *                                                       *
C*      *       * GAGE TYPE                    INPUT NAME               *
C*      *       * ---------                    ----------               *
C*      *       * RECTANGULAR ROSETTE          REC                      *
C*      *       * EQUANGULAR ROSETTE           EQU                      *
C*      *       * BENDING BRIDGE               BEN OR BBR               *
C*      *       * DELTA ROSETTE                DEL                      *
```

```
C*      *       * T-ROSETTE                     TRO                             *
C*      *       * CAPACITIVE AXIAL              CAP                             *
C*      *       * PURE AXIAL                    AXI                             *
C*      *       * SHEAR BRIDGE                  SHE OR SBR                      *
C*      *       * GENERAL ROSETTE               GEN                             *
C*------*-------*-------------------------------------------------------------*
C*      *       * NOTE- ONE ADDITIONAL CARD IS NECESSARY IF USING THE           *
C*      *       * GENERAL ROSETTE.  IT MUST IMMEDIATELY FOLLOW THE CARD         *
C*      *       * JUST DESCRIBED.  DATA TO BE SUPPLIED ON THIS CARD ARE         *
C*      *       * AS FOLLOWS-                                                   *
C*      *  1-10 * THE ANGLE BETWEEN GAGE A AND B IN DEGREES.                    *
C*      * 11-20 * THE ANGLE BETWEEN GAGE B AND C IN DEGREES.                    *
C*------*-------*-------------------------------------------------------------*
C
C
C                 ************************************************************
C
C                 +Y-    SHEAR BRIDGE DIAGRAM        RECTANGULAR ROSETTE
C                   -            ---------- +IN
C                   -            !                        X     X GAGE B
C                   --    /     / \                 GAGE C X    X
C                   -        X/   \X                      X   /
C                   -       XAX   XDX                     !  /
C                   -       /X     X\                     ! / 45 DEGREES
C                   -      / ANG. A  \                    !____XXXXXX
C                   -    --  ------   ---- +OUT               GAGE A
C                   -    ! \          /
C                   -    !  \X     X/
C                   -    !  XBX   XCX                   DELTA ROSETTE
C                   -    !   X\   /X                         *
C                   -    !     \ /                         / \
C                   -    !      !                   GAGE B X   XGAGE C
C                   -    !      !----------IN             X     X
C                   -    !                              /       \
C                   -    !------------------OUT        *---XXXXX---*
C                   -                                    GAGE A
C                   ------------------------------------------------------
C                   REFERENCE COORDINATE SYSTEM                        +X
C
C
C
C
C                 ************************************************************
C
C
      DIMENSION ITIT1(40),ITIT2(40)
      INTEGER END,REC,DEL,EQU,CAP,AXI,BBR,BEN,TRO,SBR,SHE,GEN
      REAL NU
      EQUIVALENCE(SHE,SBR),(BEN,BBR)
      DATA END,REC,DEL,EQU,AXI,BBR,BEN,TRO,CAP,SBR,SHE,COUNT/2HEN,2HRE,
     1 2HDE,2HEQ,2HAX,2HBB,2HBB,2HTR,2HCA,2HSB,2HSB,1./
      DATA GEN/2HGE/,PLANK/7777777777777777777B/
C
```

```
C       READ CARD TYPES ONE, TWO, AND THREE.
C
 40     READ (3,999) ITIT1
        READ (3,999) ITIT2
 999    FORMAT(40A2)
        READ (3,2) E,NU,G
 2      FORMAT(3E10.3)
        WRITE(1,1001)
        IF(E.EQ.BLANK) E = G*(2.*(1. + NU))
        IF(NU.EQ.BLANK) NU = (E/(2*G)) -1.
        IF(G.EQ.BLANK) G = E/(2*(1. + NU))
        IF(NU.GT.0.5.OR.NU.LT.0.0) WRITE(1,8) NU
 8      FORMAT(//////////10X,*WARNING-POISSONS RATIO HAS BEEN COMPUTED AS*
     1 F10.3)
 1002   COUNT = 1.
        WRITE(1,1001)
 1001   FORMAT(1H1)
C
C       PRINT HEADINGS.
C
        WRITE(1,1) ITIT1
 1      FORMAT (9X,32HROSETTE-2 STRAIN GAGE ANALYSIS  ,40A2)
        WRITE(1,1000) ITIT2
 1000   FORMAT     (9X,10H----------,9X,10H----------,9X,10H----------,
     1 9X,10H----------,9X,10H----------,9X,10H----------,1X,///30X,40A2/
     1 //)
        WRITE(1,3) E,NU,G
 3      FORMAT(15X,15HYOUNGS MODULUS=,2PE10.2,14X,16H POISSONS RATIO=,
     1 0PF10.3,14X 14HSHEAR MODULUS=,2PE10.2/)
 44     WRITE(1,4)
 4      FORMAT(3X,5H GAGE,4X,4HGAGE,7X,7HANGLE-A,7X,8HSTRESS-X,7X,BSTRESS
     1 -Y,7X,8HSHEAR-XY,7X,8HSTRAIN-A,7X,8HSTRAIN-B,7X,8HSTRAIN-C/5X,2HID
     1 ,5X,4HTYPE,7X,7HDEGREES,10X,3HPS1,12X,3HPSI,12X,3HPSI,11X,5HIN/IN,
     1 10X,5HIN/IN,10X,5HIN/IN/3X,5H ****,4X,4H****,7X,7H*******,7X,8H***
     1 *****,7X,8H********,7X,8H********,7X,8H********,7X,8H********,7X,
     1 8H********)
C
C       READ STRESS DATA
C
 30     READ(3,5) IL,I2,I3,I4,SX,SY,SXY,THETA,BFAC,J
 5      FORMAT(4A2,5F10.3,A2)
        IF(EOF(3)) 600,9
 9      IF(THETA.EQ.BLANK) THETA = 0.0
        IF(SX.EQ.BLANK) SX = 0.0
        IF(SY.EQ.BLANK) SY = 0.0
        IF(SXY.EQ.BLANK) SXY = 0.0
 21     EY = (1./E) * (SY - (NU*SX))
 22     EX = (1./E) * (SX - (NU*SY))
 23     GXY = SXY/G
C
C       TEST FOR TYPE OR GAGE AND TRANSFER CONTROL ACCORDINGLY.
```

```
C
      IF(J.EQ.DEL.OR.J.EQ.EQU) GO TO 16
      IF(J.EQ.AXI.OR.J.EQ.BBR.OR.J.EQ.TRO.OR.J.EQ.CAP.OR.J.EQ.SBR) GO TO
     1 17
      IF(J.EQ.REC) GO TO 15
      IF(J.EQ.GEN) GO TO 13
      WRITE(1,609)
 609  FORMAT(//////////10X,62HGAGE INPUT NAME NOT RECOGNIZED BY PROGRAM.
     1  PROGRAM TERMINATED.)
      STOP"GAGE INPUT NAME NOT RECOGNIZED"
C
C
C     READ ANGLES B AND C FOR THE GENERAL ROSETTE FROM THE DATA CARD.
C
 13   READ (3,7) ANGLEB, ANGLEC
 7    FORMAT(2F10.0)
      ANGLEA = ANGLEA * 0.0174533
      ANGLEB = (ANGLEB * 0.0174533) + ANGLEA
      ANGLEC = (ANGLEC * 0.0174533) + ANGLEB
      GO TO 14
C
C
C     SET THE PROPER ANGULAR VALUES FOR A RECTANGULAR ROSETTE.
C
 15   ANGLEA = THETA * 0.0174533
      ANGLEB = ANGLEA + 0.7854
      ANGLEC = ANGLEB + 0.7854
      GO TO 14
C
C
C      SET THE PROPER ANGULAR VALUES FOR A DELTA OR EQUIANGULAR ROSETTE.
C
 16   ANGLEA = THETA * 0.0174533
      ANGLEB = ANGLEA + 2.0944
      ANGLEC = ANGLEB + 2.0944
C
C      CALCULATE THE EXPECTED DELTA, EQUIANGULAR, RECTANGULAR OR GENERAL
C      ROSETTE STRAIN OUTPUT.
C
 14   EA = (EX*((COS(ANGLEA))**2 )) +(EY*((SIN(ANGLEA))**2 )) +
     1 GXY*(SIN(ANGLEA)*COS(ANGLEA))
      EB = (EX*((COS(ANGLEB))**2 )) +(EY*((SIN(ANGLEB))**2 )) +
     1 GXY*(SIN(ANGLEB)*COS(ANGLEB))
      EC = (EX*((COS(ANGLEC))**2 )) +(EY*((SIN(ANGLEC))**2 )) +
     1 GXY*(SIN(ANGLEC)*COS)ANGLEC))
      IF(BFAC.LE.0.) GO TO 500
C
C      USE B-FACTOR CORRECTION TO DETERMINE ACTUAL STRAIN GAGE READINGS.
C
      EA = EA + (EC/BFAC)
      EB = (EB+((EA+EC)/BFAC))/(1.+(1./BFAC))
      EC = EC + (EA/BFAC)
      GO TO 500
C
```

```
C       DETERMINE THE BASIC AXIAL GAGE RESPONSES GIVEN STRESS INPUT.
C
 17     ANGLEA = THETA * 0.0349066
        EA = (EX*((COS(ANGLEA))**2 )) +(EY*((SIN(ANGLEA))**2 )) +
     1 GXY*(SIN(ANGLEA)*COS(ANGLEA))
C
C        TEST FOR THE TYPE OF GAGE (AXIAL, BENDING BRIDGE, T-ROSETTE,
C        CAPACITIVE OF SHEAR BRIDGE) AND TRANSFER CONTROL ACCORDINGLY.
C
        IF(J.EQ.AXI.OR.J.EQ.CAP) GO TO 504
        IF(J.EQ.TRO) GO TO 19
        IF(J.EQ.SBR) GO TO 20
C
C
C        MULTIPLY BY THE PROPER FACTOR TO GET EXPECTED BENDING BRIDGE
C        OUTPUT
C
 18     EA =EA * 1.0
        GO TO 504
C
C
C        MULTIPLY BY THE PROPER FACTOR TO GET EXPECTED T-ROSETTE OUTPUT.
C
 19     EA = EA * 1.0
        GO TO 504
C
C
C        MULTIPLY BY THE PROPER FACTOR TO GET EXPECTED SHEAR BRIDGE OUTPUT
C
 20     EA = EA * 1.
C
 504    WRITE(1,502) I1,I2,I3,I4,J,THETA,SX,SY,SXY,EA
 502    FORMAT(2X,4A2,3X,A2,1X,F14.2,F15.2,F15.2,F15.2,1PE15.5,9X,4HNONE,
     1 11X,4HNONE/)
        GO TO 503
C
C       PRINT OUTPUT (GAGE/ANGLE/STRESSES/STRAINS)
C
 500    WRITE(1,6) I1,I2,I3,I4,J,THETA,SX,XY,XSY,EA,EB,EC
 6      FORMAT(2X,4A2,3X,A2,1X,F14.2,F15.2,F15.2,F15.2,1PE15.5,1PE15.5,
     1 1PE15.5/)
 503    IF(COUNT.GT.20.) GO TO 1002
        COUNT = COUNT + 1.
        GO TO 30
 600    WRITE(1,505)
505     FORMAT(50X,13H*************/50X,13H*END OF DATA*/50X,13H*********
     1 ***)
        GO TO 603
 601    WRITE(1,602)
 602    FORMAT(//////////10X,72HPROGRAM TERMINATED BECAUSE POISSONS RATIO
     1 IS LESS THAN OR EQUAL TO ZERO.)
 603    CALL EXIT
        END
```

ROOM TEMPERATURE TESTS

STRAIN GAGES ON SPAR CAPS AND WEBS

30.442+6 .3

110A1	-1033.53	6479.07	-562.92	90.0	DEL
110A2	- 232.18	-2806.69	4717.81	-90.0	DEL
110A3	673.43	12759.70	-940.58	90.0	DEL
110A4	-1561.16	4720.30	4941.85	-90.0	DEL
110A5	180.24	-2058.32	- 76.43	90.0	DEL
110A6	2031.35	-8233.30	4507.41	-90.0	DEL
310A1	3441.94	-324.38	-4008.55	0.	DEL
310A2	-6178.06	565.51	-3655.46	0.	DEL
310A3	-40.23	5995.27	+7472.22	-90.0	DEL
310A4	113.07	-1076.19	2315.23	90.0	DEL
310A5	95.99	-8088.26	7420.97	-90.0	DEL
510A1	4616.02	-211.52	-5006.81	0.	DEL
510A2	-5706.77	699.96	-4674.81	0.	DEL
510A3	-35.94	7193.19	8818.89	-90.0	DEL
510A4	140.36	-268.03	3376.98	90.0	DEL
510A5	32.13	-7766.10	8832.37	-90.0	DEL
710A1	-867.66	10637.11	2902.85	90.0	DEL
710A2	5.25	292.60	8786.44	-90.0	DEL
710A3	857.74	-10119.78	2863.24	90.0	DEL
710A4	-1644.99	8046.01	9911.71	-90.0	DEL
710A5	175.49	314.75	4195.96	90.0	DEL
710A6	1652.99	-7468.96	9933.80	-90.0	DEL
910A1	-871.77	12736.41	3904.19	90.0	DEL
910A2	139.24	1209.57	10458.77	-90.0	DEL
910A3	898.02	-10368.55	3865.18	90.0	DEL
910A4	-1814.11	9595.27	11778.84	-90.0	DEL
910A5	190.72	1178.70	5555.35	90.0	DEL
910A6	1795.21	-7377.91	11862.02	-90.0	DEL
1110A1	-549.17	16364.17	6238.86	90.0	DEL
1110A2	359.87	3165.06	13753.90	-90.0	DEL
1110A3	916.70	-9630.54	6456.17	90.0	DEL
1110A4	-2207.05	10837.90	15187.36	-90.0	DEL
1110A5	731.99	2407.45	8909.90	90.0	DEL
1110A6	1696.44	-7031.40	15829.02	-90.0	DEL
208	1196.2	73.8	-415.6		DEL
210	1179.8	104.8	-434.1		DEL
212	11670.7	-46.8	-470.3		DEL
408	12462.8	124.5	-882.6		DEL
410	12439.8	202.1	-912.1		DEL
412	13464.8	-116.6	-996.2		DEL
608	14336.9	127.9	-774.0		DEL
610	14274.4	186.5	-806.1		DEL
612	15208.6	-93.6	-878.3		DEL
808	16983.6	102.0	-357.1		DEL
810	16870.7	99.7	-389.8		DEL
812	17329.4	-14.5	-410.6		DEL
1008	21447.6	71.0	654.9		DEL
1010	21131.6	-79.5	621.6		DEL
1012	20603.0	176.1	705.8		DEL

1. Report No.	2. Government Accession No.	3. Recipient's Catalog No.
NASA CR-170413		

4. Title and Subtitle	5. Report Date
Development of a Thermal and Structural Model for a NASTRAN Finite-Element Analysis of a Hypersonic Wing Test Structure	February 1984
	6. Performing Organization Code

7. Author(s)	8. Performing Organization Report No.
Jaap Lamèris	H-1219
	10. Work Unit No.

9. Performing Organization Name and Address	11. Contract or Grant No.
The University of Kansas Center for Research, Inc. 2291 Irving Hill Drive – Campus West Lawrence, Kansas 66045	NSG 4008
	13. Type of Report and Period Covered
12. Sponsoring Agency Name and Address	Contractor Report - Final
National Aeronautics and Space Administration Washington, D.C. 20546	14. Sponsoring Agency Code RTOP 506-53-64

15. Supplementary Notes

NASA Technical Monitor: Jerald M. Jenkins, Ames Research Center, Dryden Flight Research Facility, Edwards, CA 93523

16. Abstract

As part of NASA's continuing research program into hypersonics, Dryden Flight Research Facility of Ames Research Center has conducted extensive heating and mechanical tests on a Hypersonic Wing Test Structure (HWTS). This structure was based on a structural concept developed for a hypersonic research airplane that would cruise at Mach 8. An accurate prediction of the temperature distribution is a major prerequisite for obtaining this goal.

This report describes the development of a thermal and structural model for this HWTS structure using the NASTRAN finite-element method as its primary analytical tool. A detailed analysis was defined to obtain the temperature and thermal stress distribution in the whole wing as well as at the five upper and lower root panels.

During the development of the models, it was found that the thermal application of NASTRAN and the VIEW program, used for the generation of the radiation exchange coefficients, were deficient. Although for most of these deficiencies solutions could be found, the existence of one particular deficiency in the current thermal model has prevented the final computation of the temperature distributions at this date.

A SPAR analysis of a single bay of the wing, using data converted from the original NASTRAN model, indicated that local temperature-time distributions can be obtained with good agreement with the test data. The conversion of the NASTRAN thermal model into a SPAR model is recommended to meet the immediate goal of obtaining an accurate thermal stress distribution.

17. Key Words (Suggested by Author(s))	18. Distribution Statement
Hypersonics Heat transfer Thermoelasticity	Unclassified-Unlimited STAR category 39

19. Security Classif. (of this report)	20. Security Classif. (of this page)	21. No. of Pages	22. Price*
Unclassified	Unclassified	266	A12

For Sale by the National Technical Information Service, Springfield, Virginia 22161.

End of Document